Life-like materials constructed on photoredox of perylene bisimide

Chunfeng Chen

UNIVERSITÉ DE STRASBOURG

ÉCOLE DOCTORALE 222

UMR 7140

THÈSE présentée par :

Chunfeng Chen

soutenue le : **1er Juillet 2021**

pour obtenir le grade de : **Docteur de l'université de Strasbourg**

Discipline/ Spécialité : Chimie Supramoléculaire

Life-like Materials Constructed on Photoredox of Perylene Bisimide

THÈSE dirigée par :

M Thomas Hermans Professeur, Université de Strasbourg, UMR 7140, Strasbourg, France

RAPPORTEURS :

M Florian Beuerle Privatdozent, Institut für Organische Chemie & Center for Nanosystems Chemistry, Universität Würzburg, Würzburg, Germany

M Yannick De Decker Chargé de Cours, Faculté des Sciences, Université libre de Bruxelles, Brussels, Belgium

AUTRES MEMBRES DU JURY :

Mme Emilie Moulin Directrice de recherches, Institut Charles Sadron-CNRS, Université de Strasbourg, Strasbourg, France

Contents

Chapter 1.

Introduction: From Equilibrium to Out-of-equilibrium Self-assembly

Abstract: Supramolecular assemblies based on non-covalent intermolecular interactions have outstanding properties, and bring chemistry, biology, electronics, and even information together. To better devise supramolecular materials, under thermodynamic equilibrium, the mechanism of self-assembly has been extensively studied, especially in supramolecular polymerization. For instance, chain-growth polymerization is well reported based on host-guest interactions, π–π stacking, and hydrogen bonding. Dynamic supramolecular polymers are not just limited to solution chemistry, but can also form supramolecular gels or solids. A relatively new trend is to work on open systems, where a flux of energy or matter is introduced. Many systems now use chemical fuels or light-input to achieve out-of-equilibrium states, with novel emergent properties, such as supramolecular waves, size oscillations, or dynamic patterns. This chapter reviews the development of supramolecular chemistry from the thermodynamic equilibrium to out-of-equilibrium.

1.1 Supramolecular Chemistry

Supramolecular chemistry is based on non-covalent interactions, which is different from covalent chemistry that traditionally occurs with electrons re-arrangements as the new covalent bond forms and the old covalent bond breaks. In conventional organic synthesis, compounds are coupled by multi-step organic synthesis into one entity, and later into functional (covalent) materials. However, supramolecular chemistry provides possibilities to synthesize functional materials via non-covalent bonding, with large molecules as basic units.

Non-covalent intermolecular interactions have been reported since 1960, for instance, Pedersen developed a series of crown ethers for molecular recognition.[1] A few years later, Cram extended host-guest chemistry that one molecule locates in another molecule by non-covalent bonding, leading to a new state of materials.[2] In 1978, Lehn defined supramolecular chemistry[3,4] and was jointly awarded the Nobel prize in chemistry in 1987. In his speech[5], he defined: "supramolecular chemistry is the chemistry of the intermolecular bond, covering the structures and functions of the entities formed by the association of two or more chemical species". Scientists quickly moved to this new field, and with it the journal of supramolecular chemistry was started in 1992. The journal Science, even published that chemical self-assembly was one of the 25 most compelling puzzles and questions over the next quarter-century, which reflects the importance of supramolecular chemistry.[6] So far, it has been revolutionizing conventional chemistry and material science, which brings chemistry, materials, biology, electronics, and even information processes together, broadening the materials science frontiers.

Generally, supramolecular systems are constructed by multiple identical or different chemical species via non-covalent interactions, such as hydrogen bonding, coordination, π–π stacking, Van der Waals, and hydrophobic interactions.[7–9] Comparing with covalent bonds, in most cases, intermolecular interactions are synergistically associated with one or two main driving forces, which result in reversible and dynamic materials. Thus, the design of the molecular blocks, is key to build a supramolecular system, which generally need to balance hydrophobicity and hydrophilicity. In the past 30 years, supramolecular chemistry has been well studied under thermodynamic equilibrium, such as supramolecular polymer[10–12], living materials[13–16], drug

delivery[17–19], organic electronic devices[20–23], crystallization[24,25], multi-responsive materials[26–29]. However, recently, the field, including our group, has been moving toward out-of-equilibrium where systems are sustained by a continuous energy input. [30]

1.2 Supramolecular Polymers

In supramolecular chemistry, a supramolecular polymer is essential for building dynamic materials based on non-covalent interactions. The definition of a supramolecular polymer is derived from covalent polymer. Two centuries ago, Berzelius defined a polymer as a special type of isomerization, because two different molecular weight can be obtained from the same chemical species.[31] Then, in 1953, Hermann Staudinger, the father of modern polymer chemistry, defined polymers as made of long, repeating chains of molecular units. The supramolecular polymer is analogous to covalent polymer, which also repeats molecular units to form a long chain, but with non-covalent bonding.[32] The conventional polymerization is only limited to be activated by chemicals[33,34] or photo-irradiation[35–37], whereas supramolecular polymer is mainly resulted from intermolecular aggregation that can be initialized by varied interactions, such as hydrophobic and hydrophilic interactions, π-π stacking, photo-irradiation, pH, mechanical strength.

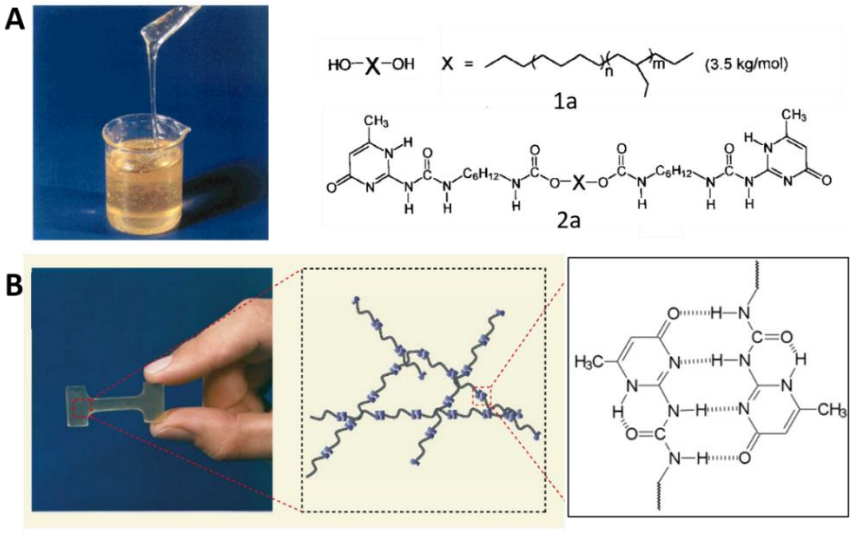

Figure 1.1. Supramolecular polymer constructed on quadruple hydrogen bonds of molecular unit ureidopyrimidinone (UPy), A) telechelic polymers (1a) product in a viscous liquid; 1a and 2a molecular structure. B) the supramolecular polymer in a plastic film that is with quadruple hydrogen bonding. Reproduced from ref. 10 and 39 with permission from Wiley, and Nature.

Although the interactions between building blocks are based on non-covalent bonding, the mechanical stiffness, can be comparable to that of a conventional polymer. For instance, in 1997, Meijier and co-workers demonstrated that a supramolecular polymer built on quadruple hydrogen bonding with 2-ureido-4-pyrimidone (UPY), could selectively form linear type supramolecular polymers with good mechanical stiffness and low melt viscosity. [38] The telechelic polymers ended by hydroxy 1a yields a viscous liquid as Figure 1A shows. But the same building blocks functionalized with 2-ureido-4[1H]-pyrimidinone 2a using a hydrosilylation reaction, led to linear supramolecular assemblies by quadruple hydrogen bonding. In comparison to 1a, the mechanical stiffness of supramolecular polymer 2a is significantly enhanced, and even forms a solid plastic film. Meanwhile, 2a supramolecular polymer is dynamically reversible when the plastic film is dissolved in dichloromethane, and consequently transformed into a highly viscous liquid. [14,39]Besides, the polymer is pH-responsive since to the quadruple hydrogen bonding can be broken by adding acid.

1.2.1 The mechanism of Supramolecular Polymerization

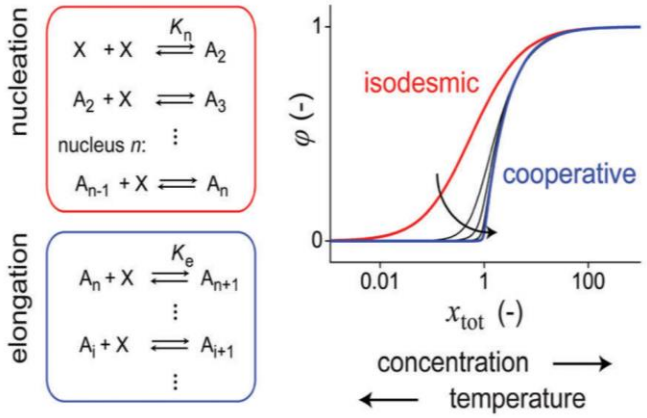

Figure 1.2. Scheme showing the equations of polymerization in the isodesmic and cooperative model, respectively. Where the X represents the molecular units, A_2 represents the dimer, and A more is the elongation of polymer, K_n is the equilibrium constant of the first step, K_e is the equilibrium constant of the rest of monomeric addition to the growing polymer chain. Reproduced from ref. 40 with permission from the Royal Society of Chemistry.

To develop supramolecular polymers, it is crucial to understand the mechanism of supramolecular polymerization. The polymerization consists of nucleation and elongation, is correlated to the Gibbs free energy.[12] Generally, there are three polymerization mechanisms: 1)

isodesmic polymerization, 2) cooperative polymerization, and 3) anti-cooperative polymerization.[40] If Gibbs free energy equivalently changes between each addition step, in other words, the nucleation constant K_n is identical to the rest of elongation constant K_e, the polymerization is isodesmic. This implies that there is no nucleation in the initial step of polymerization (Figure 1.2A). However, when the first step equilibrium constant K_n is smaller than K_e, it is a cooperative polymerization; the nucleation step is disfavored that can be single or multiple steps, corresponding to the nucleus size of two or more. In anti-cooperative polymerization the elongation is disfavoured versus the nucleation ($K_e < K_n$), and this can give rise to size control or even monodisperse assemblies.

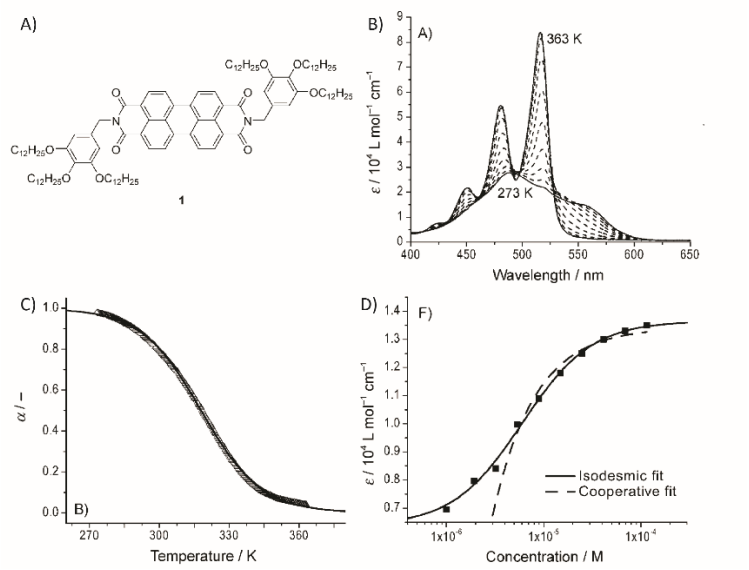

Figure 1.3. A) The molecular structure of the building blocks, perylene bisimide(PBI). B) UV spectra of PBI aggregates in MCN upon heating cooling. C) kinetics of degree of aggregation (α) in temperature-dependent experiment followed by UV absorbance at 556nm. D) kinetics of PBI aggregation in concentration-dependent measurements. Reproduced from ref. 41 with permission from Wiley.

In general, to identify the mechanism of polymerization, temperature and/or concentration dependent studies need to be performed. For instance, perylene bisimide (PBI) unidirectionally polymerizes in methylcyclohexane[41], by heating to 363 K from 273 K, which disassembled into monomer, and subsequently was cooled down back to 273 K at 0.1 K intervals, and rate 1 K min^{-1}. Over time, PBI aggregates evident from the evolution of UV absorbance at 556 nm, which indicates the polymerization is isodesmic, and the experimental data fits well with the isodesmic

model. Meanwhile, the chain growth of the PBI polymer in the concentration-dependent experiment is consistent with the temperature-dependent measurements.

In another example, C_3-symmetrical chiral building blocks vertically assembled into the one-dimensional helical polymer in diluted heptane solution[42], which has supramolecular chirality (Figure 1.4A). By heating-cooling from 363 K to 293 K, as the temperature decreases, the intensity of the positive cotton effect increases, which indicates the building blocks are aggregating over time. Figure 1.4B shows that the molar ellipticity at 223 nm was plotted as a function of temperature, suggesting that cooperatively polymerize. In the nucleation step, the equilibrium constant is temperature dependent. Once the nucleation is completed, the elongation is followed by bigger identical equilibrium constants that are more kinetically favorable. The experimental data fit well with the model developed in the Meijer group, which is based on the "K_2-K" model[43]. Meanwhile, the thermodynamic parameters can be derived from the model, such as molecular enthalpy release, entropy, and equilibrium constant.

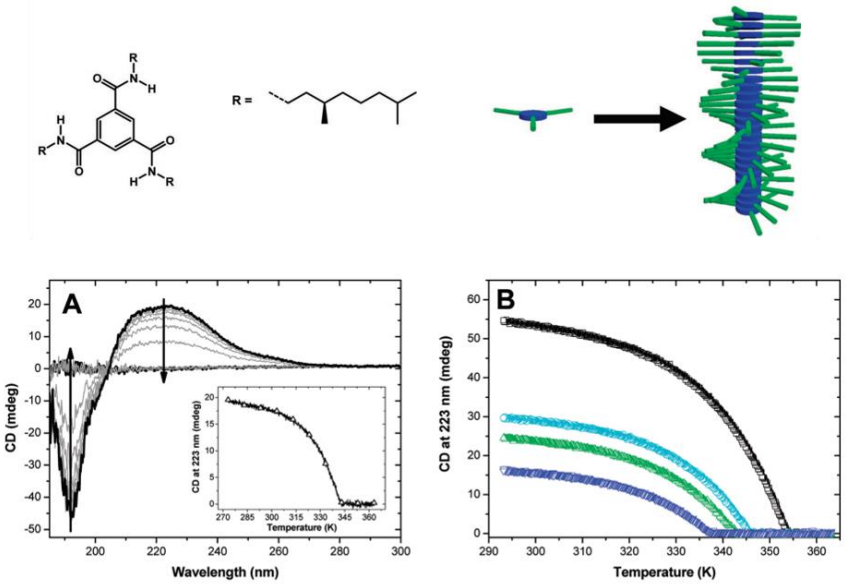

Figure 1.4. Structure of C3-Symmetrical Chiral Discotic building blocks, and the scheme of C3-Symmetrical helical assemblies. A) CD spectra of aggregation in heptane (1.4 × 10-5 M) at temperatures between 20 and 90 °C. Inset shows the molar ellipticity at 223 nm as a function of temperature for the same solution. (B) Molar ellipticity at 223 nm in different concentrations. Reproduced from ref. 42 with permission from American Chemical Society.

Chain Growth in Control

The mechanism plays the main role in constructing a one-dimensional supramolecular polymer. Recently, a well-controlled chain-growth supramolecular polymer was reported by Takuzo Aida's group[44,45]. The C_5-symmetric non-planar corannulene building blocks, M with different substituents, co-assembles into chain polymer, owing to π–π stacking and hydrogen bonding. But, in route 1, the strong competition of intramolecular hydrogen bonding intrinsically locks monomeric units, and, further, prevents π–π stacking, resulting in no polymerization. This implies that internal non-covalent bonding is the key to regulate the chain growth. However, as route 2, by introducing the initiator I with methyl group that prevents the intramolecular interactions, the ring stays open, and, further, coassemble with building blocks, M, via π–π stacking. Because the intermolecular π–π stacking between initiator I and monomer M is stronger than intra-hydrogen bonding of M. The monomer M, therefore, was activated by adding the initiator I, further, elongates into chain polymer.

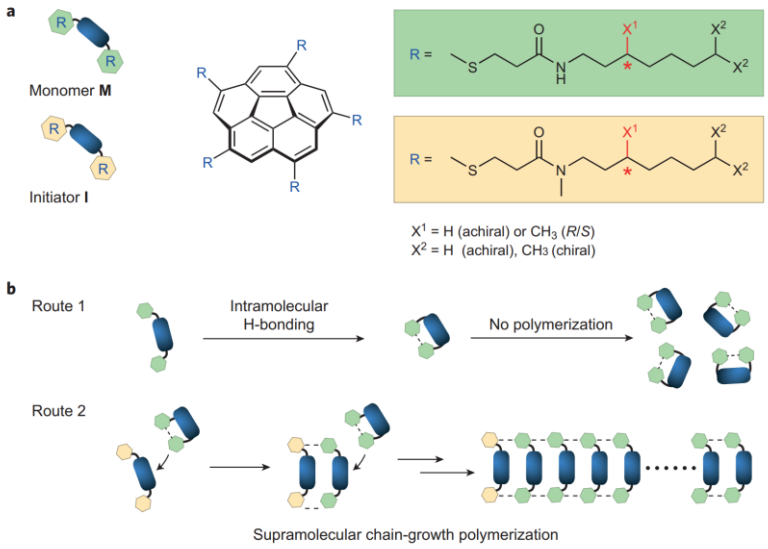

Figure 1.5. Schematic representation of the supramolecular chain-growth polymerization process involving bowl-shaped corannulene molecules. a) Structure of the monomer M and the initiator I, prepared by reductive methylamination of M. b) Route 1: In the absence of initiator I, no polymerization occurs as monomer M tends to adopt a closed cage conformation owing to strong intramolecular H-bonding. Route 2: Addition of initiator I to monomer M facilitates chain-growth polymerization through controlled intermolecular H-bonding interactions. Reproduced from ref. 45 with permission from Nature.

Given the chain growth is determined by initiator I, the length of the chain, in other words, the degree of polymerization can be regulated by the quantity of initiator. When the different amount

of initiator I added into monomer M solution, the length of polymer is extremely uniform, whose polydispersity index distributed from 1.2 to 1.3. To precisely regulate chain-growth, they introduced a chiral group in building blocks for inducing chiral aggregates. The polymerization only occurs when the initiator has the same chirality as monomer M, indicating the stereoselectivity of chain growth because the intermolecular interactions were impaired. This example shows how precisely to control supramolecular polymerization.

1.2.2 Building Linear Supramolecular Polymer Based on Host-Guest Interactions

Host-Stabilized Charge Transfer

In most cases, linear supramolecular polymers are formed by π–π stacking[46–48], hydrogen bonding[49], or metal coordination[50]. The selectivity of chain-growth and a high degree of polymerization, however, remains a challenge, but host-guest is one of the strategies to linearly co-assemble the monomeric units by head to end[51,52]. Given that cucurbit [8]uril, CB[8], is a good candidate to host methyl viologen, it has been widely used to host a series of neutral and cationic species[53–55]. For instance, Zhang and co-workers[11] have developed a linear supramolecular polymer based on host-stabilized charge transfer between cucurbit[8]uril (CB[8]) and methyl viologen. Anthracene, being an electron donor due to electron-rich in a planar shape, is incorporated in the building blocks, DADV. The host, CB[8], and the guest, DADV, both have poor solubility in water, but the complex become water-soluble when CB[8]/DADV mixed in 2:1 (molar ratio) in water because the linear DADV-2CB[8]formed by multiple host-stabilized charge-transfer interactions. In comparison to the conventional polymer, the DADV-2CB[8] polymer has a larger Kuhn length, which was characterized by AFM based on single-molecule force spectroscopy, indicating this host-guest polymer is more flexible. Meanwhile, the segment elasticity is smaller than the covalent polymer, DADV-2CB[8] behave as was spring when being lengthened.

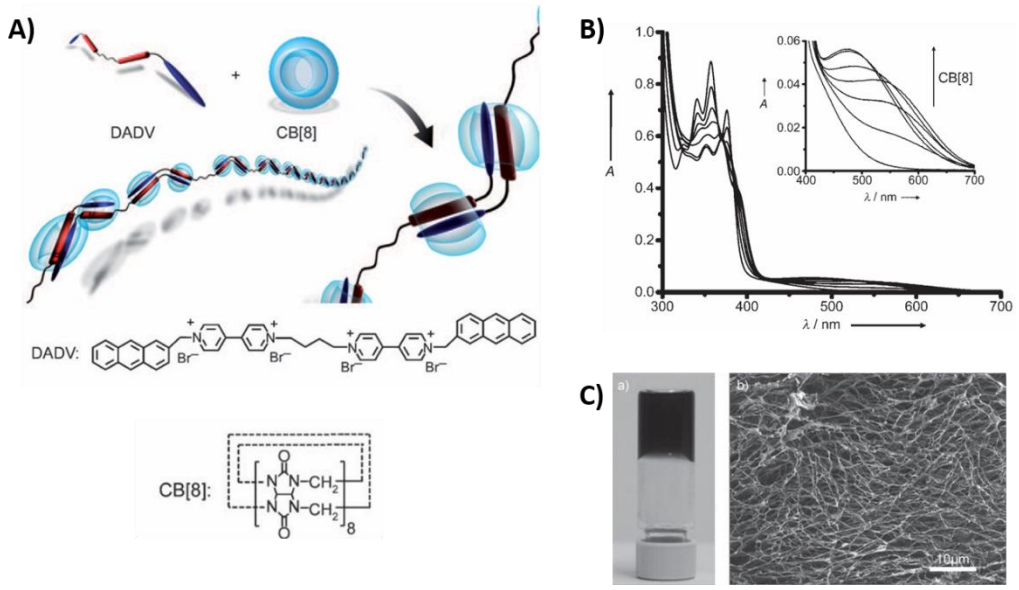

Figure 1.6. A) Representation of the formation of the supramolecular polymer based on multiple host-stabilized charge-transfer interactions, and the structures of monomers DADV and CB[8]. B) UV/Vis spectra of DADV (0.10 mm) with different ratios of CB[8] (CB[8]/DADV=0, 1:3, 2:3, 1:1, 4:3, 5:3, 2:1) C) SEM image of the gel formed by DADV-2CB[8]. Reproduced from ref. 11 with permission from Wiley.

As a control experiment, acceptor with single anthracene and methyl viologen, 1,1'-dimethyl-4,4'-bipyridine-1,1'-diium iodide, only forms 1:1 or 1:2 cyclic polymer that, by self-complex in the cavity of CB[8], is with smaller the Kuhn length and the segment elasticity, which hardly elongated into a chain-like polymer. The hydrodynamic radius of the self-cyclic polymer is only 0.4nm, but DADV-2CB[8], even, can reach 30nm. The well-complexed DADV-2CB [8] polymer even shows the new characteristic bands around 490 nm. Further, increasing the concentration of DADV-2CB[8], the deep purple gel forms with nanofibers (Figure 6C), whereas the building blocks with single anthracene and methyl viologen remain in solution, even, at higher concentration. Thus, by rational design, the host stabilized charge transfer unidirectionally contributes to chain polymer.

Linear Host-Guest Polymer Based on Cyclodextrin

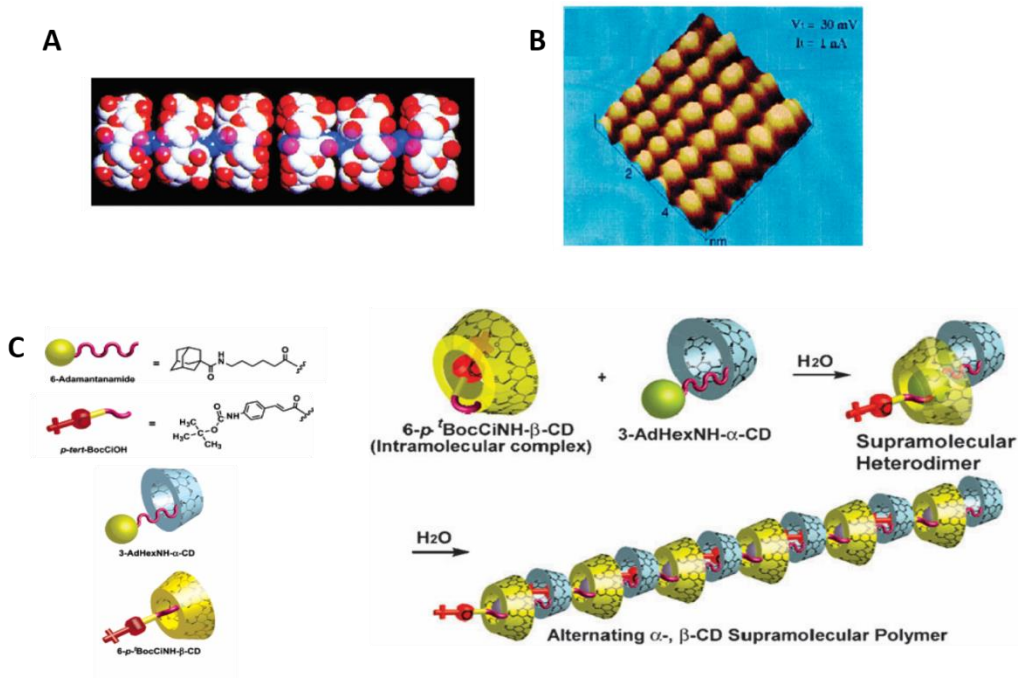

Fig. 1.7 (A) Crystal structure of a-CD-PEG. (B) STM image of a-CD- poly (ethylene glycol). (C)chemical structure and representation of 3-AdHexNH-R-CD and 6-p-t BocCiNH-α-CD. If only 6-p-t BocCiNH-α-CD in solution, there is no polymerization, caused by the intramolecular complex. By introducing 6-p-t BocCiNH-α-CD, the building blocks alternatively host and form a linear polymer. Reproduced from ref. 59, 65 with permission from Royal Society of Chemistry, and American Chemical Society, respectively.

Cyclodextrin (CD), contains 6, 7, or 8 glucose subunits, corresponding to α-CD (6 glucose subunits), β-CD (7 subunits), and γ-CD (8 subunits), respectively, which are ideal candidates being water-soluble hosts due to the hydrophobic interior in aqueous environment[56–58]. Cyclodextrin, therefore, has been widely studied in the linear supramolecular polymer. The linear rotaxane single crystal, for instance, complexed by α-CD hosting poly (ethylene glycol)[59], whose linear morphology, even, was visually observed on single-crystal X-ray and STM (Figure 1.7 A and B). As reported, such as azobenzene[60,61], adamantane[62,63], and N-methylbenzimidazole[64], are the ideal guests to the corresponding CD. For example, Harada and his co-worker have devised an alternative supramolecular polymer with substituted cyclodextrin[65]; the β-CD host adamantane and α-CD host t-Boc cinnamoyl (Figure 1.7C). If only a single 6-p-t BocCiNH-β-CD in solution, the intramolecular complex formed by β-CD and t-Boc cinnamoyl, there is no chain growth and polymerization. However, when adding 3-AdHexNH-R-CD, 6-p-t BocCiNH-β-CD intermolecularly

complexes 3-AdHexNH-R-CD because β-CD intra-hosts t-Boc cinnamoyl that replaced by the intermolecular β-CD-adamantane complex. If the molar ratio of 3-AdHexNH-R-CD/6-p-t BocCiNH-β-CD is 1:1, all the adamantane were hosted by β-CD, simultaneously, α-CD is hosting t-Boc cinnamoyl of β-CD, which allows the free monomer alternatively adding onto the chain-polymer. Therefore, the alternative linear supramolecular polymer was constructed by host-guest interaction based on cyclodextrin.

1.2.3 Supramolecular polymer gels

Since supramolecular polymerization in solution had been well-studied, the field has been moving toward three-dimensional soft materials, such as supramolecular polymer gels[66,67]. Because the main driving force is non-covalent bonding, supramolecular polymer gels show dynamic behaviors, such as reversibility, multi-responsiveness, and even adaption. However, in comparison to conventional polymers, supramolecular gels have poor mechanical properties; consequently, the study is only limited to basic research without (for the moment significant) industrial applications. Although it is challenging to make a supramolecular polymer with good mechanics, still, some groups have attempted and achieved mechanically excellent materials. As an example[68], the heteroditopic building blocks was devised based on host-guest and ligand coordination, which contains the host benzo-21-crown-7, the guest dialkylammonium, and the metallic coordination sites, 1,2,3-triazole group. By crown ether hosting dialkylammonium at high concentration in acetonitrile, the building blocks linearly polymerized, but only the polymer solution was obtained. However, when adding the ligand palladium into this solution, the linear polymers spontaneously gelated, owing to 1,2,3-triazole coordinating with metal ions. The mechanical stiffness, consequently, was enhanced from 10 to 10^4 Pa. Given the non-covalent interactions, this gel shows dynamic reversibility, such as gel-sol-gel transition by heating-cooling, pH responsive, or competition between ions. Meanwhile, the gel shows self-healing properties (Figure 1.8) and incredible elasticity, which, even, can rebound to the original point if free drops gel on the table. Such multi-interactions in one building blocks sets a good example for us to construct dynamically multi-functional supramolecular soft materials.

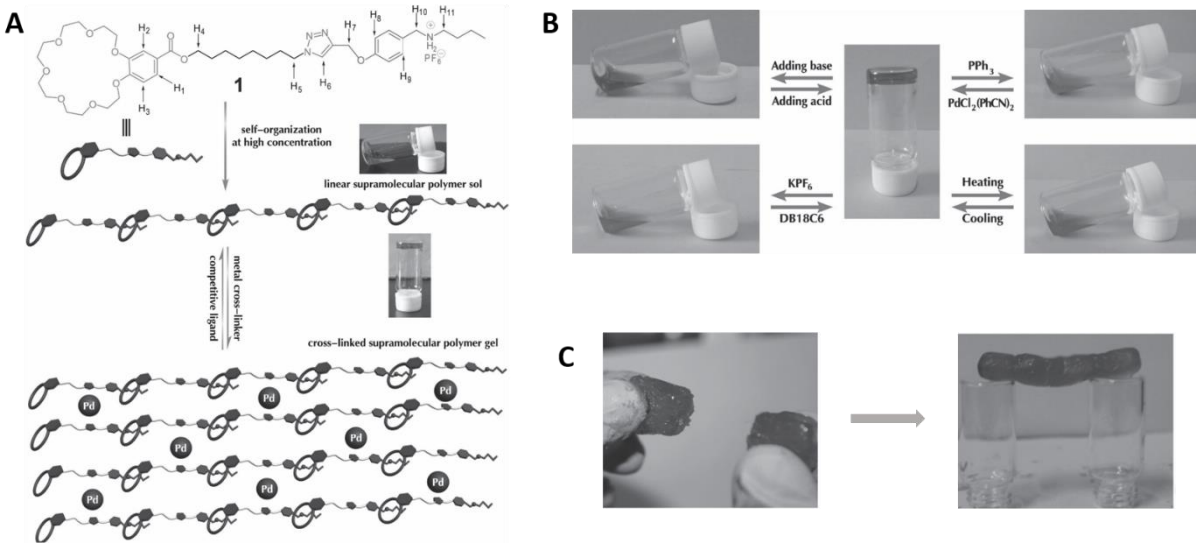

Fig. 1.8 A) the representation of supramolecular polymer constructed by building blocks, heteroditopic monomer 1. The linear polymer solution was obtained when only monomer 1 in acetonitrile, by introducing palladium ion into solution, which vertically and horizontally interacted into polymer gel. B) The reversible gel–sol transitions of the supramolecular polymer network gel by four different stimuli (pH-, thermo-, cation-, and Metallo-induced). C) The gel is self-healed after cutting. Reproduced from ref. 68 with permission from Wiley.

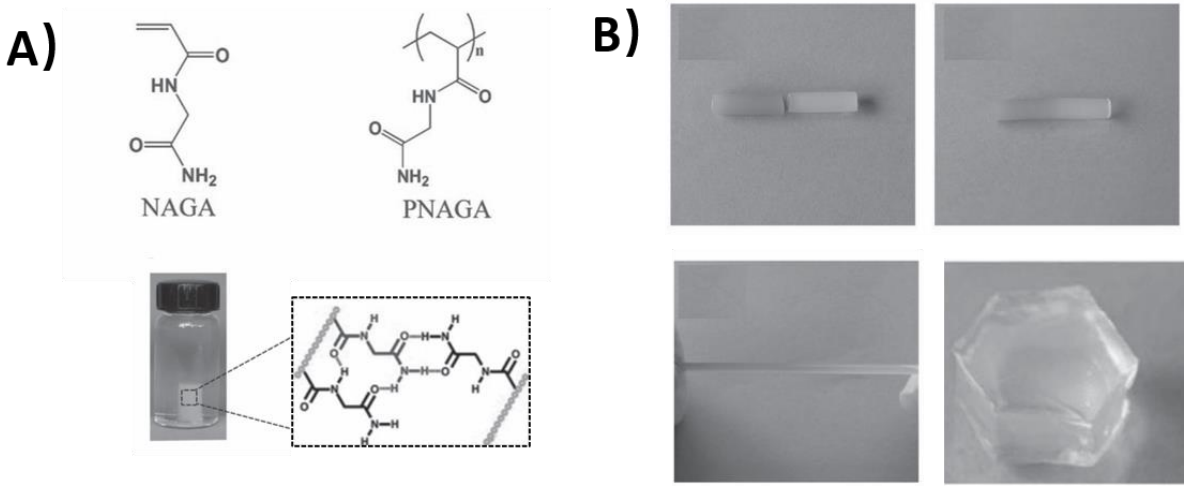

Figure 1.9 A) Molecular structures of N-acryloyl glycinamide, poly (N-acryloyl glycinamide, and the mechanisms underlying the reinforcement effect of dual amide hydrogen bonding. B) Photographs the self-reparability, stretching, and shaping of the hydrogel. Reproduced from ref. 69 with permission from Wiley.

As another example, to overcome the poor mechanical properties of the supramolecular polymer, incorporating the conventional polymer into supramolecular gel allows the materials, simultaneously, to possess expected mechanical stiffness and dynamic reversibility. Liu and his co-workers demonstrated a mechanically strong, highly stable, thermoplastic, and healable

supramolecular polymer hydrogel.[69] The monomer was designed based on multiple hydrogen bonding. N-acryloyl glycinamide (NAGA) contains two amides, upon photoinitiation, polymerizing with acryloyl chloride into poly (N -acryloyl glycinamide) (PNAGA) in water (Figure 1.9A). When the concentration up to 10-25%, the gelation in water occurs, which shows excellent mechanical properties because the hydrogen bonding was amplified after polymerization. The gel, however, is reversible in water after heating-cooling, suggesting the gel has supramolecular dynamic properties (Figure 1.9B). Due to the secondary hydrogen bonding, the tensile strength of the gel, even, can reach 1.1Mpa. The key features of this product have excellent thermo-plasticity that two-halves gels self-healed after heating to 90°C, and, even, can be stretched, shaped, and elongated (Figure 1.9B).

1.2.4 Two-component Supramolecular polymer gel

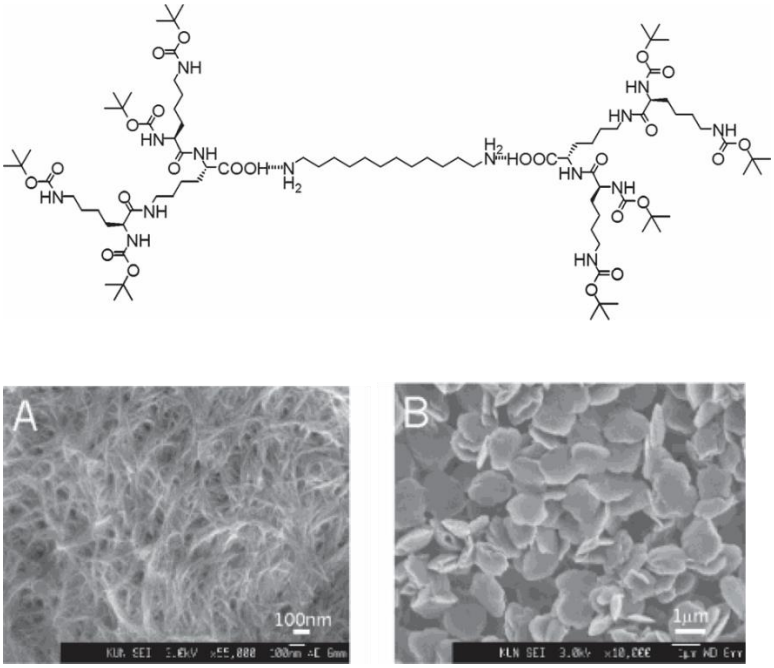

Figure 1.10. the chemical structure of two-components gelator, dendrimer, and diaminododecane. A) SEM images of a 2:1 dendrimer/diamine gel in toluene. B) SEM images of a 1:4.5 dendrimer/diamine gel in toluene. Reproduced from ref. 74 with permission from American Chemical Society.

Since gelator design needs to be balanced with delicate hydrophilicity and hydrophobicity, generally, it takes time to be optimized by a batch of organic synthesis. In comparison to the single gelator, two-component[70,71], or even multiple components gel[72,73] avoids multi-step synthesis,

synergistically combining multi-functional groups by non-covalent bonding. So far, many examples of two-component gels have been reported. Smith and co-workers, for example, constructed a two-component gel[74] based on dendrimer associating with aliphatic diaminododecane (in toluene). But the morphologies of assemblies are concentration-dependent. Thin fibers form at low concentrations (Figure 1.10B), but by increasing the concentration of the building blocks, thicker fibers were observed. At the same concentration, If the molar ratio of dendrimer/diamine is 2:1, the assemblies are nanofibers, when changing to 1:4.5, consequently, only nanoplates were observed (Figure 1.10C). Since this gel is two components, the gel properties can be easily regulated by using different aliphatic diamine spacers. The two component gels, thus, are highly flexible and being regulated.

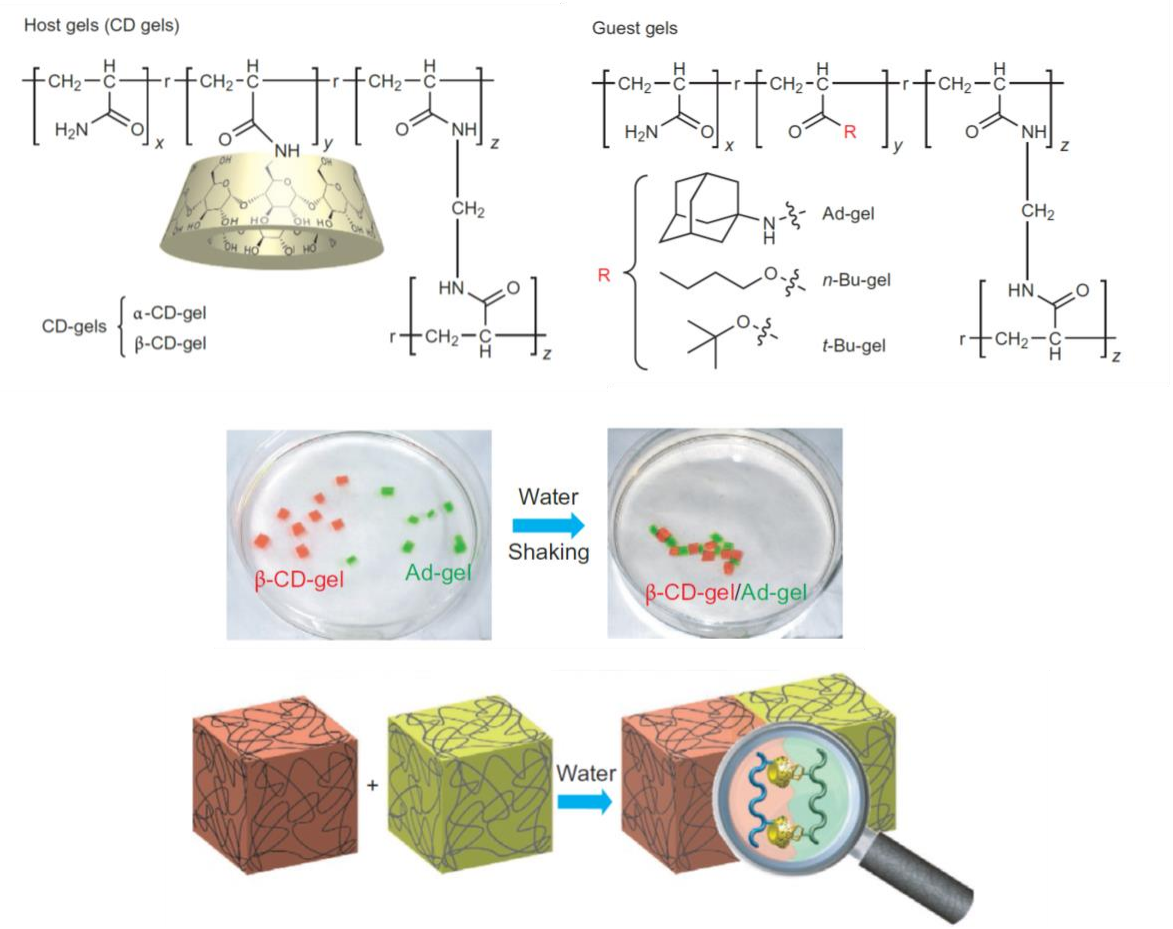

Figure 1.11. Chemical structures of host and guest gels. Host gels: a-CD-gel and b-CD-gel; guest gels: adamantyl gel (Ad-gel), n-butyl-gel (n-Bu-gel) and t-butyl-gel (t-Bu-gel). Macroscopic self-assembly between β-CD host gels and guest Ad-gel. After shaking, each gel alternatively associates it into one chain-gel. Reproduced from ref. 76 with permission from Nature.

The two-component gel is not only limited to morphological transformation, which also creates smart materials. As such, combining two or more functional building blocks allows being multi-responsive[75], even, at a macroscopic level (millimeter or centimeter). Recently, Harada and his coworkers demonstrated that bulk gels self-recognize[76]. The gelator, acrylamide substituted by cyclodextrin, forms a gel by radical copolymerization, which acts as the host. But adamantyl(AD), n-butyl (n-bu) and t-butyl (t-bu) substituted acrylamide gel act as the guests. When individual β-CD-gel met with AD-gel, which self-recognized each other, and, alternatively, associated into chain-gel after being shaken in water (Figure 1.11). The strong binding alternative gel, even, cannot be separated, only if being heated to 80°C. When introducing the β-CD compound into the mixture of β-CD-gel and AD-gel in water, the gels stop recognizing because free β-CD takes over all adamantyl moieties of AD-gel, consequently, preventing β-CD-gel from interacting with AD-gel. This suggests that macroscopic recognition is caused by host-guest interactions of β-CD and adamantly on the molecular scale. Therefore, two-component gel, provides a possibility to construct smart materials at the molecular or macroscopic level.

1.3 Out-of-equilibrium Supramolecular Assembly

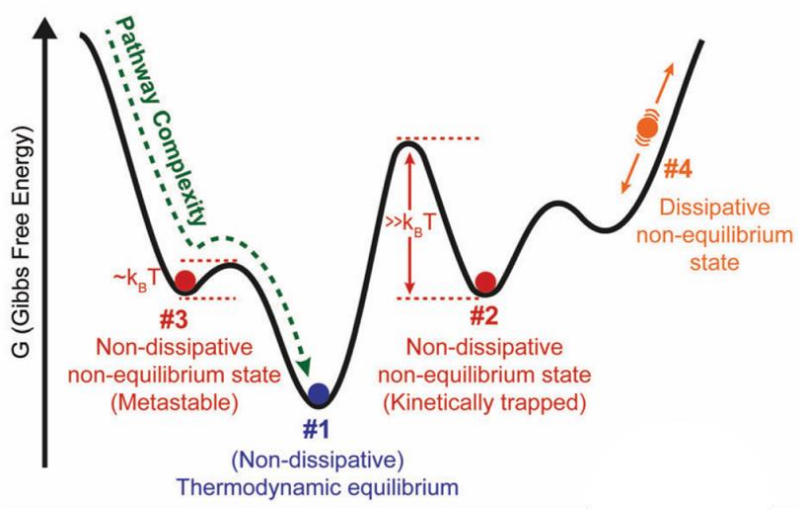

Figure. 1.12. Scheme of Gibbs free energy landscape of the different thermodynamic states in supramolecular self-assembly. Reproduced from ref. 40 with permission from Royal Society of Chemistry.

In supramolecular chemistry, the field has been moving toward out-of-equilibrium, which is classified into non-dissipative and dissipative out-of-equilibrium (Figure 1.12). Non-dissipative out of equilibrium assemblies are confined at the global minimum of the energy landscape (#1), or at local minimal (#2, #3) resulting in a kinetically trapped or metastable states.[40] If the energy barrier locates around the same magnitude as k_BT (where k_B is the Boltzmann constant and T temperature), assemblies are metastable. When the energy barrier is larger than k_BT, assemblies are kinetically trapped. To achieve dissipative out-of-equilibrium systems, continuous energy supply is key. Generally, precursors are converted into building blocks by a flux of energy, which then can aggregate. [77] Once the influx of energy is stopped, the aggregates dissipate energy and revert to the monomeric precursor. The energy input, mostly, is added in the form of chemical fuels[30,78], can be mediated by enzymes[79–81], or can be light-driven[82,83]. The reversible activation and deactivation of the building blocks is important to construct dissipative out-of-equilibrium systems.

1.3.1 Chemical Fuel Driven Dissipative Assembly

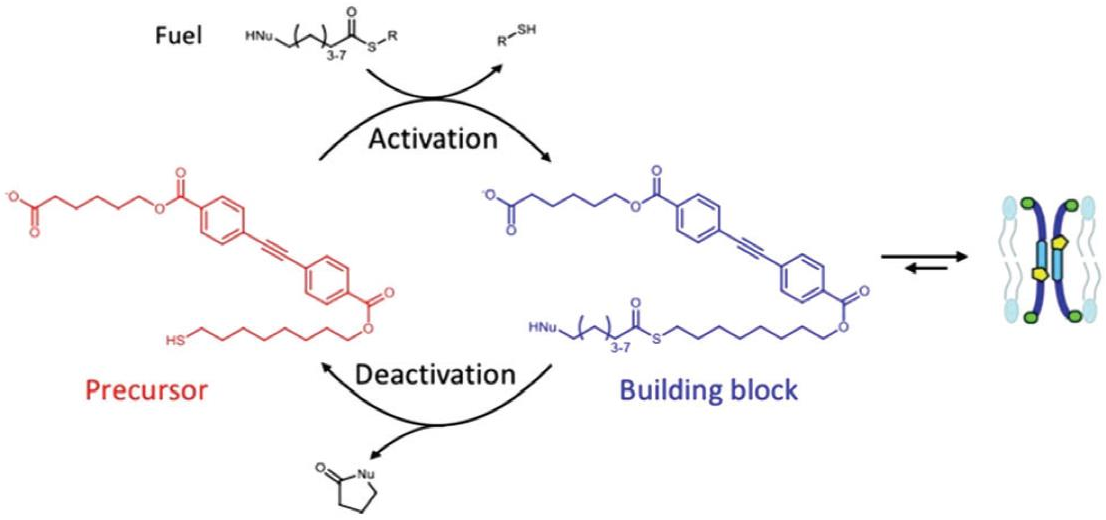

Figure 1.13. Thioester-driven dissipative assembly of membrane pores. The thioester is a chemical fuel that drives the precursor (red) to transform into the building block (blue), by exchanging thiol–thioester, consequently, assembles and forms transient membrane pores. But the aggregates intramolecularly react, finally, revert to the precursor with chemical waste. Reproduced from ref. 77 with permission from Royal Society of Chemistry.

Although several chemical reaction cycles have been reported to construct dissipative out of equilibrium systems[84], it remains in its infancy. Many supramolecular chemists are striving to enrich reaction cycles to develop new dissipative systems. As an example, Fyles designed a dissipative transient membrane pore sustained by a chemical fuel.[77,85] In the activation step, by reacting with the chemical fuel thioester, the precursor was activated into the building blocks by exchanging thiol-thioester, which further aggregates since the building blocks is more hydrophobic in comparison to the precursor. However, the aggregates are not stable due to intramolecular thioester displacement, leading to deactivation and depolymerization. The kinetics of two different reactions are key to allow the system to be out of equilibrium. In certain conditions, the deactivation is slower than the activation reactions, leading to transient aggregates that form membrane pores. Although by-product lactam generated in the deactivation step, it has no influence on the system.

In the initial definition, fuel-driven dissipative out of equilibrium materials must be initialized from monomeric precursors to building blocks, and then to aggregates. However, from a broader supramolecular perspective, fuels can also mediate depolymerization instead of polymerization. An example was reported by Hermans and co-workers[86], which is based on the chemical redox chemistry of perylene bisimide. Under thermodynamic equilibrium, PBI aggregates in buffer because of highly π–π stacking and hydrophobic interactions. When adding chemical fuel, sodium dithionate, the aggregates were reduced into radicals, consequently due to electronic repulsion, disassembling into monomer. However, once the fuel is consumed, the monomeric PBI radicals are re-oxidized back to the neutral building blocks by reacting with ambient O_2. If alternatively introducing the reductant and oxidant, the transient materials can be cycled many times.

1.3.2 Enzyme Driven Dissipative Out-of-equilibrium Assemblies

To construct biomimetic supramolecular assemblies, amphiphilic peptides are one of the ideal candidates as building blocks to build biocompatible nanostructures, which has been widely designed for bio-applications, such as bone regeneration and cartilage regeneration.[87,88] For instance, Ulijin and co-workers used α-chymotrypsin to construct a dissipative hydrogel based on a peptide.[89] In this system, the hydrophobic amino acids substituted naphthalene-tyrosine methyl

ester (1 in Figure 1.14) is the precursor, by adding the enzyme, transacylation occurs leading to a more hydrophobic building block (2). The latter assembles into nanofibers and gelates in water when the concentration is above the critical gelation concentration due to π–π stacking and hydrophobic interactions. The same enzyme, however, simultaneously hydrolyses the building blocks back to the monomer in acid form, leading to disassembly. The kinetics of catalytic transacylation and hydrolysis is key to achieve a transient gel state. The gel forms when transacylation reaction takes over, but whose lifetime is regulated by the enzyme concentration and pH. When the concentration of enzyme is 0.5 mg/mL, the gel totally transformed into solution after 16 h, whereas only 3 h was needed at 30 mg/mL. Meanwhile, the morphologies transformed from nanofibers to nanoclusters as the gel dissemble. If introducing more methyl ester (1) into the system, the transient gel can be repeated three times, which cannot be repeated more due to the chemical waste influenced on the system.

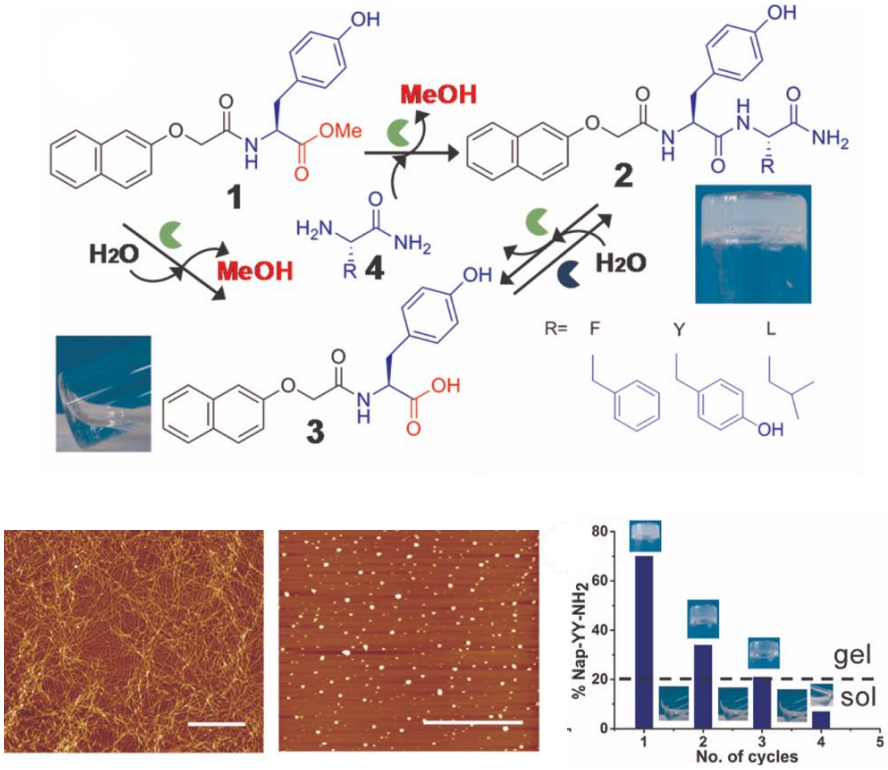

Figure 1.14. Nonequilibrium biocatalytic self-assembly: the precursor, Nap-Y-OMe (1) and different amino acid amides (X-NH2, 4) in the presence of enzyme, chymotrypsin (green), form temporal hydrogelator (2), further, forms hydrogel; but the same enzyme hydrolyze the gelator back to Nap-Y-OH (3) and 4, leading to gel disassemble to a solution, meanwhile, the morphologies transformed from nanofibers to nanoclusters. By introducing more methyl ester (1) into the system, the transient gel can be repeated three times. Reproduced from ref. 89 with permission from American Chemical Society.

1.3.3 Light-Driven Dissipative Out-of-equilibrium systems

As the abovementioned, we realize chemical waste is a big obstacle in dissipative out of equilibrium system, which affects emergent properties of transient materials. Thus, light was introduced as an energy source to push the complex systems out-of-equilibrium. Compared to chemical fuels, light can be an ideal to locally drive supramolecular assembly and disassembly by the morphological transformation of building blocks[90,91]. Photo-driven systems, often can be reversibly repeated without producing any chemical waste.

There are several photochromic molecules used as photo-responsive building blocks.[60,92] Azobenzene[93], for instance, has been extensively studied as building blocks to construct photo-responsive materials. Sleiman and co-workers have reported on nanostructures based on the photoisomerization of azobenzene.[77,94] Under thermodynamic equilibrium, the trans-azobenzene aggregates into disordered nanoplates. However, upon UVA irradiation, the trans-azobenzene photoisomerized into the cis-form, which associates into cyclic tetramers, and forms long-chain rod-like aggregates by secondary association. By heating the sample, the cis-form was reverted to the trans, leading to a morphological transformation.[94]

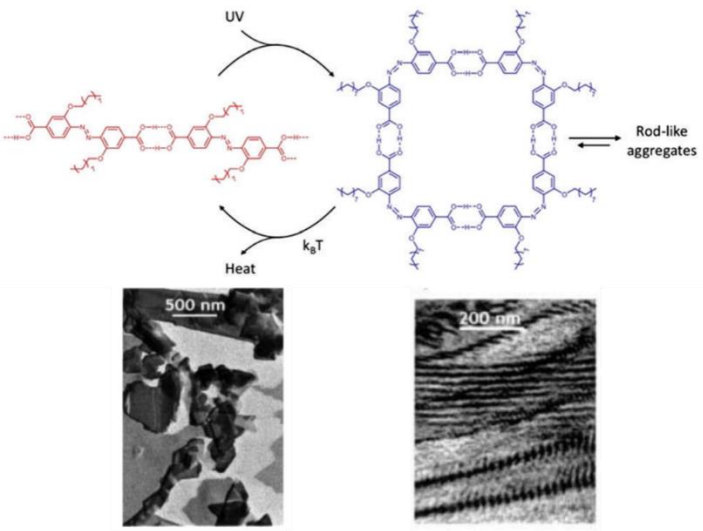

Figure 1.15. The molecular structure of the hydrogen-bonded trans-azobenzene and cis-azobenzene, SEM images of the linear assembly trans-azobenzene, and cyclic tetramers secondary assemblies. Reproduced from ref. 94 with permission from Wiley.

In light-driven systems, the activation and deactivation of building blocks, can be fully controlled by different photons, i.e., by two different light sources. Yagai and co-workers, for instance, reported that the aggregates based on diarylethene can be regulated by photoisomerization,[92] owning to the movement of the two central methyl groups. The open form of the diarylethene is more flexible and allows monomer, to assemble into aggregates, but the closed form is more rigid and prohibits aggregation. The two states of the diarylethene can be switched by UV and visible light (Figure 1.16A). These dual responsive light properties give us the possibility to create fully light-controlled emergent materials.

Van Esch and coworkers constructed a spatiotemporally controlled gel.[95] The open form diarylethene is toluene-soluble, upon UV irradiation, converting into the closed-form that, consequently, assembles into nanofibers and forms an organogel. Under a gradient intensity of UV light irradiation, the gel locally forms in the strong UV region, and simultaneously, the gelator diffuses to the weak UV area. This mass transfer is caused by the transformation of the building blockings 2 is faster than the diffusion of the building blocks 2 (Figure 1.16B).

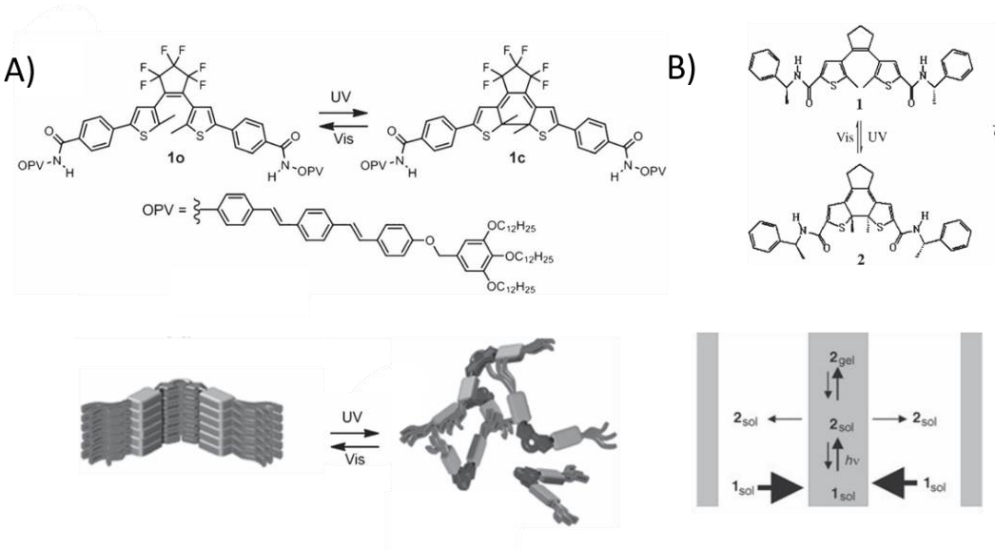

Figure 1.16. A) Molecular structures of OPV-equipped diarylethene 1 in the open (1 o) and closed forms (1 c), and the representation of the open form and assembled closed form. B) the building block, dithienylcyclopentene, can be switched between the open form 1 and the closed-form 2 upon UV and visible light irradiation. Mass-transfer during photoinduced gel formation in inhomogeneous optical fields. Reproduced from ref. 92 and 95 with permission from Wiley.

1.4 Perylene Bisimides as Building Blocks

Perylene-3,4,9,10-tetracarboxylic acid bisimide is abbreviated as PBI that is extensively studied as building blocks to construct hierarchical architectures in supramolecular chemistry[96]. The parent perylene bisimide substituted by two carboxylic acid and imide groups at 3,4- and 9,10-positions, respectively (Figure 1.17), leading to a rigid planar scaffold. Given the large π-conjugation, PBI is a good candidate as a supramolecular building block. Interestingly, PBI has a low reduction potential,[97] and generally is an acceptor. In dichloromethane, when the PBI was electrically reduced, two reversible reduction redox cycles were obtained around -1.0 and -1.2 V, corresponding to the PBI radical anion and dianion. The monomer PBI absorbs from 440 nm to 525 nm with three maxima in UV/vis absorption, and the fluorescence is totally mirrored; the quantum yield, reaches 0.9 in common solvents. Because a large energy gap exits between the singlet and the triplet, S_1—T_1 intersystem crossing is negligible[96]. When PBI aggregates, the UV absorption has a blue or red shift, which corresponds to H and J-aggregation, respectively. In comparison to other dyes, PBI has pronounced photo-thermo-stability[98], without degrading even when exposed to UV light. Thus, the PBI is widely studied in supramolecular polymerization[99,100], luminescent architectures[101,102], organic electron devices[103,104], and photocatalysis[105].

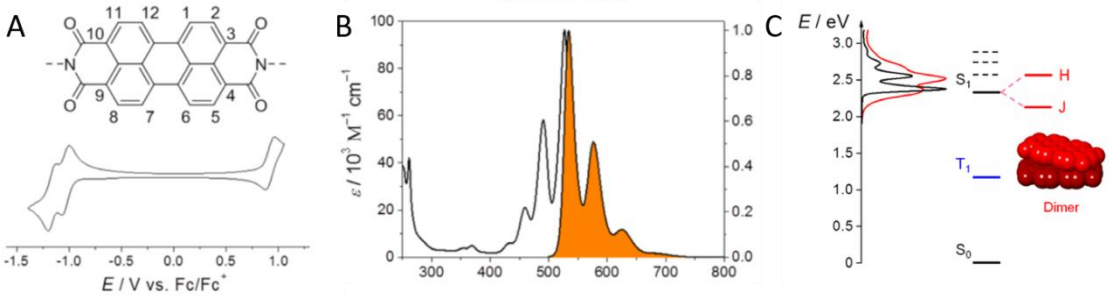

Figure 1.17. A) Molecular structure of the parent perylene-3,4:9,10-tetracarboxylic acid bisimide scaffold, and typical cyclic voltammogram of PBI monomer in dichloromethane (ferrocene/ferrocenium as reference). B) UV/vis and fluorescence spectrum of PBI monomer. C) Simplified Jablonski diagram showing the energy levels of singlet and triplet states of the parent PBI chromophore and including the H- and J-coupled Frenkel states of a typical rotationally displaced π- stacked dimer aggregate. Reproduced from ref. 96 with permission from American Chemical Society.

1.4.1 PBI as Building Blocks for Polymerization

As an example, Würthner and co-workers reported fluorescent J-aggregates based on PBI living supramolecular polymerization.[106] In this system, monomeric MeO-PBI forms H-aggregates in

1,1,2,2-tetrachloroethane when the hot solution was cooled down from 90°C to 10°C at a rate of 5°C/min. However, J-aggregates were obtained at a slower cooling rate 1°C/min (Figure 1.18). This corresponds to two different pathways: 1) isodesmic polymerization in H-aggregation, and 2) cooperative polymerization in J-aggregation. The main reason leading to different pathways in the hydrogen bonding; in H-aggregates, the amide groups intramolecularly associates with imide ring by hydrogen bonding, subsequently, π-π stacks, whereas the hydrogen bonding in J-aggregates intermolecularly interacts. But the intramolecular hydrogen-bonded H-aggregates are kinetically metastable, over time, transforming to thermodynamically favorable J-aggregates. The initial state of H-aggregates, interestingly, is almost fluorescent silent, whereas the fluorescence of J-aggregates is turned on with a quantum yield of 0.14. The transition of H to J aggregates is not just dependent on the competitive π-π stacking and intramolecular hydrogen bonding, but can also be induced by seeding. The elongated J-aggregates are equivalently added into the incubated H-aggregated solution, the H-aggregates instantaneously transformed into J-aggregates, simultaneously, the fluorescence was turned on.

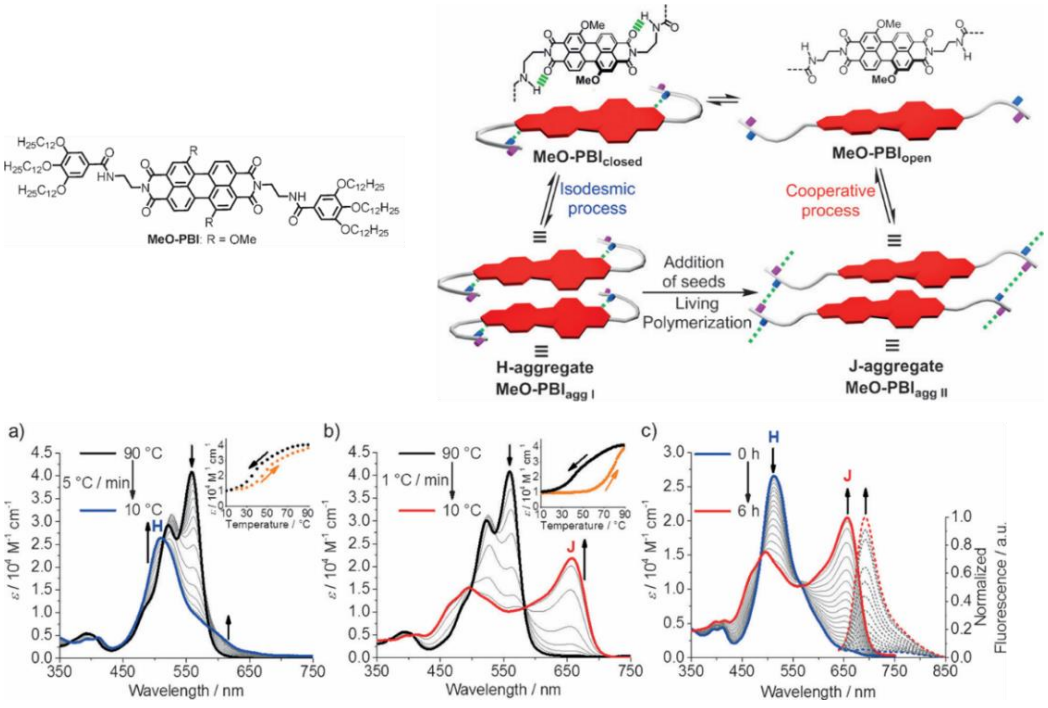

Figure 1.18. the molecular structure of perylene bisimide derivative. The equilibrium between the open (MeO-PBIopen) and the closed conformation (MeO-PBIclosed) and formation of the metastable H-aggregate Meo-PBIagg I and the thermodynamically favored J-aggregate Meo-PBIagg II; the UV spectra of the H and J aggregation from the monomer upon cooling from 90 °C to 10 °C at the rate 5, 1 °C/min, respectively, and UV spectra of the transformation from H aggregates to J aggregates. Reproduced from ref. 106 with permission from Wiley.

Very recently, a self-sorting supramolecular polymerization based on P- and M- chiral atropoenantiomers was reported.[107] The core distorted perylene bisimide substituted by acyloxyl (PBI1) has P and M chirality (Figure 1.19), whose aggregation is temperature-dependent. PBI1 cooperatively aggregates into nanofibers when monomeric PBI1 in hot methylcyclohexane is cooled down at a fast rate, which further assembles into the purple columnar liquid crystal. In contrast, with a slow cooling rate, nanosheets formed, leading to a red lamellar crystal. The two aggregates show different optical properties; the Agg1 mainly absorbs around 600 nm, but 544 nm is the main absorption in Agg2. When equivalently mixing the stock solution of Agg1 and Agg2, Agg1 converted into Agg2 at 35 °C, indicating Agg2 nanosheets are thermodynamically favorable. The main reason leading to this self-sorting polymerization is homochiral and heterochiral self-assembly. If M/M or P/P PBI1 nucleated and elongated, the nanofibers form. But P/M or M/P atropisomers alternatively polymerize into two-dimensional nanosheets.

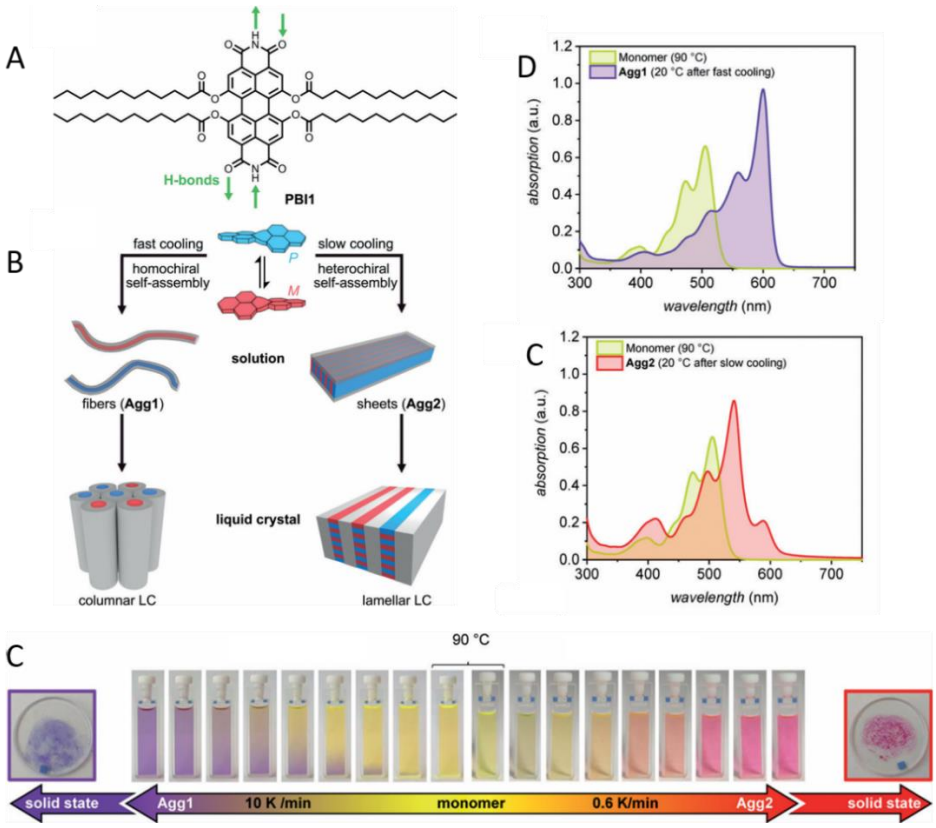

Figure 1.19. a) Chemical structure of PBI1. b) Schematic illustration of the cooling-rate dependent homo- or heterochiral self-assembly into fibers or sheets, respectively, and their subsequent organization into columnar or lamellar liquid crystals. C) the blue and red liquid crystals obtained with a fast and slow cooling rate from the hot PBI solution. D, E) UV/Vis absorption spectra of a solution of monomers and aggregates of PBI1 Agg1 and Agg2. Reproduced from ref. 107 with permission from Wiley.

1.4.2 PBI Chemical Reduction

Given perylene bisimides (PBI) with low reduction potential, PBI easily gets reduced by sodium dithionate,[108] leading to one, or two-electron transfer, which corresponds to PBI radical anion ($PBI^{\bullet-}$), and dianion (PBI^{2-}). After reduction, PBI aggregates spontaneously disassemble into monomer, due to electronic repulsions. As an example, Rybtchinski and co-workers demonstrated a robust supramolecular gel based on perylene bisimides in response to multiple stimuli[109]. In this system, gelator PP2b is designed with two conjugated perylene core and hydrophilic polyethylene glycol, which allows gelation in water/THF (80/20 vol%). In the gel, the π-π interactions are the main driving force contributing to nucleation and elongation; simultaneously, hydrophobic interactions also play a role in the segmented fiber secondary association.

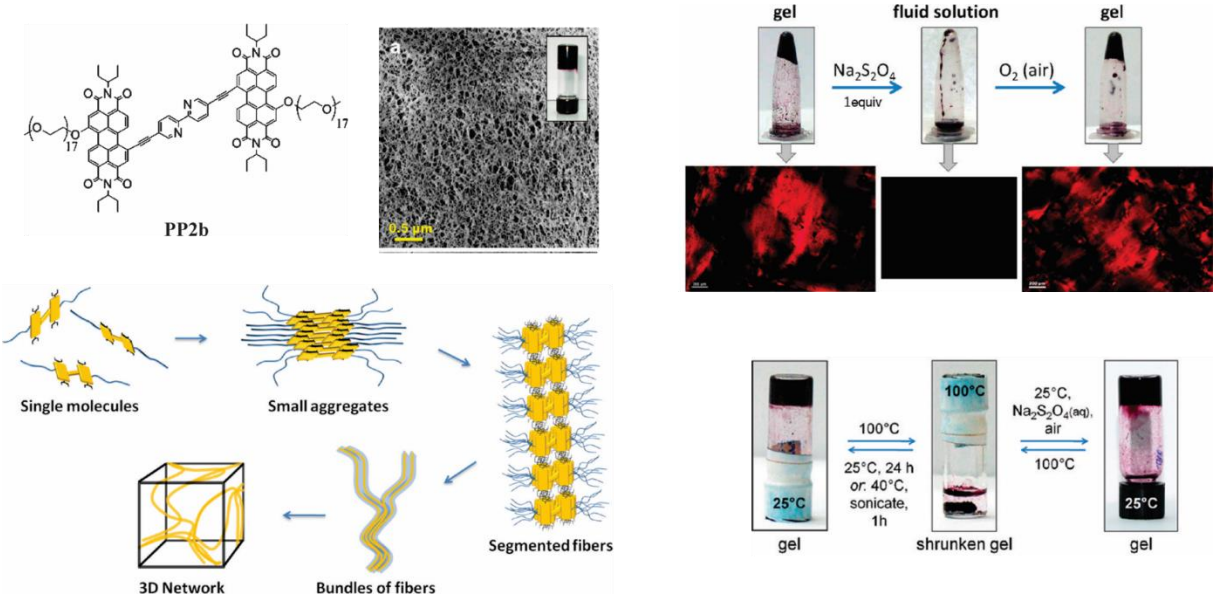

Figure 1.20. The gelator PP2b forms gel in water/THF with nanofibers as single building block nucleates, elongates, and further, secondarily bundled into gels by segmented fibers. By introducing the chemical reductant $Na_2S_2O_4$, the red gel is reduced into solution; meanwhile, the red fluorescent nanostructure was quenched. When PP2b gel was heated to 100°C, the gel is shrunken instead of disassembled, but which reverts to the gel state after 24h relaxation without any interference. If introducing the chemical reductant or sonication, the swelling rate was accelerated. Reproduced from ref. 109 with permission from American Chemical Society.

Nanofibers, ultimately, bundled and entangled into three dimensional hierarchical structures, leading to a gel. By adding sodium dithionate, PBI was reduced into $PBI^{\bullet-}$, and PBI^{2-}; over time, the gel collapse into solution caused by electronic repulsions. Once the reduced solution was

exposed in atmospheric O_2, $PBI^{\bullet-}/PBI^{2-}$ were spontaneously re-oxidized back to the neutral PBI, which then re-gelated. By alternatively introducing the reductant and oxidant, the gel-sol-gel transition can be repeated three times, but no more due to chemical waste influences on gelation. The aggregated gel, meanwhile, shows strong red fluorescence, whereas the fluorescence of the reduced solution is quenched. In addition, the gel is responsive to multiple stimuli, such as temperature, chemical fuels. Heating to 100 °C, the gel contracted instead of disassembly, which gradually reverts to the gel state in 24h without any interference. If introducing the chemical redox, or by sonication, the swelling rate was accelerated.

1.4.3 PBI Photoreduction

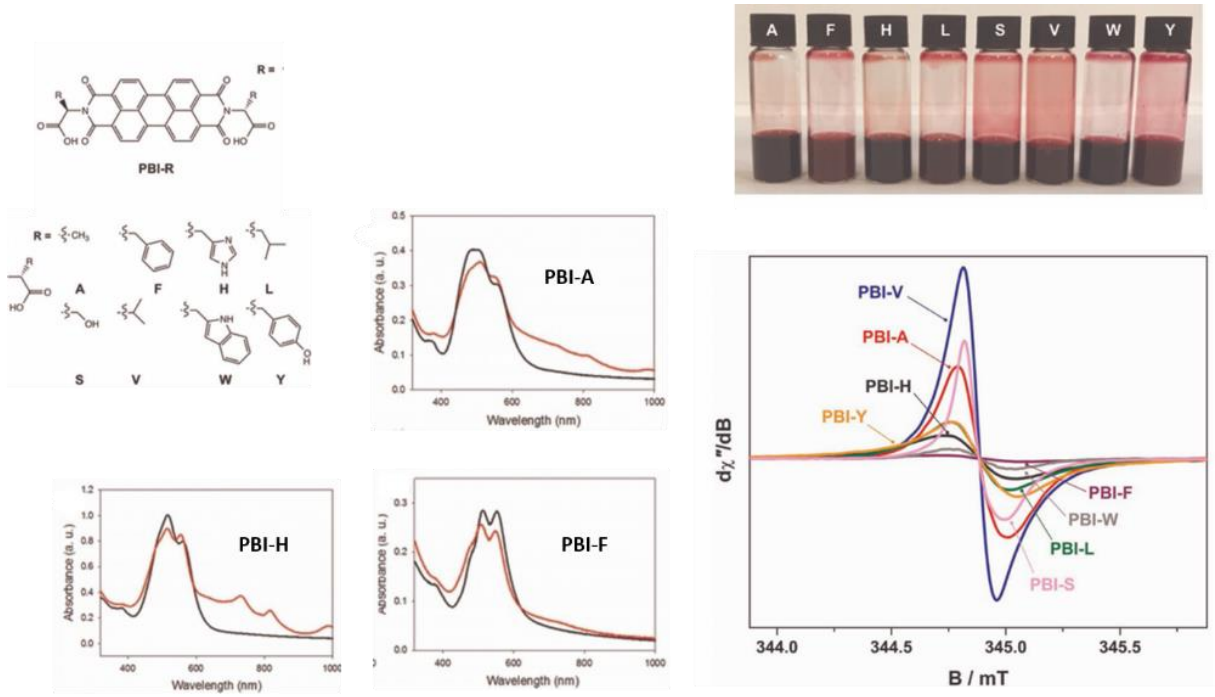

Figure 1.21. The different PBIs substituted by amino acids coassembled, upon UVA irradiation, which selectively gets reduced into $PBI^{\bullet-}/PBI^{2-}$, leading to aggregates disassemble. The reduced was tracked by UV spectroscopy and EPR: PBI-A, PBI-H (black line) was reduced into PBI^{2-} (red line), and $PBI^{\bullet-}$, respectively, but no reduction in PBI-H. Reproduced from ref. 110 with permission from Wiley.

To overcome the issue of chemical waste in PBI reduction systems, light can be ideal energy input to in situ photoreduce PBI with negligible reduced chemical waste. Due to outstanding thermal and photochemical stabilities, PBI has been widely studied as a photoreponsive building blocks in supramolecular chemistry. For instance, Adams and co-workers studied photoreduction of

supramolecular assembled films with different PBI derivatives substituted by amino acids[110]. In alkaline conditions, all PBIs assembled in water, which was tracked by UV/vis spectroscopy, a weak absorption around 380 nm, and broadband from 450-600 nm, corresponds to PBI S_0-S_2, S_0-S_1 transition. Although the nanostructures individually assembled by different PBIs are the same, under UV 365nm irradiation, the aggregates are disassembled, and the film photoreduction is substituents dependent (Figure 1.21). Upon light irradiation, PBI-A, PBI-S, PBI-V, and PBI-S was reduced into PBI dianion, whereas PBI-L, PBI-H, PBY only allows one-electron transfer; even, the decomposition was observed in PBI-F and PBI-W. Further, the controlled photoreduction has a different intensity in EPR measurements, leading to different photoconductive PBI films.

1.5 Aim and outline of this thesis.

The main aim of this thesis is to achieve chemical fuel- and light-driven supramolecular systems and materials using redox chemistry on perylene diimide building blocks. In general, reactions are involved to either activate or deactivate the used building blocks, leading to assembly or disassembly, respectively. These reactions are key to achieve out-of-equilibrium conditions.

In chapter 2, we study photoinduced electron transfer of perylene bisimide (PBI) in a donor-acceptor system under vacuum conditions, regulating assembly and disassembly of aggregates due to the electrostatic repulsion. In the PBI monomer state, only a single electron transfer (and following reduction) occurs, whereas in the PBI assembled state, a two-electron transfer can be achieved. By introducing atmospheric O_2, the reduced species are spontaneously re-oxidized back to the neutral, then further, nucleate, and elongate into large aggregates.

In chapter 3, we greatly accelerate PBI photoreduction by using a UV-activated chemical fuel (acetone), which allows full reduction under ambient air conditions. This opens the possibility to achieve different non-equilibrium steady states, where there is a combination by light-driven photoreduction and chemical oxidation (by stirring the solution in air).

In chapter 4, the PBI photoreduction system was developed from solution to the gel state. We, selectively photoreduced perylene bisimides gels with one or two-electron transfer resulting in two types of rapid, reversible, and photoresponsive organogels. Interestingly, the mechanical

stiffness of the photoinduced one-electron transfer gel was enhanced, whereas two-electron transfer (and reduction) lead to gel weakening.

In chapter 5, we temporally controlled out-of-equilibrium assemblies based on synergistic reactions: PBI photoreduction, and PBI chemical reduction. In the presence of fuel (dithiothreitol, DTT), PBI aggregates are chemically reduced into monomeric $PBI^{\bullet-}$ or PBI^{2-}. Interestingly, upon UV irradiation, the reduction rate is significantly accelerated, suggesting that PBI photoreduction synergistically occurs. By introducing O_2, $PBI^{\bullet-}$/PBI^{2-} were spontaneously re-oxidized back to the neutral, and further aggregated. Various steady states and oscillating states were observed.

1.6 References

(1) Pedersen, C. J. The Discovery of Crown Ethers. *Science* **1988**, *241* (4865), 536–540. https://doi.org/10.1126/science.241.4865.536.

(2) Cram, D. J.; Cram, J. M. Host-Guest Chemistry: Complexes between Organic Compounds Simulate the Substrate Selectivity of Enzymes. *Science* **1974**, *183* (4127), 803–809. https://doi.org/10.1126/science.183.4127.803.

(3) Diederich, F. 40 Years of Supramolecular Chemistry. *Angewandte Chemie International Edition* **2007**, *46* (1–2), 68–69. https://doi.org/10.1002/anie.200602704.

(4) Lehn, J. M. Cryptates: The Chemistry of Macropolycyclic Inclusion Complexes. *Acc. Chem. Res.* **1978**, *11* (2), 49–57. https://doi.org/10.1021/ar50122a001.

(5) Lehn, J.-M. Supramolecular Chemistry—Scope and Perspectives Molecules, Supermolecules, and Molecular Devices (Nobel Lecture). *Angewandte Chemie International Edition in English* **1988**, *27* (1), 89–112. https://doi.org/10.1002/anie.198800891.

(6) Kennedy, D. What Don't We Know? *Science* **2005**, *309* (5731), 75–75. https://doi.org/10.1126/science.309.5731.75.

(7) Lehn, J. M. Supramolecular Chemistry. *Science* **1993**, *260* (5115), 1762–1763. https://doi.org/10.1126/science.8511582.

(8) Self-Processes — Programmed Supramolecular Systems. In *Supramolecular Chemistry*; John Wiley & Sons, Ltd, 1995; pp 139–197. https://doi.org/10.1002/3527607439.ch9.

(9) Luminescent Lanthanide Complexes as Photochemical Supramolecular Devices. *Coordination Chemistry Reviews* **1993**, *123* (1–2), 201–228. https://doi.org/10.1016/0010-8545(93)85056-A.

(10) Reichert, A.; Nagy, J. O.; Spevak, W.; Charych, D. Supramolecular Polymer Materials: Chain Extension of Telechelic Polymers Using a Reactive Hydrogen-Bonding Synthon. 2000, 12 (12), 874-878. https://doi-org/10.1002/1521-4095(200006)12:12<874::AID-ADMA874>3.0.CO;2-C

(11) Liu, Y.; Yu, Y.; Gao, J.; Wang, Z.; Zhang, X. Water-Soluble Supramolecular Polymerization Driven by Multiple Host-Stabilized Charge-Transfer Interactions. *Angewandte Chemie International Edition* **2010**, *49* (37), 6576–6579. https://doi.org/10.1002/anie.201002415.

(12) De Greef, T. F. A.; Smulders, M. M. J.; Wolffs, M.; Schenning, A. P. H. J.; Sijbesma, R. P.; Meijer, E. W. Supramolecular Polymerization. *Chem. Rev.* **2009**, *109* (11), 5687–5754. https://doi.org/10.1021/cr900181u.

(13) Ogi, S.; Sugiyasu, K.; Manna, S.; Samitsu, S.; Takeuchi, M. Living Supramolecular Polymerization Realized through a Biomimetic Approach. *Nature Chemistry* **2014**, *6* (3), 188–195. https://doi.org/10.1038/nchem.1849.

(14) Brunsveld, L.; Folmer, B. J. B.; Meijer, E. W.; Sijbesma, R. P. Supramolecular Polymers. *Chem. Rev.* **2001**, *101* (12), 4071–4098. https://doi.org/10.1021/cr990125q.

(15) Zhao, D.; Moore, J. S. Nucleation–Elongation: A Mechanism for Cooperative Supramolecular Polymerization. *Org. Biomol. Chem.* **2003**, *1* (20), 3471–3491. https://doi.org/10.1039/B308788C.

(16) Korevaar, P. A.; George, S. J.; Markvoort, A. J.; Smulders, M. M. J.; Hilbers, P. A. J.; Schenning, A. P. H. J.; De Greef, T. F. A.; Meijer, E. W. Pathway Complexity in Supramolecular Polymerization. *Nature* **2012**, *481* (7382), 492–496. https://doi.org/10.1038/nature10720.

(17) O'Reilly, R. K.; Hawker, C. J.; Wooley, K. L. Cross-Linked Block Copolymer Micelles: Functional Nanostructures of Great Potential and Versatility. *Chem. Soc. Rev.* **2006**, *35* (11), 1068–1083. https://doi.org/10.1039/B514858H.
(18) Zhang, Q.; Ko, N. R.; Oh, J. K. Recent Advances in Stimuli-Responsive Degradable Block Copolymer Micelles: Synthesis and Controlled Drug Delivery Applications. *Chem. Commun.* **2012**, *48* (61), 7542–7552. https://doi.org/10.1039/C2CC32408C.
(19) Chi, X.; Ji, X.; Xia, D.; Huang, F. A Dual-Responsive Supra-Amphiphilic Polypseudorotaxane Constructed from a Water-Soluble Pillar[7]Arene and an Azobenzene-Containing Random Copolymer. *J. Am. Chem. Soc.* **2015**, *137* (4), 1440–1443. https://doi.org/10.1021/ja512978n.
(20) Lehn, J.-M. Perspectives in Supramolecular Chemistry—From Molecular Recognition towards Molecular Information Processing and Self-Organization. *Angewandte Chemie International Edition in English* **1990**, *29* (11), 1304–1319. https://doi.org/10.1002/anie.199013041.
(21) Allendorf, M. D.; Schwartzberg, A.; Stavila, V.; Talin, A. A. A Roadmap to Implementing Metal–Organic Frameworks in Electronic Devices: Challenges and Critical Directions. *Chemistry – A European Journal* **2011**, *17* (41), 11372–11388. https://doi.org/10.1002/chem.201101595.
(22) Mei, J.; Leung, N. L. C.; Kwok, R. T. K.; Lam, J. W. Y.; Tang, B. Z. Aggregation-Induced Emission: Together We Shine, United We Soar! *Chem. Rev.* **2015**, *115* (21), 11718–11940. https://doi.org/10.1021/acs.chemrev.5b00263.
(23) Huang, X.; Sheng, P.; Tu, Z.; Zhang, F.; Wang, J.; Geng, H.; Zou, Y.; Di, C.; Yi, Y.; Sun, Y.; Xu, W.; Zhu, D. A Two-Dimensional π–d Conjugated Coordination Polymer with Extremely High Electrical Conductivity and Ambipolar Transport Behaviour. *Nature Communications* **2015**, *6* (1), 7408. https://doi.org/10.1038/ncomms8408.
(24) Sergeyev, S.; Pisula, W.; Geerts, Y. H. Discotic Liquid Crystals: A New Generation of Organic Semiconductors. *Chem. Soc. Rev.* **2007**, *36* (12), 1902–1929. https://doi.org/10.1039/B417320C.
(25) Zaworotko, M. J. Superstructural Diversity in Two Dimensions: Crystal Engineering of Laminated Solids. *Chem. Commun.* **2001**, No. 1, 1–9. https://doi.org/10.1039/B007127G.
(26) Ma, X.; Tian, H. Stimuli-Responsive Supramolecular Polymers in Aqueous Solution. *Acc. Chem. Res.* **2014**, *47* (7), 1971–1981. https://doi.org/10.1021/ar500033n.
(27) Yamaguchi, H.; Kobayashi, Y.; Kobayashi, R.; Takashima, Y.; Hashidzume, A.; Harada, A. Photoswitchable Gel Assembly Based on Molecular Recognition. *Nature Communications* **2012**, *3* (1), 603. https://doi.org/10.1038/ncomms1617.
(28) Zhang, Q.; Qu, D.-H.; Wu, J.; Ma, X.; Wang, Q.; Tian, H. A Dual-Modality Photoswitchable Supramolecular Polymer. *Langmuir* **2013**, *29* (17), 5345–5350. https://doi.org/10.1021/la4012444.
(29) Nakahata, M.; Takashima, Y.; Yamaguchi, H.; Harada, A. Redox-Responsive Self-Healing Materials Formed from Host–Guest Polymers. *Nature Communications* **2011**, *2* (1), 511. https://doi.org/10.1038/ncomms1521.
(30) Boekhoven, J.; Brizard, A. M.; Kowlgi, K. N. K.; Koper, G. J. M.; Eelkema, R.; van Esch, J. H. Dissipative Self-Assembly of a Molecular Gelator by Using a Chemical Fuel. *Angewandte Chemie International Edition* **2010**, *49* (28), 4825–4828. https://doi.org/10.1002/anie.201001511.

(31) Jensen, W. B. The Origin of the Polymer Concept. *J. Chem. Educ.* **2008**, *85* (5), 624. https://doi.org/10.1021/ed085p624.
(32) Mülhaupt, R. Hermann Staudinger and the Origin of Macromolecular Chemistry. *Angewandte Chemie International Edition* **2004**, *43* (9), 1054–1063. https://doi.org/10.1002/anie.200330070.
(33) Lu, S.; Fan, Q.-L.; Chua, S.-J.; Huang, W. Synthesis of Conjugated−Ionic Block Copolymers by Controlled Radical Polymerization. *Macromolecules* **2003**, *36* (2), 304–310. https://doi.org/10.1021/ma020408b.
(34) Ouchi, M.; Terashima, T.; Sawamoto, M. Transition Metal-Catalyzed Living Radical Polymerization: Toward Perfection in Catalysis and Precision Polymer Synthesis. *Chem. Rev.* **2009**, *109* (11), 4963–5050. https://doi.org/10.1021/cr900234b.
(35) Photoinitiated Crosslinking Polymerisation. *Progress in Polymer Science* **1996**, *21* (4), 593–650. https://doi.org/10.1016/0079-6700(95)00027-5.
(36) Decker, C. The Use of UV Irradiation in Polymerization. *Polymer International* **1998**, *45* (2), 133–141. https://doi.org/10.1002/(SICI)1097-0126(199802)45:2<133::AID-PI969>3.0.CO;2-F.
(37) Decker, C.; Nguyen Thi Viet, T.; Decker, D.; Weber-Koehl, E. UV-Radiation Curing of Acrylate/Epoxide Systems. *Polymer* **2001**, *42* (13), 5531–5541. https://doi.org/10.1016/S0032-3861(01)00065-9.
(38) Sijbesma, R. P.; Beijer, F. H.; Brunsveld, L.; Folmer, B. J. B.; Lange, R. F. M.; Lowe, J. K. L.; Meijer, E. W. Reversible Polymers Formed from Self-Complementary Monomers Using Quadruple Hydrogen Bonding. **1997**, *278*, 5.
(39) de Greef, T. F. A.; Meijer, E. W. Supramolecular Polymers. *Nature* **2008**, *453* (7192), 171–173. https://doi.org/10.1038/453171a.
(40) Sorrenti, A. Non-Equilibrium Supramolecular Polymerization. *Chem Soc Rev* **2017**, 16.
(41) Smulders, M. M. J.; Nieuwenhuizen, M. M. L.; de Greef, T. F. A.; van der Schoot, P.; Schenning, A. P. H. J.; Meijer, E. W. How to Distinguish Isodesmic from Cooperative Supramolecular Polymerisation. *Chemistry – A European Journal* **2010**, *16* (1), 362–367. https://doi.org/10.1002/chem.200902415.
(42) Smulders, M. M. J.; Schenning, A. P. H. J.; Meijer, E. W. Insight into the Mechanisms of Cooperative Self-Assembly: The "Sergeants-and-Soldiers" Principle of Chiral and Achiral C_3 -Symmetrical Discotic Triamides. *J. Am. Chem. Soc.* **2008**, *130* (2), 606–611. https://doi.org/10.1021/ja075987k.
(43) Gershberg, J.; Fennel, F.; Rehm, T. H.; Lochbrunner, S.; Würthner, F. Anti-Cooperative Supramolecular Polymerization: A New K2–K Model Applied to the Self-Assembly of Perylene Bisimide Dye Proceeding via Well-Defined Hydrogen-Bonded Dimers. *Chem. Sci.* **2016**, *7* (3), 1729–1737. https://doi.org/10.1039/C5SC03759J.
(44) Kang, J.; Miyajima, D.; Mori, T.; Inoue, Y.; Itoh, Y.; Aida, T. A Rational Strategy for the Realization of Chain-Growth Supramolecular Polymerization. *Science* **2015**, *347* (6222), 646–651. https://doi.org/10.1126/science.aaa4249.
(45) Deng, R.; Liu, X. Chain Growth in Control. *Nature Chem* **2015**, *7* (6), 472–473. https://doi.org/10.1038/nchem.2265.

(46) Huang, Y.; Fu, L.; Zou, W.; Zhang, F.; Wei, Z. Ammonia Sensory Properties Based on Single-Crystalline Micro/Nanostructures of Perylenediimide Derivatives: Core-Substituted Effect. *J. Phys. Chem. C* **2011**, *115* (21), 10399–10404. https://doi.org/10.1021/jp200735m.
(47) Supur, M.; Fukuzumi, S. Photodriven Electron Transport within the Columnar Perylenediimide Nanostructures Self-Assembled with Sulfonated Porphyrins in Water. *J. Phys. Chem. C* **2012**, *116* (44), 23274–23282. https://doi.org/10.1021/jp308549w.
(48) Chen, S.; Slattum, P.; Wang, C.; Zang, L. Self-Assembly of Perylene Imide Molecules into 1D Nanostructures: Methods, Morphologies, and Applications. *Chem. Rev.* **2015**, *115* (21), 11967–11998. https://doi.org/10.1021/acs.chemrev.5b00312.
(49) Sijbesma, R. P.; Meijer, E. W. Quadruple Hydrogen Bonded Systems. *Chem. Commun.* **2003**, No. 1, 5–16. https://doi.org/10.1039/B205873C.
(50) Wang, F.; Zhang, J.; Ding, X.; Dong, S.; Liu, M.; Zheng, B.; Li, S.; Wu, L.; Yu, Y.; Gibson, H. W.; Huang, F. Metal Coordination Mediated Reversible Conversion between Linear and Cross-Linked Supramolecular Polymers. *Angewandte Chemie International Edition* **2010**, *49* (6), 1090–1094. https://doi.org/10.1002/anie.200906389.
(51) Sun, R.; Xue, C.; Ma, X.; Gao, M.; Tian, H.; Li, Q. Light-Driven Linear Helical Supramolecular Polymer Formed by Molecular-Recognition-Directed Self-Assembly of Bis(p-Sulfonatocalix[4]Arene) and Pseudorotaxane. *J. Am. Chem. Soc.* **2013**, *135* (16), 5990–5993. https://doi.org/10.1021/ja4016952.
(52) Xia, D.; Wang, P.; Ji, X.; Khashab, N. M.; Sessler, J. L.; Huang, F. Functional Supramolecular Polymeric Networks: The Marriage of Covalent Polymers and Macrocycle-Based Host–Guest Interactions. *Chem. Rev.* **2020**, *120* (13), 6070–6123. https://doi.org/10.1021/acs.chemrev.9b00839.
(53) Lagona, J.; Mukhopadhyay, P.; Chakrabarti, S.; Isaacs, L. The Cucurbit[n]Uril Family. *Angewandte Chemie International Edition* **2005**, *44* (31), 4844–4870. https://doi.org/10.1002/anie.200460675.
(54) Appel, E. A.; Biedermann, F.; Rauwald, U.; Jones, S. T.; Zayed, J. M.; Scherman, O. A. Supramolecular Cross-Linked Networks via Host−Guest Complexation with Cucurbit[8]Uril. *J. Am. Chem. Soc.* **2010**, *132* (40), 14251–14260. https://doi.org/10.1021/ja106362w.
(55) Kim, H.-J.; Heo, J.; Jeon, W. S.; Lee, E.; Kim, J.; Sakamoto, S.; Yamaguchi, K.; Kim, K. Selective Inclusion of a Hetero-Guest Pair in a Molecular Host: Formation of Stable Charge-Transfer Complexes in Cucurbit[8]Uril. *Angewandte Chemie International Edition* **2001**, *40* (8), 1526–1529. https://doi.org/10.1002/1521-3773(20010417)40:8<1526::AID-ANIE1526>3.0.CO;2-T.
(56) Harada, A.; Okada, M. Complex Formation between Hydrophobic Polymers and Methylated Cyclodextrins. Oligo(Ethylene) and Poly(Propylene). *Polymer Journal* **1999**, *31* (11), 1095–1098. https://doi.org/10.1295/polymj.31.1095.
(57) Harada, A. Construction of Supramolecular Structures from Cyclodextrins, Polymers. *Carbohydrate Polymers* **1997**, *34* (3), 183–188. https://doi.org/10.1016/S0144-8617(97)00023-4.
(58) Harada, A.; Li, J.; Suzuki, S.; Kamachi, M. Complex Formation between Polyisobutylene and Cyclodextrins: Inversion of Chain-Length Selectivity between .Beta.-Cyclodextrin and .Gamma.-Cyclodextrin. *Macromolecules* **1993**, *26* (19), 5267–5268. https://doi.org/10.1021/ma00071a047.

(59) Harada, A.; Takashima, Y.; Yamaguchi, H. Cyclodextrin-Based Supramolecular Polymers. *Chem. Soc. Rev.* **2009**, *38* (4), 875. https://doi.org/10.1039/b705458k.
(60) Tamesue, S.; Takashima, Y.; Yamaguchi, H.; Shinkai, S.; Harada, A. Photoswitchable Supramolecular Hydrogels Formed by Cyclodextrins and Azobenzene Polymers. *Angewandte Chemie International Edition* **2010**, *49* (41), 7461–7464. https://doi.org/10.1002/anie.201003567.
(61) Wang, D.; Wagner, M.; Butt, H.-J.; Wu, S. Supramolecular Hydrogels Constructed by Red-Light-Responsive Host–Guest Interactions for Photo-Controlled Protein Release in Deep Tissue. *Soft Matter* **2015**, *11* (38), 7656–7662. https://doi.org/10.1039/C5SM01888A.
(62) Miyamae, K.; Nakahata, M.; Takashima, Y.; Harada, A. Self-Healing, Expansion–Contraction, and Shape-Memory Properties of a Preorganized Supramolecular Hydrogel through Host–Guest Interactions. *Angewandte Chemie International Edition* **2015**, *54* (31), 8984–8987. https://doi.org/10.1002/anie.201502957.
(63) Liu, H.; Zhang, Y.; Hu, J.; Li, C.; Liu, S. Multi-Responsive Supramolecular Double Hydrophilic Diblock Copolymer Driven by Host-Guest Inclusion Complexation between β-Cyclodextrin and Adamantyl Moieties. *Macromolecular Chemistry and Physics* **2009**, *210* (24), 2125–2137. https://doi.org/10.1002/macp.200900279.
(64) Yi, S.; Zheng, J.; Lv, P.; Zhang, D.; Zheng, X.; Zhang, Y.; Liao, R. Controlled Drug Release from Cyclodextrin-Gated Mesoporous Silica Nanoparticles Based on Switchable Host–Guest Interactions. *Bioconjugate Chem.* **2018**, *29* (9), 2884–2891. https://doi.org/10.1021/acs.bioconjchem.8b00416.
(65) Miyauchi, M.; Harada, A. Construction of Supramolecular Polymers with Alternating α-, β-Cyclodextrin Units Using Conformational Change Induced by Competitive Guests. *J. Am. Chem. Soc.* **2004**, *126* (37), 11418–11419. https://doi.org/10.1021/ja046562q.
(66) Liu, Q.; Wang, Y.; Li, W.; Wu, L. Structural Characterization and Chemical Response of a Ag-Coordinated Supramolecular Gel. *Langmuir* **2007**, *23* (15), 8217–8223. https://doi.org/10.1021/la700364t.
(67) Naota, T.; Koori, H. Molecules That Assemble by Sound: An Application to the Instant Gelation of Stable Organic Fluids. *J. Am. Chem. Soc.* **2005**, *127* (26), 9324–9325. https://doi.org/10.1021/ja050809h.
(68) Yan, X.; Xu, D.; Chi, X.; Chen, J.; Dong, S.; Ding, X.; Yu, Y.; Huang, F. A Multiresponsive, Shape-Persistent, and Elastic Supramolecular Polymer Network Gel Constructed by Orthogonal Self-Assembly. *Adv. Mater.* **2012**, *24* (3), 362–369. https://doi.org/10.1002/adma.201103220.
(69) Dai, X.; Zhang, Y.; Gao, L.; Bai, T.; Wang, W.; Cui, Y.; Liu, W. A Mechanically Strong, Highly Stable, Thermoplastic, and Self-Healable Supramolecular Polymer Hydrogel. *Adv. Mater.* **2015**, *27* (23), 3566–3571. https://doi.org/10.1002/adma.201500534.
(70) Rao, K. V.; Jayaramulu, K.; Maji, T. K.; George, S. J. Supramolecular Hydrogels and High-Aspect-Ratio Nanofibers through Charge-Transfer-Induced Alternate Coassembly. *Angewandte Chemie International Edition* **2010**, *49* (25), 4218–4222. https://doi.org/10.1002/anie.201000527.
(71) Foster, J. A.; Piepenbrock, M.-O. M.; Lloyd, G. O.; Clarke, N.; Howard, J. A. K.; Steed, J. W. Anion-Switchable Supramolecular Gels for Controlling Pharmaceutical Crystal Growth. *Nature Chemistry* **2010**, *2* (12), 1037–1043. https://doi.org/10.1038/nchem.859.

(72) Buerkle, L. E.; Rowan, S. J. Supramolecular Gels Formed from Multi-Component Low Molecular Weight Species. *Chem. Soc. Rev.* **2012**, *41* (18), 6089–6102. https://doi.org/10.1039/C2CS35106D.
(73) Cornwell, D. J.; Daubney, O. J.; Smith, D. K. Photopatterned Multidomain Gels: Multi-Component Self-Assembled Hydrogels Based on Partially Self-Sorting 1,3:2,4-Dibenzylidene-d-Sorbitol Derivatives. J. Am. Chem. Soc. 2015, 137 (49), 15486–15492. https://doi.org/10.1021/jacs.5b09691.
(74) Hirst, A. R.; Smith, D. K.; Feiters, M. C.; Geurts, H. P. M.; Wright, A. C. Two-Component Dendritic Gels: Easily Tunable Materials. J. Am. Chem. Soc. 2003, 125 (30), 9010–9011. https://doi.org/10.1021/ja036111q.
(75) Gong, G.-F.; Chen, Y.-Y.; Zhang, Y.-M.; Fan, Y.-Q.; Zhou, Q.; Yang, H.-L.; Zhang, Q.-P.; Yao, H.; Wei, T.-B.; Lin, Q. A Novel Bis-Component AIE Smart Gel with High Selectivity and Sensitivity to Detect CN^-, Fe^{3+} and $H_2PO_4^-$. *Soft Matter* **2019**, *15* (31), 6348–6352. https://doi.org/10.1039/C9SM01035A.
(76) Harada, A.; Kobayashi, R.; Takashima, Y.; Hashidzume, A.; Yamaguchi, H. Macroscopic Self-Assembly through Molecular Recognition. *Nature Chem* **2011**, *3* (1), 34–37. https://doi.org/10.1038/nchem.893.
(77) van Rossum, S. A. P.; Tena-Solsona, M.; van Esch, J. H.; Eelkema, R.; Boekhoven, J. Dissipative Out-of-Equilibrium Assembly of Man-Made Supramolecular Materials. *Chem. Soc. Rev.* **2017**, *46* (18), 5519–5535. https://doi.org/10.1039/C7CS00246G.
(78) Singh, N.; Lainer, B.; Formon, G. J. M.; De Piccoli, S.; Hermans, T. M. Re-Programming Hydrogel Properties Using a Fuel-Driven Reaction Cycle. *J. Am. Chem. Soc.* **2020**, *142* (9), 4083–4087. https://doi.org/10.1021/jacs.9b11503.
(79) Semenov, S. N.; Wong, A. S. Y.; van der Made, R. M.; Postma, S. G. J.; Groen, J.; van Roekel, H. W. H.; de Greef, T. F. A.; Huck, W. T. S. Rational Design of Functional and Tunable Oscillating Enzymatic Networks. *Nature Chemistry* **2015**, *7* (2), 160–165. https://doi.org/10.1038/nchem.2142.
(80) Del Grosso, E.; Ragazzon, G.; Prins, L. J.; Ricci, F. Fuel-Responsive Allosteric DNA-Based Aptamers for the Transient Release of ATP and Cocaine. *Angewandte Chemie International Edition* **2019**, *58* (17), 5582–5586. https://doi.org/10.1002/anie.201812885.
(81) Sorrenti, A.; Leira-Iglesias, J.; Sato, A.; Hermans, T. M. Non-Equilibrium Steady States in Supramolecular Polymerization. *Nature Communications* **2017**, *8* (1), 15899. https://doi.org/10.1038/ncomms15899.
(82) Monreal Santiago, G.; Liu, K.; Browne, W. R.; Otto, S. Emergence of Light-Driven Protometabolism on Recruitment of a Photocatalytic Cofactor by a Self-Replicator. *Nat. Chem.* **2020**, *12* (7), 603–607. https://doi.org/10.1038/s41557-020-0494-4.
(83) Ikegami, T.; Kageyama, Y.; Obara, K.; Takeda, S. Dissipative and Autonomous Square-Wave Self-Oscillation of a Macroscopic Hybrid Self-Assembly under Continuous Light Irradiation. *Angewandte Chemie International Edition* **2016**, *55* (29), 8239–8243. https://doi.org/10.1002/anie.201600218.
(84) Singh, N.; Formon, G. J. M.; Piccoli, S. D.; Hermans, T. M. Devising Synthetic Reaction Cycles for Dissipative Nonequilibrium Self-Assembly. *Advanced Materials* **2020**, *32* (20), 1906834. https://doi.org/10.1002/adma.201906834.

(85) Dambenieks, A. K.; Vu, P. H. Q.; Fyles, T. M. Dissipative Assembly of a Membrane Transport System. *Chem. Sci.* **2014**, *5* (9), 3396–3403. https://doi.org/10.1039/C4SC01258E.
(86) Leira-Iglesias, J.; Sorrenti, A.; Sato, A.; Dunne, P. A.; Hermans, T. M. Supramolecular Pathway Selection of Perylenediimides Mediated by Chemical Fuels. *Chem. Commun.* **2016**, *52* (58), 9009–9012. https://doi.org/10.1039/C6CC01192F.
(87) Mata, A.; Geng, Y.; Henrikson, K. J.; Aparicio, C.; Stock, S. R.; Satcher, R. L.; Stupp, S. I. Bone Regeneration Mediated by Biomimetic Mineralization of a Nanofiber Matrix. *Biomaterials* **2010**, *31* (23), 6004–6012. https://doi.org/10.1016/j.biomaterials.2010.04.013.
(88) Shah, R. N.; Shah, N. A.; Del Rosario Lim, M. M.; Hsieh, C.; Nuber, G.; Stupp, S. I. Supramolecular Design of Self-Assembling Nanofibers for Cartilage Regeneration. *Proc Natl Acad Sci USA* **2010**, *107* (8), 3293–3298. https://doi.org/10.1073/pnas.0906501107.
(89) Debnath, S.; Roy, S.; Ulijn, R. V. Peptide Nanofibers with Dynamic Instability through Nonequilibrium Biocatalytic Assembly. *J. Am. Chem. Soc.* **2013**, *135* (45), 16789–16792. https://doi.org/10.1021/ja4086353.
(90) Jong, J. J. D. de; Lucas, L. N.; Kellogg, R. M.; Esch, J. H. van; Feringa, B. L. Reversible Optical Transcription of Supramolecular Chirality into Molecular Chirality. *Science* **2004**, *304* (5668), 278–281. https://doi.org/10.1126/science.1095353.
(91) Qu, D.-H.; Wang, Q.-C.; Zhang, Q.-W.; Ma, X.; Tian, H. Photoresponsive Host–Guest Functional Systems. *Chem. Rev.* **2015**, *115* (15), 7543–7588. https://doi.org/10.1021/cr5006342.
(92) Yagai, S.; Ishiwatari, K.; Lin, X.; Karatsu, T.; Kitamura, A.; Uemura, S. Rational Design of Photoresponsive Supramolecular Assemblies Based on Diarylethene. *Chem. Eur. J.* **2013**, *19* (22), 6971–6975. https://doi.org/10.1002/chem.201300282.
(93) Salzano de Luna, M.; Marturano, V.; Manganelli, M.; Santillo, C.; Ambrogi, V.; Filippone, G.; Cerruti, P. Light-Responsive and Self-Healing Behavior of Azobenzene-Based Supramolecular Hydrogels. *Journal of Colloid and Interface Science* **2020**, *568*, 16–24. https://doi.org/10.1016/j.jcis.2020.02.038.
(94) Rakotondradany, F.; Whitehead, M. A.; Lebuis, A.-M.; Sleiman, H. F. Photoresponsive Supramolecular Systems: Self-Assembly of Azodibenzoic Acid Linear Tapes and Cyclic Tetramers. *Chem. Eur. J.* **2003**, *9* (19), 4771–4780. https://doi.org/10.1002/chem.200304864.
(95) de Jong, J. J. D.; Hania, P. R.; Pug?lys, A.; Lucas, L. N.; de Loos, M.; Kellogg, R. M.; Feringa, B. L.; Duppen, K.; van Esch, J. H. Light-Driven Dynamic Pattern Formation. *Angew. Chem. Int. Ed.* **2005**, *44* (16), 2373–2376. https://doi.org/10.1002/anie.200462500.
(96) Wurthner, F.; Saha-Moller, C. R.; Fimmel, B.; Ogi, S.; Leowanawat, P.; Schmidt, D. Perylene Bisimide Dye Assemblies as Archetype Functional Supramolecular Materials. *Chem Rev* **2016**, *116* (3), 962–1052. https://doi.org/10.1021/acs.chemrev.5b00188.
(97) Würthner, F. Perylene Bisimide Dyes as Versatile Building Blocks for Functional Supramolecular Architectures. *Chem. Commun.* **2004**, No. 14, 1564–1579. https://doi.org/10.1039/B401630K.
(98) Zhong, L.; Xing, F.; Shi, W.; Yan, L.; Xie, L.; Zhu, S. Synthesis, Spectra, and Electron-Transfer Reaction of Aspartic Acid-Functionalized Water-Soluble Perylene Bisimide in Aqueous Solution. *ACS Appl Mater Interfaces* **2013**, *5* (8), 3401–3407. https://doi.org/10.1021/am4004446.

(99) Zang, L.; Che, Y.; Moore, J. S. One-Dimensional Self-Assembly of Planar π-Conjugated Molecules: Adaptable Building Blocks for Organic Nanodevices. *Acc. Chem. Res.* **2008**, *41* (12), 1596–1608. https://doi.org/10.1021/ar800030w.

(100) Che, Y.; Datar, A.; Balakrishnan, K.; Zang, L. Ultralong Nanobelts Self-Assembled from an Asymmetric Perylene Tetracarboxylic Diimide. *J. Am. Chem. Soc.* **2007**, *129* (23), 7234–7235. https://doi.org/10.1021/ja071903w.

(101) Yu, Y.; Shi, Q.; Li, Y.; Liu, T.; Zhang, L.; Shuai, Z.; Li, Y. Solid Supramolecular Architecture of a Perylene Diimide Derivative for Fluorescent Enhancement. *Chemistry – An Asian Journal* **2012**, *7* (12), 2904–2911. https://doi.org/10.1002/asia.201200659.

(102) Li, F.; Li, Y.; Wei, G.; Wang, Y.; Li, S.; Cheng, Y. Circularly Polarized Luminescence of Chiral Perylene Diimide Based Enantiomers Triggered by Supramolecular Self-Assembly. *Chemistry – A European Journal* **2016**, *22* (36), 12910–12915. https://doi.org/10.1002/chem.201601328.

(103) Datar, A.; Oitker, R.; Zang, L. Surface-Assisted One-Dimensional Self-Assembly of a Perylene Based Semiconductor Molecule. *Chem. Commun.* **2006**, No. 15, 1649–1651. https://doi.org/10.1039/B518060K.

(104) Sun, J.-P.; Hendsbee, A. D.; Dobson, A. J.; Welch, G. C.; Hill, I. G. Perylene Diimide Based All Small-Molecule Organic Solar Cells: Impact of Branched-Alkyl Side Chains on Solubility, Photophysics, Self-Assembly, and Photovoltaic Parameters. *Organic Electronics* **2016**, *35*, 151–157. https://doi.org/10.1016/j.orgel.2016.05.012.

(105) Ghosh, I.; Ghosh, T.; Bardagi, J. I.; Konig, B. Reduction of Aryl Halides by Consecutive Visible Light-Induced Electron Transfer Processes. *Science* **2014**, *346* (6210), 725–728. https://doi.org/10.1126/science.1258232.

(106) Wagner, W.; Wehner, M.; Stepanenko, V.; Ogi, S.; Würthner, F. Living Supramolecular Polymerization of a Perylene Bisimide Dye into Fluorescent J-Aggregates. *Angew. Chem. Int. Ed.* **2017**, *56* (50), 16008–16012. https://doi.org/10.1002/anie.201709307.

(107) Hecht, M.; Leowanawat, P.; Gerlach, T.; Stepanenko, V.; Stolte, M.; Lehmann, M.; Würthner, F. Self-Sorting Supramolecular Polymerization: Helical and Lamellar Aggregates of Tetra-Bay-Acyloxy Perylene Bisimide. *Angew. Chem.* **2020**, *132* (39), 17232–17238. https://doi.org/10.1002/ange.202006744.

(108) Leira-Iglesias, J.; Sorrenti, A.; Sato, A.; Dunne, P. A.; Hermans, T. M. Supramolecular Pathway Selection of Perylenediimides Mediated by Chemical Fuels. *Chem. Commun.* **2016**, *52* (58), 9009–9012. https://doi.org/10.1039/C6CC01192F.

(109) Krieg, E.; Shirman, E.; Weissman, H.; Shimoni, E.; Wolf, S. G.; Pinkas, I.; Rybtchinski, B. Supramolecular Gel Based on a Perylene Diimide Dye: Multiple Stimuli Responsiveness, Robustness, and Photofunction. *J. Am. Chem. Soc.* **2009**, *131* (40), 14365–14373. https://doi.org/10.1021/ja903938g.

(110) Draper, E. R.; Archibald, L. J.; Nolan, M. C.; Schweins, R.; Zwijnenburg, M. A.; Sproules, S.; Adams, D. J. Controlling Photoconductivity in PBI Films by Supramolecular Assembly. *Chemistry* **2018**, *24* (16), 4006–4010. https://doi.org/10.1002/chem.201800201.

Chapter 2.

Photoreduction of a Perylene Bisimide Derivative in Its Monomeric and Aggregated State

Abstract: The reversible assembly and disassembly of aggregates is driven by the photoreduction and oxidation of perylene bisimides (**PBI-1**). Upon UV or visible light irradiation, the radical anion (**PBI-1**$^{\bullet-}$) easily forms both in monomer and in aggregated form under vacuum conditions. The dianion (**PBI-1**$^{2-}$), however, only forms in aggregates, due to changes in the electronic landscape upon assembly. We show that photoreduction is key to drive **PBI-1** disassemble into monomers due to electrostatic repulsion. The latter is reversible by introducing molecular dioxygen, which converts **PBI-1**$^{2-}$ rapidly into **PBI-1**$^{\bullet-}$ and subsequently neutral **PBI-1**, leading to reassembly.

2.1 Introduction

2.1.1 Photoinduced Electron Transfer

Photoinduced electron transfer plays a key role in chemistry[1–4], materials[5–7], and biology[8,9]. Photosynthesis in plants[10,11], for instance, is one of the major contributions of electron transfer, which converts photoenergy into chemical energy by light-harvesting. To unravel this highly advanced natural system, many chemists are striving to get insights into the mechanism, and developing photo-harvesting materials, such as photocatalysts[12,13], photo-imaging materials[14,15], and organic electronic devices[16–18]. Particularly in supramolecular systems[19], photoinduced electron transfer provides the possibility to locally adjust optical or mechanical properties of materials. To rationally construct a photoinduced electron-transfer system, the mechanism of photoinduced electron transfer is fundamental in molecular or complex systems. Photoinduced electron transfer, as equation (1), is a simple movement of an electron from electron-rich species (donor D) to electron-deficient species (acceptor A). Generally, there are four types of excitation mechanisms in systems: (i) The excited donor provides an electron to the acceptor (equation 2), (ii) The excited acceptor gets one electron from the donor (equation 3), (iii) The complex that the donor associated with the acceptor in the ground states, is excited and further electron transfers (equation 4), (iv) The donor complexed with the acceptor after excitation, subsequently, the electron transfers (equation 5).

$$D + A \xrightarrow{h\nu} D^+ + A^- \qquad (1)$$

$$D + A \xrightarrow{h\nu} D^* + A \longrightarrow D^+ + A^- \qquad (2)$$

$$D + A \xrightarrow{h\nu} D + A^* \longrightarrow D^+ + A^- \qquad (3)$$

$$D \text{ --- } A \xrightarrow{h\nu} (D \text{ --- } A)^* \longrightarrow D^+ + A^- \qquad (4)$$

$$D + A \xrightarrow{h\nu} (D \text{ --- } A)^* \longrightarrow D^+ + A^- \qquad (5)$$

Figure 2.1. the excitation of donor or acceptor followed by electron transfer.

Building a photoinduced electron transfer system, strict rules should be followed[20]: (i) The incident photon energy must fit with the energy level of the donor or acceptor that brings one of them to the excited state from the ground state, (ii) The light can drive the electron transfer from the donor to the acceptor, (iii) The lifetime of the excited state is long enough to allow transfer electron, which must be unidirectional. But why is the light source essential to induce electron transfer? Because for photoexcitation, relating to the right wavelength rather than light intensity, is the key in electron transfer. When a molecule is photoexcited, an electron is promoted from the highest occupied molecular orbital (HOMO) to the lowest unoccupied molecular orbital (LUMO), resulting in the enhancement of the redox activity due weakening of the covalent bonding[21]. Meanwhile, the ionization potential (IP) of the excited molecules, which is the energy needed for electron releasing to vacuum from the LUMO, is lower than the corresponding ground state. Thus, the light-induced generation of a vacancy in the HOMO opens the possibility for the electron transfer to happen.

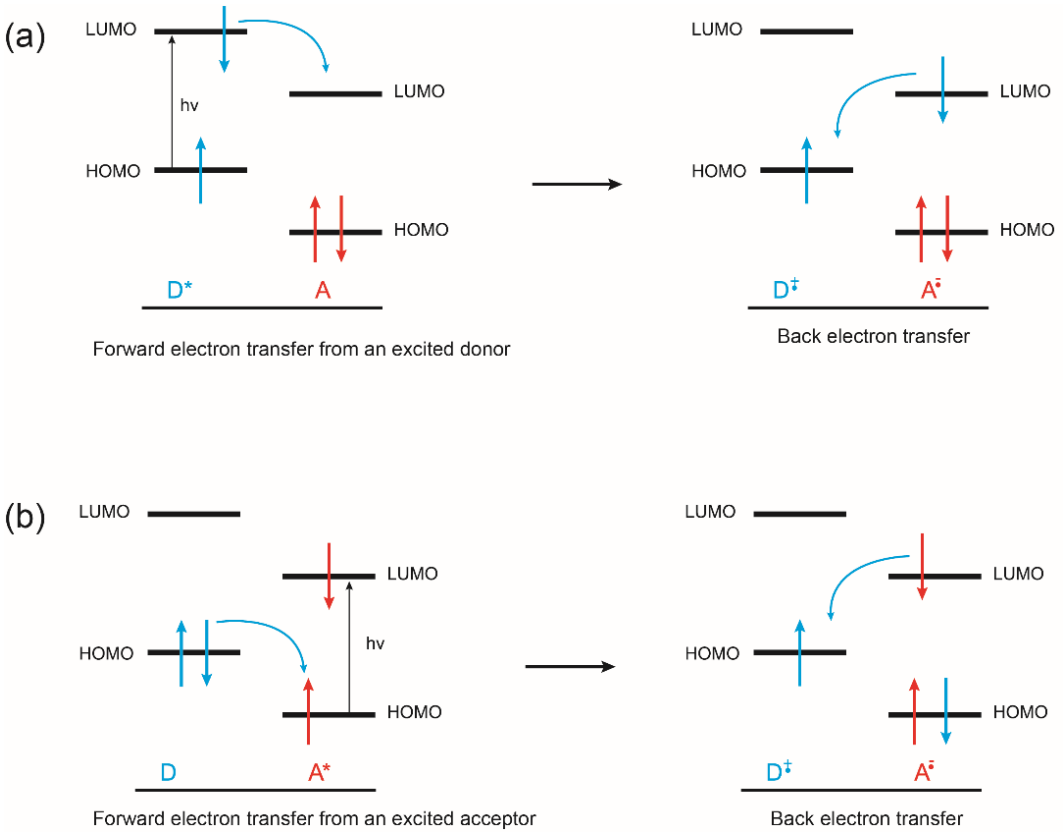

Figure 2.2. the representation of free energy changes for the forward and back electron-transfer. Reproduced from ref. 20 with permission from Wiley.

The frontier molecular orbital, simplifying the prediction of reactivity of the electron movement between HOMO and LUMO in the D-A system, clearly elucidates the mechanism of photoinduced electron transfer. Figure 2.2 shows, upon light irradiation, the free energy changes as electrons move. The donor, by definition, is more energetic with high lying occupied molecular orbitals, whereas the unfilled orbitals of the acceptor are relatively lower. When inputting a photon, the free energy changes, and the electron transfers forward and back. Figure 2.2 shows the electron moves: (a) When the donor is excited with the promotion of one electron from HOMO to LUMO, then, subsequently, one electron transfers to the acceptor LUMO from the donor LUMO forming radical anion; meanwhile, the radical pairs $D^{\bullet+} + A^{\bullet-}$, reverts to the ground state D + A, by back electron transfer via releasing one electron from the acceptor LUMO to the donor HOMO. (b) In another case, the acceptor gets excited, then electron forward transfers to the vacant acceptor HOMO from the donor HOMO, whereas the part of radical pairs simultaneously back to the corresponding ground state with exothermic electron transfer[22].

Here, we aim to regulate the assembly and disassembly of supramolecular aggregates by electron transfer in a donor-acceptor system. Given the highly π-conjugated aromatic core[23], photostability[24–26], and electron deficiency[27], perylene bisimides, are ideal candidate as the building block to construct photoresponsive supramolecular materials.

2.1.2 Photoinduced Electron Transfer in Perylene Bisimide

Perylene bisimides (PBIs) represented a highly versatile class of compounds with outstanding features, such as photo-thermal stability[24] and high electron mobility[28]. Specifically, their electron-poor character renders them excellent electron acceptors that can produce stable radical anions.[29]. Recently, König and co-workers have demonstrated that PBI was used to photo-catalyze the reduction of aryl halides.[30] The PBI (see. Fig.2.3A) monomer formed in DMF or DMSO, which can photo-induce one-electron transfer to form $PBI^{\bullet-}$ in the presence of donor, triethylamine, upon blue light irradiation under inert conditions. The process of the photoreduction can be tracked by UV/vis spectroscopy. The neutral PBI absorbs from 400 to 530 nm with three maxima. When the reduction occurs, $PBI^{\bullet-}$ generated three maxima from 600 to

1000 nm on the top of the neutral spectrum (see. Fig.2.3B). Meanwhile, the color of the PBI solution also visually changed upon photoreduction from the red to the green. Once oxygen was introduced into the $PBI^{\bullet-}$ solution, it was quickly oxidized back to the neutral PBI, thus restoring the original (red) color. Interestingly, the photoexcited $PBI^{\bullet-}$ with high redox activity due to the vacant site in the HOMOA, can be a photocatalyst to contribute to the generation of stable aryl radicals from the corresponding aryl chloride (see. Fig.2.3C), further reacting with a trapping agent to form the target products.

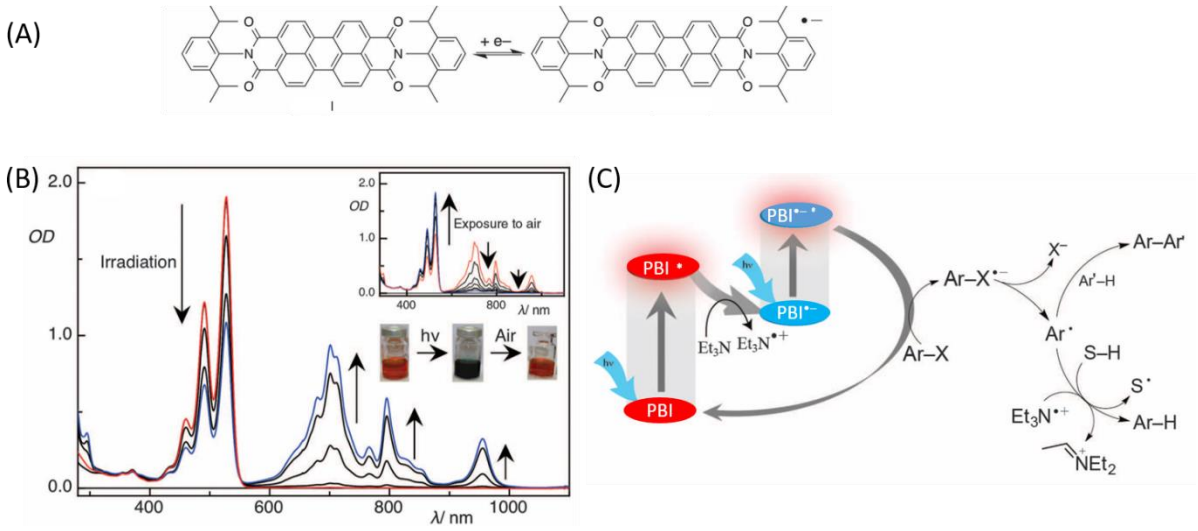

Figure 2.3. PBI radical anion ($PBI^{\bullet-}$) being a photocatalyst when PBI as an acceptor and triethylamine as a donor which is photoreduced upon blue light 450 nm irradiation. (A) Molecular structure of the neutral PBI, N, N-bis(2,6-diisopropylphenyl) perylene3,4,9,10-bis(dicarboximide), and its $PBI^{\bullet-}$. (B) UV spectra of PBI and $PBI^{\bullet-}$, the neutral PBI absorbs from 400 to 600 nm with three maxima whereas the characteristic UV absorption of the $PBI^{\bullet-}$ is from 600 to 100 nm on top of its neutral spectrum. Meanwhile, the PBI solution has a color change from the red to the green as the photoreduction occurs. (C) The mechanism of $PBI^{\bullet-}$ being a photocatalyst. The subsequent excitation of the $PBI^{\bullet-}$ accumulates sufficient energy for the reduction of stable aryl chlorides giving aryl radicals, which were trapped by hydrogen atom donors or used in carbon-carbon bond formation. Reproduced from ref. 30 with permission from Science.

Although PBI is easily photoreduced by a one-electron transfer in the absence of oxygen, achieving two-electron transfer from a donor remains challenging. PBI, however, can get two electrons followed by: i) chemical reduction by sodium dithionate[31,32], or ii) (bulk) electrochemical reduction in cyclic voltammetry[33].

To facilitate photoinduced dianion creation, Xie et al substituted the PBI core with electron-withdrawing substituents, 4-carboxy phenoxy groups, at bay positions.[34] Their PBI dianion formed, upon irradiation of the $PBI^{\bullet-}$ analog, which was obtained by a one-electron photoreduction upon irradiation of green light in the deoxygenated DMF. The photoexcited radical anion $PBI^{*\bullet-}$ could be used as a photo-catalyst to achieve hydrogen evolution. Using substitution chemistry, Würthner and co-workers developed a series of air-stable $PBI^{\bullet-}$ radicals by introducing electron-withdrawing substituents at perylene bay positions, such as -Cl, , -CN, or $-CF_3$[23,35]. And even the stable zwitterionic PBI-centered radical was isolated using catatonic bay substituents.[35] Still, there are numerous challenges associated with constructing a photo-responsive supramolecular material, that is: 1) the dianion PBI^{2-} is rarely formed without substitution at the *ortho* or bay position of the perylene bisimide[30,34], which is only limited to the multiple synthesis instead of photoreduction; 2) the mechanism of formation of photo-reduction to PBI^{2-} is not completely understood.

In this chapter, therefore, we devise systems without substitution at PBI bay positions, in a molecular and supramolecular complex system under vacuum, capable of selectively reaching either $PBI^{\bullet-}$ or PBI^{2-}, and in this way control their assembly and disassembly. The key finding is that two-electron transfer can be easily achieved in aggregates due to delocalization of electrons.

2.2 Photoreducion of Perylene Bisimides

2.2.1 Synthesis

We synthesized a water-soluble perylene bisimide derivative (**PBI-1**)[31], by coupling a diamine substituted PBI-1 core and oligoethyleneglycol derivative of the gallic acid (see Fig.2.4). First, a commercial triethyleneglycol monomethylether was activated by tosyl chloride into the corresponding tosyl oligoethyleneglycol derivative **2**, which underwent nucleophilic substitution by methyl gallate to form compound **3**. Subsequently, the methyl gallate was hydrolyzed into the corresponding gallic acid moiety **4**, enabling coupling with a diamine in the next step.

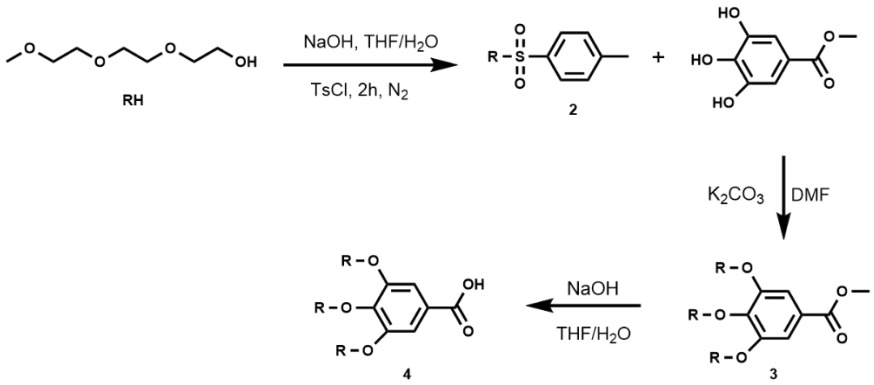

Figure 2.4. Synthesis of the gallic derivative. Synthesis of the water-soluble part of **PBI-1** for balancing the hydrophobicity. The synthesis followed reference 31.

To get the high yield of the compound (5), we developed a novel method to improve the literature method to optimize the yield, we reacted Perylene-3,4,9,10-tetracarboxylic acid dianhydride with ethylenediamine in pure imidazole at 140°C under N_2 flow, resulting in the 95% yield of compound **5** (see. Fig.2.5). Finally, the latter was coupled with compound **4** into the final product **PBI-1**.

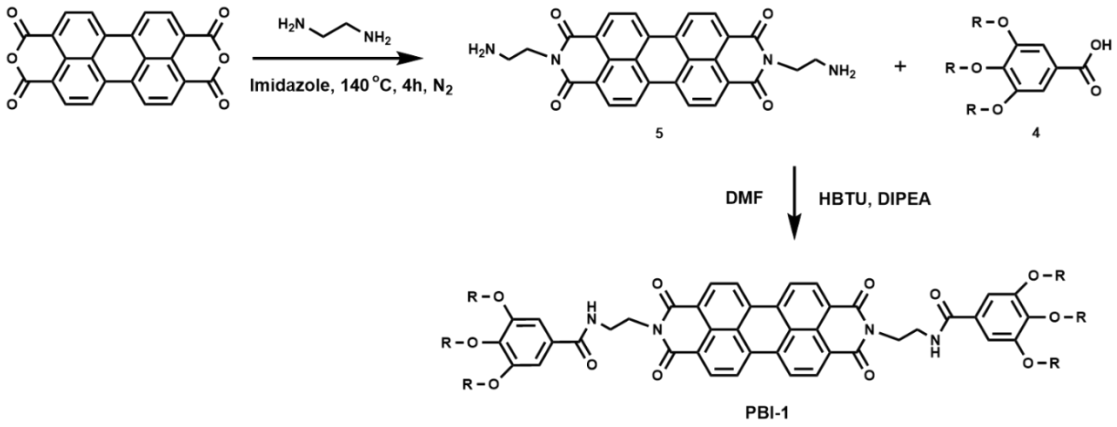

Figure 2.5. Synthesis of PBI-1. the amine-terminated perylene bisimide coupled with compound 4 into the final product[31].

2.2.2 Self-Assembly of PBI-1

Our group recently have employed **PBI-1** as building block to construct non-equilibrium supramolecular polymers driven by chemical redox in aqueous borate buffer, which displays large-scale emergent properties, such as oscillations, travelling fronts and patterns.[36] In my projects, we aim to use **PBI-1** photoreduction and oxidation as driving forces to build dynamic

supramolecular polymers. Since triethanolamine (TEOA) as an electron donor in photoinduced eletron-transfer system is a must, we first studied the **PBI-1** at 33 μM self-assembly in sodium bicarbonate-carbonate buffer (50 mM) at pH 10.8 (TEOA can be buffered in this range of pH). **PBI-1** is water-soluble but has a strong tendency to aggregate due to the π - π stacking of aromatic cores, hydrogen bonding between amide and carbonyl, and hydrophilic intertwines of oligoethyleneglycol. In contrast, in "good solvents", such as DMF or DMSO, **PBI-1** remains in its monomeric state. Figure 2.6A shows that the UV/Vis absorption of **PBI-1** in DMF has a well-resolved vibronic structure[37–39], spanning the range of 400 to 600 nm, with three maxima at 458, 490, and 527 nm, corresponding to the characteristic 0–2, 0–1, and 0–0 transitions of the monomeric PBI from S_0–S_1, respectively. In general[40,41], the degree of PBI aggregation can be derived from the ratio of UV absorbance of the 0–1 versus the 0–0 transition: A^{0-1}/ A^{0-0} , where 0.63 indicates a monomeric state, but upon aggregation the ratio increases to 0.7 or higher . When **PBI-1** is in the buffer, however, only one broad band is observed from 400 to 550 nm, with a characteristic new absorption band at 569 nm, indicative of a highly aggregated state in the buffer (see. Fig.2.6). A new band in the UV region from 200 to 300 nm[42], interestingly, blue shifted that rarely discussed in PBI aggregates studying, which corresponds to the transitions from the higher energy level. Although **PBI-1** is in aggregates, it is still fluorescent in buffer, which mirrored with the UV absorption from 600 to 800 nm with maxima 700 nm (See. Fig. 2.6B).

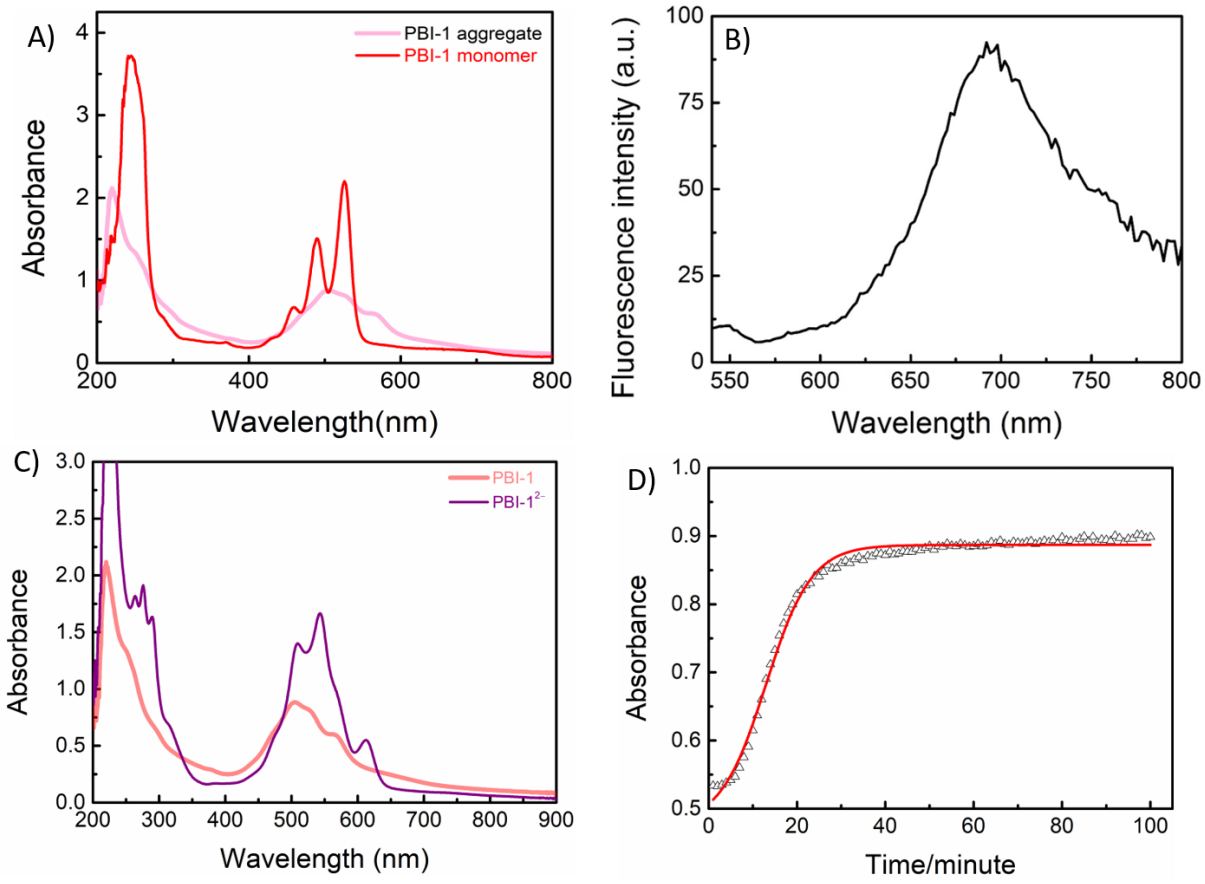

Figure 2.6. **The monomeric and aggregated PBI-1.** A) the UV spectra of 33 µM aggregated **PBI-1** in 50 mM bicarbonate-carbonate buffer pH=10.80, absorbing from 220 to 270, and 400 to 600 nm with four maximum peaks at 220, 506, 528, and 565 nm, while the 33 µM monomeric **PBI-1** in dichloromethane absorbs maximum at 245, 458,490, and 527 nm. B) the fluorescence emission spectrum of **PBI-1** aggregates in 50 mM bicarbonate-carbonate buffer pH=10.80, the exciting wavelength is at 510 nm. C) the UV spectra of the **PBI-1** aggregates in the buffer before and after chemical reduction with sodium dithionate. D) the kinetics of **PBI-1** aggregation in the buffer after one reduction-oxidation cycle monitored at 528 nm in 100 minutes with UV spectroscopy.

Heating-cooling experiments, generally, are used as a tool to study the assembly and disassembly of supramolecular aggregates. However, for **PBI-1** the latter method does not work due to the precipitation slightly above 60 °C in the buffer[43]. A better way, therefore, to achieve disassembly and assembly of **PBI-1** is to use chemical reduction and oxidation, respectively (as previously demonstrated in our group ref. 31). First, **PBI-1** aggregates in the buffer were chemically, sequentially, reduced into **PBI-1**$^{\bullet-}$ and **PBI-1**$^{2-}$ by $Na_2S_2O_4$, which, subsequently, disassembled into monomer due to the electronic repulsions. The chemical reduction is confirmed by UV characteristic absorption of **PBI-1**$^{2-}$, at 510, 547, and 615 nm[42] (see. Fig. 2.6 C). By introducing

ambient dioxygen, then, into the reduced **PBI-1** solution, the **PBI-1**$^{2-}$ was immediately re-oxidized back to neutral; still, in a monomeric state. The monomer, then, aggregates over time followed by UV absorbance of **PBI-1** aggregation at 528 nm. As shown in Figure 2.5 D that **PBI-1** cooperatively aggregated in the buffer, which nucleated, elongated in the first 40 mins, then reaches a plateau in a thermodynamic equilibrium state. This suggests that chemical reduction as a force is sufficient to drive **PBI-1** assembly and disassembly in aqueous solution.

2.2.3 PBI-1 Photoreduction

Although the **PBI-1** out-of-assemblies have been well studied with chemical reduction (sodium dithionate being a reductant, as previously demonstrated in our group ref. 31), the chemical waste (the product of **PBI-1** chemical reduction) pose an obstacle if one wants to repeat many redox cycles. To locally drive assembly and disassembly of **PBI-1** aggregates with negligible wastes, here we studied the photoreduction upon irradiation with different wavelengths. In most experiments we used 33 μM **PBI-1** in buffer (pH=10.8) and a large excess (3000 equivalents) of TEOA (triethanolamine) as electron donor. The whole reaction mixture was degassed by free-pump-thaw cycles until there were no more visible bubbles (typically four cycles with a duration of 90 mins). The degassed samples were irradiated by UVC lamp at 10 cm (235 to 280 nm, 184.5 mW/m^2), then the solution color changed from red to blue in ~ 2 minutes, and finally evolved to purple after 5 minutes (Figure 2.7 A, B, and C), corresponding to the **PBI-1**$^{\bullet-}$ (radical anion), and **PBI-1**$^{2-}$ (dianion), respectively (and similarly to the chemical reduction reported[36]). In contrast to UVC irradiation, only a blue solution was obtained upon UVA (316 to 400 nm, 1422 mW/m^2) irradiation even after 20 mins. In addition, UVB irradiation (281 to 315 nm, 227.5 mW/m^2), however, there is no photoreduction. It is reasonable due to **PBI-1** absorbs less UVB light in comparison to UVC region. Lastly, only **PBI-1**$^{\bullet-}$ was achieved, even irradiating more than 2 hours by blue light (390 to 480 nm, 402 mW/m^2), and still no **PBI-1**$^{2-}$ formation, which is in agreement with the literature reported[30,44].

In addition to visual color changes, the photoreduction can be tracked by UV/vis spectroscopy. The neutral **PBI-1** aggregates absorb from 400 to 600 nm with three maxima at 505, 530, and 569 nm (Figure 2.7 D); after UVA or blue light irradiation 30 mins, the absorbance of the neutral **PBI-**

1 decreases, whereas three new peaks with maxima at 727, 815, and 982 nm appear, corresponding to characteristic absorption of **PBI-1**$^{\bullet-}$.[30] In contrast, when the sample was irradiated by UVC, **PBI-1**$^{2-}$ quickly formed with three maxima at 510, 547, and 615 nm. Meanwhile, a new band from 200 to 300 nm emerges as **PBI-1**$^{2-}$ forms, which is rarely reported, corresponding to the electronic transition of the **PBI-1**$^{2-}$. Hence, the **PBI-1** can be selectively photoreduced in buffer by using different wavelengths.

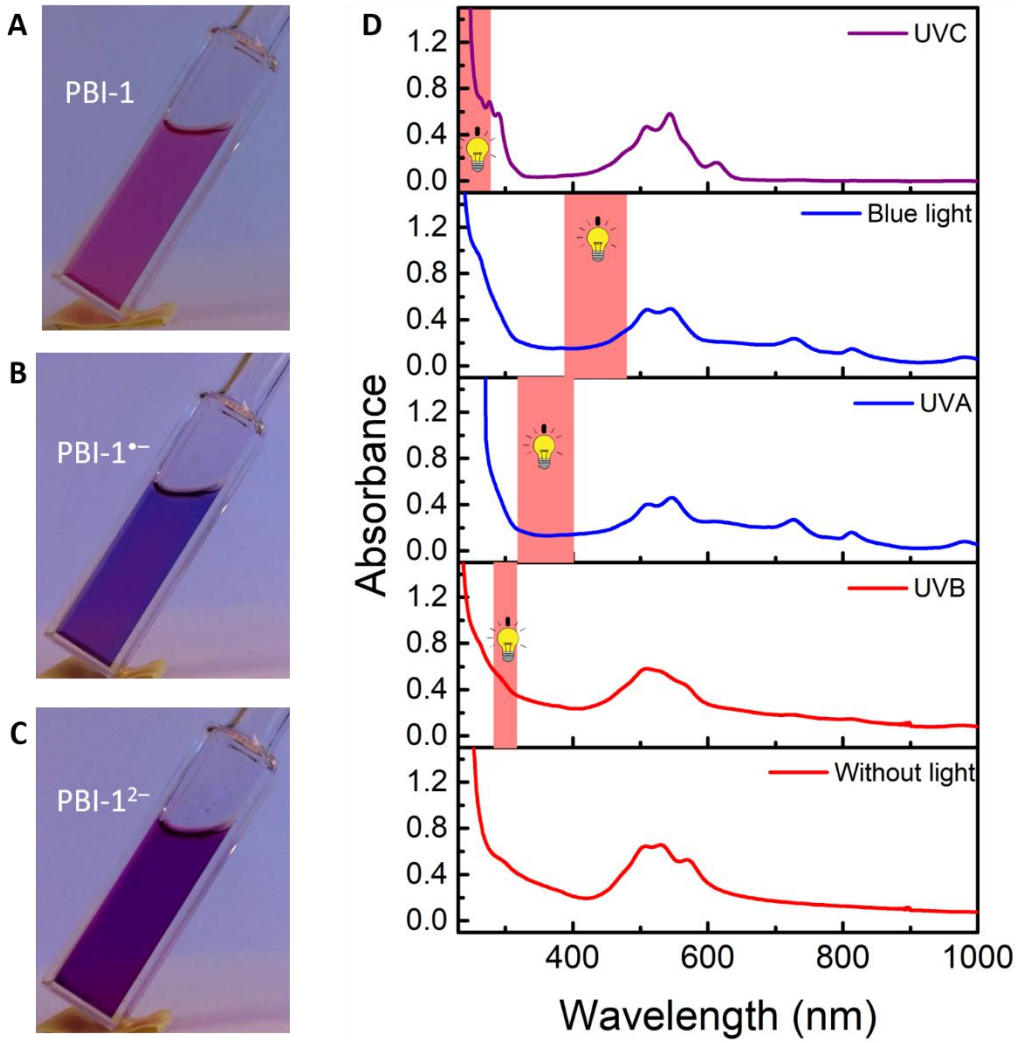

Figure 2.7. **PBI-1 photoreduction with different irradiated wavelength.** The photoreduction of 3 mL **PBI-1** in 50 mM bicarbonate-carbonate buffer pH=10.80 with 3000 eq. of TEOA (degassed by free-pump-thaw 4 cycles), was irradiated by blue light (irradiation time 30 mins, 390 to 480 nm, 402 mW/m^2), UVA (irradiation time 30 mins, 316 to 400 nm, 1422 mW/m^2), UVB (irradiation time 60 mins, 281 to 315 nm, 227.5 mW/m^2), and UVC (irradiation time 5 mins 235 to 280 nm, 184.5 mW/m^2). A) The image of the neutral **PBI-1**. B) The image of the **PBI-1**$^{\bullet-}$. C) The image of the **PBI-1**$^{2-}$. D) UV spectra of the aggregated **PBI-1** in the buffer after irradiation of UVB, UVA, UVC, Blue light.

2.2.4 The Mechanism of Photoreduction in PBI-1 aggregates

From the experiments in the previous section, we have seen that upon UVC irradiation, two electron reduction is fast in **PBI-1** aggregates, whereas previous literature[30] (and experiments on monomeric **PBI-1** below) show only a one-electron transfer. Here, we hypothesize that the aggregation contributes to the delocalization of electrons, thus allowing for facile two-electron reduction. After the first reduction to **PBI-1**$^{\bullet-}$, its electrons are shared by other conjugated neutral **PBI-1** in the aggregate, enabling transfer of one more electron from the donor TEOA. In contrast, **PBI-1** in the monomeric state, would stop after a single reduction to **PBI-1**$^{\bullet-}$ since delocalization would be absent. What follows is the comparison of photoreduction in the aggregated versus the monomeric state.

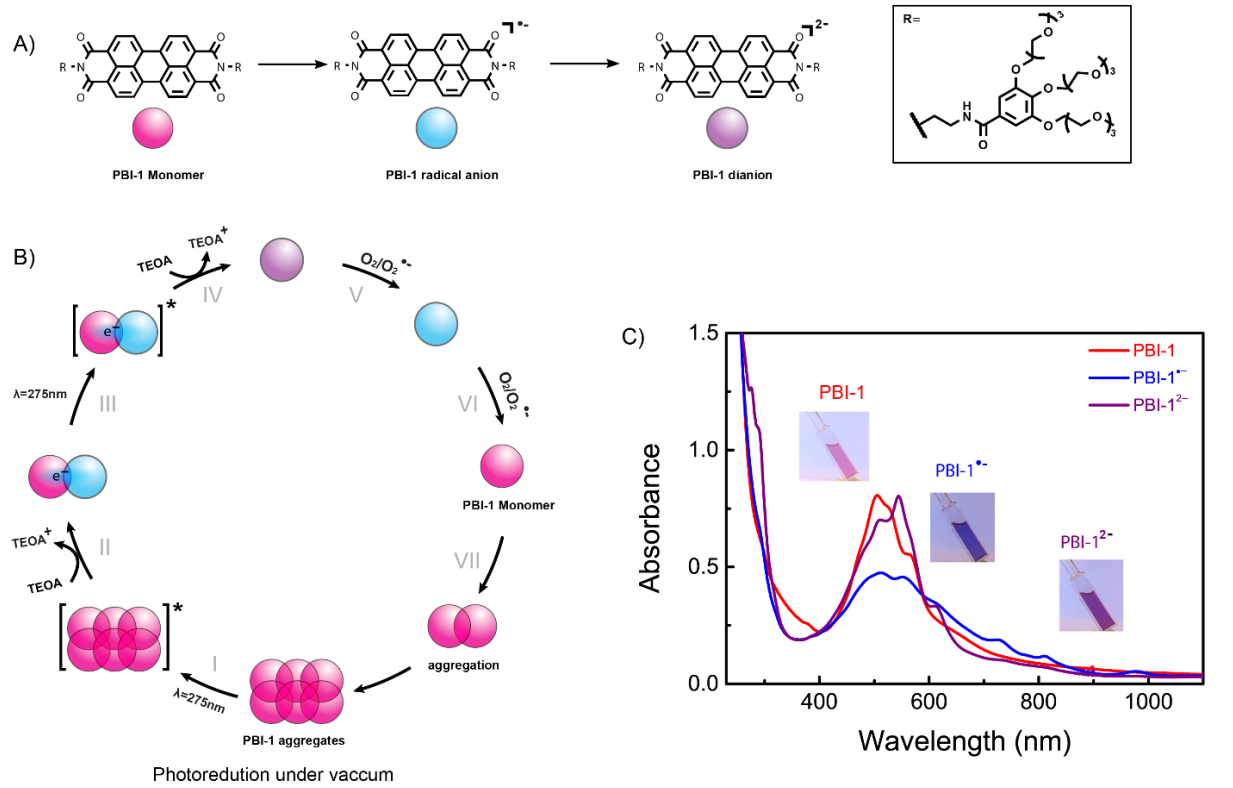

Figure 2.8. **The disassembly and re-assembly of PBI-1 driven by photoreduction and oxidation.** A) The molecular structure of the monomeric **PBI-1** (the pink ball), **PBI-1**$^{\bullet-}$ (the blue ball), and **PBI-1**$^{2-}$ (the purple ball). B) The scheme of **PBI-1** disassembly and re-assembly driven by photoreduction and oxidation as phases I (the excitation of **PBI-1** aggregate), II (one electron-transfer between excited **PBI-1** aggregate and TEOA), III (the excitation of the mixture **PBI-1**$^{\bullet-}$/**PBI-1** by UVC), IV (one more electron-transfer to **PBI-1**$^{\bullet-}$ forming **PBI-1**$^{2-}$), V (the oxidation of **PBI-1**$^{2-}$), VI (the oxidation of **PBI-1**$^{\bullet-}$), VII (the aggregation of the monomeric **PBI-1** over time). C) The UV spectra of the **PBI-1** (33 µM in the presence of 3000. eq of TEOA) in deoxygenated sodium bicarbonate-carbonate buffer upon UVC LED (275 nm, 5 mW/cm^2 forming **PBI-1**$^{\bullet-}$ (the blue solution) and **PBI-1**$^{2-}$ (the purple solution).

The deoxygenated **PBI-1** aggregates (33 μM) with 3000. eq of TEOA in buffer were irradiated 2 mins by UVC LED (275 nm, 5 mW/cm^2). The **PBI-1** solution evolves from the pink to the blue as the **PBI-1**$^{\bullet-}$ formation which has characteristic UV/vis absorption as shown in Figure 2.8 C (the same as abovementioned). After 5 mins irradiation, the color sequentially changes to the purple when a new UV absorption appears at 615 nm (see Fig 2.8 C purple line), indicative of the **PBI-1**$^{2-}$ formation. As the photoredox happens, the PBI-1 shuttles between the monomer and aggregates as illustrated in Figure 2.8. When **PBI-1** aggregates were illuminated by UVC (see Fig. 2.8B. Phase I), it is in an excited state that enable abstracting one electron from the donor TEOA. As the **PBI-1**$^{\bullet-}$ formation the aggregates disassembled due to the electronic repulsions (see Fig. 2.8B. Phase II). Interestingly, the aggregates are not fully disassembled. The **PBI-1**$^{\bullet-}$ remains co-assembled with the neutral **PBI-1** but in a smaller assembly in comparison to the non-reduced **PBI-1** (as our group previously reported. Ref. 36). In this scenario, the electron delocalizes between the **PBI-1**$^{\bullet-}$ and **PBI-1** in aggregates (electron density is redistributed as reported in Kasha's exciton model[45], which facilitates a continuous electron-transfer to occur — **PBI-1**$^{2-}$ formation after a consecutive excitation (see Fig. 2.8B. Phase III and IV).

To recover **PBI-1** aggregates, **PBI-1**$^{2-}$ oxidation is needed. Introducing atmospheric O_2 into the vacuum cuvette, the color of the solution spontaneously reverts to pink from purple but blue as an intermediate color. **PBI-1**$^{2-}$ is sequentially re-oxidized back to **PBI-1**$^{\bullet-}$ (see. Fig. 2.8B. Phase V and VI), and **PBI-1** that reassembles over time (see Fig. 2.8B. Phase VII).

Notably, for photo-inducing **PBI-1** electron transfer, substitution at bay positions with electron-withdrawing groups is to shift the energy level of the lowest unoccupied molecular orbital (LUMO) for enhancing electron transfer[23]. Generally, there are two possible mechanisms of excitation in a two-electron transfer system: (i) Sequential excitation— first, photoexcited **PBI-1** forms **PBI-1**$^{\bullet-}$, further get excited and obtain one more electron from TEOA to form **PBI-1**$^{2-}$. (ii) Simultaneous excitation— photoexcited **PBI-1** directly gets two electrons from TEOA. According to what we observed in Figure 2.8 C, the **PBI-1**$^{\bullet-}$, first, formed upon UVC irradiation under vacuum with characteristic absorptions at 727, 815, and 982 nm; sequentially, irradiating on **PBI-1**$^{\bullet-}$, **PBI-1**$^{2-}$ was observed with characteristic UV absorption at 510, 547, and 615 nm as the majority of **PBI-**

1$^{\bullet-}$ consumed (Figure 2.8 C). This implies that **PBI-1**$^{\bullet-}$ is sequentially excited to further react with electron donor TEOA.

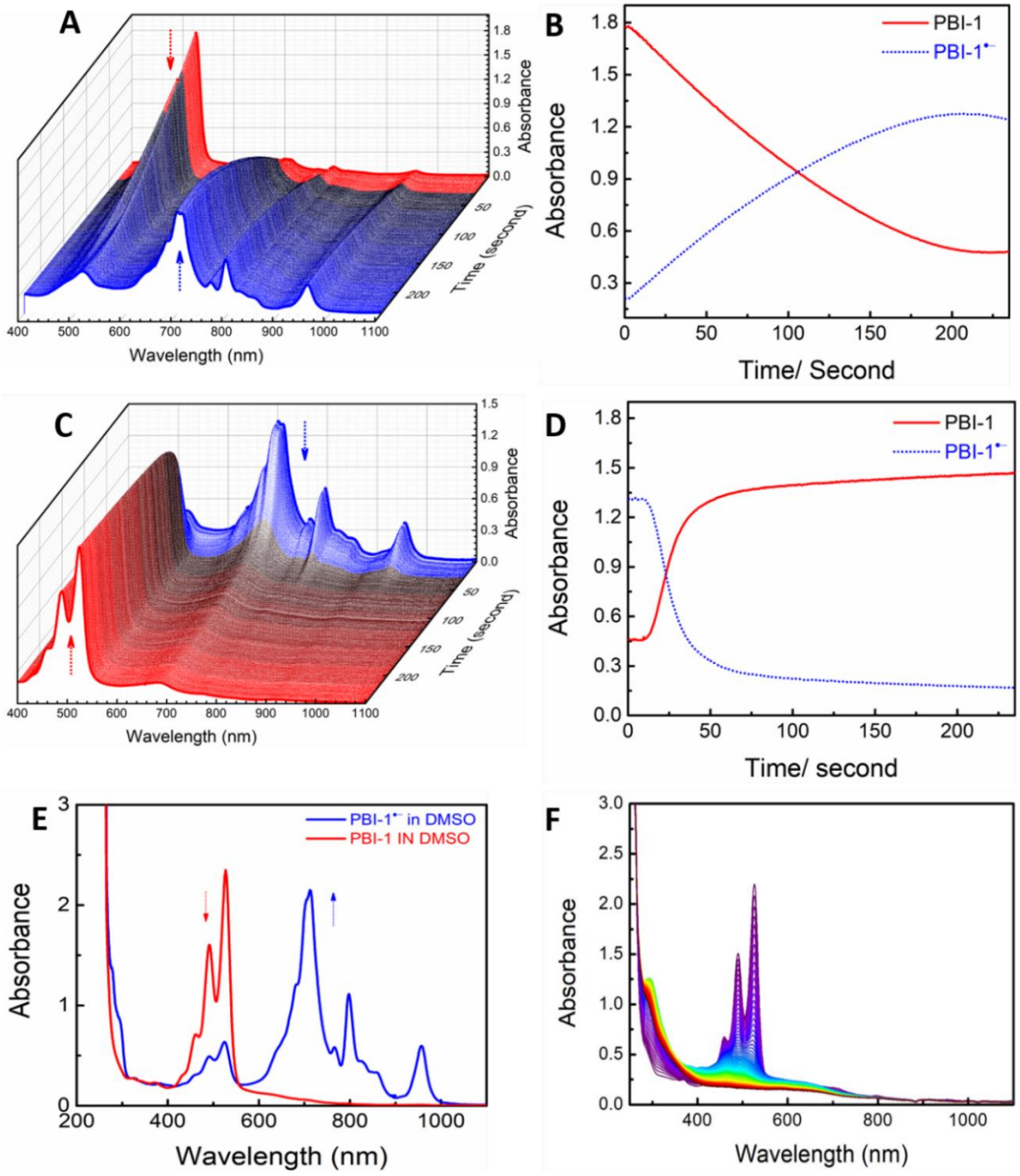

Figure 2.9. **The monomeric PBI-1 photoreduction.** A, B) the kinetics of **PBI-1** (33 µM with 3000 eq. of TEOA) photoreduction in DMF upon UVC (275 nm, 5 mW) irradiation 235 seconds. C, D) the kinetics of **PBI-1**$^{\bullet-}$ oxidation by introducing the air into the closed cuvette (with stirring). E) the UV spectra of **PBI-1** in DMSO (the same conditions as the former experiment) before and after the photoreduction (irradiated by UVC 2 mins). F) the UV spectra of **PBI-1** in dichloromethane upon UVC irradiation 10 mins.

To prove delocalization of electrons in aggregates contributing to **PBI-1**$^{2-}$ formation, **PBI-1** monomer photoreduction in good solvents, DMF and DMSO, was conducted. The degassed **PBI-1** in DMF was irradiated by UVC 275 nm, only **PBI-1**$^{\bullet-}$ was obtained with three maxima UV absorption at 727, 815, 982 nm (Figure 2.9 A), respectively, which is consistent with literature reported.[30] The kinetics of photoreduction was monitored with a UV-diode array, indicating the electron transfers in about 100 seconds, then the rate of the reduction becomes slows down and reaches a plateau (Figure 2.9 B).

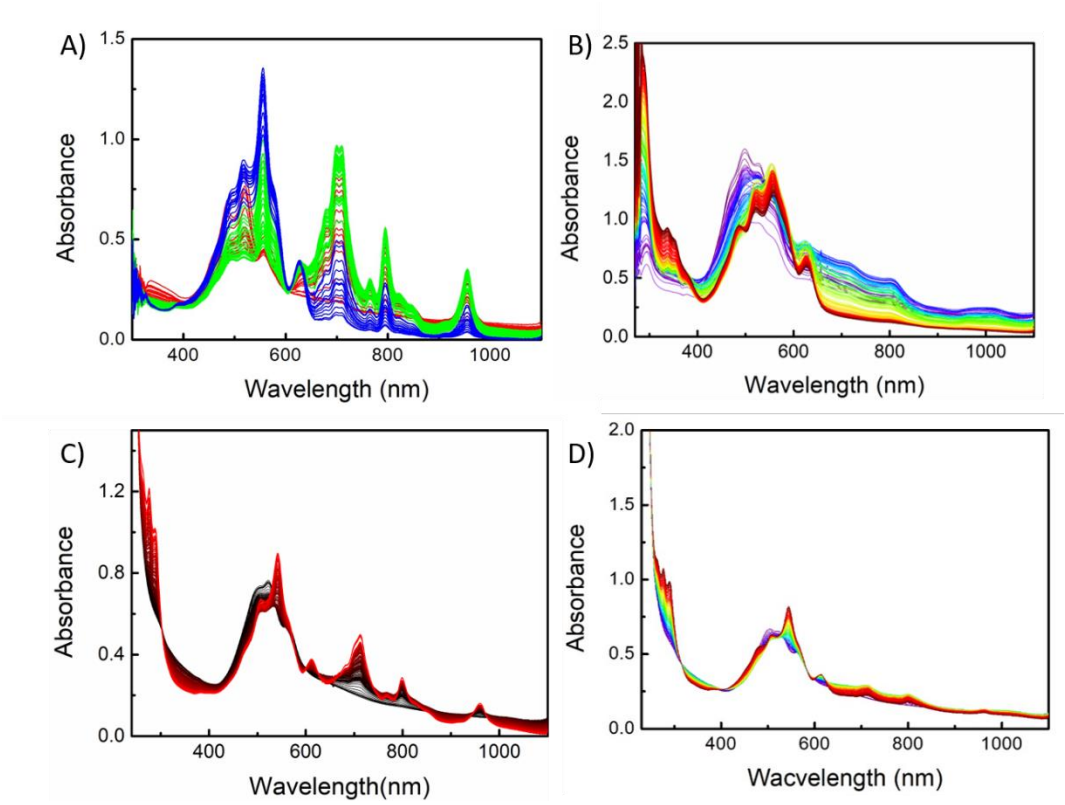

Figure 2.10**. The photoreduction of the aggregated PBI-1 in different solvents.** A) **PBI-1** in acetone (33µM with 3000 eq. of TEOA) before and after 1 hour of UVC irradiation (275 nm, 5 mW, at 5 cm). (B) **PBI-1** in toluene (33 µM with 3000 eq. of TEOA) before and after 1 hour of UVC irradiation (275 nm, 5 mW, at 5 cm). (C) **PBI-1** in ethanol (33 µM with 3000 eq. of TEOA) before and after 1 hour of UVC irradiation (275 nm, 5 mW, at 5 cm). (D) **PBI-1** in isopropanol (33 µM with 3000 eq. of TEOA) before and after 1 hour of UVC irradiation (275 nm, 5 mW, at 5 cm).

However, neutral **PBI-1** is not completely transformed into **PBI-1**$^{\bullet-}$ because the electron transfer stays at an equilibrium state between the forward and back electron transfer (see. Fig.2.2B). By introducing ambient dioxygen into the vacuum, the **PBI-1**$^{\bullet-}$ was re-oxidized back to neutral in 75 seconds under stirring (Figure 2.9 C and D), which indicates the rate of the oxygen reacting with

PBI-1$^{\bullet-}$ is much faster than the rate of photoreduction. Overall, these experiments indicate that it would be very difficult to photoreduce **PBI-1** under atmospheric conditions. Figure 2.9 E shows that the **PBI-1** photoreduction in DMSO behaved the same as in DMF. Thus, **PBI-1** two-electron transfer only takes place when **PBI-1** in the aggregates state, but not in the monomer, which is in agreement with our initial hypothesis. Meanwhile, we also studied **PBI-1** monomer in other solvents, unfortunately, the **PBI-1** monomer in dichloromethane and chloroform is unstable under UVC irradiation, leading to fast photobleaching (see. Fig 2.9F).

Table 1: the information of PBI-1 in different solvents.

Solvent	Dielectric constant (ε)	Reduced species	Assembly	**α ratio**
Buffer	80.1	PBI$^{\bullet-}$, PBI-1^{2-}	aggregate	0.95
Ethanol	24.5	PBI-1$^{\bullet-}$, PBI-1^{2-}	aggregate	0.95
acetone	20.7	PBI-1$^{\bullet-}$, PBI-1^{2-}	aggregate	0.80
isopropanol	17.9	PBI-1$^{\bullet-}$, PBI-1^{2-}	aggregate	1.03
toluene	2.38	PBI-1$^{\bullet-}$, PBI-1^{2-}	aggregate	1.08
DMSO	46.7	PBI-1$^{\bullet-}$	monomer	0.69
DMF	36.7	PBI-1$^{\bullet-}$	monomer	0.65
dichloromethane	8.93	none	monomer	0.68
chloroform	4.81	None	monomer	0.62

(**α ratio:** UV absorption of the 0–1 versus the 0–0 transition: A^{0-1}/ A^{0-0}, where 0.63 indicates a monomeric state, but upon aggregation the ratio increases to 0.7 or higher).

However, we noticed **PBI-1**$^{2-}$ forms, in ethanol, acetone, isopropanol, and toluene, only when **PBI-1** in the aggregates state. The degassed **PBI-1** sample in acetone, 33 μM acceptor with 3000 eq. of TEOA, was irradiated by UVC; the neutral **PBI-1**, sequentially, was photoreduced into **PBI-1**$^{\bullet-}$ and **PBI-1**$^{2-}$, but, still, there is a minor part of **PBI-1**$^{\bullet-}$ that stays in radical anion state (Figure 2.10 A). For the **PBI-1** in toluene under the same conditions, the intermediate **PBI-1**$^{\bullet-}$ transformed into the **PBI-1**$^{2-}$; notably, the **PBI-1** aggregates lead to the obvious scattering in the neutral state, whereas the **PBI-1**$^{2-}$ is much less scattering (Figure 2.10 B). On the contrary, **PBI-1**$^{\bullet-}$ coexists with **PBI-1**$^{2-}$ in ethanol and isopropanol (Figure 2.10 C, D), even after a long time of UVC irradiation.

Thus, the information of **PBI-1**$^{\bullet-}$ and **PBI-1**$^{2-}$ in different solvents suggests that the aggregates mainly contribute to the **PBI-1**$^{2-}$ formation.

According to Marcus theory, the driving force of electron transfer correlates with the dielectric constants of the medium. Thus, we conducted the **PBI-1** photoreduction in different solvents, with dielectric constants from 80.1 to 2.38, including buffer, ethanol, acetone, isopropanol, and toluene. From table 1, it is clear that the dianion can be obtained for a very wide range of dielectric constants, but only if **PBI-1** is in the aggregated state. Compare, for example, DMF (ε = 36.7) with ethanol (24.5). They have quite comparable constants, but only the latter leads to **PBI-1**$^{2-}$.

Overall, we conclude from these series of experiments that the dielectric constant is not the main factor in determining whether two-electron reduction is possible. Instead, it is the formation of aggregates.

2.2.5 Photodynamic Study with Transient Absorption, and Steady-State Spectroscopy.

To get more quantitative insights into the rapid electronic processes ongoing in **PBI-1** aggregates, we used transient absorption spectroscopy. Its working principle is the pump-probe. Two very short pulses of light from an ultrafast laser are needed: the first excite (pump) a molecule to an excited state, and then the probe detected with whole spectra (wavelength range) from femtosecond to nanosecond when the excited molecule reverts to the ground state. In deoxygenated buffer, 500 µM PBI aggregates with 3000 eq. of TEOA were pumped using a 450 nm femtosecond laser. The spectrum is taken at 400 fs after laser excitation, then, a new band around 710 nm appears, which indicates **PBI-1**$^{\bullet-}$ formation, but without **PBI-1**$^{2-}$ formation (Figure 2.11. A and B). Under the same conditions, only **PBI-1**$^{\bullet-}$ was observed when **PBI-1** monomer in DMSO (Figure 2.10. C, D). However, the lifetime of the excited **PBI-1** and **PBI-1**$^{\bullet-}$ in the monomer is about 10 times shorter than **PBI-1** aggregates, which implies that the aggregation induces different **PBI-1** photophysical properties in comparison to the monomer. Hence, the photodynamic of excited **PBI-1** and **PBI-1**$^{\bullet-}$ is different in aggregate, and in monomer.

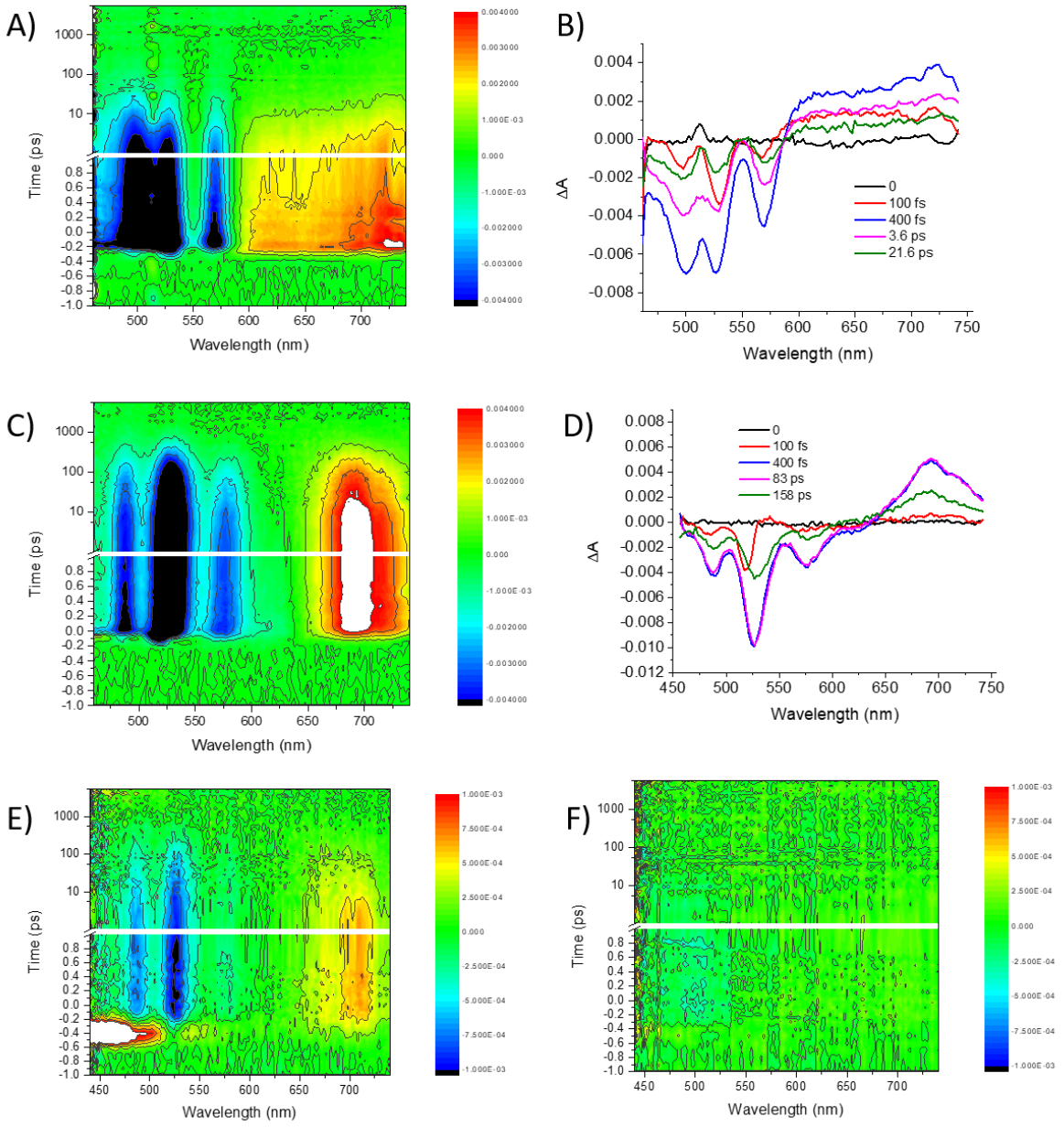

Figure 2.11. **PBI-1 photoreduction studied with transient absorption spectra.** A, B) the aggregated **PBI-1** (500 µM with 3000 eq. of TEOA) in buffer was pumped by 450nm laser and detected from 450 to 750 nm. C, D) The monomeric **PBI-1** in DMSO was pumped by 450 nm laser and detected from 450 to 750 nm. E) The monomeric **PBI-1** in DMSO was pumped by 350 nm laser and detected from 450 to 750 nm. F) The aggregated **PBI-1** in buffer were pumped by 350nm laser detected from 450 to 750 nm.

We also followed the photodynamics of **PBI-1** photoreduction with other excitation wavelengths. For instance, at 350 nm, even less radical anion forms in **PBI-1** monomeric state (**PBI-1** in DMSO, see. Fig. 2.11E) whereas no reduction occurs in **PBI-1** aggregated solution (**PBI-1** in buffer, see.

Fig. 2.11F). This maybe correlates with low UV absorbance of **PBI-1** solution from 300 to 400 nm (see. Fig. 2.6D). From a technical perspective, it is quite challenging to follow the photodynamic of the **PBI-1** radicals under transient absorption spectroscopy. For instance, constantly removing dioxygen and keeping circulating **PBI-1** solution, which brings some unexpected chemical or physical influences.

Instead to track the photoreduction kinetics all the way to **PBI-1**$^{2-}$, we devised a set-up based on a commercial UV diode array, combined with a 3D-printed holder and a home-made stirring plate (there is no stirring accessary with UV-8454 diode array), which allowed the UVC LED to constantly excite the sample from the side of the cuvette (Figure 2.11 A).

The **PBI-1** (33 μM contentration with 3000. Eq. of TEOA) photoreduction is in real time followed with the UV diode array (with our devised set-up). As our prior demonstration (see 2.23 section), **PBI-1** and its reduced species all have their own unique absorption (Fig. 2.12B). We selected 729 and 612 nm as indicators of **PBI-1**$^{\bullet-}$, and **PBI-1**$^{2-}$ formation, respectively. As the photoreduction taking place in the first 210 seconds, the **PBI-1**$^{\bullet-}$ UV/vis absorbance reached a plateau (see Fig. 2.12 C) due to **PBI-1** fully converted into **PBI-1**$^{\bullet-}$, but then had a rapid decline in 470 s. In contrast, **PBI-1**$^{2-}$ absorbance keeps growing until 470 s to a maximum (see Fig. 2.12 D). This suggests that, between 210 s and 470 s, the **PBI-1**$^{\bullet-}$ converts into **PBI-1**$^{2-}$. Therefore, the photodynamic of **PBI-1**$^{2-}$ formation characterized with steady-state spectroscopy is a sequential excitation (the dianion forms after a radical anion).

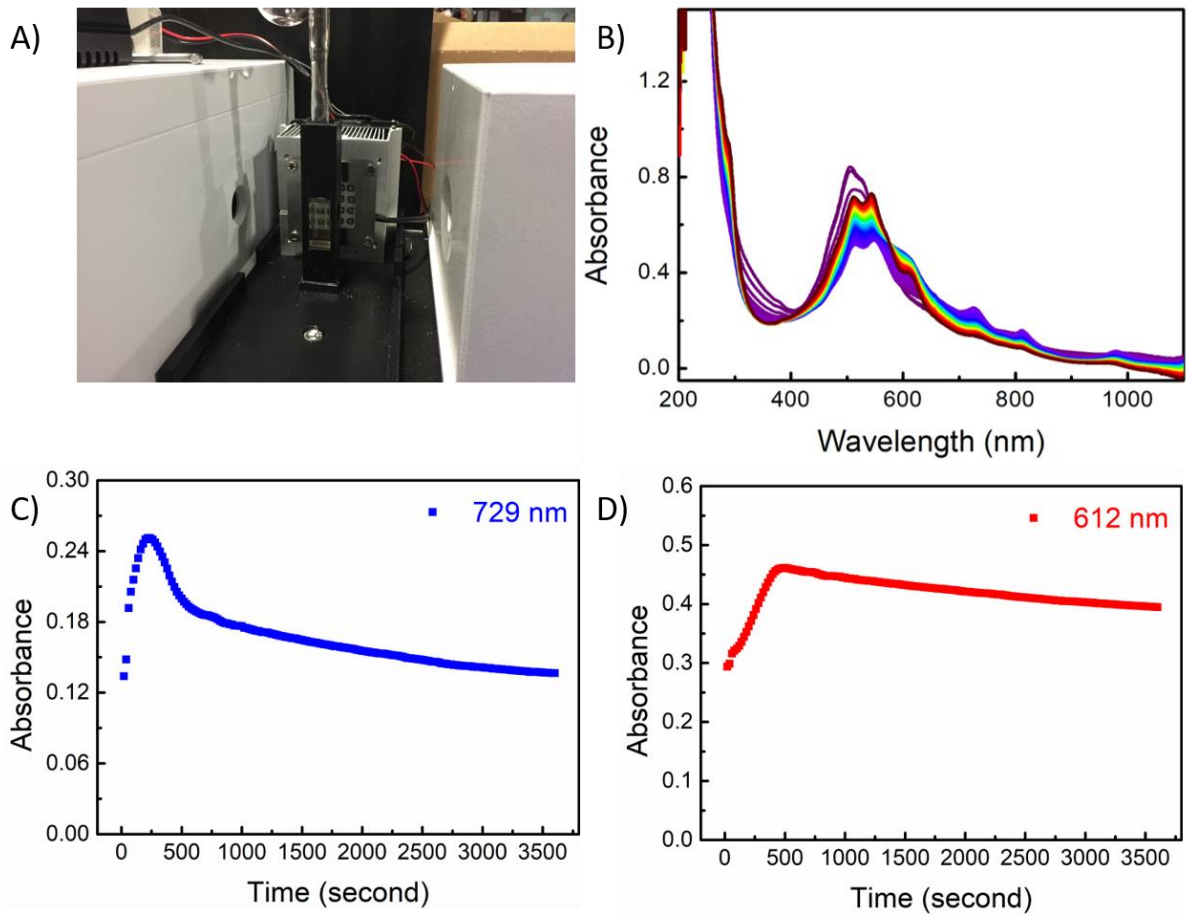

Figure 2.12. **The PBI-1 dianion formation was tracked with a home-modified UV 8454 diode array.** A) The image of home-modified set-up. B) the UV spectra of 33 µM deoxygenated **PBI-1** in buffer with 3000 eq. of TEOA was constantly irradiated by UVC LED 1 hour (275 nm, 5 mW/cm^2). C, D) the kinetics of the UV absorbance at 729 (**PBI-1**$^{\bullet-}$), and 612 nm (**PBI-1**$^{2-}$) in 1 hour.

2.2.6 Photo-Driven Disassembly of PBI-1 Aggregates

To see the effect of photoreduction up close we used confocal microscopy, where a circular region could be selectively illuminated to locally reduce the **PBI-1** aggregates. Before irradiation, the size of neutral **PBI-1** is around 2–5 µm, with red fluorescence, as shown in Figure 2.13 A. When a second laser at 380 nm irradiated the **PBI-1** aggregates residing in the green circle, after 10 seconds, the aggregates start to disassemble; and the red fluorescence is fading (Figure 2.13B). In previous work from the group,[36] it was shown that reduction changes the local solution density, and thus causes convective flows to start. In the experiment in Figure 2.12, the combination of reduction and convection leads to an apparent depletion of aggregates in the top right corner (cf. panel c). In the photoreduced regions, the fluorescence emission changed from 674 nm to 596

nm due to disassembly. These rather visual experiments confirm our other spectroscopic experiments (shown earlier in this chapter), and yet again demonstrate that light is a promising tool to control the disassembly of **PBI-1**.

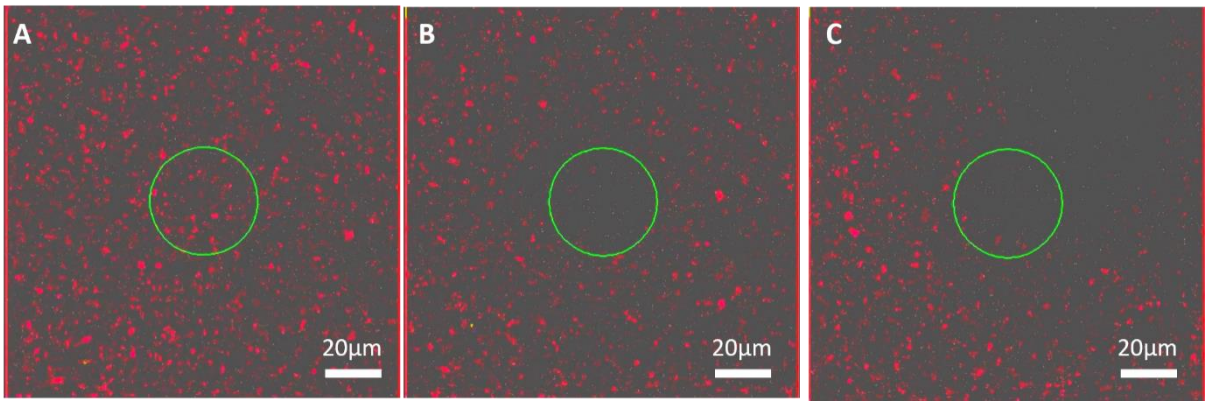

Figure 2.13. **The PBI-1 photoreduction under confocal microscopy.** A) the degassed **PBI-1** with 3000 eq. of TEOA (33 µM) in buffer before UV irradiation. B) The former sample was irradiated with 380 nm laser in the circular region for 10 seconds. (C) The sample was continuously irradiated for 60s.

2.3 Conclusions

In conclusion, we have achieved selective photoreduction of perylene bisimide derivative **PBI-1** in degassed solutions, under vacuum conditions. Only one electron transfers for **PBI-1** in solvents where it is in its monomeric form. In contrast, two-electron transfer occurs when **PBI-1** is aggregated. The aggregates contribute to **PBI-1**$^{2-}$ formation due to the delocalization of electrons. Our qualitative and quantitative studies indicate that the formation of **PBI-1**$^{2-}$ occurs sequentially; first from **PBI-1** to **PBI-1**$^{\bullet-}$, and then further to **PBI-1**$^{2-}$. When the vacuum was released, and ambient dioxygen entered the system, the reduced species quickly re-oxidize back to the neutral (and assembled) state. Applying light locally, can lead to spatiotemporal control over **PBI-1** assembly, and was shown to induce small-scale convective flows (due to density differences). In the following chapters, we will show that **PBI-1**, due to its fast and complete photoreduction behavior, is interesting building block to construct out-of-equilibrium systems.

2.4 Acknowledgements

Chunfeng Chen performed the synthesis and all the experiments apart from transient absorption spectra, that was collected by Dr. Takuji Adachi, Dr. Johanna Brazard, and Prof. Prof.Stefan Haacke. Prof. Thomas Hermans helped with confocal measurements. Prof. Thomas Hermans and Dr. Takuji Adachi supervised the research.

2.5 Experimental Section

2.5.1 Synthesis of PBI-1. PBI-1 was synthesized as our group previously reported[43]. Methyl gallate was purchased from TCI chemicals. Triethyleneglycol monomethylether and perylene-3,4,9,10-tetracarboxylic dianhydride were purchased from Sigma-Aldrich. All other chemicals and solvents were purchased from Sigma-Aldrich and VWR. NMR spectra were recorded on an NMR Bruker AVANCE 400 MHz.

[2-[2-(2-Methoxyethoxy)ethoxy]ethoxy]p-toluenesulfonate (2). To a solution of triethyleneglycol monomethylether (10 g, 0.061 mol, 1 eq) in 20 mL THF, a solution of NaOH (5 g, 0.125 mol, 2 eq) in H_2O (20 mL) was added under stirring at 0 ºC. To this mixture, a solution of tosyl chloride (15 g, 0.078 mol, 1.3 eq) dissolved in 20 mL THF was added dropwise under an inert atmosphere. Then, the reaction was allowed to warm to rt and stirred for 2 hours. Afterward, 120 mL of diethyl ether were added, and the organic layer was washed with 1 M NaOH (3 x 100 mL), water (2 x 100 mL), and dried over anhydrous $MgSO_4$. After evaporation and drying under vacuum, the title product was obtained as a yellowish oil (18.53 g, 95%). ^{1}H NMR (400 MHz, $CDCl_3$) δ 7.84 (d, J = 8.3 Hz, 2H), 7.39 (d, J = 8.5 Hz, 2H), 4.25 –4.16 (m, 2H), 3.75 – 3.70 (m, 2H), 3.69 – 3.61 (m, 6H), 3.57 (dd, J = 5.8, 3.3 Hz, 2H), 3.41 (s, 3H), 2.49 (s, 3H).

Methyl 3,4,5-tris[2-[2-(2-Methoxyethoxy) ethoxy] ethoxy] benzoate (3). Methyl gallate (2 g, 10.8 mmol, 1 eq) and potassium carbonate (15 g, 108 mmol, 10 eq) were added to a solution of **2** (13.7 g, 43.2 mmol, 4 eq) in DMF (50 mL). The reaction mixture was heated at 80 ºC overnight under an inert atmosphere. Then, the solvent was removed under vacuum, and CH_2Cl_2 (100 mL) was added to the solid residue. The obtained solution was collected in a separatory funnel and

washed with saturated $NaHCO_3$ (50 mL) and brine (50 mL). The organic layer was dried over anhydrous $MgSO_4$, followed by evaporation and drying under vacuum. Purification by flash chromatography using hexane/ethyl acetate (1:5) as eluent afforded **3** (6.02 g,90%) as a yellow oil. ^{1}H NMR (400 MHz, CDCl3) δ 7.31 (s, 2H), 4.23 – 4.19 (m, 6H), 3.88 (dd, J = 8.8, 3.6 Hz, 9H), 3.77 –3.70 (m, 6H), 3.70 – 3.62 (m, 12H), 3.56 (dd, J = 5.9, 3.2 Hz, 6H), 3.39 (s, 9H).

3,4,5-tris[2-[2-(2-Methoxyethoxy)ethoxy]ethoxy]benzoic acid (4). To a solution of **3** (6.02 g, 10.61 mmol, 1 eq) in 50 mL of a THF/H_2O 1.5:1 mixture at 0 °C, 10 mL of a 10.6 M solution of NaOH (100.61 mmol, 10 eq) were added. The reaction mixture was allowed to warm to rt and stirred overnight, after that, it was acidified to pH 2 with HCl (1 M) and extracted with CH_2Cl_2 (3 x 70 mL). The collected organic phase was dried over anhydrous $MgSO_4$, concentrated, and dried under vacuum to give **4** (6.35 g, 98%) as a yellow oil. ^{1}H NMR (400 MHz, DMSO) δ 7.22 (s, 2H), 4.18 – 4.12 (m, 6H), 3.80 – 3.72 (m, 6H), 3.56 (m, 18H), 3.43 – 3.39 (m, 6H), 3.23 (s, 9H).

N,N'-bis(aminoethyl) perylene-3,4,9,10-tetracarboxylic bisimide (5). perylene-3,4,9,10-tetracarboxylic acid dianhydride (1 g, 2.95 mmol, 1 eq) with imidazole (20 g, 100 eq) in 100mL flask were heated to 140°C under N2. In 20 min, the solid imidazole was melted into solution, followed by injection of 8mL ethylenediamine (0.12 mol, 40.67 eq). The color of solution changed from the red from the black in 2 mins, which was stirred for 2h at 140°C. Then the solution was cooled down to 90°C, whose reaction was stopped by adding 20mL H2O. After one hour stirring at 90 °C, the solution was cooled down to the room temperature. by adding HCl to adjust the Ph of solution to 12, the solution was stirred overnight. The precipitate was filtered and washed with water 3 times, which subsequently was washed with dichloromethane 3 times. The final compound perylene bisimide (5) was obtained (1.18g, 83.69%). ^{1}H NMR (400 MHz, D_2O) δ 7.98 (8H), 4.35 (4H), 3.33 (4H).

N,N'-Di[3,4,5-tris[2-[2-(2-Methoxyethoxy)ethoxy]ethoxy]benzoylaminoethyl]-perylene-3,4,9,10-tetracarboxylic bisimide (PBI-1). Carboxylic acid **4** (0.157 g, 0.26 mmol, 2.4 eq) was dissolved in 20 mL of DMF. To this solution, HBTU (0.098 g, 0.26 mmol, 2.4 eq) and DIPEA (190 μL,

1.07 mmol, 10 eq) were added under an inert atmosphere. After 5 min, perylene bisimide **5** (0.061 g, 0.11 mmol, 1 eq) was added and the reaction mixture was stirred at rt for 48 hours, after which 50 mL of CH_2Cl_2 were added. The organic phase was washed with saturated $NaHCO_3$ (2 x 50 mL) and brine, dried over anhydrous $MgSO_4$, and the solvent was evaporated under vacuum. The crude **PBI-1** was dissolved in 20mL DMSO, then added into 300 mL cold methanol for stirring 30mins. The solution was stored in fridge for 2 hours to precipitate, which was filtered and dried to get pure PBI-1 (0.143 mg, 78.57%). ^{1}H NMR (400 MHz, DMSO) δ 8.70 (s, 4H), 8.48 (s, 2H), 8.39 (s, 4H), 7.00 (s, 4H), 4.55 (s, 12H), 4.28 (s, 4H), 4.03 (s, 16H), 3.78 – 3.40 (m, 68H), 3.19 (s, 18H). ^{13}C NMR (101 MHz, DMSO) δ 166.53, 163.38, 152.13, 140.20, 134.16, 130.05, 124.37, 123.12, 106.68, 72.30, 71.68, 70.29, 70.01, 69.31, 68.73, 63.49, 58.45. HRMS (ESI$^+$) Calculated Mass for $C_{84}H_{112}N_4O_{30}Na_2$ [M+2Na$^+$]: 851.3573. Found: 851.3539.

2.5.2. PBI-1 aggregation after one shot chemical reduction. 33μM PBI-1 in 50 mM bicarbonate-carbonate buffer (pH 10.80) was added 3 μL of a 400 mM $Na_2S_2O_4$ solution. Then, the solution spontaneously gets reduced with color evolution from redness to purple after blue. By introducing ambient dioxygen, subsequently, the purple PBI-1 solution was re-oxidized back to the red, but which is still in the monomer. The PBI-1 aggregation was recorded by UV spectroscopy (JASCO V-670) in 100 mins.

2.5.3. UV-Vis measurements. UV-Vis spectra were taken by a JASCO V-670 spectrometer equipped with a stirring plate. All the neutral and reduced species were performed in a 1cm quartz cuvette.

2.5.4. Fluorescence measurements. Emission spectra were recorded with a Fluorolog®-3 spectrofluorometer by exciting at 488 nm and recording between 500 nm and 800 nm.

2.5.5. Home-modified UV-diode array. The holder with four windows was 3D-printed, which allows the UVC LED to constantly excite the sample from the sidewall of the Schlenk cuvette. The

kinetics of the sample, simultaneously, is detected by UV-diode array from another two open windows, which facing to the detector of UV spectroscopy.

2.5.6. PBI-1 photoreduction. All PBI-1 solutions in a different solvent were 33uM, 3mL in the presence of 3000 eq. of TEOA, which was degassed by free-pump-thaw until there is no bubble observed. Next, using a UV lamp or LED irradiating on the sample, the color of the sample changes from red to blue, finally halted on purple. The distance between UVC LED and sample holder is 2cm. Four big power lamp UVA, UVB, blue light, the distance is 10 cm.

2.5.7. Confocal measurements. Confocal micrographs were taken by using Zeiss LSM 710 confocal microscope system with 63x magnification, numerical aperture, NA, 1.3 of Zeiss LCI Plan-NEOFLUAR immersion objective lens (Zeiss GmbH). The samples inside of the green circle were excited by a continuous-wave laser at 380 nm, whereas only visible light in the left areas. The emission was measured from 500 nm to 800 nm using a spectral detector. The PBI-1 aggregates in the buffer in the presence of 3000 eq. of TEOA, which is degassed by free-pump-thaw before light irradiation.

2.6 References

(1) Menzel, J. P.; de Groot, H. J. M.; Buda, F. Photoinduced Electron Transfer in Donor–Acceptor Complexes: Isotope Effect and Dynamic Symmetry Breaking. *J. Phys. Chem. Lett.* **2019**, *10* (21), 6504–6511. https://doi.org/10.1021/acs.jpclett.9b02408.

(2) La Porte, N. T.; Martinez, J. F.; Hedstrom, S.; Rudshteyn, B.; Phelan, B. T.; Mauck, C. M.; Young, R. M.; Batista, V. S.; Wasielewski, M. R. Photoinduced Electron Transfer from Rylenediimide Radical Anions and Dianions to Re(Bpy)$(CO)_3$ Using Red and near-Infrared Light. *Chem Sci* **2017**, *8* (5), 3821–3831. https://doi.org/10.1039/c6sc05103k.

(3) Shi, Y.; Zhang, T.; Jiang, X.-M.; Xu, G.; He, C.; Duan, C. Synergistic Photoredox and Copper Catalysis by Diode-like Coordination Polymer with Twisted and Polar Copper–Dye Conjugation. *Nature Communications* **2020**, *11* (1), 5384. https://doi.org/10.1038/s41467-020-19172-3.

(4) Antón-García, D.; Warnan, J.; Reisner, E. A Diketopyrrolopyrrole Dye-Based Dyad on a Porous TiO2 Photoanode for Solar-Driven Water Oxidation. *Chem. Sci.* **2020**, *11* (47), 12769–12776. https://doi.org/10.1039/D0SC04509H..

(5) Kamat, P. V. Quantum Dot Solar Cells. Semiconductor Nanocrystals as Light Harvesters. *J. Phys. Chem. C* **2008**, *112* (48), 18737–18753. https://doi.org/10.1021/jp806791s.

(6) Greenham, N. C.; Peng, X.; Alivisatos, A. P. Charge Separation and Transport in Conjugated-Polymer/Semiconductor-Nanocrystal Composites Studied by Photoluminescence Quenching and Photoconductivity. *Phys. Rev. B* **1996**, *54* (24), 17628–17637. https://doi.org/10.1103/PhysRevB.54.17628.

(7) Ardo, S.; Meyer, G. J. Photodriven Heterogeneous Charge Transfer with Transition-Metal Compounds Anchored to TiO2 Semiconductor Surfaces. *Chem. Soc. Rev.* **2008**, *38* (1), 115–164. https://doi.org/10.1039/B804321N.

(8) Reece, S. Y.; Hodgkiss, J. M.; Stubbe, J.; Nocera, D. G. Proton-Coupled Electron Transfer: The Mechanistic Underpinning for Radical Transport and Catalysis in Biology. *Philosophical Transactions of the Royal Society B: Biological Sciences* **2006**, *361* (1472), 1351–1364. https://doi.org/10.1098/rstb.2006.1874.

(9) Hambourger, M.; Moore, G. F.; Kramer, D. M.; Gust, D.; Moore, A. L.; Moore, T. A. Biology and Technology for Photochemical Fuel Production. *Chem. Soc. Rev.* **2008**, *38* (1), 25–35. https://doi.org/10.1039/B800582F.

(10) von Caemmerer, S.; Farquhar, G. D. Some Relationships between the Biochemistry of Photosynthesis and the Gas Exchange of Leaves. *Planta* **1981**, *153* (4), 376–387. https://doi.org/10.1007/BF00384257.

(11) von Caemmerer, S.; Farquhar, G. D. Some Relationships between the Biochemistry of Photosynthesis and the Gas Exchange of Leaves. *Planta* **1981**, *153* (4), 376–387. https://doi.org/10.1007/BF00384257.

(12) Kudo, A.; Miseki, Y. Heterogeneous Photocatalyst Materials for Water Splitting. *Chem. Soc. Rev.* **2008**, *38* (1), 253–278. https://doi.org/10.1039/B800489G.

(13) Xiang, Q.; Yu, J.; Jaroniec, M. Graphene-Based Semiconductor Photocatalysts. *Chem. Soc. Rev.* **2012**, *41* (2), 782–796. https://doi.org/10.1039/C1CS15172J.

(14) Kobayashi, H.; Longmire, M. R.; Ogawa, M.; Choyke, P. L. Rational Chemical Design of the next Generation of Molecular Imaging Probes Based on Physics and Biology: Mixing Modalities, Colors and Signals. *Chem. Soc. Rev.* **2011**, *40* (9), 4626–4648. https://doi.org/10.1039/C1CS15077D.
(15) Liang, L.; Liu, C.; Jiao, X.; Zhao, L.; Zeng, X. A Highly Selective and Sensitive Photoinduced Electron Transfer (PET) Based HOCl Fluorescent Probe in Water and Its Endogenous Imaging in Living Cells. *Chem. Commun.* **2016**, *52* (51), 7982–7985. https://doi.org/10.1039/C6CC02603F.
(16) Laquindanum, J. G.; Katz, H. E.; Dodabalapur, A.; Lovinger, A. J. N-Channel Organic Transistor Materials Based on Naphthalene Frameworks. *J. Am. Chem. Soc.* **1996**, *118* (45), 11331–11332. https://doi.org/10.1021/ja962461j.
(17) Katz, H. E.; Johnson, J.; Lovinger, A. J.; Li, W. Naphthalene tetracarboxylic Diimide-Based n-Channel Transistor Semiconductors: Structural Variation and Thiol-Enhanced Gold Contacts. *J. Am. Chem. Soc.* **2000**, *122* (32), 7787–7792. https://doi.org/10.1021/ja000870g.
(18) Katz, H. E.; Lovinger, A. J.; Johnson, J.; Kloc, C.; Siegrist, T.; Li, W.; Lin, Y.-Y.; Dodabalapur, A. A Soluble and Air-Stable Organic Semiconductor with High Electron Mobility. *Nature* **2000**, *404* (6777), 478–481. https://doi.org/10.1038/35006603.
(19) Wasielewski, M. R. Photoinduced Electron Transfer in Supramolecular Systems for Artificial Photosynthesis. *Chem. Rev.* **1992**, *92* (3), 435–461. https://doi.org/10.1021/cr00011a005.
(20) Fox, M. A. Photoinduced Electron Transfer. *Photochemistry and Photobiology* **1990**, *52* (3), 617–627. https://doi.org/10.1111/j.1751-1097.1990.tb01808.x.
(21) Spanggaard, H.; Krebs, F. C. A Brief History of the Development of Organic and Polymeric Photovoltaics. *Solar Energy Materials and Solar Cells* **2004**, *83* (2), 125–146. https://doi.org/10.1016/j.solmat.2004.02.021.
(22) Mentel, K. K.; Serra, A.; Abreu, P. E.; Arnaut, L. G. Higher Activation Barriers Can Lift Exothermic Rate Restrictions in Electron Transfer and Enable Faster Reactions. *Nature Communications* **2018**, *9* (1), 2903. https://doi.org/10.1038/s41467-018-05267-5.
(23) Seifert, S.; Schmidt, D.; Wurthner, F. An Ambient Stable Core-Substituted Perylene Bisimide Dianion: Isolation and Single Crystal Structure Analysis. *Chem Sci* **2015**, *6* (3), 1663–1667. https://doi.org/10.1039/c4sc03671a.
(24) Jung, C.; Müller, B. K.; Lamb, D. C.; Nolde, F.; Müllen, K.; Bräuchle, C. A New Photostable Terrylene Diimide Dye for Applications in Single Molecule Studies and Membrane Labeling. *J. Am. Chem. Soc.* **2006**, *128* (15), 5283–5291. https://doi.org/10.1021/ja0588104.
(25) Dubois, A.; Canva, M.; Brun, A.; Chaput, F.; Boilot, J.-P. Photostability of Dye Molecules Trapped in Solid Matrices. *Appl. Opt., AO* **1996**, *35* (18), 3193–3199. https://doi.org/10.1364/AO.35.003193.
(26) New Perylene and Violanthrone Dyestuffs for Fluorescent Collectors. *Dyes and Pigments***1989**, *11* (4), 303–317. https://doi.org/10.1016/0143-7208(89)85048-X.
(27) Gosztola, D.; Niemczyk, M. P.; Svec, W.; Lukas, A. S.; Wasielewski, M. R. Excited Doublet States of Electrochemically Generated Aromatic Imide and Diimide Radical Anions. *Journal of Physical Chemistry A* **2000**, *104* (28), 6545–6551. https://doi.org/10.1021/jp000706f.
(28) Zhan, X.; Tan, Z.; Domercq, B.; An, Z.; Zhang, X.; Barlow, S.; Li, Y.; Zhu, D.; Kippelen, B.; Marder, S. R. A High-Mobility Electron-Transport Polymer with Broad Absorption and Its Use in Field-

Effect Transistors and All-Polymer Solar Cells. *J. Am. Chem. Soc.* **2007**, *129* (23), 7246–7247. https://doi.org/10.1021/ja071760d.
(29) Schmidt, D.; Bialas, D.; Wurthner, F. Ambient Stable Zwitterionic Perylene Bisimide-Centered Radical. *Angew Chem Int Ed Engl* **2015**, *54* (12), 3611–3614. https://doi.org/10.1002/anie.201408067.
(30) Ghosh, I.; Ghosh, T.; Bardagi, J. I.; Konig, B. Reduction of Aryl Halides by Consecutive Visible Light-Induced Electron Transfer Processes. *Science* **2014**, *346* (6210), 725–728. https://doi.org/10.1126/science.1258232.
(31) Leira-Iglesias, J.; Sorrenti, A.; Sato, A.; Dunne, P. A.; Hermans, T. M. Supramolecular Pathway Selection of Perylenediimides Mediated by Chemical Fuels. *Chem. Commun.* **2016**, *52* (58), 9009–9012. https://doi.org/10.1039/C6CC01192F.
(32) Marcon, R. O.; Brochsztain, S. Aggregation of 3,4,9,10-Perylenediimide Radical Anions and Dianions Generated by Reduction with Dithionite in Aqueous Solutions. *J. Phys. Chem. A* **2009**, *113* (9), 1747–1752. https://doi.org/10.1021/jp808383e.
(33) Goodson, F. S.; Panda, D. K.; Ray, S.; Mitra, A.; Guha, S.; Saha, S. Tunable Electronic Interactions between Anions and Perylenediimide. *Org. Biomol. Chem.* **2013**, *11* (29), 4797–4803. https://doi.org/10.1039/C3OB40703A.
(34) Xu, Y.; Zheng, J.; Lindner, J. O.; Wen, X.; Jiang, N.; Hu, Z.; Liu, L.; Huang, F.; Würthner, F.; Xie, Z. Consecutive Charging of a Perylene Bisimide Dye by Multistep Low-Energy Solar-Light-Induced Electron Transfer Towards H_2 Evolution. *Angew. Chem.* **2020**, *132* (26), 10449–10453. https://doi.org/10.1002/ange.202001231.
(35) Schmidt, D.; Bialas, D.; Wurthner, F. Ambient Stable Zwitterionic Perylene Bisimide-Centered Radical. *Angew Chem Int Ed Engl* **2015**, *54* (12), 3611–3614. https://doi.org/10.1002/anie.201408067.
(36) Leira-Iglesias, J.; Tassoni, A.; Adachi, T.; Stich, M.; Hermans, T. M. Oscillations, Travelling Fronts and Patterns in a Supramolecular System. *Nature Nanotech* **2018**, *13* (11), 1021–1027. https://doi.org/10.1038/s41565-018-0270-4.
(37) Dehm, V.; Büchner, M.; Seibt, J.; Engel, V.; Würthner, F. Foldamer with a Spiral Perylene Bisimide Staircase Aggregate Structure. *Chem. Sci.* **2011**, *2* (11), 2094. https://doi.org/10.1039/c1sc00435b.
(38) Gershberg, J.; Fennel, F.; Rehm, T. H.; Lochbrunner, S.; Würthner, F. Anti-Cooperative Supramolecular Polymerization: A New K_2 –K Model Applied to the Self-Assembly of Perylene Bisimide Dye Proceeding via Well-Defined Hydrogen-Bonded Dimers. *Chem. Sci.* **2016**, *7* (3), 1729–1737. https://doi.org/10.1039/C5SC03759J.
(39) Wurthner, F.; Saha-Moller, C. R.; Fimmel, B.; Ogi, S.; Leowanawat, P.; Schmidt, D. Perylene Bisimide Dye Assemblies as Archetype Functional Supramolecular Materials. *Chem Rev* **2016**, *116* (3), 962–1052. https://doi.org/10.1021/acs.chemrev.5b00188.
(40) Han, J. J.; Shaller, A. D.; Wang, W.; Li, A. D. Q. Architecturally Diverse Nanostructured Foldamers Reveal Insightful Photoinduced Single-Molecule Dynamics. *J. Am. Chem. Soc.* **2008**, *130* (22), 6974–6982. https://doi.org/10.1021/ja078302p.
(41) Shaller, A. D.; Wang, W.; Li, A.; Moyna, G.; Han, J. J.; Helms, G. L.; Li, A. D. Q. Sequence-Controlled Oligomers Fold into Nanosolenoids and Impart Unusual Optical Properties. *Chem. Eur. J.* **2011**, *17* (30), 8350–8362. https://doi.org/10.1002/chem.201100612.

(42) Zhong, L.; Xing, F.; Shi, W.; Yan, L.; Xie, L.; Zhu, S. Synthesis, Spectra, and Electron-Transfer Reaction of Aspartic Acid- Functionalized Water-Soluble Perylene Bisimide in Aqueous Solution. *ACS Appl. Mater. Interfaces* **2013**, 7.
(43) Leira-Iglesias, J.; Sorrenti, A.; Sato, A.; Dunne, P. A.; Hermans, T. M. Supramolecular Pathway Selection of Perylenediimides Mediated by Chemical Fuels. *Chem. Commun.* **2016**, *52* (58), 9009–9012. https://doi.org/10.1039/C6CC01192F.
(44) Gong, H.-X.; Cao, Z.; Li, M.-H.; Liao, S.-H.; Lin, M.-J. Photoexcited Perylene Diimide Radical Anions for the Reduction of Aryl Halides: A Bay-Substituent Effect. *Organic Chemistry Frontiers* **2018**. https://doi.org/10.1039/c8qo00445e.
(45) Kasha, M.; Rawls, H. R.; El-Bayoumi, M. A. The exciton model in molecular spectroscopy. *Pure and Applied Chemistry* **1965**, *11* (3–4), 371–392. https://doi.org/10.1351/pac196511030371.

Chapter 3.

Dissipative Out-of-equilibrium Systems of Perylene Bisimide Driven by UV-Activated Chemical Fuel

Abstract: The photoreduction of perylene bisimides (PBI) has been widely studied in photocatalysis, hydrogen evolution, photo-responsive gel, and organic semiconductors. Upon UV or visible light irradiation, one or two-electron transfer to PBI radical anion ($PBI^{\bullet-}$) and dianion (PBI^{2-}) can occur under vacuum conditions. However, in the presence of O_2, it is nearly impossible to achieve photoreduction. Here, we introduce UV-activated chemical fuel acetone, which significantly accelerates the rate of photoreduction, enabling bulk-scale atmospheric photoreduction. Using our method, we could reversibly photoreduce and oxidize (by O_2) a PBI derivative for more than 10 times. Interestingly, this strategy is not limited to PBI, but also to other rylene bisimides and even methyl viologen. This brings us one step closer to photochemically controllable life-like materials.

3.1 Introduction

Supramolecular chemistry, traditionally, has been done under equilibrium conditions.[1–4] However, in living systems, the relevant thermodynamic state is not the equilibrium.[5] Inspired by the latter, recent reports show a shift towards developing life-like systems out-of-equilibrium.[6–8] Living systems can only sustain themselves because there is a continuous supply of fuels. For example, the dynamic microtubules driven by enzymes are crucial in cells.[9,10] In Supramolecular Chemistry, hierarchical structures are generally constructed by non-covalent interactions, such as hydrogen bonding[11,12], π-π stacking[13,14], and the hydrophobic effect[15,16]. The advantage of using non-covalent bonding is the reversibility of assemblies. A relatively new direction is the one taken in the growing field of Supramolecular Systems Chemistry, where using a 'chemical fuel' a building block can be turned 'on' or 'off'. In the 'on' state, the building block can assemble into supramolecular structures, whereas in the 'off' state it would disassemble.[17–19] What is of great importance is that the reactions to turn on/off are efficient and completely reversible, so many switching events can be achieved. [20]

Recently, our research group has demonstrated that supramolecular oscillation, traveling fronts, and patterns could be achieved by using chemical redox reactions (Fig. 3.1A) of perylene bisimides (PBI). [21] In the latter work, the PBI system was oscillating in cycles between aggregates and monomeric units by continuous influx of the reductant (dithionite) and oxidant (oxygen). In one such redox cycle (Fig. 3.1B), the PBI aggregates first get reduced to the dianion PBI^{-2} and therefore disassemble. Next, the dianions can be oxidized back to the neutral PBI, resulting in nucleation and growth into colloidal aggregates. In the oscillating regime (Fig. 3.1C), positive feedback stems from the cooperative supramolecular polymerization of PBI. That is, the assembly rate keeps increasing sharply when going from an all-monomeric state to the colloidal state. On the other hand, there is also a negative feedback mechanism. Namely, the chemical reduction by dithionite is size-dependent. Larger colloids will take longer to reduce and disassemble, as compared to smaller aggregates (or monomers). The nonlinearity of the kinetics of the assembly/disassembly and the reduction, are key in pushing the system far from equilibrium. In addition, interesting spatiotemporal behaviors, such as traveling fronts, and patterns were observed in that system.

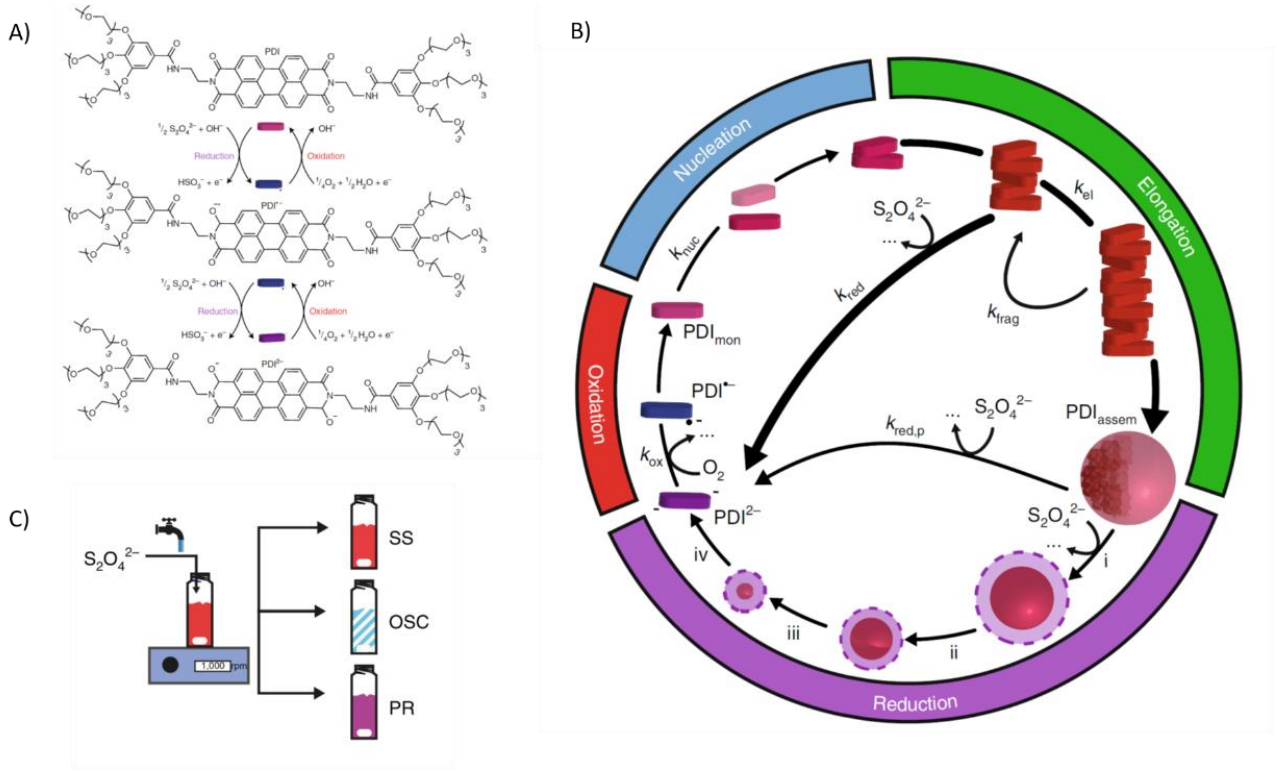

Figure 3.1. **Prior work from the group, in which chemical redox drives PBI oscillating between the monomer and aggregates.** (A) PBI is chemically reduced into $PBI^{\bullet-}$ and dianion PBI^{-2} upon the addition of $Na_2S_2O_4$. By introducing oxygen, spontaneous oxidation leads first to a radical anion $PBI^{\bullet-}$ and then to the neutral PBI. (B) The scheme of PBI assembly and disassembly driven by $Na_2S_2O_4$ and O_2. Upon chemical reduction, PBI aggregates disassemble into monomer due to electronic repulsions. In a subsequent oxidation (by O_2), the electronically active $PBI^{\bullet-}$/ PBI^{2-} revert to PBI and further re-aggregate. (C) When the chemical reduction and oxidation simultaneously occur in a semi-batch reactor, where the reductant $Na_2S_2O_4$ was constantly flowed in, while and the oxidant molecular dioxygen was introduced by keeping stirring solution. Under certain conditions, the oscillation was observed in a narrow window. Reproduced from ref. 21 with permission from Nature.

A general issue in chemically fueled system is that chemical reactions produce waste products. The accumulation of the latter often leads to poisoning or dampening of the response of the system (i.e., the on/off switching gets fatigued)[18]. In contrast to chemical fuels, light-based switching can be done reversibly and repeatedly without producing any chemical waste.[22] For example, the photoisomerization of azobenzene and diarylethene[19,23], has been employed to regulate the assembly and disassembly of supramolecular aggregates. The trans-cis transformation of azobenzene is reversible under UV light irradiation and heating, whereas the morphological transformation of aggregates constructed by diarylethene can be regulated via the open and closed ring conformations, using different wavelength illumination. As mentioned earlier, PBI is an ideal candidate as building blocks that can transform between aggregates and

monomers.[24] Additionally, PBI is a good acceptor due to the electron deficiency of perylene core[25,26], and can be photoreduced. Several groups have reported one or two-electron transfer in solution or gels under vacuum conditions.[27,28] Although the $PBI^{\bullet-}$ and PBI^{2-} can be easily formed with PBI aggregates under vacuum (see Chapter 2), only one photoredox cycle is achieved after oxygen is introduced into the sealed cuvette. If more photoredox cycles are required, additional degassing steps would be necessary. It thus remains a challenge to accumulate work with reduced PBI under ambient conditions, which we want to overcome in this chapter.

In photochemistry, the carbonyl chromophore is widely used to study H abstraction or charge transfer.[29–31] Acetone, especially, shows a dramatic photo-reactivity when it is in singlet or triplet excited sate. [32] In the presence of amines[33,34], upon UV irradiation, amine-acetone exciplex forms a singlet excited state; the acetone radical, further, generated by charge separation. In this scenario, acetone is being a UV-activated chemical fuel, meanwhile, as an electron acceptor to TEOA. Herein, we show a photo-driven system, where perylene bisimide can efficiently be reduced under ambient conditions by a UV-activated chemical fuel—acetone. As shown in Figure 3.2A, an acetone[35] radical initialized by UV irradiation was used to fuel the formation of the dianion **PBI-1**$^{2-}$ in the presence of O_2, thus allowing the assembly/disassembly of the **PBI-1** aggregates under ambient conditions. Interestingly, we could kinetically control the rate of the reaction by adjusting the amount of acetone, such that increasing to 9% vol of acetone in buffer significantly accelerated the rate of the reaction. Thus, the photoreduction and oxidation simultaneously occur in the presence of light under ambient conditions, which pushed the system away from equilibrium. And we can selectively obtain the **PBI-1**$^{\bullet-}$ and **PBI-1**$^{2-}$ by introducing the different chemical fuels. Additionally, we also developed other photo-driven out of equilibrium assemblies under ambient oxygen, such as PBI-alanine (PBIA), napthalenedimide-aminoisophthalic acid (NDI), and methyl viologen (MV).

3.2 Monomeric PBI-1 Photoreduction by UV-activated Acetone

As shown in Chapter 2, **PBI-1** monomer in DMF solutions has three characteristic absorption maxima at 456, 490, and 525 nm. In contrast to the conditions in chapter 2 (i.e., 33 μM **PBI-1** in

DMF, 3000 eq. of triethanolamine TEOA as a donor), where photoreduction in vacuum was achieved after 5 mins upon UVC (275 nm, 5 mW/cm^2), no reduction is observed in an open (to the ambient) cuvette. Even, after 1 hour of UVC irradiation, the UV absorbance of **PBI-1** at 525 nm (an indicator of neutral **PBI-1**) is still unchanged, as shown in Figure 3.2 A and B. The main reason is that the oxidation rate of **PBI-1**$^{\bullet-}$/ **PBI-1**$^{2-}$ is faster than the photoreduction, as shown in Chapter 2.

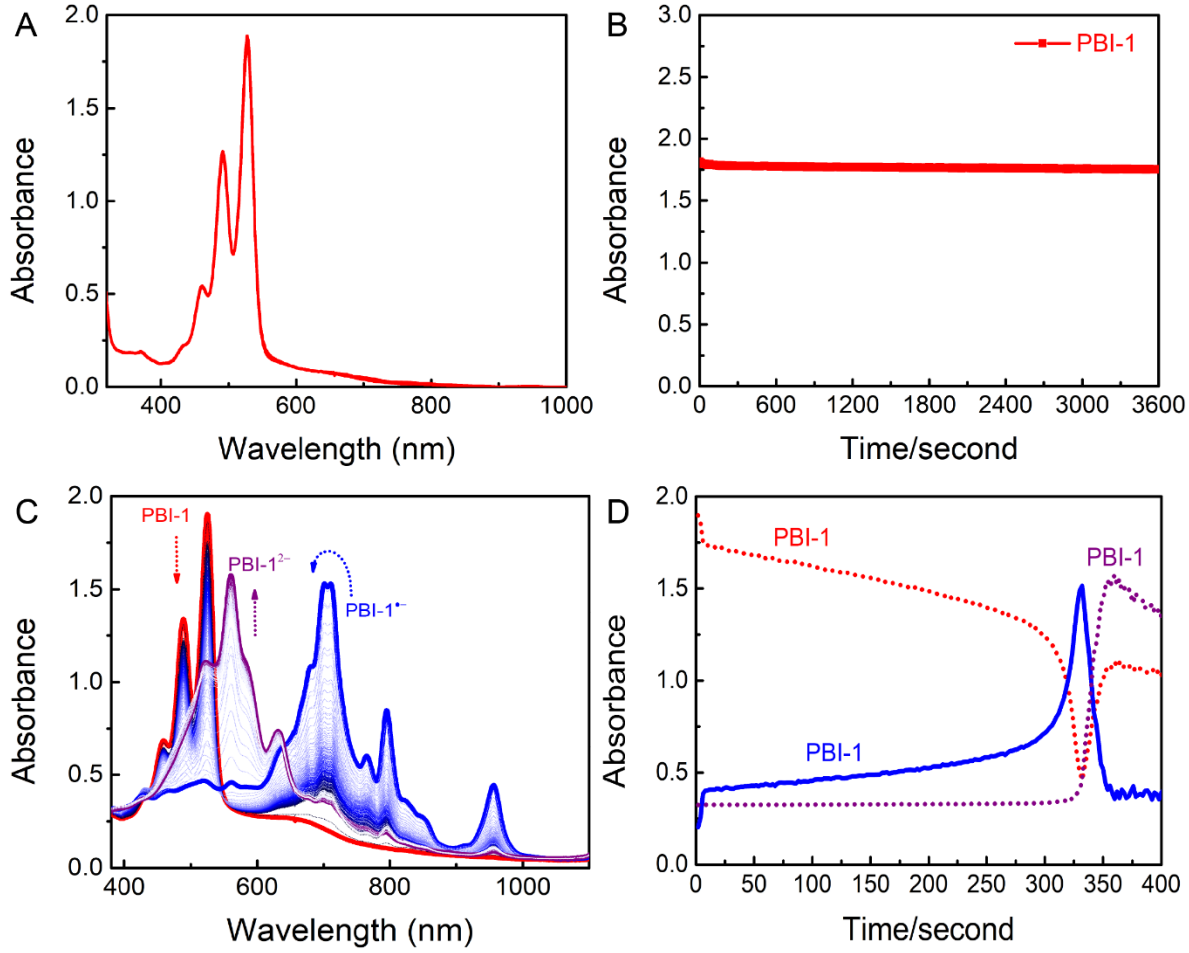

Figure 3.2. **The monomeric PBI-1 Photoreduction in DMF.** (A) The UV spectrum of 33 µM **PBI-1** with 3000 eq.of TEOA in DMF before and after 1 hour of UVC irradiation (275 nm, 5 mW/cm^2) in an opening cuvette. (B) the kinetic of the former solution irradiated by UVC 1 hour at 525 nm. (C) The UV spectrum of 33 µM **PBI-1** with 3000 eq.of TEOA in acetone (9% vol)/DMF before and after 400s of UVC irradiation (275 nm, 5 mW/cm^2) in an opening cuvette with stirring. (D) the kinetic of **PBI-1** (the same sample in C) irradiated by UVC 400s at 525 (red line), 705 (blue line), and 561 nm (purple line).

By introducing a photo-activated chemical fuel (9% vol. acetone) into the system (as earlier mentioned), however, the electron is transferred quickly, and **PBI-1** could be sequentially reduced into **PBI-1**$^{\bullet-}$ with three characteristic absorption maxima at 705, 794, and 956 nm[27], and **PBI-1**$^{2-}$ with three characteristic absorption maxima at 520, 561, and 631 nm[36] (see. Fig. 3.2C). The kinetics of **PBI-1** photoreduction is followed at 525, 705, and 561 nm corresponding to **PBI-1**, **PBI-1**$^{\bullet-}$, and **PBI-1**$^{2-}$, respectively. Figure 3.2 D demonstrates that **PBI-1**$^{2-}$ forms after **PBI-1** fully converted into **PBI-1**$^{\bullet-}$, which further proves that **PBI-1**$^{2-}$ is a sequential reaction (only **PBI-1**$^{\bullet-}$ forms in the absence of acetone in Chapter 2). This UV-activated fuel acetone provides a possibility using photoreduction to drive **PBI-1** aggregates out-of-equilibrium.

3.3 Aggregated PBI-1 Photoreduction by UV-activated Acetone

We further extend this strategy to induce aggregated **PBI-1** for electron-transfer under ambient condition. In this section, we first studied the acetone influence on the electron-transfer rate (tracked with UV-diode array). 33 μM **PBI-1** with 3000 eq. of TEOA in buffer (the solution was stirred in an open cuvette) but with different eq. of acetone, was reduced in 1 hour of UVC irradiation (275 nm, 5 mW/cm^2). At 1000 eq., no reduction occurs (see. Fig. 3.3A) and a slight degradation was observed after a UVC long irradiation. But the photoinduced electron-transfer starts with 3000 eq. of acetone (reaching **PBI-1**$^{2-}$ in 20 mins), if more acetone involved (6000, 10000 eq.), a faster reduction would take place (see Fig. 3.3C, the time taking to reach **PBI-1**$^{2-}$), which is confirmed with UV characteristic absorption (Figure 3.3B, the reduction with 10000 eq. of acetone). Especially in 20000 eq. (4.9% v/v, acetone/buffer), **PBI-1**$^{2-}$ only takes 3 mins reaching to **PBI-1**$^{2-}$ (Figure 3.3C).

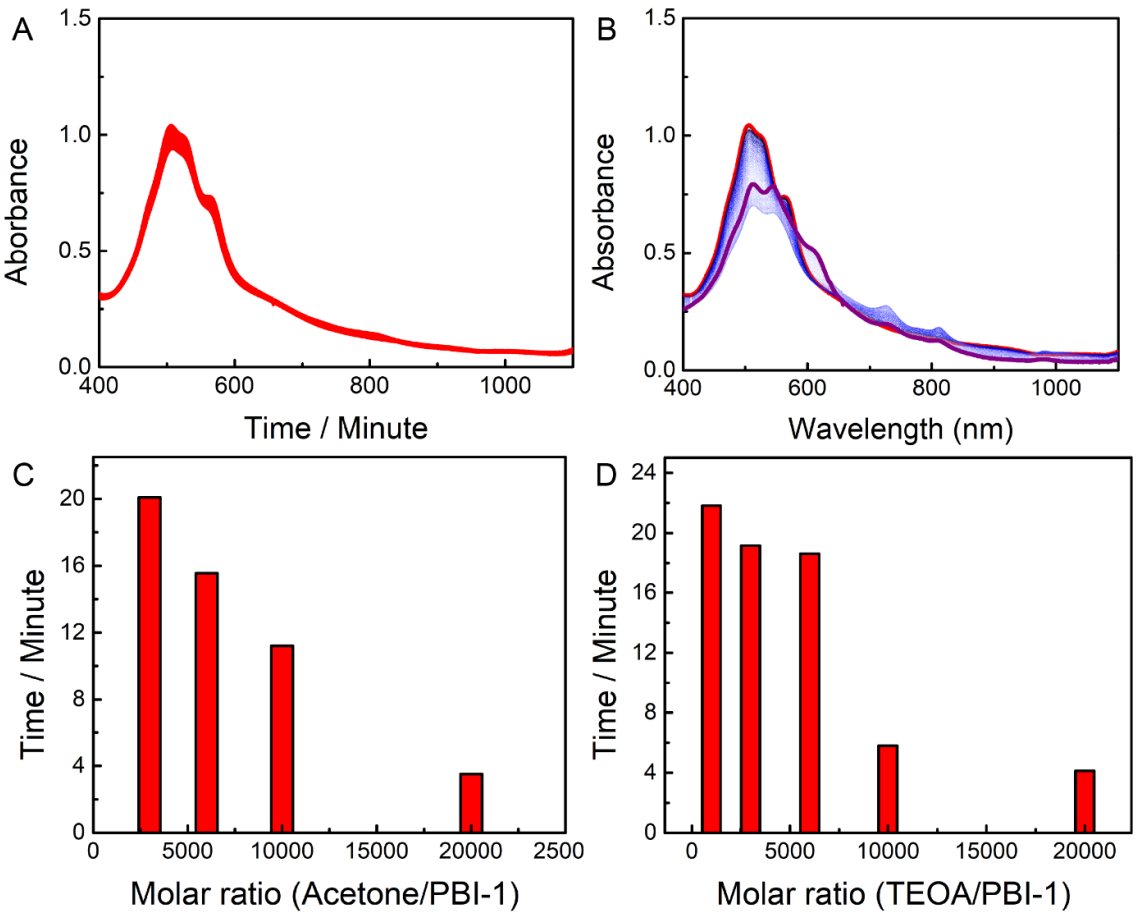

Figure 3.3. **The aggregated PBI-1 photoreduction by UV-activated acetone.** A) The UV spectra of **PBI-1** with 3000 eq. of TEOA in buffer (with 1000 eq. of acetone to **PBI-1**), in 1 hour of UVC (275 nm, 5 mW/cm^2). B) The UV spectra of **PBI-1** with 3000 eq. of TEOA in buffer (with 10000 eq. of acetone to **PBI-1**), in 1 hour of UVC (275 nm, 5 mW/cm^2). C) The reduction rate (the time needed to reach to the maximum of **PBI-1**$^{2-}$ uv absorbance at 610 nm, 33 µM **PBI-1** in buffer with 3000, 6000, 10000, 20000 eq. of acetone (with 3000 eq. of TEOA, the solution is stirred in an open cuvette) upon UVC irradiation at 3 cm. D) The reduction rate (the time needed to reach to the maximum of **PBI-1**$^{2-}$ uv absorbance at 610 nm, 33 µM **PBI-1** in buffer with 3000, 6000, 10000, 20000 eq. of TEOA (with 6000 eq. of acetone, the solution is stirred in an open cuvette) upon UVC irradiation at 3 cm.

In acetone radical generation, TEOA works as electron donor that also determines the rate of further **PBI-1** photoreduction. In contrast to a fixed concentration of TEOA, we varied TEOA from 100 to 20000 eq. (including 100, 1000, 3000, 6000, 10000 eq.) at a fixed acetone concentration (6000 eq.) to monitor the rate of photoreduction (the time needed to reach **PBI-1**$^{2-}$ when UV absorbance at 610 nm is up to the maximum). Electrons only transfer when TEOA is more than 1000 eq., after that, the reaction undergoes faster as an increase of TEOA eq.. Reaching to the final product **PBI-1**$^{2-}$ needs only 3.5 mins in comparison to 22 mins needed with 1000 eq. of TEOA (see Fig. 3.4D). In short, the first photoinduced electron-transfer between TEOA and acetone (acetone radical formation) is essential to initialize **PBI-1** photoreduction.

3.4 PBI-1 out-of-Equilibrium Systems with UV-Activated Chemical Fuels—Acetone.

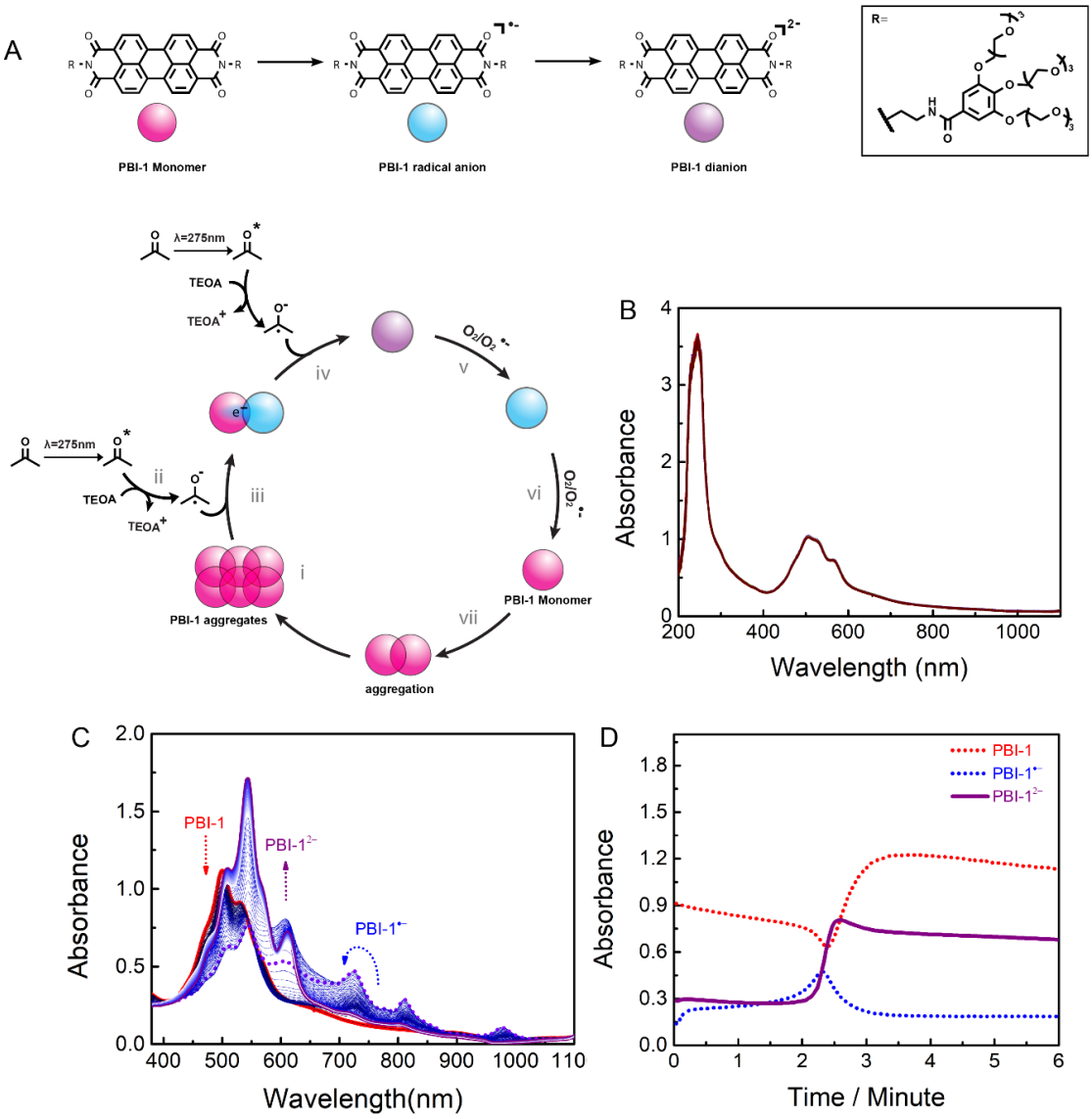

Figure 3.4. **PBI-1 out-of equilibrium assemblies driven by UV-activated acetone.** (A) The illustration of **PBI-1** out-of-equilibrium assemblies is photo-driven by UV activated chemical fuel, acetone, under ambient conditions: (i) 33 μM PBI aggregated in the bicarbonate-carbonate buffer (pH=10.80) with 9% vol acetone, in the presence of 3000 eq. of TEOA. (ii) Upon UVC LED irradiation (275 nm, 5 mW/cm^2), acetone radical forms by electron-transfer. (iii) Acetone radical as electron donor transfers electrons to **PBI-1** aggregates, leading to sequentially disassemble into smaller **PBI-1**$^{\bullet-}$/**PBI-1** aggregates. (iv) The small aggregates further disassemble with **PBI-1**$^{2-}$ formation. (v, vi) The oxidation of **PBI-1**$^{2-}$ and **PBI-1**$^{\bullet-}$ by O_2. (vii) The monomeric **PBI-1** aggregation over time. (B) UV spectra of 33 μM **PBI-1** aggregate in the bicarbonate-carbonate buffer (pH=10.80), in the presence of 3000 eq, before and after UVC irradiation. (C) Adding 9% vol acetone in sample (B), UV spectra of **PBI-1** aggregates irradiated by UVC 6 mins. (D) The kinetics of **PBI-1**, **PBI-1**$^{\bullet-}$, and **PBI-1**$^{2-}$ by followed UV absorbance at 526, 725, and 543 nm, respectively.

We have explored the influence of TEOA and acetone on the rate of **PBI-1**$^{2-}$ formation. Herein we used an optimized condition to establish an efficient photoreduction system pushing **PBI-1** assemblies out-of-equilibrium. First, as a control experiment, upon UVC irradiation there is no reduction and UV absorption is unchanged in the absence of acetone when **PBI-1** solution (33 μM **PBI-1** with 3000 eq. of TEOA in buffer) was rigorously stirred (introducing O_2) in an open cuvette, as shown in Figure 3.4B. When 9% vol of acetone was added into the former system, electron quickly transfers. **PBI-1** could be sequentially reduced into **PBI-1**$^{\bullet-}$ with three characteristic absorption maxima at 725, 811, and 981 nm, and **PBI-1**$^{2-}$ with three characteristic absorption maxima at 507, 542, and 610 nm (see Fig. 3.4).

Acetone is not a normal 'chemical fuel' but rather a 'pre-fuel'. It can stay dormant in the system, but upon exposure to UVC it can be activated. Specifically, UVC (275 nm) irradiation excites acetone, which then abstracts one electron from the donor TEOA forming acetone radicals (see Fig. 3.4A, step ii).[32] Next, the electron-rich acetone radical donates electrons to **PBI-1** aggregates, resulting in the formation of **PBI-1**$^{\bullet-}$/ **PBI-1**$^{2-}$ by one- or two-electron transfer Fig. 3.4A, step iii), leading to a disassembly due to electronic repulsion. When the UVC irradiation was stopped, the **PBI-1**$^{\bullet-}$/ **PBI-1**$^{2-}$ was spontaneously re-oxidized back to the neutral PBI-1 (Fig. 3.4A, step iv, v), as one would expect. Over time, **PBI-1** cooperatively polymerizes back to its aggregated state (as our group previously characterized with DLS).[21]

The kinetics of all **PBI-1** species were recorded with a home-modified UV-diode array (see Chapter 2) in real time. Figure 3.4 C shows that more **PBI-1**$^{2-}$ forms in the presence of 9% vol of acetone in buffer comparing to the studied with 2.45% vol. of acetone (namely, 10000 eq., as shown in Fig. 3.3B). Since this redox undergoes under ambient oxygen, the **PBI-1** reduction competes with **PBI-1**$^{\bullet-}$/ **PBI-1**$^{2-}$ oxidation. If less acetone involved, the oxidation would be in a dominant role, leading to a fast backward oxidation, namely, less **PBI-1**$^{\bullet-}$/ **PBI-1**$^{2-}$ formation. To get further insights into the depolymerization process, we tracked the kinetics of UV absorbance at 526, 725, and 543 nm corresponding to **PBI-1**, **PBI-1**$^{\bullet-}$, and **PBI-1**$^{2-}$, respectively. In contrast to reported in Chapter 2 (**PBI-1**$^{\bullet-}$ and **PBI-1**$^{2-}$ simultaneously forms in the beginning of photoreduction), **PBI-1**$^{\bullet-}$ first forms in 2 mins accompanied by a decrease of **PBI-1**, sequentially followed by **PBI-1**$^{2-}$ formation. When the absorbance of **PBI-1**$^{\bullet-}$ reaches a plateau at 2.4 mins, **PBI-1**$^{2-}$ formation has

an exponential growth (Figure 3.4D). This implies that the aggregated **PBI-1**$^{2-}$ formation assisted with acetone is a sequential reaction. But, still, non-linear depolymerization affects the reduction rate, resulting in **PBI-1**$^{2-}$ formation before **PBI-1**$^{\bullet-}$ reaches its maximum (In monomeric **PBI-1** photoreduction, **PBI-1**$^{2-}$ only forms when **PBI-1**$^{\bullet-}$ reaches its maximum).

3.5 Repeatability and reversibility of the photoredox cycle.

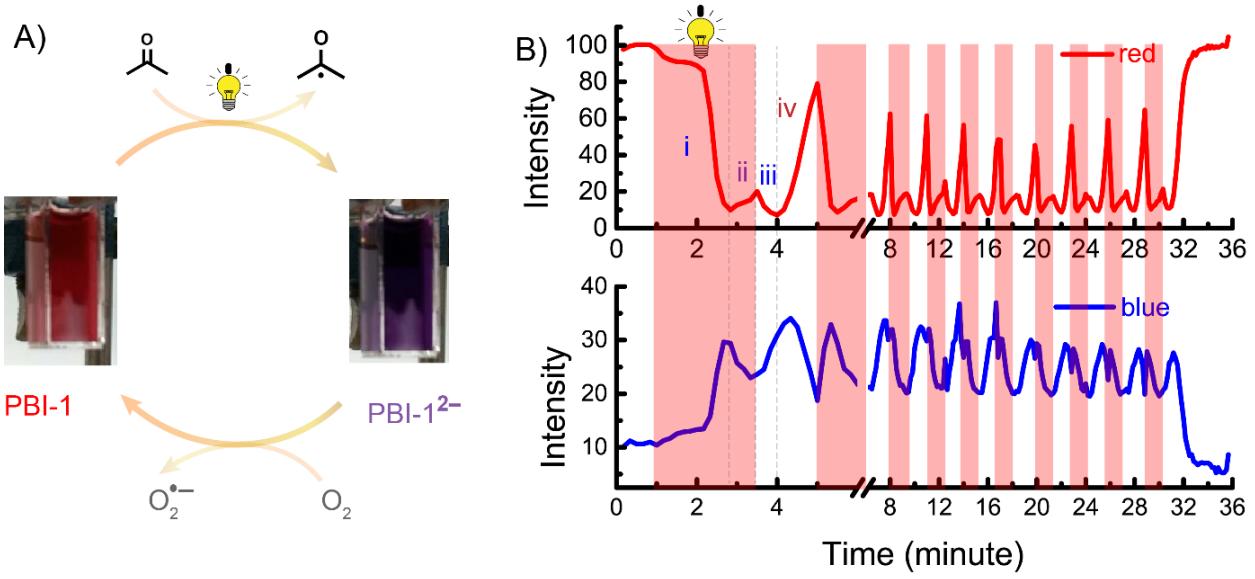

Figure 3.5. **Multiple PBI-1 photoredox cycles.** A) The image of **PBI-1** in buffer (2.25 mL, 50 µM, 3000 eq. of TEOA) with acetone (9% vol) before and after photoreduction. (B) 10 photoredox cycles of the former solution (constantly stirring solution for introducing O_2) by switching on/off light was tracked by the camera. The red and blue channel represents the evolution of **PBI-1** species: The reduction of **PBI**$^{-1}$ to **PBI-1**$^{\bullet-}$ (as step i), and **PBI-1**$^{\bullet-}$ to **PBI-1**$^{2-}$ (as step ii). The oxidation of **PBI-1**$^{2-}$ to **PBI-1**$^{\bullet-}$ as step iii, and **PBI-1**$^{\bullet-}$ to **PBI-1** as step iv.

PBI-1 aggregates can be disassembled and re-assembled with multiple redox cycles in the presence of UV-activated pre-fuel, acetone. Because the absorbance of **PBI-1** in the buffer is saturated in UV/vis spectroscopy, we used a camera to track the kinetics of the depolymerization. The evolution of the intensity of the red and blue channels represents the process of the **PBI-1** photoreduction. **PBI-1** aggregates (2.25 mL, 50 µM) in buffer with 9% vol acetone in the presence of 3000 eq. of TEOA was irradiated by the UVC LED, but along with the constant introduction of O_2 by 500 rpm stirring rate, which was sequentially reduced into **PBI-1**$^{\bullet-}$ and **PBI-1**$^{2-}$. In the first 3.5 minutes, the **PBI-1** solution was reduced into **PBI-1**$^{\bullet-}$, corresponding to the red channel (Figure

3.5, step i), reaching the minimum; however, the intensity arises as purple **PBI-1**$^{2-}$ forms (step ii). By switching off the UVC, the **PBI-1**$^{2-}$ was re-oxidized back to the **PBI-1**$^{\bullet-}$, thus, the red channel back to the minimum intensity (step iii); finally, **PBI-1**$^{\bullet-}$ reverted the neutral **PBI-1** when the red intensity backs to the maximum (step iv). By switching on and off the UVC LED every 90 seconds, the photoredox can be cycled 10 times. Interestingly, the second reduction is faster than the first, which indicates that (similarly to previous work from the group[21]), the photoreduction is faster during the assembly phase of **PBI-1** versus fully assembled **PBI-1** aggregates. The way to understand the latter is the following: fully formed **PBI-1** assemblies are micro-sized whereas during the assembly phase they are 1-2 order of magnitude smaller. The surface-to-volume ratio is therefore much greater when **PBI-1** is still assembling, and therefore, the photoreduction (either directly abstracting an electron from TEOA or via the acetone pathway) is faster. Due to the high photostability of **PBI-1**, many photoreduction/oxidation cycles can be performed, even in the presence of oxygen.

3.6 Selectively Photoinduced Electron-Transfer by UV-Activated Chemical Fuel—Terephthaldehyde.

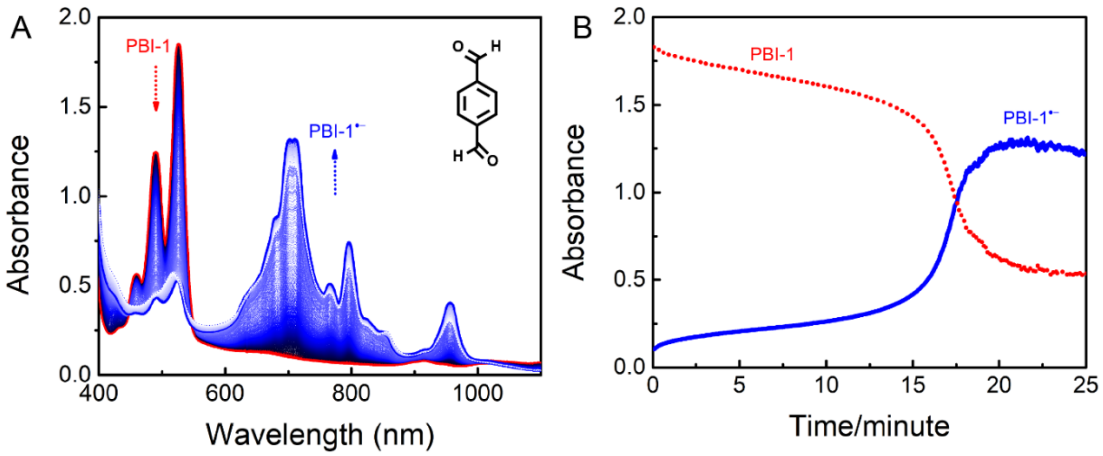

Figure 3.6. **Photoreduction of PBI-1 with UV-activated terephthaldyhyde.** A) The UV spectra of **PBI-1** in DMF (33 µM with 3000 eq. of TEOA and 6000 eq. of terephthaldyhyde) evolution to **PBI-1**$^{\bullet-}$ upon UVC irradiation. B) the kinetics of **PBI-1**, and **PBI-1**$^{\bullet-}$ at 525, and 706 nm in 25 mins UVC irradiation.

We herein explore another UV-activated prefuel terephthaldyhyde to precisely achieve one-eletron transfer under ambient oxygen. **PBI-1** (33 µM) with 6000 eq. of terephthaldehyde in the

presence of 3000 eq. of TEOA in DMF (the solution was stirred), was irradiated by UVC (275 nm, 5 mW/cm^2). After 15 mins, **PBI-1**$^{\bullet-}$ was generated with three characteristic absorption maxima at 705, 794, and 956 nm (Fig. 3.6A). The kinetics at 525 and 706 nm were followed by UV-diode array, indicative of **PBI-1** and **PBI-1**$^{\bullet-}$, respectively. In 20 mins of UVC irradiation, the absorbance of **PBI-1**$^{\bullet-}$ as a final product reaches a plateau (Fig. 3.6B, in contrast to the intermediate **PBI-1**$^{\bullet-}$ fueled by acetone as in Figure 3.2C)

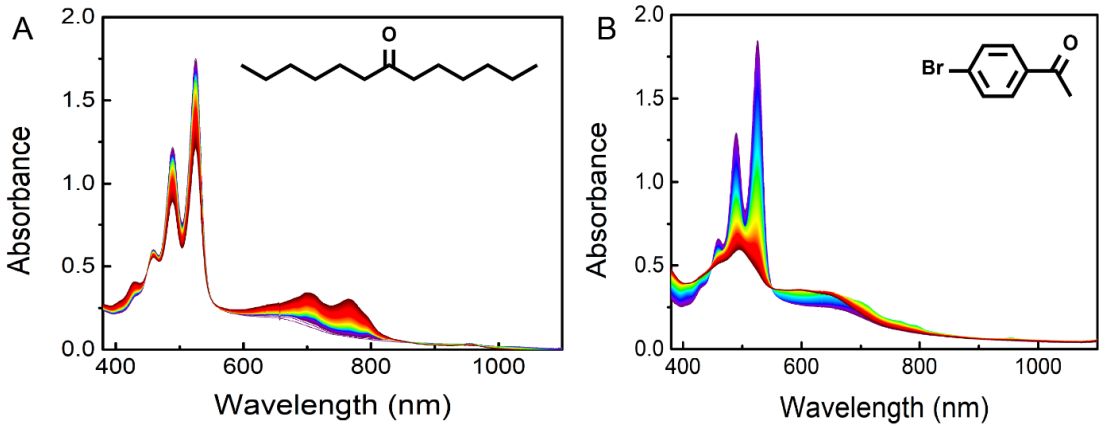

Figure 3.7. **The photoirradiation of PBI-1 with dihexyl ketone, or 4'-Bromoacetophenone.** A) The UV spectra of **PBI-1** in DMF (33 µM with 3000 eq. of TEOA and 6000 eq. of dihexyl ketone) upon UVC irradiation 1 hour. B) The UV spectra of kinetics of **PBI-1** with 4'-Bromoacetophenone in DMF (the same condition as the former experiment).

In addition, we explored other ketones as chemical fuels to initialize **PBI-1** reduction. The same condition as we used as the terephthaldyhyde case, dihexyl ketone, or aromatic ketone – 4'-Bromoacetophenone even have carbonyl group but fail to facilitate **PBI-1** redcution. Figure 3.7 A and B shows that after 1 hour of UVC irradiation photodegradation takes place. In short, some carbonyl compounds can be UV-activated fuels to induce **PBI-1** photoreduction.

3.7 Acetone as a general aid in ambient photoreduction

We explored the generality of our photoreduction approach by trying to photoreduce other dyes in presence of acetone. Namely, PBI alanine (**PBIA**), napthalenedimide-aminoisophthalic acid (NDI-PA), and methyl viologen. These dyes are widely used as building blocks in supramolecular aggregates, for example, methyl viologen in host–guest chemistry with cucurbiturils[37]. The first one we explored was PBI alanine (Figure 3.8 A) in a non-degassed aqueous solution in a closed

cuvette, which was sequentially photoreduced into **PBIA**$^{\bullet-}$ and **PBIA**$^{2-}$ in only 40 seconds (Figure 3.8 B). This is even quicker than normal azo-benzene(450-W xenon arc lamp, 5 mins irradiation)[38] or diarylethene (590 nm, 30 min, 250– 255 mW)[39] switches reported so far.

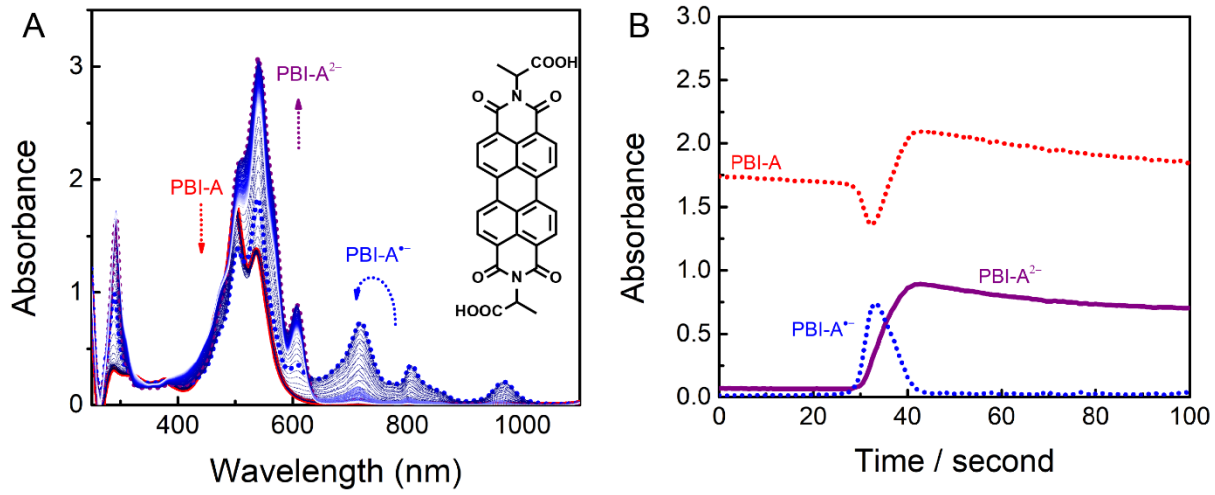

Figure 3.8. **The photoreuduction of PBI-alanine fueled by acetone.** A, B) the kinetic of **PBIA** (PBI-alanine) aggregates photoreduction in100s of UVC irradiation, 46.7 µM PBI in buffer with 9% acetone, in the presence of O_2. The evolution of the neutral **PBIA**, **PBIA**$^{\bullet-}$, and **PBIA**$^{2-}$ was followed by a UV-diode array at 525, 711, and 611 nm, respectively.

In addition, naphthalene bisimide (NDI) and methyl viologen are frequently used as electron acceptors. Figure 3.9 A shows that charge-neutral NDI-PA mainly absorbs at 353 nm, which is quickly consumed as the NDI-PA$^{\bullet-}$ is generated with absorption maxima 309, 438, and 821 nm[40–43], again in only 40 seconds upon UVC irradiation.

Lastly, also methyl viologen (Fig 3.9B) can be reduced in 70 seconds upon UVC irradiation, showing MV$^{\bullet-}$ signals at 312, 390, and 600 nm[44,45]. For **PBI-1** and PBI-alanine we noticed that photodegradation can occur under long time UVC irradiation. To resolve this issue, there are two solutions: (1) selecting an optimum amount of acetone and donor TEOA, which can quickly transform **PBI-1** into radicals without, or with extremely less decomposition, because the **PBI-1** radical anion and dianion is much more stable as literature reported[46,47], and (2) We can prevent the decomposition by introducing DABCO[32], which inhibits the formation of singlet oxygen in water, thus slowing down the decomposition rate. Overall, our approach of using photoexcited acetone as an aid in achieving rapid photoreduction is working for quite different classes of molecules,and can be a steppingstone to develop light-driven materials.

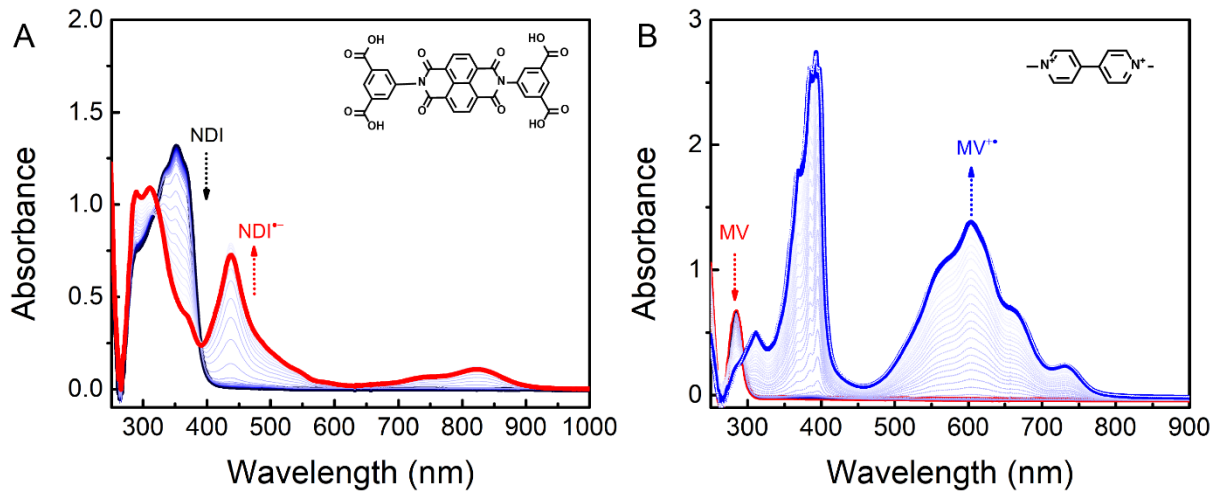

Figure 3.9. **The photoreduction of NDI and methyl viologen by UV-activated acetone.** A, B) The UV spectra of napthalenedimide-aminoisophthalic acid (NDI) (100 µM), and methyl viologen (134 µM) photoreduction with 3000 eq. TEOA in buffer with 9% acetone, upon UVC irradiation, in the presence of O_2. NDI absorbs at 353 nm, but $NDI^{\bullet-}$ absorbs at 309, 438, and 821 nm. the neutral MV absorbs at 285 nm, whereas $MV^{\bullet-}$ absorbs at 312, 390, and 600 nm.

3.8 Conclusions

In conclusion, we have drastically improved the rates of **PBI-1** photoreduction by using a UV-activated chemical pre-fuel—acetone, even in the presence of O_2. We found that, similarly to the photoreduction under inert conditions in Chapter 2, the **PBI-1** is first reduced to **PBI-1**$^{\bullet-}$ and then sequentially to **PBI-1**$^{2-}$. The acetone approach also works for helping in the photoreduction of other rylene bisimides, such as perylene alanine, NDI, and for methyl viologen. It is therefore an easy to implement approach in life-like materials where photoreduction and oxidation by air need to be balanced.

3.9 Acknowledgements

Chunfeng Chen performed the synthesis and all the experiments apart from the compound napthalenedimide-aminoisophthalic acid (NDI), that was synthesized by Michaela Schicho. Prof. Thomas Hermans supervised the research.

3.10 Experimental Section

3.10.1 Compound and Chemicals: The building blocks perylene bisimides (PBI-1) were synthesized as described in chapter 2. Perylene bisimide- alanine (PBIP)[48], and Napthalenebisimide-aminoisophthalic acid (NDI)[49] were synthesized as reported in literature by coupling perylene bisimide and alanine, and napthalenebismide and aminoisophthalic acid, respectively. Methyl viologen and all the other chemicals and solvents were purchased from Sigma-Aldrich, TCI, and VWR without further purification.

3.10.2 UV-vis Measurements. UV/vis spectra were taken by Home-modified UV-diode array 8454. The holder with four windows was 3D-printed, which allows the UVC LED (275 nm, 5.0 mW) to constantly excite the sample from the sidewall of 1cm quartz cuvette.

3.10.3 PBI-1/ NDI/Methyl Viologen Photoreduction. 33 μM PBI-1 (46.7 μM PBI-alanine, 100 μM NDI, or 134 μM methyl viologen) in 3 mL bicarbonate-carbonate buffer with 9% v/v acetone, in the presence of 3000 eq. of TEOA, which was stirred at 500 rpm, and simultaneously irradiated by UVC LED (275nm, 5mW) in a 1 cm open cuvette. The distance between UVC LED and sample holder is 2 cm.

3.11 References

(1) Zhao, T.; Han, J.; Duan, P.; Liu, M. New Perspectives to Trigger and Modulate Circularly Polarized Luminescence of Complex and Aggregated Systems: Energy Transfer, Photon Upconversion, Charge Transfer, and Organic Radical. *Acc. Chem. Res.* **2020**, *53* (7), 1279–1292. https://doi.org/10.1021/acs.accounts.0c00112.

(2) Liu, M.; Zhang, L.; Wang, T. Supramolecular Chirality in Self-Assembled Systems. *Chem. Rev.* **2015**, *115* (15), 7304–7397. https://doi.org/10.1021/cr500671p.

(3) Iseki, S.; Nonomura, K.; Kishida, S.; Ogata, D.; Yuasa, J. Zinc-Ion-Stabilized Charge-Transfer Interactions Drive Self-Complementary or Complementary Molecular Recognition. *J. Am. Chem. Soc.* **2020**, *142* (37), 15842–15851. https://doi.org/10.1021/jacs.0c05940.

(4) Roche, C.; Sun, H.-J.; Prendergast, M. E.; Leowanawat, P.; Partridge, B. E.; Heiney, P. A.; Araoka, F.; Graf, R.; Spiess, H. W.; Zeng, X.; Ungar, G.; Percec, V. Homochiral Columns Constructed by Chiral Self-Sorting During Supramolecular Helical Organization of Hat-Shaped Molecules. *J. Am. Chem. Soc.* **2014**, *136* (19), 7169–7185. https://doi.org/10.1021/ja5035107.

(5) Weisenberg, R. C.; Deery, W. J.; Dickinson, P. J. Tubulin-Nucleotide Interactions during the Polymerization and Depolymerization of Microtubules. *Biochemistry* **1976**, *15* (19), 4248–4254. https://doi.org/10.1021/bi00664a018.

(6) van Rossum, S. A. P.; Tena-Solsona, M.; van Esch, J. H.; Eelkema, R.; Boekhoven, J. Dissipative Out-of-Equilibrium Assembly of Man-Made Supramolecular Materials. *Chem. Soc. Rev.* **2017**, *46* (18), 5519–5535. https://doi.org/10.1039/C7CS00246G.

(7) Mattia, E.; Otto, S. Supramolecular Systems Chemistry. *Nature Nanotechnology* **2015**, *10* (2), 111–119. https://doi.org/10.1038/nnano.2014.337.

(8) Grzybowski, B. A.; Huck, W. T. S. The Nanotechnology of Life-Inspired Systems. *Nature Nanotechnology* **2016**, *11* (7), 585–592. https://doi.org/10.1038/nnano.2016.116.

(9) Valiron, O.; Caudron, N.; Job, D. Review Microtubule Dynamics. **2001**, *58*, 16.

(10) Muroyama, A.; Lechler, T. Microtubule Organization, Dynamics and Functions in Differentiated Cells. *Development* **2017**, *144* (17), 3012–3021. https://doi.org/10.1242/dev.153171.

(11) de Greef, T. F. A.; Meijer, E. W. Supramolecular Polymers. *Nature* **2008**, *453* (7192), 171–173. https://doi.org/10.1038/453171a.

(12) Haino, T. Molecular-Recognition-Directed Formation of Supramolecular Polymers. *Polymer Journal* **2013**, *45* (4), 363–383. https://doi.org/10.1038/pj.2012.144.

(13) Burattini, S.; Colquhoun, H. M.; Fox, J. D.; Friedmann, D.; Greenland, B. W.; Harris, P. J. F.; Hayes, W.; Mackay, M. E.; Rowan, S. J. A Self-Repairing, Supramolecular Polymer System: Healability as a Consequence of Donor–Acceptor π–π Stacking Interactions. *Chem. Commun.* **2009**, No. 44, 6717–6719. https://doi.org/10.1039/B910648K.

(14) Venkata Rao, K.; Miyajima, D.; Nihonyanagi, A.; Aida, T. Thermally Bisignate Supramolecular Polymerization. *Nature Chemistry* **2017**, *9* (11), 1133–1139. https://doi.org/10.1038/nchem.2812.

(15) Fukui, T.; Sasaki, N.; Takeuchi, M.; Sugiyasu, K. Living Supramolecular Polymerization Based on Reversible Deactivation of a Monomer by Using a 'Dummy' Monomer. *Chem. Sci.* **2019**, *10* (28), 6770–6776. https://doi.org/10.1039/C9SC02151E.

(16) Gruschwitz, F. V.; Klein, T.; Catrouillet, S.; Brendel, J. C. Supramolecular Polymer Bottlebrushes. *Chem. Commun.* **2020**, *56* (38), 5079–5110. https://doi.org/10.1039/D0CC01202E.
(17) Dambenieks, A. K.; Vu, P. H. Q.; Fyles, T. M. Dissipative Assembly of a Membrane Transport System. *Chem. Sci.* **2014**, *5* (9), 3396–3403. https://doi.org/10.1039/C4SC01258E.
(18) Debnath, S.; Roy, S.; Ulijn, R. V. Peptide Nanofibers with Dynamic Instability through Nonequilibrium Biocatalytic Assembly. *J. Am. Chem. Soc.* **2013**, *135* (45), 16789–16792. https://doi.org/10.1021/ja4086353.
(19) de Jong, J. J. D.; Hania, P. R.; Pug?lys, A.; Lucas, L. N.; de Loos, M.; Kellogg, R. M.; Feringa, B. L.; Duppen, K.; van Esch, J. H. Light-Driven Dynamic Pattern Formation. *Angew. Chem. Int. Ed.* **2005**, *44* (16), 2373–2376. https://doi.org/10.1002/anie.200462500.
(20) Boekhoven, J.; Hendriksen, W. E.; Koper, G. J. M.; Eelkema, R.; van Esch, J. H. Transient Assembly of Active Materials Fueled by a Chemical Reaction. *Science* **2015**, *349* (6252), 1075–1079. https://doi.org/10.1126/science.aac6103.
(21) Leira-Iglesias, J.; Tassoni, A.; Adachi, T.; Stich, M.; Hermans, T. M. Oscillations, Travelling Fronts and Patterns in a Supramolecular System. *Nature Nanotech* **2018**, *13* (11), 1021–1027. https://doi.org/10.1038/s41565-018-0270-4.
(22) Yagai, S.; Ishiwatari, K.; Lin, X.; Karatsu, T.; Kitamura, A.; Uemura, S. Rational Design of Photoresponsive Supramolecular Assemblies Based on Diarylethene. *Chem. Eur. J.* **2013**, *19* (22), 6971–6975. https://doi.org/10.1002/chem.201300282.
(23) Rakotondradany, F.; Whitehead, M. A.; Lebuis, A.-M.; Sleiman, H. F. Photoresponsive Supramolecular Systems: Self-Assembly of Azodibenzoic Acid Linear Tapes and Cyclic Tetramers. *Chem. Eur. J.* **2003**, *9* (19), 4771–4780. https://doi.org/10.1002/chem.200304864.
(24) Leira-Iglesias, J.; Sorrenti, A.; Sato, A.; Dunne, P. A.; Hermans, T. M. Supramolecular Pathway Selection of Perylenediimides Mediated by Chemical Fuels. *Chem. Commun.* **2016**, *52* (58), 9009–9012. https://doi.org/10.1039/C6CC01192F.
(25) Zhang, X.; Lu, Z.; Ye, L.; Zhan, C.; Hou, J.; Zhang, S.; Jiang, B.; Zhao, Y.; Huang, J.; Zhang, S.; Liu, Y.; Shi, Q.; Liu, Y.; Yao, J. A Potential Perylene Diimide Dimer-Based Acceptor Material for Highly Efficient Solution-Processed Non-Fullerene Organic Solar Cells with 4.03% Efficiency. *Advanced Materials* **2013**, *25* (40), 5791–5797. https://doi.org/10.1002/adma.201300897.
(26) Zhong, Y.; Trinh, M. T.; Chen, R.; Wang, W.; Khlyabich, P. P.; Kumar, B.; Xu, Q.; Nam, C.-Y.; Sfeir, M. Y.; Black, C.; Steigerwald, M. L.; Loo, Y.-L.; Xiao, S.; Ng, F.; Zhu, X.-Y.; Nuckolls, C. Efficient Organic Solar Cells with Helical Perylene Diimide Electron Acceptors. *J. Am. Chem. Soc.* **2014**, *136* (43), 15215–15221. https://doi.org/10.1021/ja5092613.
(27) Ghosh, I.; Ghosh, T.; Bardagi, J. I.; Konig, B. Reduction of Aryl Halides by Consecutive Visible Light-Induced Electron Transfer Processes. *Science* **2014**, *346* (6210), 725–728. https://doi.org/10.1126/science.1258232.
(28) Draper, E. R.; Schweins, R.; Akhtar, R.; Groves, P.; Chechik, V.; Zwijnenburg, M. A.; Adams, D. J. Reversible Photoreduction as a Trigger for Photoresponsive Gels. *Chem. Mater.* **2016**, *28* (17), 6336–6341. https://doi.org/10.1021/acs.chemmater.6b02677.
(29) Turro, N. J.; Dalton, J. C.; Dawes, K.; Farrington, G.; Hautala, R.; Morton, D.; Niemczyk, M.; Schore, N. Molecular Photochemistry. L. Molecular Photochemistry of Alkanones in

Solution. .Alpha.-Cleavage, Hydrogen Abstraction, Cycloaddition, and Sensitization Reactions. *Acc. Chem. Res.* **1972**, *5* (3), 92–101. https://doi.org/10.1021/ar50051a002.

(30) Scaiano, J. C. Intermolecular Photoreductions of Ketones. *Journal of Photochemistry* **1973**, *2* (2), 81–118. https://doi.org/10.1016/0047-2670(73)80010-3.

(31) Salem, L. Surface Crossings and Surface Touchings in Photochemistry. *J. Am. Chem. Soc.* **1974**, *96* (11), 3486–3501. https://doi.org/10.1021/ja00818a024.

(32) Pischel, U.; Nau, W. M. Switch-Over in Photochemical Reaction Mechanism from Hydrogen Abstraction to Exciplex-Induced Quenching: Interaction of Triplet-Excited versus Singlet-Excited Acetone versus Cumyloxyl Radicals with Amines. *J. Am. Chem. Soc.* **2001**, *123* (40), 9727–9737. https://doi.org/10.1021/ja011212e.

(33) Yang, N.-C.; Elliott, S. P. Photochemistry of (s)-(+)-5-Methyl-2-Heptanone. *J. Am. Chem. Soc.* **1969**, *91* (26), 7550–7551. https://doi.org/10.1021/ja01054a078.

(34) Griller, D.; Howard, J. A.; Marriott, P. R.; Scaiano, J. C. Absolute Rate Constants for the Reactions of Tert-Butoxyl, Tert-Butylperoxyl, and Benzophenone Triplet with Amines: The Importance of a Stereoelectronic Effect. *J. Am. Chem. Soc.* **1981**, *103* (3), 619–623. https://doi.org/10.1021/ja00393a020.

(35) Yonezawa, Y.; Sato, T.; Kuroda, S.; Kuge, K. Photochemical Formation of Colloidal Silver: Peptizing Action of Acetone Ketyl Radical. *Faraday Trans.* **1991**, *87* (12), 1905. https://doi.org/10.1039/ft9918701905.

(36) Zhong, L.; Xing, F.; Shi, W.; Yan, L.; Xie, L.; Zhu, S. Synthesis, Spectra, and Electron-Transfer Reaction of Aspartic Acid-Functionalized Water-Soluble Perylene Bisimide in Aqueous Solution. *ACS Appl Mater Interfaces* **2013**, *5* (8), 3401–3407. https://doi.org/10.1021/am4004446.

(37) Liu, Y.; Yu, Y.; Gao, J.; Wang, Z.; Zhang, X. Water-Soluble Supramolecular Polymerization Driven by Multiple Host-Stabilized Charge-Transfer Interactions. *Angewandte Chemie International Edition* **2010**, *49* (37), 6576–6579. https://doi.org/10.1002/anie.201002415.

(38) Kumita, J. R.; Smart, O. S.; Woolley, G. A. Photo-Control of Helix Content in a Short Peptide. *PNAS* **2000**, *97* (8), 3803–3808. https://doi.org/10.1073/pnas.97.8.3803.

(39) Kim, Y.; Jung, H.; Choe, Y. H.; Lee, C.; Ko, S.-K.; Koun, S.; Choi, Y.; Chung, B. H.; Park, B. C.; Huh, T.-L.; Shin, I.; Kim, E. High-Contrast Reversible Fluorescence Photoswitching of Dye-Crosslinked Dendritic Nanoclusters in Living Vertebrates. *Angewandte Chemie International Edition* **2012**, *51* (12), 2878–2882. https://doi.org/10.1002/anie.201107086.

(40) Kumar, S.; Mukhopadhyay, P. Ambient Stable Naphthalenediimide Radical Ions: Synthesis by Solvent-Free, Sonication, Mechanical Grinding or Milling Protocols. *Green Chem.* **2018**, *20* (20), 4620–4628. https://doi.org/10.1039/C8GC01614C.

(41) Bhosale, S. V.; Jani, C. H.; Langford, S. J. Chemistry of Naphthalene Diimides. *Chem. Soc. Rev.* **2008**, *37* (2), 331–342. https://doi.org/10.1039/B615857A.

(42) La Porte, N. T.; Martinez, J. F.; Chaudhuri, S.; Hedström, S.; Batista, V. S.; Wasielewski, M. R. Photoexcited Radical Anion Super-Reductants for Solar Fuels Catalysis. *Coordination Chemistry Reviews* **2018**, *361*, 98–119. https://doi.org/10.1016/j.ccr.2018.01.018.

(43) La Porte, N. T.; Martinez, J. F.; Hedstrom, S.; Rudshteyn, B.; Phelan, B. T.; Mauck, C. M.; Young, R. M.; Batista, V. S.; Wasielewski, M. R. Photoinduced Electron Transfer from Rylenediimide Radical Anions and Dianions to Re(Bpy)(CO)3 Using Red and near-Infrared Light. *Chem Sci* **2017**, *8* (5), 3821–3831. https://doi.org/10.1039/c6sc05103k.

(44) Ding, J.; Zheng, C.; Wang, L.; Lu, C.; Zhang, B.; Chen, Y.; Li, M.; Zhai, G.; Zhuang, X. Viologen-Inspired Functional Materials: Synthetic Strategies and Applications. *J. Mater. Chem. A* **2019**, *7* (41), 23337–23360. https://doi.org/10.1039/C9TA01724K.
(45) Trabolsi, A.; Khashab, N.; Fahrenbach, A. C.; Friedman, D. C.; Colvin, M. T.; Cotí, K. K.; Benítez, D.; Tkatchouk, E.; Olsen, J.-C.; Belowich, M. E.; Carmielli, R.; Khatib, H. A.; Goddard, W. A.; Wasielewski, M. R.; Stoddart, J. F. Radically Enhanced Molecular Recognition. *Nature Chemistry* **2010**, *2* (1), 42–49. https://doi.org/10.1038/nchem.479.
(46) Shirman, E.; Ustinov, A.; Ben-Shitrit, N.; Weissman, H.; Iron, M. A.; Cohen, R.; Rybtchinski, B. Stable Aromatic Dianion in Water. *J. Phys. Chem. B* **2008**, *112* (30), 8855–8858. https://doi.org/10.1021/jp8029743.
(47) Marcon, R. O.; Brochsztain, S. Highly Stable 3,4,9,10-Perylenediimide Radical Anions Immobilized in Robust Zirconium Phosphonate Self-Assembled Films. *Langmuir* **2007**, *23* (24), 11972–11976. https://doi.org/10.1021/la702642h.
(48) Draper, E. R.; Walsh, J. J.; McDonald, T. O.; Zwijnenburg, M. A.; Cameron, P. J.; Cowan, A. J.; Adams, D. J. Air-Stable Photoconductive Films Formed from Perylene Bisimide Gelators. *J. Mater. Chem. C* **2014**, *2* (28), 5570–5575. https://doi.org/10.1039/c4tc00744a.
(49) Zhang, H.-Y.; Yao, L.-J.; Chen, X.; Huang, J.-Y. Two Coordination Polymers: Treatment Activity on the Bacterial Infection in the Hemodialysis Patients via Inhibiting *Staphylococcus Aureus* Survival. *Journal of Coordination Chemistry* **2020**, *73* (24), 3332–3343. https://doi.org/10.1080/00958972.2020.1846187.

Chapter 4.

Reversible Photoreduction Gels Based on Perylene Bisimides: One, or Two-Electron Selectively Transfer

Abstract: Photoresponsive gels, generally, are constructed, and in situ regulated by photoisomerization of azobenzene, or diarylethene. However, the rapid responsiveness to light-input remains a big challenge. We, here, demonstrate two types of rapid, reversible, and photoresponsive perylene bisimide- aminoisophthalic acid (PDBA) organogels with one or two-electron transfers, corresponding to PDBA radical anion ($PDBA^{\bullet -}$) and dianion ($PDBA^{2-}$). The only difference that makes two-electron transfer is in the presence of electron donor—triethylamine (TEA). Interestingly, the mechanical stiffness of the photoinduced one-electron transfer gel was enhanced, whereas two-electron transfer led to a weak gel. In comparison to the photoreduction of monomeric PDBA in DMF solution, only $PDBA^{2-}$ was photoinduced in aggregates, that is, in the gel state, owing to delocalization of electrons and slow diffusion of O_2.

4.1 Introduction

Low-molecular-weight gels generally respond to stimuli[1,2], such as pH[3,4], temperature[5,6], mechanical strength[7], light-input[8], chemicals[9,10], etc. In comparison to polymer gels, these gels are more dynamic and are often consisting of two[11–14], or more components[15–17]. An attractive feature of such gels is that by mixing and matching different components, a wide range of functional materials[18] can be obtained, without repeating the organic synthesis and purification for each material. After applying an external stimulus, these gels can show dynamic behaviors, such as gel-sol-gel transitions[19], color changes[20], locally morphological transformation[21], or optical electronic properties changes[22].

In recent years, chemical fuels have been used to regulate supramolecular structures[2,23–26], leading to interactive materials. Chemical waste (left after reaction of the chemical fuels), however, poses an obstacle when one wants to achieve repeated changes in the interactive material. Compared to chemical fuels, light can be an ideal energy input to in situ regulate supramolecular morphologies without any extra chemical additives[27]. The light intensity, wavelength, or polarization[28,29], are key elements that need to be controlled. Often, light-controllable systems consist of a photochromic molecule that is also a gelator.

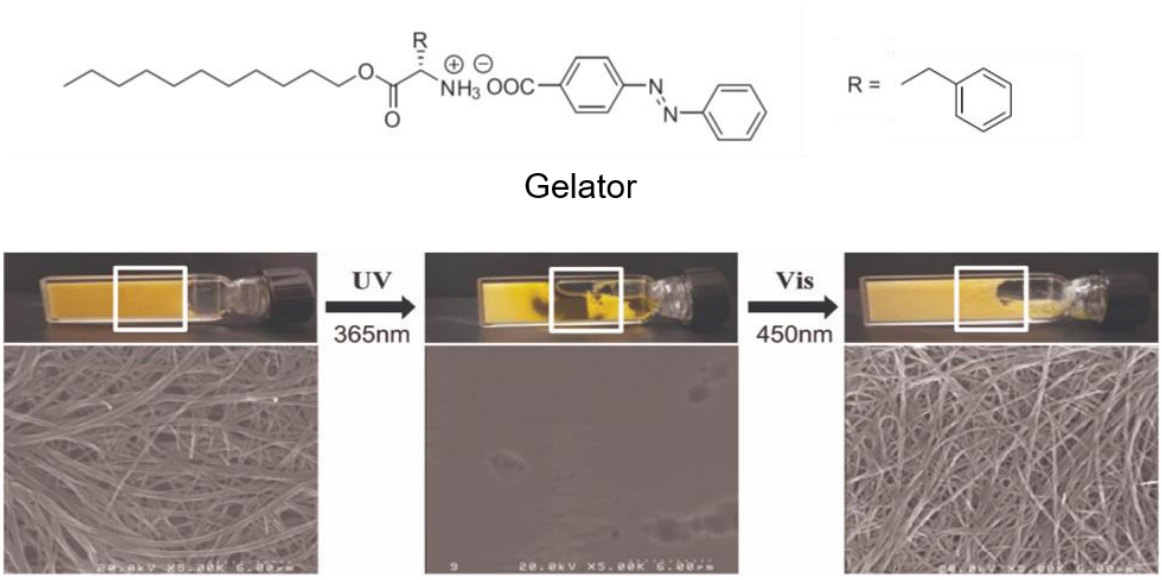

Figure 4.1. The molecular structure of the gelator, and the SEM images of the sample before and after UV, visible light irradiation: Left) before UV 365 nm irradiation. Center) after UVA 365 nm irradiation 4h. Right) after visible light irradiation 30 mins. Reproduced from ref. 33 with permission from the Elsevier.

A prime examples is azobenzene, which can be photo-isomerized by switching UV/visible light or by heating[30–32]. The thermodynamically favorable trans-form is isomerized into the less stable cis-azobenzene upon UVA irradiation, and reverts to the former when exposed to visible light or upon heating. As an example (Figure 4.1), an organic gelator in its trans-form assembled into nanofibers[33], leading to yellow gels. Upon UVC irradiation for 4 hours, the trans-azobenzene was photoisomerized into the cis-form, which causes the gel to fall apart. But the gel could be restored upon exposure to visible light (at 450 nm).

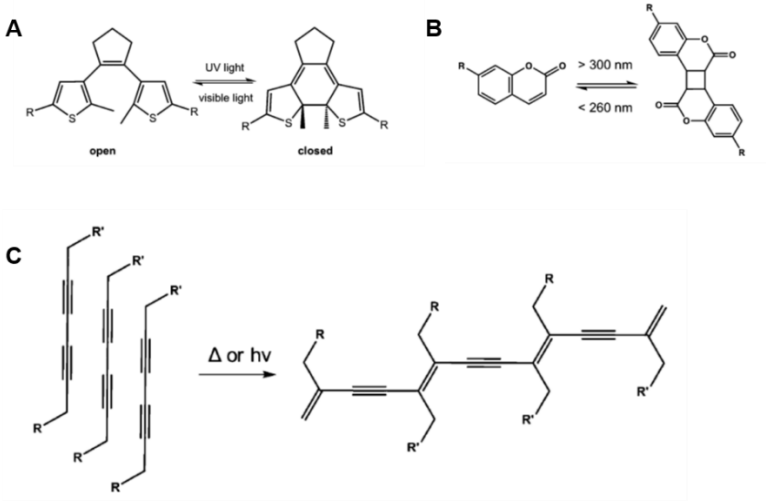

Figure 4.2. A) the molecular structure of dithienylethene in ring open and close form. B) the reversible photodimerization of coumarin in monomer and dimer. C) UV induced polymerization of diacetylene into polymeric networks. Reproduced from ref. * (see page 3) with permission from the Royal Society of Chemistry.

Whereas the azobenzene undergoes shape changes to regulate gelation, there are also light-mediated chemistry that reversibly form and break covalent bonds. Diarylethene (Figure 4.2A), for instance, is a photo-reversible building block[34–39]. Upon UV irradiation, the gelator dithienylcyclopentene ring closes[29], whereas the reverse process occurs upon visible light irradiation. The gelator in the closed ring is more conjugated due to the larger entropic penalty of the flexible open isomer upon aggregation[29,40]. The transformation of the building blocks, even, leads to color changes when building blocks in solution. But in some cases[41], the closed ring is more conjugated and aggregated due to the rotation of a single methyl bond is restricted. If extending into photoinduced polymerization, coumarin[42–46] can be dimerized into building blocks (Figure 4.2B). When the light source is over 300 nm, dimerization occurs, which leads to aggregate because the dimer is more hydrophobic. Upon UVC irradiation, the dimer easily reverts to the

corresponding monomers. In addition, the mechanical stiffness of diacetylene gel[47,48] can be enhanced upon UVC irradiation, owning to photoinduced irreversible polymerization (Figure 4.2C).

Although millions of organic molecules have been discovered and synthesized so far, only a limited number of photochromophores can be used as light-responsive building blocks in supramolecular chemistry. We are thus striving to develop new reversibly photoresponsive supramolecular materials using different photochromophores.

Perylene bisimide (PBI) has been widely studied as building blocks to construct supramolecular polymer in the ground state due to highly conjugated perylene core[49,50], high electron affinity[51,52], thermal-photo stability[53], etc. Although the PBI has been widely studied in organic electronic devices[54], it is barely reported that using light regulates PBI aggregates. Very recently, Adams and coworkers demonstrated reversible photoreduction as a trigger for photoresponsive gels[20]. In water, an amino acid-functionalized PBI gelates in the presence of glucono-δ-lactone (GDL) that neutralizes carboxylic acid groups for enhancing PBI hydrophobicity. When the pH is at 9, PBI formed micelles in the solution that was reduced into PBI radical anion ($PBI^{\bullet-}$), which is sensitive to ambient oxygen, upon UVA irradiation at inert conditions. By lowering the pH below 7, a gel forms, which was reduced into $PBI^{\bullet-}$ gel (with a color change of red to purple) that is stable for two hours in air. Once O_2 was introduced, the $PBI^{\bullet-}$ gel was re-oxidized back to the neutral. The mechanical stiffness of gel, interestingly, is enhanced after photoreduction, which differs from the other gels, such as azobenzene gels[55,56], or a dithienylthene gel[39] that was decomposed after exposure to light.

As we have seen in Chapter 2 and Chapter 3, most PBI-based systems only achieve a one-electron reduction in solution. For the gel example of Adams[20] discussed above this is also the case. Interestingly, there are several reports when photoreduction on PBI gels was achieved, but in absence of a compound acting as an electron donor[57–59]. It has been argued that in a PBI molecule, the perylene core plays the role of (electron-deficient) electron acceptor, whereas the imide ring would acts as an electron donor.[60] Upon irradiation of PBI aggregates, the excited PBI could abstract one electron from the nearby imides. However, in some cases[61] an extra free donor, such

as triethylamine, can facilitate the photoinduced electron-transfer in a donor-acceptor system, which has different mechanism.

In this chapter, we report a reversible photoreduction in two-component gels based on perylene bisimides, which reveals the mechanisms of PBI photoreduction. The gelator perylene bisimide-aminoisophthalic acid (**PDBA**) co-assembles with cetrimonium bromide (CTAB) in the presence of triethylamine (TEA) or helxyamine (HLA) into the corresponding neutral gels by heating-cooling. For the gelation, HLA only works as an organic base to deprotonate **PDBA**, in contrast to TEA that has two functions— an organic base, as well as an electron donor. The deprotonated **PDBA**, subsequently co-assembles with CTAB into two-component gels due to electrostatic interactions. Upon UV irradiation, the gels could be reduced. Under ambient conditions, the PDBA/CTAB/HLA gel only allows one-electron transfer, whereas two electrons are transferred in the PDBA/CTAB/TEA gel. Surprisingly, the rheological properties of the latter two gels are very different after photoreduction. The former leads to stiffening, whereas the latter becomes weaker upon light irradiation.

4.2 Synthesis

We synthesized perylene bisimide aminoisophthalic acid (**PDBA**)[62]: Perylene-3,4,9,10-tetracarboxylic acid dianhydride reacted with 5-aminoisophthalic acid in pure imidazole at 140°C under N_2 flow, resulting in a 95% yield of the compound (Figure 4.3). **PDBA** is soluble in water and DMSO in the presence of a base.

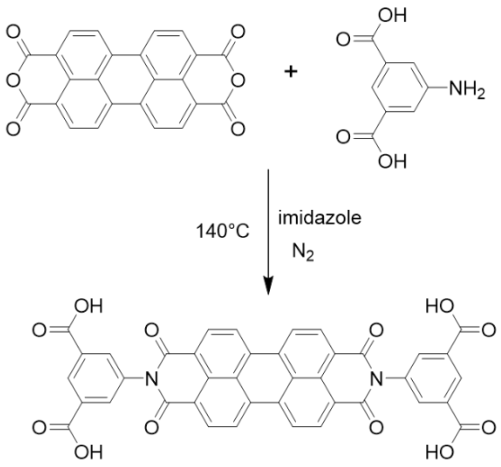

Figure 4.3. the synthesis of the gelator, perylene bisimide -aminoisophthalic acid (**PDBA**)

4.3 Photoinduced one-Electron Transfer in PDBA/CTAB/HLA Gel.

4.3.1 Gelation

Perylene bisimide-aminoisophthalic acid (**PDBA**) is highly π-conjugated, and its solubility is not ideal, even in solvents such as DMSO (solubility = 2.78 μM) or DMF (solubility = 2.08 μM) when the pH is below 7. By increasing the pH above 7, in the presence of organic base hexylamine (HLA, 6 equivalents), the **PDBA** at 25 μM concentration is soluble in DMSO, but precipitates after heating-cooling.

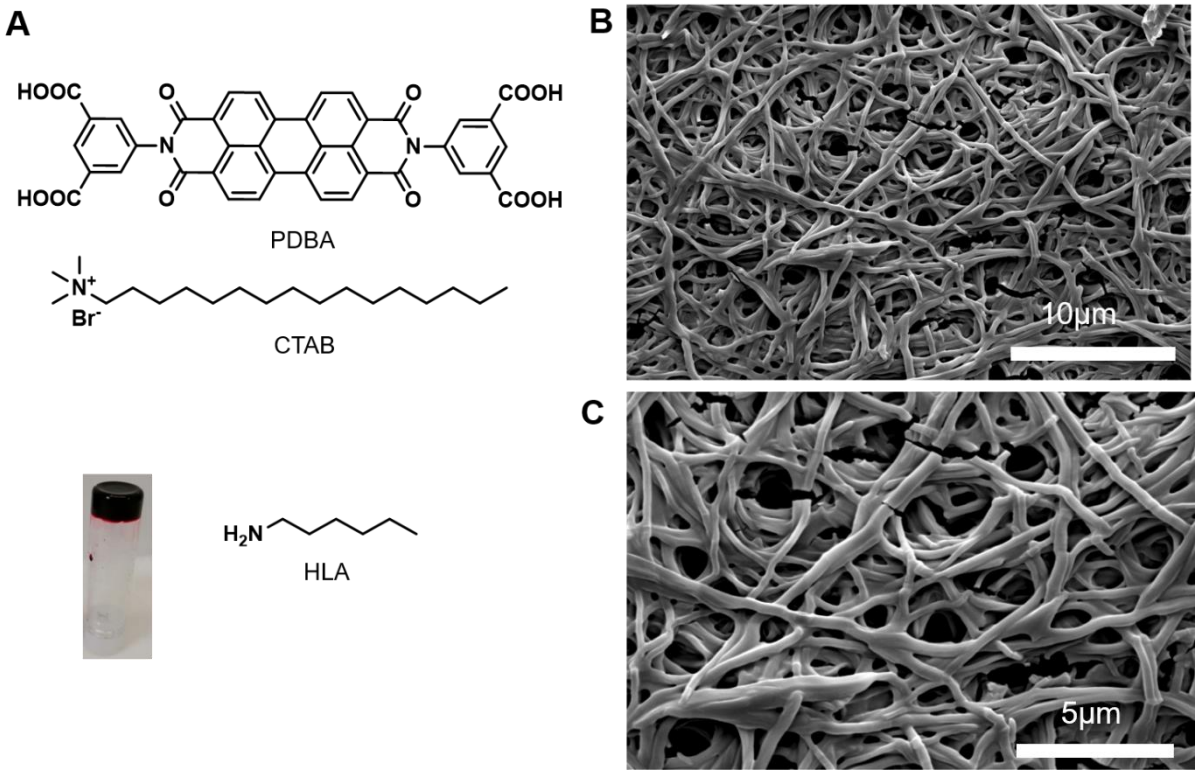

Figure 4.4. **PDBA/CTAB/HLA gel formation in DMSO (4.95 wt %) after heating-cooling. (A)** The molecular structure of **PDBA**, CTAB, and hexylamine and the image of the gel. **(B, C)** SEM images of xerogel of the PDBA/CTAB/HLA in different scales.

Apparently, only the π–π stacking interaction is not sufficient to form three-dimensional networks. Given the four deprotonated carboxylic groups with negative charges, we introduced a commercially available compound, cetrimonium bromide (CTAB) with a positive charge, to form coassembled structures (Figure 4.4 A). Upon heating to the solution and cooling back to room

temperature, the PDBA/CTAB/HLA mixture forms a red gel within 5 mins, which was confirmed by inverse vial experiments (see Fig. 4.4A) and quantitatively using rheology (see below). Figure 4.4B and C show that this organogel consists of entangled long nanofibers, with a typical width of 500 nm and length of 30 μm (though, the latter is difficult to establish exactly from the images). Due to the heating-cooling process, an amine with a high boiling point is necessary.

4.3.2 Photoreduction of PDBA/CTAB/HLA Gel

In Chapter 2 and Chapter 3 we reported that, in the presence of a donor (i.e., TEOA or TEA), perylene bisimdes can be selectively photoreduced to just the radical anion, or all the way to the dianion. The wavelength of the irradiated light is vital for the **PDBA** photoreduction. Since, as the UV spectra of **PDBA** shows, the gel, here, absorbs from 300 to 700 nm with two maxima 508 and 554 nm that indicates the **PDBA** is highly aggregated, meanwhile, the intensity from 300 to 400 nm is pronounced. Thus, we used UVA LED (from 350 to 410 nm, 3-6 W/cm^2) as photon input. Given the high electron affinity of perylene bisimides, the PDBA/CTAB/HLA gel was photoreduced. After reduction, the gel color remains in the dark and simultaneously emits red fluorescence when irradiated by UVA LED, which, subsequently, transformed into purple (Figure 4.5A). Given the characteristic UV absorption of neutral **PDBA** and reduced species, the photoreduction was tracked with UV-vis spectroscopy (Figure 4.5B). When the neutral PDBA/CTAB/HLA gel gets reduced, **PDBA** absorbance is declining, whereas the new UV absorptions appear from 600 to 1000 nm with three maxima 710, 795, and 958 nm on the top of neutral **PDBA**, which are assigned to the PBDA radical anion (**PDBA**$^{\bullet-}$)[61]. Notably, the broad absorption of the neutral **PDBA** neutral splits two peaks, and the ratio of 492/517 becomes lower, indicating the gel is less assembled. In comparison to the Adams work[20], this PDBA/CTAB/HLA gel easily gets reduced, even accumulating more **PDBA**$^{\bullet-}$ at ambient conditions (see Fig/ 4.5B).

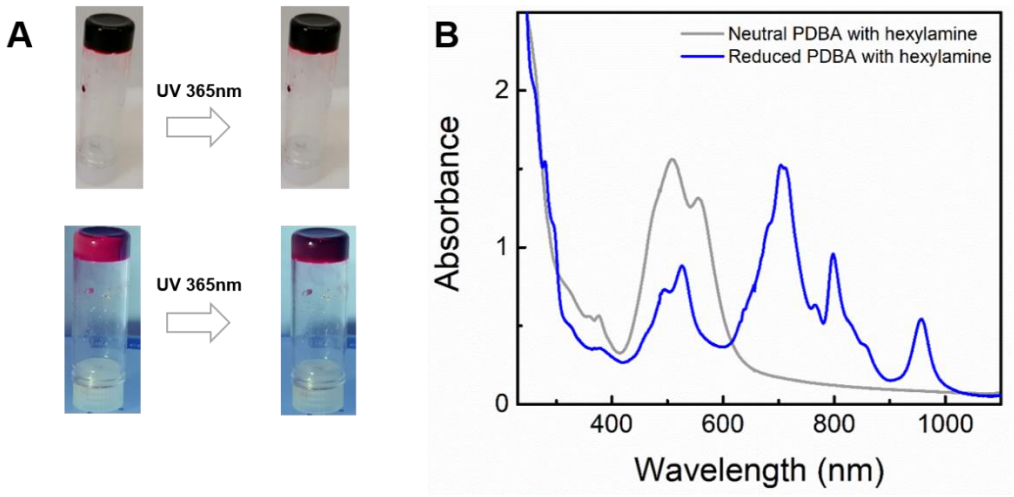

Figure 4.5. **The photoreduction of the PDBA/CTAB/HLA gel.** A) images of PDBA/CTAB/HLA gel before and after UVA irradiation, no obvious color change when the gel was irradiated by UVA LED (350-410 nm, 3-6 W/cm^2) placed at 20 cm.The neutral gel is fluorescent if exposed to UVA illumination, but fluorescence tends to be quenched as being photoreducned in 2 mins. B) the UV spectra of **PDBA** before and after UVA 365nm irradiation, the gel in 0.1 mm quartz cuvette that was transferred from the gel prepared in a vial was irradiated 1 minute by UVA LED placed at 2 cm.

To track the kinetics of gel photoreduction, ptochology is promising as compared to purely spectroscopic methods, such as UV spectroscopy, because the kinetics of the photophysical information in gel, generally is challenging to be followed due to low optical transmittance. But kinetics of mechanical properties is easily obtained with rheometer. A viscoelastic material is quantified with a storage modulus (G') and loss modulus (G'') that correspondingly represents the elastic and viscous portion of the materials. When the storage modulus is higher than the loss modulus (G'>G''), the materials are more solid-like, by contrast, a viscous liquid has a lower storage modulus than loss modulus (G'<G'').

The perylene bisimide gels are semisolid with a higher storage modulus when sandwiched in a two-parallel-plates rheometer (see Figure 4.6A). Applying a given shearing strain in the process of deformation and restorage is a must. For instance, the viscous (fluid) and elastic (solid) properties of the thermodynamic supramolecular gels are dependent on the timescale of rheological experiments with a sweeping strain, which allows us to observe the transition between the gel and the liquid at a critical strain.

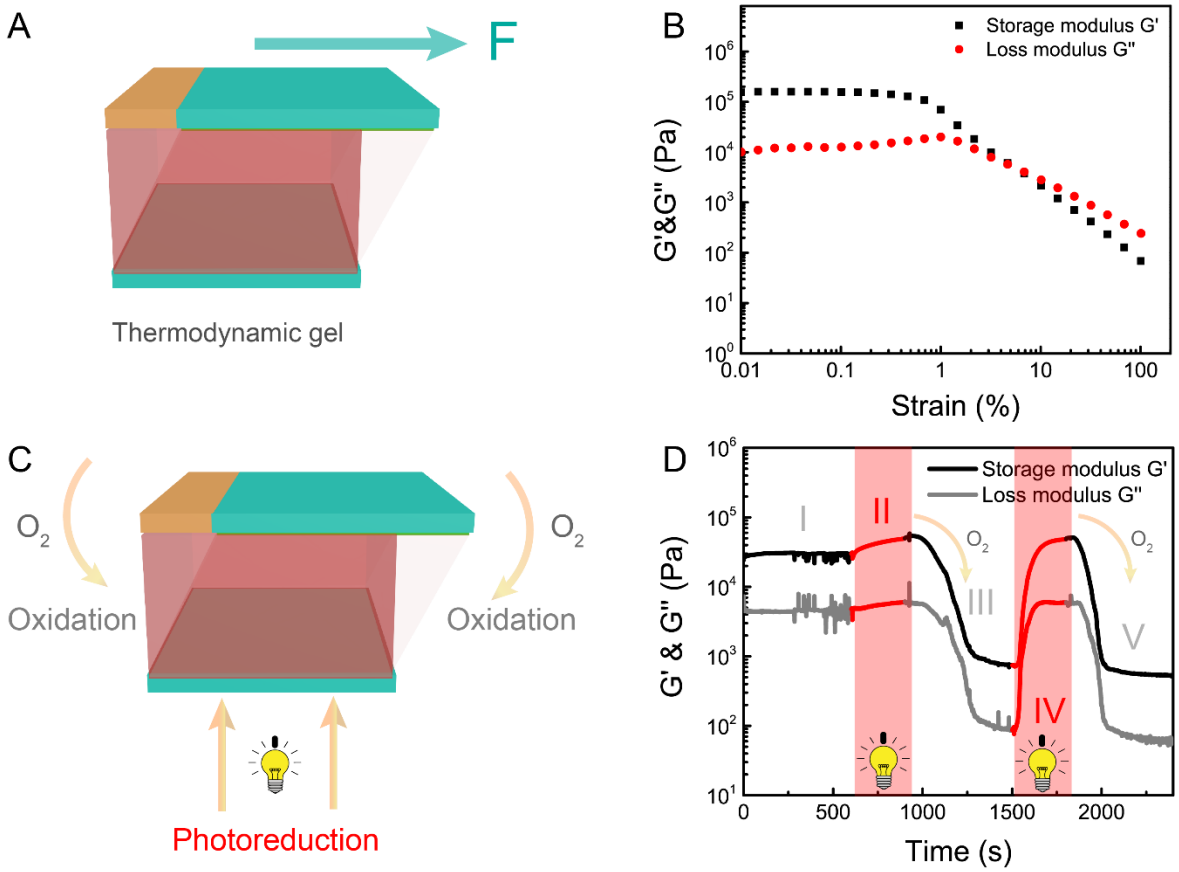

Figure 4.6. **PDBA/CTAB/HLA gel photoreduction tracked with photorheology. A)** the scheme of the most common thermodynamic gels measured with a given force when sandwiched in two-parallel-plates. **B)** PDBA/CTAB/HLA gel (4.9 wt%) made in a vial was transferred to a rheometer (with two stainless steel parallel plates) and measured with sweeping strain from 0.01 to 100% at shearing rate 10 rad/s and 20°C. **C)** The scheme of the PDBA/CTAB/HLA gel in situ photoreduction in real time under photo-rheometer. When light is on, the photoreduction is dominated as **PDBA** reduced into ***PDBA***$^{\bullet-}$ but a weak oxidation simultaneously *occurs* (**PDBA**•– is oxidized back to the neutral **PDBA**). ***D)*** The PDBA CTAB/HLA gel *(*4.9 wt%*)* in situ photoreduction in real time under photo-rheometer (the bottom parallel plate is transparent with a cooling system at 20°C) in an oscillatory shearing mode with a constant shearing rate 10 rad/s and shearing strain 0.1%. The first measurement without light stays in a plateau 600s (phase I), in phase II, applying UVA lamp (from 32 0nm to 500 nm, 27.7 W/cm^2) 300s in situ to the **PDBA** gel. After switching off the light 600s in phase III. In phase IV and V the light was switched on (300s) and off (600s) again.

Figure 4.6B demonstrates that the breakage strain was around 0.47% when a 4.9 wt% PDBA/CTAB/HLA organogel in DMSO was sheared by a strain from 0.01 to 100%. But measuring the rheological properties of the PBI (perylene bisimide) gels in real time remain a big challenge. Adams and his coworkers[20] reported an air-stable PBI$^{\bullet-}$ gel which was first obtained by UVA LED irradiation in different timescales. Subsequently, the PBI$^{\bullet-}$ gel was transferred to a rheometer and measured with a sweeping strain, which has a higher storage/loss modulus as compared to a non-irradiated PBI gel. Although this PBI$^{\bullet-}$ gel is relatively air-stable, the gel is not in steady state

which constantly dissipates energy to the surrounding environment due to an oxidation caused by atmospheric O_2. Meanwhile, the kinetics of the photoreduction is still missing.

We assumed the above experiments have been done with most common non-oscillatory sweeping mode (always rotating in the same direction). Herein we employ the photo-rheology with an oscillatory sweeping to track the kinetics of photoreduction of the PDBA/CTAB/HLA gel in real time. In the oscillatory study, applying a constant shearing strain and angular frequency is a must. As abovementioned (Figure 4.6 B), we know the critical strain is around 0.47%. To ensure a non-destructive gel, a constant shearing strain at 0.1% and a fixed shearing rate at 10 rad/s were applied to the gel. So far, we have established rheometer settings where the gel can be probed non-destructively. In a typical experiment, the sample was probed first for 600 seconds without light, showing plateau values for G' and G'' (see Fig. 4.6 D, region I). UVA lamp (from 320 nm to 500 nm, 27.7W/cm^2) was in situ applied on the sample through a transparent bottom plate (see Fig. 4.6 C); whose temperature was fixed at 20°C by a cooling system. After 300 seconds, the storage G' was enhanced from 30000 Pa to 51310 Pa (see Fig. 4.6 D, region II). By switching off the light, the G' drops back to the initial value and even down to 730 Pa (see Fig. 4.6 D, region III). The increase was photoinduced because the **PDBA** was photoreduced into **PDBA**$^{\bullet-}$, then the electrons delocalized between neutral **PDBA** and **PDBA**$^{\bullet-}$ contributes to a stronger bonding[20].

Further, this enhancement was amplified from the molecular to the macroscopic scale, resulting in a higher mechanical stiffness. This hypothesis might be contradicted to what we have elaborated in chapter 2 and 3 (photoreduction induced PBI-1 disassembly in solution due to electronic repulsion). But in the reported PBI gel[20], photoreduction leading to an increase in mechanical stiffness has been experimentally proven; together with a cluster model (DFT+D calculation) that is composed of PBI and PBI$^{\bullet-}$ suggests a significant increase of the binding energy. Interestingly, the enhancement of the rheological properties in PDBA/CTAB/HLA gel is only temporally maintained by light irradiation. Switching off the light the G'/G'' eventually recovers to the before (non-irradiated gel) and even down to 100 Pa because when without light irradiation only **PDBA**$^{\bullet-}$ oxidation takes place via constantly reacting with atmospheric O_2 (see Fig. 4.6 C oxidation). To achieve multiple photoredox cycles, only Fig. 4.6 D IV and V shows a second photoredox only by switching on/off of the UVA lamp.

4.4 Photoinduced Two-Electron Transfer in PDBA/CTAB/TEA gels

4.4.1 Gelation

To achieve two-electron transfer, we replaced HLA with electron donor TEA in the gelation step. The co-gelators PDBA/CTAB (4.95 wt%) in the presence of TEA in DMSO (see. Fig. 4.7A) was heated until becoming a solution then cooled down to the room temperature, the PDBA/CTAB/TEA gel formed in 20 mins (see. Fig. 4.7 A) which has a longer gelation time in comparison to the PDBA/CTAB/HLA gel (see above, gelation in 5 mins). Because the HLA has a longer alkyl chain which is involved in hydrophobic interactions, by contrast, TEA serves as an organic base with short alkyl group. Even the difference of the gelation abilities can be explained from its microstructures. The PDBA/CTAB/TEA organogel formed smaller entangled nanofibers (compared to PDBA/CTAB/HLA, see above), with widths of 0.25 µm and lengths of around 5 µm (see. Fig. 4.7 B and C). As said before, in the PDBA/CTAB/TEA gel the TEA has a dual function: it is an organic base, as well as the electron donor. As reported in literature[61,63], TEA is a good electron donor, which is widely used in photochemistry, especially in the photoreduction of perylene bisimides.

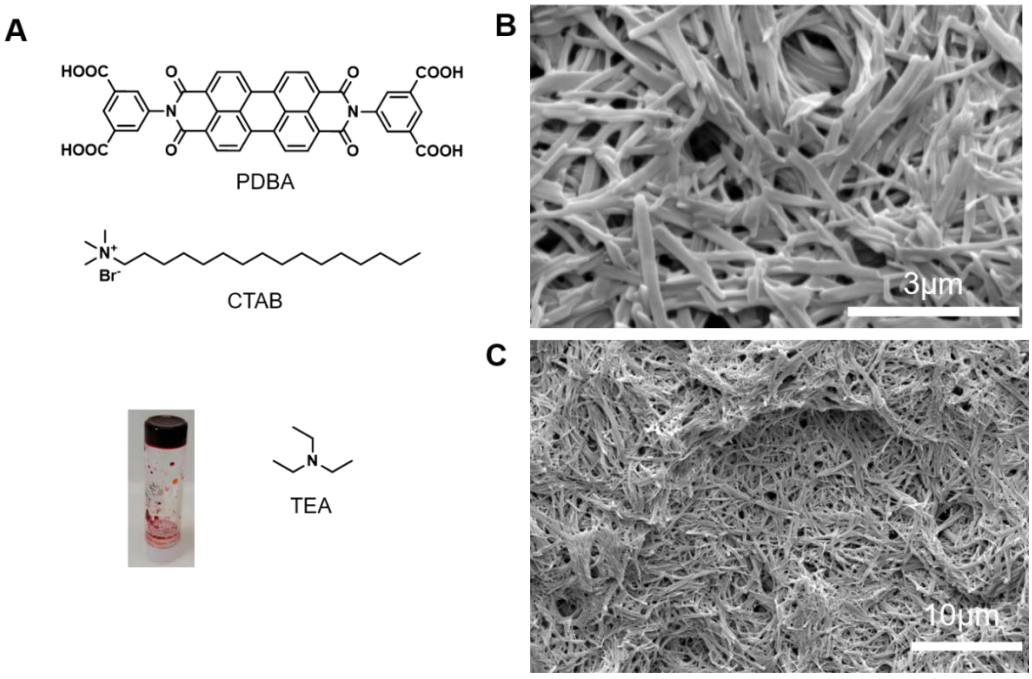

Figure 4.7. **PDBA/CTAB/TEA gel formation in DMSO (4.95 wt%) by heating-cooling.** (A) The molecular structures of the **PDBA**, CTAB, and TEA and the image of PDBA/CTAB/TEA gel. B, C) the SEM images of **PDBA** gel in different scales.

4.4.2 Photoinduced Two-Electron Transfer in PDBA/CTAB/TEA gels

Upon UVA (LED from 350 to 410 nm, 3-6 W/cm^2) irradiation of a PDBA/CTAB/TEA gel, a two-electron transfer process takes place. After 5 minutes of shining light, no changes were observed in the visible color of the gel (Figure 4.8 A, top). However, the gel developed a yellow-red fluorescence when viewed under a UVA lamp (Figure 4.8 A, bottom). In general, monomeric PBI radical anions are fluorescence quenched, but **PDBA** radicals in this case are more fluorescent, likely resulting from aggregation-induced emission. The photoreduction was also tracked quantitatively using UV-vis spectroscopy (Figure 4.8 B). The neutral PDBA/CTAB/TEA gel is less aggregated in comparison to the PDBA/CTAB/HLA gel, determined by the lower ratio of 493/528 absorptions, but overall still in the aggregated state. The gel has a broad UV absorption with five maxima at 324, 378, 493, 528, and 575 nm (Figure 4.8 B). Upon UVA irradiation, the **PDBA** was converted into **PDBA**$^{\bullet-}$ with maxima at 710, 795, and 958 nm. Upon further reduction to **PDBA**$^{2-}$ peaks appeared at 522 and 574 nm[64], in addition to characteristic bands at 264, 281, and 294 nm[65]. Full conversion of **PDBA**$^{\bullet-}$ to **PDBA**$^{2-}$ was not possible, as it stopped at 12.5%. As a control experiment, the monomeric **PDBA** with 3000 eq.of TEA in DMSO only can be reduced into **PDBA**$^{\bullet-}$ without a trace of **PDBA**$^{2-}$ formation (see. Appendix 4.10), which suggests that only **PDBA**$^{2-}$ was photoinduced in aggregates (in agreement with our study in Chapter 2), that is, in the gel state, owing to delocalization of electrons and slow diffusion of O_2.

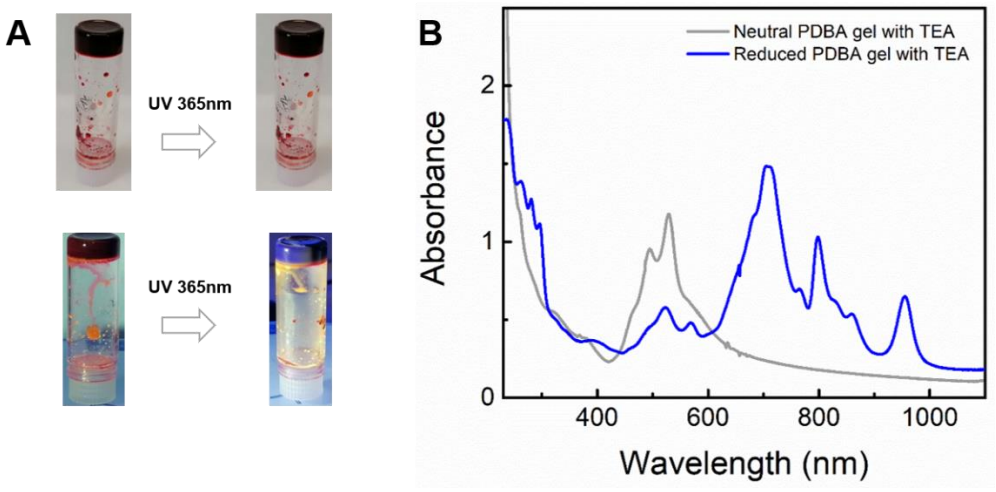

Figure 4.8. **The photoreduction of PDBA/CTAB/TEA gel upon UVA irradiation.** A) images of the PDBA/CTAB/TEA gel before and after UVA irradiation (LED from 350 to 410 nm, 3-6 W/cm^2, irradiation distance 20 cm between gel and lamp). B) the UV spectrum of the PDBA/CTAB/TEA gel in 0.1 mm quartz cuvette before and after UVA 365 nm irradiation 1 min (irradiation distance 2 cm between gel and lamp).

The rheological properties of the PDBA/CTAB/TEA are quite different. The gel (4.9 wt%) was swept by an incremental strain from 0.01 to 100% at a constant shearing rate 10 rad/s. The initial modulus G' and loss modulus G'' are 3600 and 380 Pa (see. Appendix Fig.4.11), respectively, which is weaker than the PDBA/CTAB/HLA gel (compared to the Fig. 4.6B). The difference can corelate with the gel microstructures. Since TEA with a shorter alkyl chain that mainly works as an organic base, the main non-covalent interactions in gel are electrostatic interaction between **PDBA** and CTAB and π–π interaction (between perylene bismide) which leads to shorter entangled nanofibers (see 4.7 B SEM image). In contrast, longer and wider nanofibers are observed (see 4.4 C SEM image) because that the HLA has hydrophobic interactions with CTAB which enhance the mechanical stiffness of the PDBA/CTAB/HLA gel.

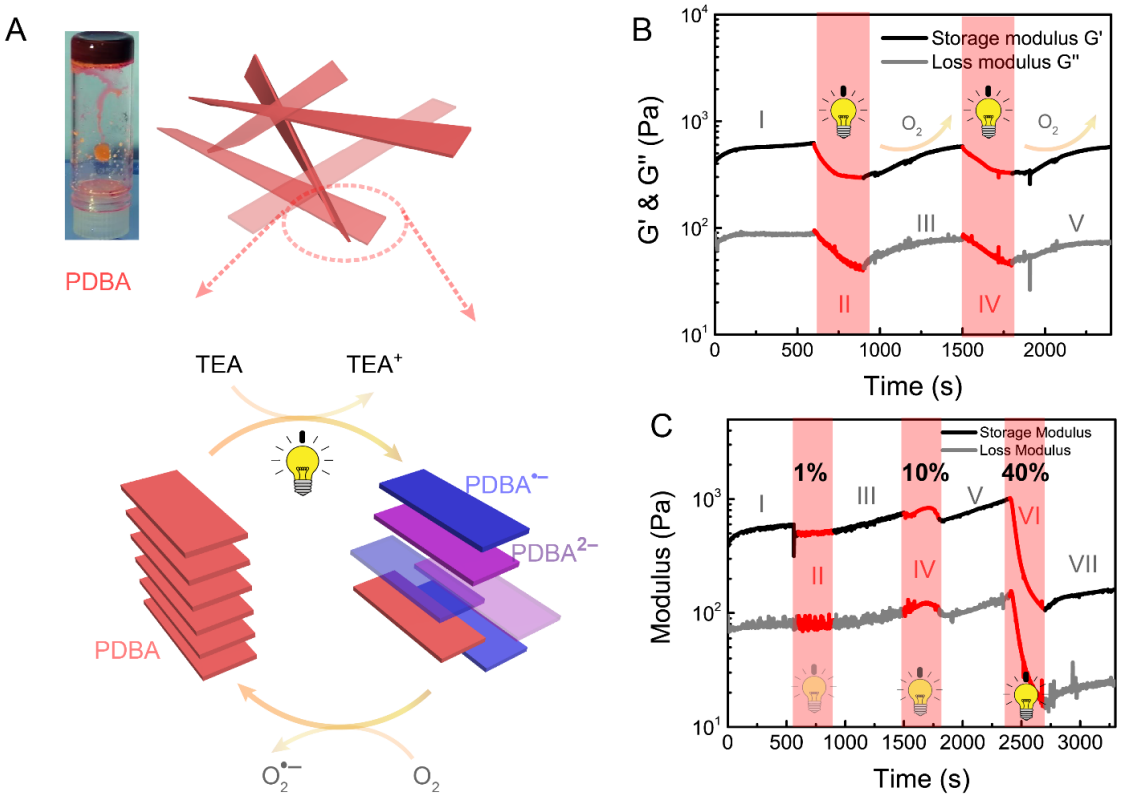

Figure 4.9 **PDBA/CTAB/TEA gel photoreduction tracked with photorheology.** (A) the scheme of the photoreduction and oxidation of the PDBA/CTAB/TEA gel. (B) PDBA/CTAB/TEA (4.9 wt%) gel was sheared at a constant strain 0.05% and shearing rate 10 rad/s in a plateau (phase I), after 600s applying UV lamp in situ with 20% light intensity (from 320 nm to 500 nm, 27.7 W/cm^2) to a gel 300s (phase II) for photoreduction. Switching off UV lamp 300s, only **PDBA$^{\bullet-}$ / PDBA^{2-}** oxidation occurs (by reacting with atmospheric O_2, phase III). One more photoredox was repeated as phase IV and V by light on/off. (C) Incremental UVA (1%, 10%, and 40% in phase II, IV, and VI, respectively) was employed to a PDBA/CTAB/TEA gel (light is off in phase I, III, and V).

We tracked the kinetics of the PDBA/CTAB/TEA gel photoreduction by photorheology in the oscillatory mode, at constant shear strain 0.05% and shearing rate 10 rad/s. A plateau is maintained in the first 600s. When switching on the UVA lamp (20% light intensity), both the storage G' and loss moduli G" decrease (see Fig.4.9B. phase II), likely due to electrostatic repulsion between **PDBA**$^{2-}$ and **PDBA**$^{\bullet-}$ species, resulting in disassembly and gel weakening (see Fig. 4.9A). When stopping light irradiation, the **PDBA**$^{\bullet-}$ and **PDBA**$^{2-}$ are oxidized back to the neutral **PDBA**, whose mechanical stiffness recover to before irradiation (see Fig.4.9B. phase III). Oxygen solubilities in DMSO are 1.83×10^{-5} mol m^{-3} Pa^{-1} (see DOI: 10.1021/acs.jpcc.7b09218), which would allow for **PDBA** reduction/oxidation cycles in principle (note 2 cycles are shown in Figure 4.9B).

Using incremental light intensities, we could obtain deeper insights into the photoreduction influences on the gel. There are no changes in rheological properties when PDBA/CTAB/TEA gel was irradiated with 1% light, since the oxidation rate is faster than the reduction. But the gel shows dynamic properties with 10% light irradiation. In the first 200s UVA irradiation as shown in (see IV in Fig. 4.9 C), the storage/loss moduli increase over time; if continuously irradiating on the gel, the mechanical stiffness declines from 840 Pa to 690 Pa (see IV in Fig. 4.9 C). When the light intensity was increased further to 40%, the gel quickly disassembled and lost all structural integrity (see VI in Figure 4.9 C). This is likely due to the full reduction to **PDBA**$^{2-}$, which would be disassembled, whereas for lower light intensities only the **PDBA**$^{\bullet-}$ (and thus stronger assembled) state is reached. After full reduction, the gel recovery is no longer possible (see VII in Figure 4.9 C), likely because dissolved oxygen is also depleted, and would need to be replenished by diffusion through the viscous solution (which would be slow given the parallel plate geometry of the rheometer).

4.5 Conclusions

In this chapter, we have presented two similar gels PDBA/CTAB/HLA and PDBA/CTAB/TEA, which can undergo a one-electron or two-electron reduction, respectively. In the PDBA/CTAB/HLA gel, the HLA only acts as an organic base to deprotonate **PDBA**. In contrast, in the PDBA/CTAB/TEA

gel the TEA has two functions: as an organic base to deprotonate **PDBA**, but also act as an electron donor. The resulting photorheological properties of the two gels are qualitatively similar for low light illumination, where in both cases the **PDBA** is only reduced to **PDBA**$^{\bullet-}$, which co-assembled with neutral **PDBA** lead to charge delocalization and stiffe gels as previously found in the literature. For stronger illumination, only the PDBA/CTAB/TEA gel can be further reduced to PDBA^{2-} that causes structural disintegration. Our approach can therefore lead to real-time tunable material properties.

4.6 Acknowledgements

Chunfeng Chen performed the synthesis and all the experiments. Prof. Thomas Hermans supervised the research.

4.7 Experimental Section

Synthesis of N, N ' -Di-(Phenyl-3, 5-Dicarboxylic Acid)-Perylene-3,4:9,10-Tetracarboxylic Acid Diimide(PDBA): 1g (2.55 mmol) of perylene-3,4:9,10-tetracarboxylic dianhydride, 1.154 g (6.37 mmol) 5-aminoisophthalic acid and 8 g of imidazole were heated at 140 °C under nitrogen atmosphere. After 2 hours reaction, adding 100 mL of ethanol into the hot mixture the solution was refluxed for 2 hours, then adjusting the pH to 2 for precipitating the target compound. The precipitate was filtered and washed with ethanol and then dried under a vacuum oven (Yield: 90%). ^{1}H NMR of PDBA (400 MHz, DMSO,25°C) ð: 8.54 (s, 2H), 8.13 (s, 4H), 7.21 (m, 8H). MS (MALDI-TOF): m/z calc. for $C_{40}H_{18}N_2O_{12}$: 718.58, found: 741.12 [M+Na$^+$]. ^{13}C NMR (400 MHz, d_6-DMSO) δ (ppm): 165.98, 162.99, 136.44, 134.34, 132.25, 130.28, 129.89, 127.15, 126.77.

PDBA/CTAB/HLA Gelation. The gelator PDBA (9mg) and 18.22 mg CTAB (cetrimonium bromide) in the presence of 6 eq. helxyamine (HLA) in 500 ul DMSO was heated until becoming a transparent solution, then cooling down to the room temperature and gelated in 5 mins. The gelation was both confirmed with reversing the vial and rheological measurements.

PDBA/CTAB/TEA Gelation. The gelator PDBA (9mg) and 18.22 mg CTAB (cetrimonium bromide) in the presence of 5 eq. helxyamine (TEA) in 500 ul DMSO was heated until becoming a transparent solution, then cooling down to the room temperature and gelated in 20mins. The gelation was both confirmed with reversing the vial and rheological measurements.

Gels Photoreduction In Vial. PDBA/CTAB/TEA (PDBA/CTAB/HLA) gel in glass vial was irradiated by UVA LED 365 nm at 20 cm (from 350 to 410 nm, 3-6 W/cm^2). After 2 mins irradiation, The PDBA/CTAB/TEA gel had a color change from the red to the blue (the PDBA/CTAB/HLA gel changed from the red to the dark red).

UV-vis Measurements. UV-vis spectra were recorded with a UV diode array 8454 after PDBA/CTAB/TEA (PDBA/CTAB/HLA) gelation for 1 hour. The gels were transferred to a 0.1 mm quartz cuvette in which was irradiated by UVA LED (from 350 to 410 nm, 3-6 W/cm^2) 2 mins.

Scanning Electron Microscopy (SEM): The microstructure of the PDBA/CTAB/TEA (PDBA/CTAB/HLA) gel was characterized with an FEI Quanta FEG 450 Microscope. The sample was sputtered with 15 nm of gold and characterized with a 5.0 kV High Voltage and dwell time of 60 µs.

Rheology: The measurements were performed with an Anton Paar Physica MCR 302 rheometer equipped with laser supplement—OmniCure S1500, whose laser ranges from 320 to 500nm with maximum irradiance 27.7 W/cm^2. The neutral gels were prepared as above (see. PDBA/CTAB/HLA Gelation) and transferred to a rheometer with a 25 mm plate. All neutral gels at 20 °C were swept (the gap between two parallel plates is 0.3 mm) by a shearing strain from 0.1% to 100% at 10 rad/s.

Photoredox on Rheometer: The photoreduction of PDBA/CTAB/TEA (PDBA/CTAB/HLA) gel was performed with an oscillatory mode at a fixed shearing strain 0.1% and shearing rate 10 rad/s. The gels in vial were prepared and then transferred to a glass bottom plate with a cooling system at 20°. The photoreduction and oxidation was achieved by switching on/off UV lamp.

4.8 References

(1) Cheng, W.; Zhao, D.; Qiu, Y.; Hu, H.; Wang, H.; Wang, Q.; Liao, Y.; Peng, H.; Xie, X. Robust Multi-Responsive Supramolecular Hydrogel Based on a Mono-Component Host–Guest Gelator. *Soft Matter* **2018**, *14* (25), 5213–5221. https://doi.org/10.1039/C8SM00639C.

(2) Cao, Z.-Q.; Wang, G.-J. Multi-Stimuli-Responsive Polymer Materials: Particles, Films, and Bulk Gels. *Chem. Rec.* **2016**, *16* (3), 1398–1435. https://doi.org/10.1002/tcr.201500281.

(3) Muñoz Resta, I.; Manzano, V. E.; Cecchi, F.; Spagnuolo, C. C.; Cukiernik, F. D.; Di Chenna, P. H. Supramolecular Assembly of PH-Sensitive Triphenylene Derived π-Gelators and Their Application as Molecular Template for the Preparation of Silica Nanotubes. *Gels* **2016**, *2* (1), 7. https://doi.org/10.3390/gels2010007.

(4) Cafferty, B. J.; Avirah, R. R.; Schuster, G. B.; Hud, N. V. Ultra-Sensitive PH Control of Supramolecular Polymers and Hydrogels: PKa Matching of Biomimetic Monomers. *Chem. Sci.* **2014**, *5* (12), 4681–4686. https://doi.org/10.1039/C4SC02182G.

(5) Grande, V.; Soberats, B.; Herbst, S.; Stepanenko, V.; Würthner, F. Hydrogen-Bonded Perylene Bisimide J-Aggregate Aqua Material. *Chem. Sci.* **2018**, *9* (34), 6904–6911. https://doi.org/10.1039/C8SC02409J.

(6) Li, X.; Zhang, Y.; Chen, A.; Zhang, B.; Zhang, B.; Song, J. A Ferrocene-Based Organogel with Multi-Stimuli Properties and Applications in Naked-Eye Recognition of F− and Al3+. *RSC Adv.* **2017**, *7* (59), 37105–37111. https://doi.org/10.1039/C7RA06722D.

(7) Zhang, Y.-M.; Li, Y.-F.; Fang, H.; He, J.-X.; Yong, B.-R.; Yao, H.; Wei, T.-B.; Lin, Q. Multi-Stimuli-Responsive Supramolecular Gel Constructed by Pillar[5]Arene-Based Pseudorotaxanes for Efficient Detection and Separation of Multi-Analytes in Aqueous Solution. *Soft Matter* **2018**, *14* (42), 8529–8536. https://doi.org/10.1039/C8SM01838C.

(8) Roy, S.; Maiti, D. K.; Panigrahi, S.; Basak, D.; Banerjee, A. A Bolaamphiphilic Amino Acid Appended Photo-Switching Supramolecular Gel and Tuning of Photo-Switching Behaviour. *Phys. Chem. Chem. Phys.* **2014**, *16* (13), 6041–6049. https://doi.org/10.1039/C3CP55108C.

(9) Sun, P.; Ren, S.; Liu, F.; Wu, A.; Sun, N.; Shi, L.; Zheng, L. Smart Low Molecular Weight Hydrogels with Dynamic Covalent Skeletons. *Soft Matter* **2018**, *14* (32), 6678–6683. https://doi.org/10.1039/C8SM01482E.

(10) Krieg, E.; Shirman, E.; Weissman, H.; Shimoni, E.; Wolf, S. G.; Pinkas, I.; Rybtchinski, B. Supramolecular Gel Based on a Perylene Diimide Dye: Multiple Stimuli Responsiveness, Robustness, and Photofunction. *J. Am. Chem. Soc.* **2009**, *131* (40), 14365–14373. https://doi.org/10.1021/ja903938g.

(11) Patterson, A. K.; Smith, D. K. Two-Component Supramolecular Hydrogel for Controlled Drug Release. *Chem. Commun.* **2020**, *56* (75), 11046–11049. https://doi.org/10.1039/D0CC03962D.

(12) Kar, H.; Ghosh, S. Remote Control for Self-Assembly. *Nat. Chem.* **2015**, *7* (10), 765–767. https://doi.org/10.1038/nchem.2351.

(13) Onogi, S.; Shigemitsu, H.; Yoshii, T.; Tanida, T.; Ikeda, M.; Kubota, R.; Hamachi, I. In Situ Real-Time Imaging of Self-Sorted Supramolecular Nanofibres. *Nat. Chem.* **2016**, *8* (8), 743–752. https://doi.org/10.1038/nchem.2526.

(14) Draper, E. R.; Dietrich, B.; Adams, D. J. Self-Assembly, Self-Sorting, and Electronic Properties of a Diketopyrrolopyrrole Hydrogelator. *Chem. Commun.* **2017**, *53* (11), 1864–1867. https://doi.org/10.1039/C6CC10083J.
(15) Draper, E. R.; Adams, D. J. How Should Multicomponent Supramolecular Gels Be Characterised? *Chem. Soc. Rev.* **2018**, *47* (10), 3395–3405. https://doi.org/10.1039/C7CS00804J.
(16) Moffat, J. R.; Smith, D. K. Controlled Self-Sorting in the Assembly of 'Multi-Gelator' Gels. *Chem. Commun.* **2009**, No. 3, 316–318. https://doi.org/10.1039/B818058J.
(17) Okesola, B. O.; Wu, Y.; Derkus, B.; Gani, S.; Wu, D.; Knani, D.; Smith, D. K.; Adams, D. J.; Mata, A. Supramolecular Self-Assembly To Control Structural and Biological Properties of Multicomponent Hydrogels. *Chem. Mater.* **2019**, *31* (19), 7883–7897. https://doi.org/10.1021/acs.chemmater.9b01882.
(18) Das, A.; Ghosh, S. A Generalized Supramolecular Strategy for Self-Sorted Assembly between Donor and Acceptor Gelators. *Chem. Commun.* **2011**, *47* (31), 8922–8924. https://doi.org/10.1039/C1CC12915E.
(19) Liu, Z.-X.; Feng, Y.; Yan, Z.-C.; He, Y.-M.; Liu, C.-Y.; Fan, Q.-H. Multistimuli Responsive Dendritic Organogels Based on Azobenzene-Containing Poly(Aryl Ether) Dendron. *Chem. Mater.* **2012**, *24* (19), 3751–3757. https://doi.org/10.1021/cm302318b.
(20) Draper, E. R.; Schweins, R.; Akhtar, R.; Groves, P.; Chechik, V.; Zwijnenburg, M. A.; Adams, D. J. Reversible Photoreduction as a Trigger for Photoresponsive Gels. *Chem. Mater.* **2016**, *28* (17), 6336–6341. https://doi.org/10.1021/acs.chemmater.6b02677.
(21) Rakotondradany, F.; Whitehead, M. A.; Lebuis, A.-M.; Sleiman, H. F. Photoresponsive Supramolecular Systems: Self-Assembly of Azodibenzoic Acid Linear Tapes and Cyclic Tetramers. *Chem. - Eur. J.* **2003**, *9* (19), 4771–4780. https://doi.org/10.1002/chem.200304864.
(22) Sangeetha, N. M.; Maitra, U. Supramolecular Gels: Functions and Uses. *Chem. Soc. Rev.* **2005**, *34* (10), 821–836. https://doi.org/10.1039/B417081B.
(23) Adhikari, B.; Kraatz, H.-B. Redox-Triggered Changes in the Self-Assembly of a Ferrocene–Peptide Conjugate. *Chem. Commun.* **2014**, *50* (42), 5551–5553. https://doi.org/10.1039/C3CC49268K.
(24) Ma, N.; Li, Y.; Xu, H.; Wang, Z.; Zhang, X. Dual Redox Responsive Assemblies Formed from Diselenide Block Copolymers. *J. Am. Chem. Soc.* **2010**, *132* (2), 442–443. https://doi.org/10.1021/ja908124g.
(25) Napoli, A.; Valentini, M.; Tirelli, N.; Müller, M.; Hubbell, J. A. Oxidation-Responsive Polymeric Vesicles. *Nat. Mater.* **2004**, *3* (3), 183–189. https://doi.org/10.1038/nmat1081.
(26) Dong, W.-F.; Kishimura, A.; Anraku, Y.; Chuanoi, S.; Kataoka, K. Monodispersed Polymeric Nanocapsules: Spontaneous Evolution and Morphology Transition from Reducible Hetero-PEG PICmicelles by Controlled Degradation. *J. Am. Chem. Soc.* **2009**, *131* (11), 3804–3805. https://doi.org/10.1021/ja808419b.
(27) Li, L.; Jiang, H.; Messmore, B. W.; Bull, S. R.; Stupp, S. I. A Torsional Strain Mechanism To Tune Pitch in Supramolecular Helices. *Angew. Chem. Int. Ed.* **2007**, *46* (31), 5873–5876. https://doi.org/10.1002/anie.200701328.

(28) Monreal Santiago, G.; Liu, K.; Browne, W. R.; Otto, S. Emergence of Light-Driven Protometabolism on Recruitment of a Photocatalytic Cofactor by a Self-Replicator. *Nat. Chem.* **2020**, *12* (7), 603–607. https://doi.org/10.1038/s41557-020-0494-4.
(29) de Jong, J. J. D.; Hania, P. R.; Pug?lys, A.; Lucas, L. N.; de Loos, M.; Kellogg, R. M.; Feringa, B. L.; Duppen, K.; van Esch, J. H. Light-Driven Dynamic Pattern Formation. *Angew. Chem. Int. Ed.* **2005**, *44* (16), 2373–2376. https://doi.org/10.1002/anie.200462500.
(30) Wang, J.; Jiang, Q.; Hao, X.; Yan, H.; Peng, H.; Xiong, B.; Liao, Y.; Xie, X. Reversible Photo-Responsive Gel–Sol Transitions of Robust Organogels Based on an Azobenzene-Containing Main-Chain Liquid Crystalline Polymer. *RSC Adv.* **2020**, *10* (7), 3726–3733. https://doi.org/10.1039/C9RA10161F.
(31) Chen, L.; Zhao, X.; Lin, Y.; Su, Z.; Wang, Q. Dual Stimuli-Responsive Supramolecular Hydrogel of Bionanoparticles and Hyaluronan. *Polym. Chem.* **2014**, *5* (23), 6754–6760. https://doi.org/10.1039/C4PY00819G.
(32) Bhavya, P. V.; Jenifer, V. R.; Muthuvel, P.; Das, T. M. Insights into a Novel Class of Azobenzenes Incorporating 4,6-O-Protected Sugars as Photo-Responsive Organogelators. *RSC Adv.* **2019**, *9* (72), 42219–42227. https://doi.org/10.1039/C9RA08033C.
(33) Suzuki, M.; Maruyama, Y.; Hanabusa, K. Gel-Solution Phase Transition of Organogels with Photoreversibility: L-Amino Acid Organogelators with Azobenzene. *Tetrahedron Lett.* **2016**, *57* (31), 3540–3543. https://doi.org/10.1016/j.tetlet.2016.06.111.
(34) Chen, S.; Li, W.; Li, X.; Zhu, W.-H. Aggregation-Controlled Photochromism Based on a Dithienylethene Derivative with Aggregation-Induced Emission. *J. Mater. Chem. C* **2017**, *5* (10), 2717–2722. https://doi.org/10.1039/C7TC00023E.
(35) Wan, H.; Xue, H.; Ling, Y.; Qiao, Y.; Chen, Y.; Zhou, G. Electron Donor and Acceptor Functionalized Dithienylethenes: Effects of Charge Density on Photochromic Properties. *Phys. Chem. Chem. Phys.* **2018**, *20* (21), 14348–14356. https://doi.org/10.1039/C8CP02238K.
(36) Pace, T. C. S.; Müller, V.; Li, S.; Lincoln, P.; Andréasson, J. Enantioselective Cyclization of Photochromic Dithienylethenes Bound to DNA. *Angew. Chem. Int. Ed.* **2013**, *52* (16), 4393–4396. https://doi.org/10.1002/anie.201209773.
(37) Li, Z.; Xie, Y.; Zhu, M.; Song, Y.; Qin, M.; Hu, X. Dithienylethene-Functionalized Difluoroboron β-Diketonate Complexes: Synthesis, Photophysical Properties and NIR Photochromism. *Opt. Mater.* **2019**, *94*, 257–265. https://doi.org/10.1016/j.optmat.2019.05.052.
(38) Zhang, Z.; Wang, W.; Jin, P.; Xue, J.; Sun, L.; Huang, J.; Zhang, J.; Tian, H. A Building-Block Design for Enhanced Visible-Light Switching of Diarylethenes. *Nat. Commun.* **2019**, *10* (1), 4232. https://doi.org/10.1038/s41467-019-12302-6.
(39) R. Draper, E.; J. Adams, D. Photoresponsive Gelators. *Chem. Commun.* **2016**, *52* (53), 8196–8206. https://doi.org/10.1039/C6CC03485C.
(40) Jong, J. J. D. de; Lucas, L. N.; Kellogg, R. M.; Esch, J. H. van; Feringa, B. L. Reversible Optical Transcription of Supramolecular Chirality into Molecular Chirality. *Science* **2004**, *304* (5668), 278–281. https://doi.org/10.1126/science.1095353.
(41) Yagai, S.; Ishiwatari, K.; Lin, X.; Karatsu, T.; Kitamura, A.; Uemura, S. Rational Design of Photoresponsive Supramolecular Assemblies Based on Diarylethene. *Chem. - Eur. J.* **2013**, *19* (22), 6971–6975. https://doi.org/10.1002/chem.201300282.
(42) D'Auria, M.; Racioppi, R. The Photodimerisation of Coumarin. *J. Photochem. Photobiol. Chem.* **2004**, *163* (3), 557–559. https://doi.org/10.1016/j.jphotochem.2004.02.012.

(43) Ikeda, M.; Tanida, T.; Yoshii, T.; Hamachi, I. Rational Molecular Design of Stimulus-Responsive Supramolecular Hydrogels Based on Dipeptides. *Adv. Mater.* **2011**, *23* (25), 2819–2822. https://doi.org/10.1002/adma.201004658.
(44) Draper, E. R.; McDonald, T. O.; Adams, D. J. Photodimerisation of a Coumarin-Dipeptide Gelator. *Chem. Commun.* **2015**, *51* (64), 12827–12830. https://doi.org/10.1039/C5CC03817K.
(45) Huang, Y.; Zhang, Y.; Yuan, Y.; Cao, W. Organogelators Based on Iodo 1,2,3-Triazole Functionalized with Coumarin: Properties and Gelator-Solvent Interaction. *Tetrahedron* **2015**, *71* (14), 2124–2133. https://doi.org/10.1016/j.tet.2015.02.044.
(46) Ji, W.; Liu, G.; Xu, M.; Dou, X.; Feng, C. Rational Design of Coumarin-Based Supramolecular Hydrogelators for Cell Imaging. *Chem. Commun.* **2014**, *50* (98), 15545–15548. https://doi.org/10.1039/C4CC06376G.
(47) Inoue, K.; Ono, Y.; Kanekiyo, Y.; Hanabusa, K.; Shinkai, S. Preparation of New Robust Organic Gels by in Situ Cross-Link of a Bis(Diacetylene) Gelator. *Chem. Lett.* **1999**, *28* (5), 429–430. https://doi.org/10.1246/cl.1999.429.
(48) Chen, C.; Chen, J.; Wang, T.; Liu, M. Fabrication of Helical Nanoribbon Polydiacetylene via Supramolecular Gelation: Circularly Polarized Luminescence and Novel Diagnostic Chiroptical Signals for Sensing. *ACS Appl. Mater. Interfaces* **2016**, *8* (44), 30608–30615. https://doi.org/10.1021/acsami.6b10392.
(49) Wagner, W.; Wehner, M.; Stepanenko, V.; Ogi, S.; Würthner, F. Living Supramolecular Polymerization of a Perylene Bisimide Dye into Fluorescent J-Aggregates. *Angew. Chem. Int. Ed.* **2017**, *56* (50), 16008–16012. https://doi.org/10.1002/anie.201709307.
(50) Gallaher, J. K.; Aitken, E. J.; Keyzers, R. A.; Hodgkiss, J. M. Controlled Aggregation of Peptide-Substituted Perylene-Bisimides. *Chem. Commun.* **2012**, *48* (64), 7961–7963. https://doi.org/10.1039/C2CC31465G.
(51) Zhan, X.; Tan, Z.; Domercq, B.; An, Z.; Zhang, X.; Barlow, S.; Li, Y.; Zhu, D.; Kippelen, B.; Marder, S. R. A High-Mobility Electron-Transport Polymer with Broad Absorption and Its Use in Field-Effect Transistors and All-Polymer Solar Cells. 2.
(52) An, Z.; Yu, J.; Jones, S. C.; Barlow, S.; Yoo, S.; Domercq, B.; Prins, P.; Siebbeles, L. D. A.; Kippelen, B.; Marder, S. R. High Electron Mobility in Room-Temperature Discotic Liquid-Crystalline Perylene Diimides. *Adv. Mater.* **2005**, *17* (21), 2580–2583. https://doi.org/10.1002/adma.200500027.
(53) Jung, C.; Müller, B. K.; Lamb, D. C.; Nolde, F.; Müllen, K.; Bräuchle, C. A New Photostable Terrylene Diimide Dye for Applications in Single Molecule Studies and Membrane Labeling. *J. Am. Chem. Soc.* **2006**, *128* (15), 5283–5291. https://doi.org/10.1021/ja0588104.
(54) King, S.; Sommer, M.; Huettner, S.; Thelakkat, M.; Haque, S. A. Charge Separation and Recombination in Self-Organizing Nanostructured Donor–Acceptor Block Copolymer Films. *J. Mater. Chem.* **2009**, *19* (30), 5436. https://doi.org/10.1039/b905708k.
(55) Clemente, M. J.; Tejedor, R. M.; Romero, P.; Fitremann, J.; Oriol, L. Photoresponsive Supramolecular Gels Based on Amphiphiles with Azobenzene and Maltose or Polyethyleneglycol Polar Head. *New J. Chem.* **2015**, *39* (5), 4009–4019. https://doi.org/10.1039/C4NJ02012J.

(56) Tamesue, S.; Takashima, Y.; Yamaguchi, H.; Shinkai, S.; Harada, A. Photoswitchable Supramolecular Hydrogels Formed by Cyclodextrins and Azobenzene Polymers. *Angew. Chem. Int. Ed.* **2010**, *49* (41), 7461–7464. https://doi.org/10.1002/anie.201003567.
(57) Guo, Z.; Zhang, X.; Wang, Y.; Li, Z. Supramolecular Self-Assembly of Perylene Bisimide Derivatives Assisted by Various Groups. *Langmuir* **2018**. https://doi.org/10.1021/acs.langmuir.8b02964.
(58) Draper, E. R.; Walsh, J. J.; McDonald, T. O.; Zwijnenburg, M. A.; Cameron, P. J.; Cowan, A. J.; Adams, D. J. Air-Stable Photoconductive Films Formed from Perylene Bisimide Gelators. *J Mater Chem C* **2014**, *2* (28), 5570–5575. https://doi.org/10.1039/c4tc00744a.
(59) Roy, S.; Maiti, D. K.; Panigrahi, S.; Basak, D.; Banerjee, A. A New Hydrogel from an Amino Acid-Based Perylene Bisimide and Its Semiconducting, Photo-Switching Behaviour. *RSC Adv.* **2012**, *2* (29), 11053–11060. https://doi.org/10.1039/C2RA21319B.
(60) Zhan, X.; Facchetti, A.; Barlow, S.; Marks, T. J.; Ratner, M. A.; Wasielewski, M. R.; Marder, S. R. Rylene and Related Diimides for Organic Electronics. *Adv. Mater.* **2011**, *23* (2), 268–284. https://doi.org/10.1002/adma.201001402.
(61) Ghosh, I.; Ghosh, T.; Bardagi, J. I.; Konig, B. Reduction of Aryl Halides by Consecutive Visible Light-Induced Electron Transfer Processes. *Science* **2014**, *346* (6210), 725–728. https://doi.org/10.1126/science.1258232.
(62) Sukul, P. K.; Santra, D. C.; Singh, P. K.; Maji, S. K.; Malik, S. Water Soluble Perylene Bisimide and Its Turn off/on Fluorescence Are Used to Detect Cysteine and Homocysteine. *New J. Chem.* **2015**, *39* (7), 5084–5087. https://doi.org/10.1039/C5NJ00608B.
(63) Pellegrin, Y.; Odobel, F. Sacrificial Electron Donor Reagents for Solar Fuel Production. *Comptes Rendus Chim.* **2017**, *20* (3), 283–295. https://doi.org/10.1016/j.crci.2015.11.026.
(64) Kang, R.; Miao, R.; Qi, Y.; Chang, X.; Shang, C.; Wang, L.; Fang, Y. Tuning the Formation of Reductive Species of Perylene-Bisimide Derivatives in DMF via Aggregation Matter. *Chem. Commun.* **2017**, *53* (72), 10018–10021. https://doi.org/10.1039/C7CC05645A.
(65) Marcon, R. O.; Brochsztain, S. Aggregation of 3,4,9,10-Perylenediimide Radical Anions and Dianions Generated by Reduction with Dithionite in Aqueous Solutions. *J. Phys. Chem. A* **2009**, *113* (9), 1747–1752. https://doi.org/10.1021/jp808383e.

4.9 Appendix

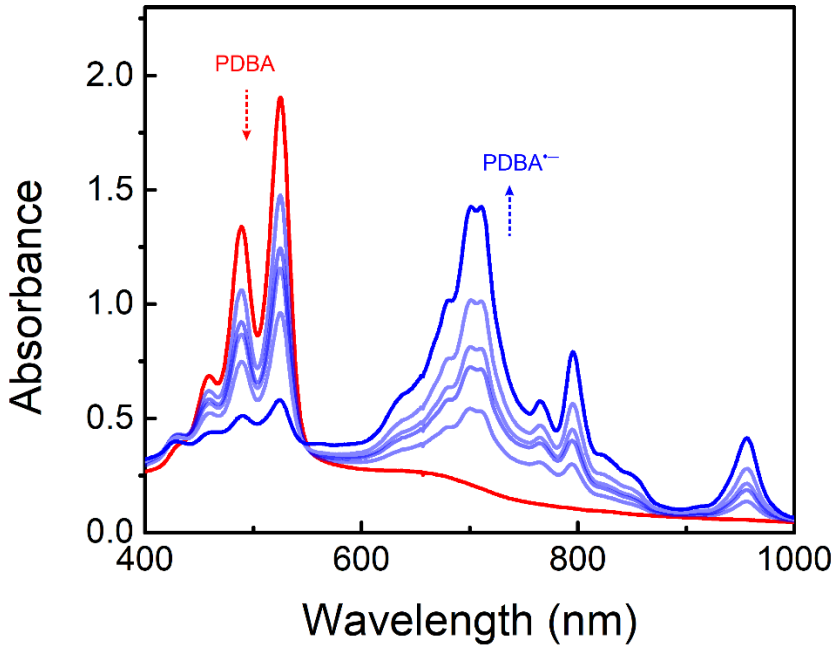

Figure 4.10. The photoreduction of 33 µM PDBA in DMSO with 3000 TEA upon UVA irradiation 5mins (LED from 350 to 410 nm, 3-6 W/cm^2, irradiation distance 40cm between the sample and lamp) under vacuum conditions.

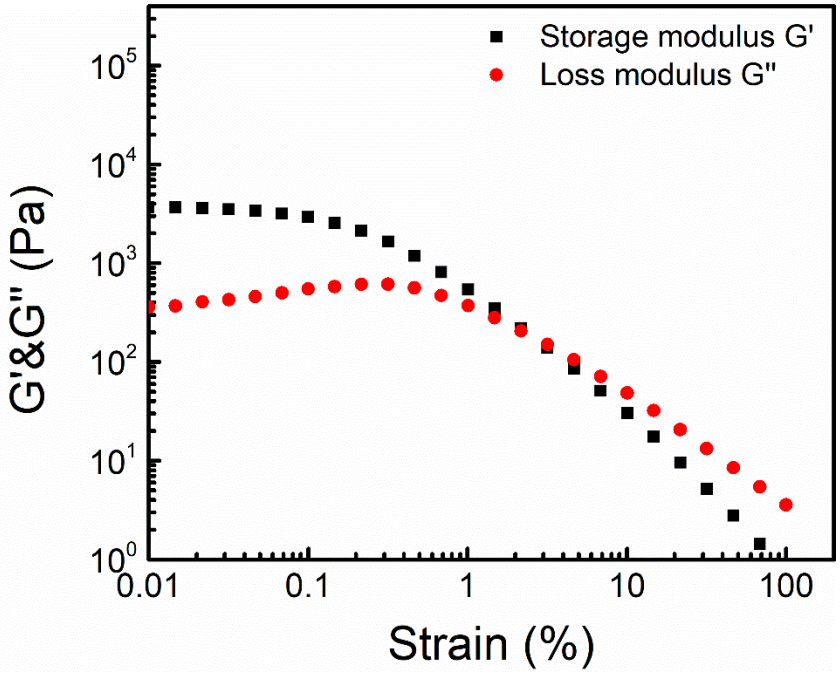

Figure 4.11. PDBA/CTAB/TEA gel (4.7 wt%) made in a vial was transferred to a rheometer (with two stainless steel parallel plates) at 20 °C and swept with a strain from 0.01 to 100% at shearing rate 10 rad/s.

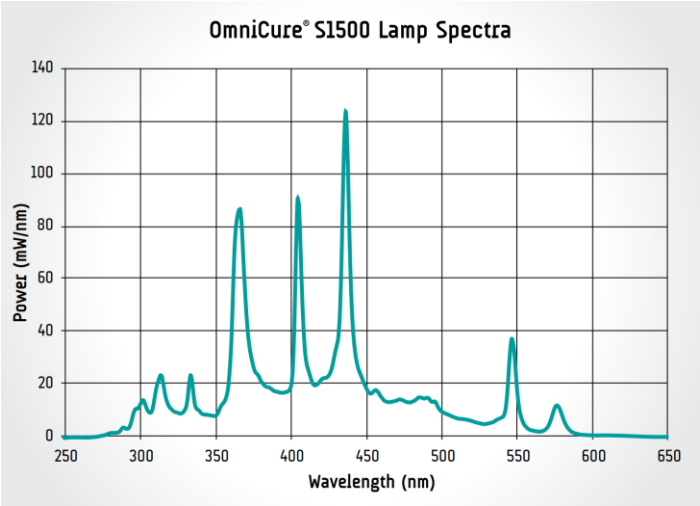

Figure 4.12. The lamp spectra on photo-rheometer.

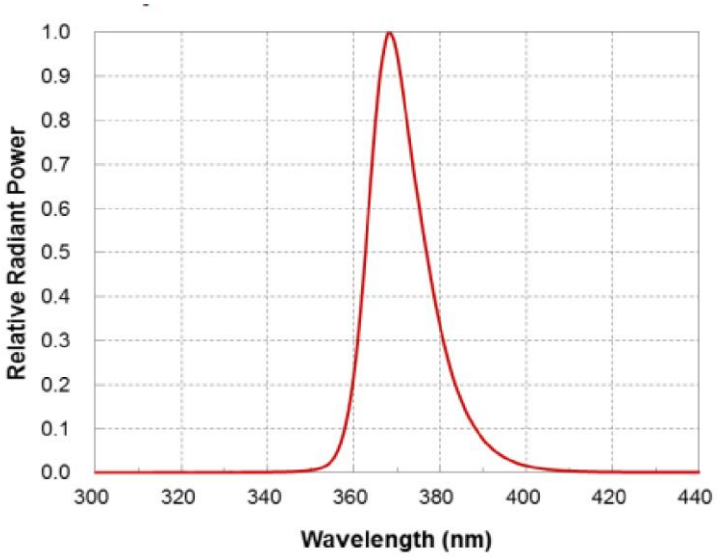

Figure 4.13. The lamp spectra of UVA LED for the gel photoreduction in vials.

Chapter 5.

Temporally Controlled out-of-Equilibrium Systems Based on Synergistic Reactions: Photoreduction and Chemical Reduction of Perylene Bisimide

Abstract: We construct **PBI-1** (a perylene bisimide derivative) out of equilibrium systems, temporally mediated by synergistic reduction: both chemical reduction and photoreduction are possible. In all-chemical reduction, the electron transfers slowly from DTT to **PBI-1** leading to reduced/disassembled species, i.e., the radical anion (**PBI-1**$^{\bullet-}$) and **PBI-1** dianion (**PBI-1**$^{2-}$). Introducing an aliquot of oxygen into the system by shaking leads to a short-lived re-assembled state of mostly neutral **PBI-1** species. Such a process is currently called Transient Self-assembly in the literature. The chemical reduction can greatly be accelerated when exposed to UV irradiation, leading to photoreduction. Simultaneously employing these two (synergistic) reductions, and combined with (ambient oxygen) oxidation, leads to emergent properties, such as oscillation between the aggregates and the monomers. Additionally, we developed other photoredox cycles with DTT being an electron-donor, such as naphthalene bisimide (NDI), thus showing the approach is generally applicable.

5.1 Introduction.

Supramolecular assemblies have been extensively studied at the thermodynamical equilibrium from the nanoscale to the macroscale[1–6]. Many stimuli such as pH[7–9], temperature[10,11], mechanical stress[12,13], and light irradiation[14,15] have been used to control self-assembly[16–18]. Meanwhile, well-organized π-conjugates that even plays the leading roles in constructing organic semiconductor[19–22] and contribute to electron-hole transfer. In recent years, the field has started moving toward studying out-of-equilibrium states that can be obtained using chemical fuels (in a batch-wise or sustained addition regime), enabling the materials with emergent properties, such as transient membrane transport[23], spatiotemporally controlled patterns[24,25], traveling waves, and oscillations[26].

Out-of-equilibrium systems often show a transient self-assembly behavior, where assemblies are formed for a predetermined amount of time. Typically, two irreversible reactions are used: one that activates a monomer (enabling self-assembly) and one deactivating the monomer (resulting in disassembly)[23,27–30]. The initial (deactivated) monomer lacks the capability of the assembly. After putting energy into the system, for example, in the form of chemical fuels or photon[31], the monomer is activated and now has the potential to aggregate. Overall, the assemblies in the system are sustained only when the system is constantly provided with energy that keeps pushing the system away from the equilibrium. Once the influx of energy is stopped, the building blocks are deactivated and revert to deactivated disassembled monomers. Since, in such systems, researchers have found emergent properties (such as non-equilibrium gel and vesicle membranes),[32,33] there has been an increased effort to develop new systems.

The most elegant dissipative out of equilibrium assemblies, however, are found in living beings. Take microtubules, for instance, where dynamic assembly and disassembly of microtubules is driven by guanosine-5'-triphosphate (GTP) hydrolysis to temporally control the functions in cells.[34,35] An artificial look-alike of microtubules was introduced by van Esch co-workers, where they demonstrated that dibenzoyl-(L)-cystine (DBC) could be alkylated to form more hydrophobic mono- or di-esters upon addition of an aliquot of methyliodide (MeI), leading to self-assembled fibers and gels(Figure 5.1).[36] Meanwhile, the hydrolysis of the DBC-esters reverting to the

carboxylate DBC leads to disassembly, which results in gel collapse after the energy source (MeI) was consumed. The latter type of process was called “transient self-assembly.”

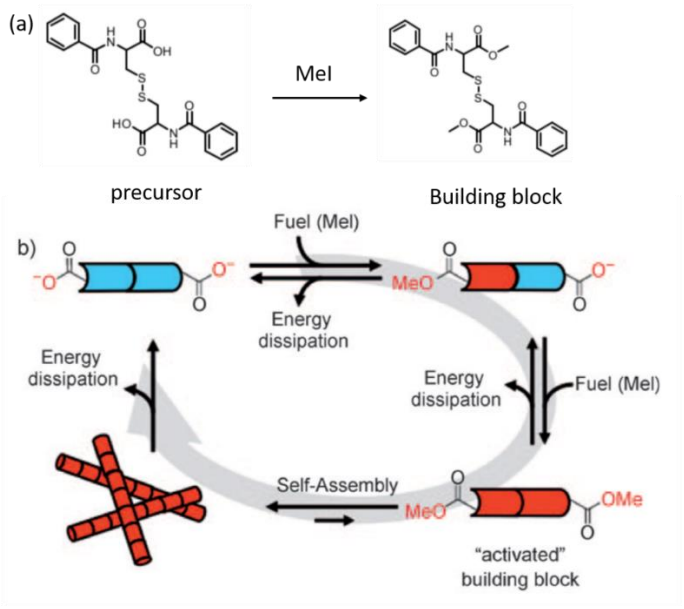

Figure 5.1 **The scheme of dissipative self-assembly.** (a) The transformation of building blocks from the precursor by fueling of MeI. (b) The carboxylate precursor (blue), dibenzoyl-(L)-cystine (DBC), is monomeric. By adding fuel, MeI, the precursor was activated and converted into di-ester building blocks (red) that further aggregates and gelates. As the fuel, MeI is consumed, the building blocks revert to the precursor and disassemble back to the solution. Reproduced from ref. 36 with permission from the Wiley.

When trying to do multiple transient cycles (i.e., adding a shot of fuel, having transient self-assembly, and then disassembly) is often possible, but the response is damped. This is because the chemical fuels produce chemical waste products that accumulate in the system.[37,38] To overcome this issue, light is an ideal energy source to push the system out of equilibrium[29,39], which leaves no chemical waste and can be applied spatiotemporally. For example, systems based on photoisomerizable building blocks like azobenzene[40] or diarylethene[24] have been used. One drawback is the slow response of the latter materials. For instance, the cis-azobenzene relaxes back to the trans that even takes 30 mins upon exposure to a mercury lamp[41] in most cases.

In this chapter, we demonstrate temporally controlled assemblies based on synergistic reductions of a perylene bisimide derivative. We use the same molecule **PBI-1** as in chapter 3 (and as previously studied[26,42] in our research group. As a reminder, it is highly aggregated in water but can be disassembled upon chemical reduction (using sodium dithionite $Na_2S_2O_4$) to its radical anion (**PBI-1**$^{\bullet-}$) and dianion (**PBI-1**$^{2-}$). In chapter 3, we showed that efficient photoreduction could

be achieved by exciting acetone. In this chapter, we use a different approach by adding DTT (1,4-Dithiothreitol), which can fulfill two roles: i) it can chemically reduce **PBI-1**, and ii) it can act as an electron donor in photoreduction (Fig. 5.2). It is, therefore, a "synergistic reduction" system (Figure 5.2a). As usual (see chapter 3), the reduced **PBI-1** species are quickly re-oxidized back to the neutral **PBI-1**, followed by their self-assembly. The unique dual function of DTT in this system leads to pathway selection and supramolecular oscillations driven by light (Figure 5.2b and c).

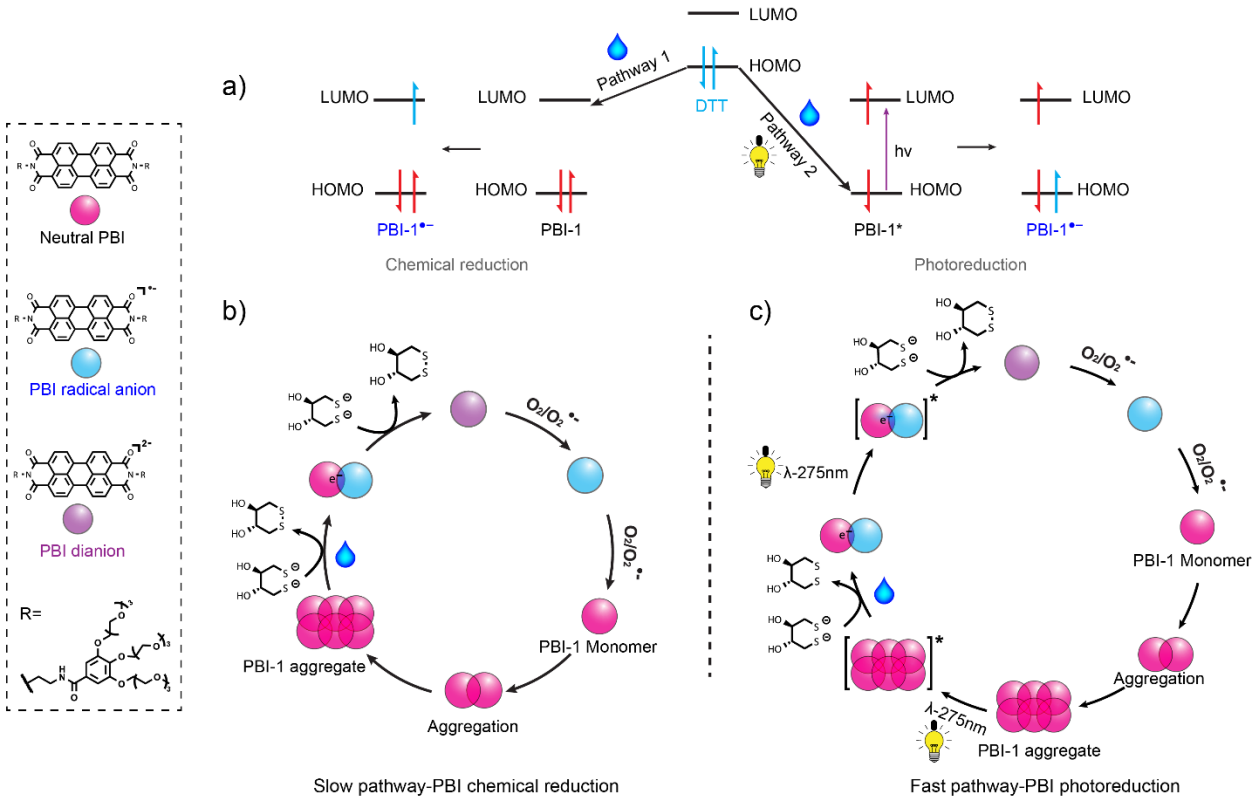

Figure 5.2. **Chemical reduction versus photoreduction of PBI-1.** a) The scheme of two pathways of electron transfer in the donor-acceptor system, where the **PBI-1** is acceptor and dithiothreitol (DTT) as an electron donor. Pathway 1, chemical reduction: the electron transfer is thermodynamically favorable. Pathway 2, photoreduction: upon UV irradiation, excited **PBI-1** gets electrons from DTT faster. b) The scheme of assembly and disassembly of **PBI-1** aggregates upon chemical reduction: the **PBI-1** aggregate (red aggregated balls on the left side) in H_2O, in the presence of DTT, is sequentially reduced into the monomeric **PBI-1**$^{\bullet-}$ and **PBI-1**$^{2-}$ (blue and purple balls). Introducing O_2, **PBI-1**$^{\bullet-}$/**PBI-1**$^{2-}$ were spontaneously re-oxidized back to the neutral, which, over time, aggregated. c) In the photoreduction system: **PBI-1** aggregate, upon UV irradiation, is excited, which subsequently gets electrons from DTT at a fast rate, leading to disassembly after forming **PBI-1**$^{\bullet-}$/**PBI-1**$^{2-}$, which are reverted to the neutral **PBI-1** and further re-aggregated.

5.2. PBI-1 chemical reduction and transient aggregates

As shown in Figure 5.2a (pathway 1), DTT works as a chemical reductant because its highest occupied molecular orbitals (HOMOs) are located above the lowest unoccupied molecular orbitals (LUMO) of **PBI-1** (as determined previously[43] by cyclic voltammetry). The reduction kinetics were monitored using a UV-diode array for an aqueous solution at pH = 10, 33 µM **PBI-1** in the presence of 600 equivalents of DTT (Figure 5.3A). As a reminder, the aggregated **PBI-1** absorbs from 400 to 600 nm with three maxima 502, 526 nm, 565 nm.

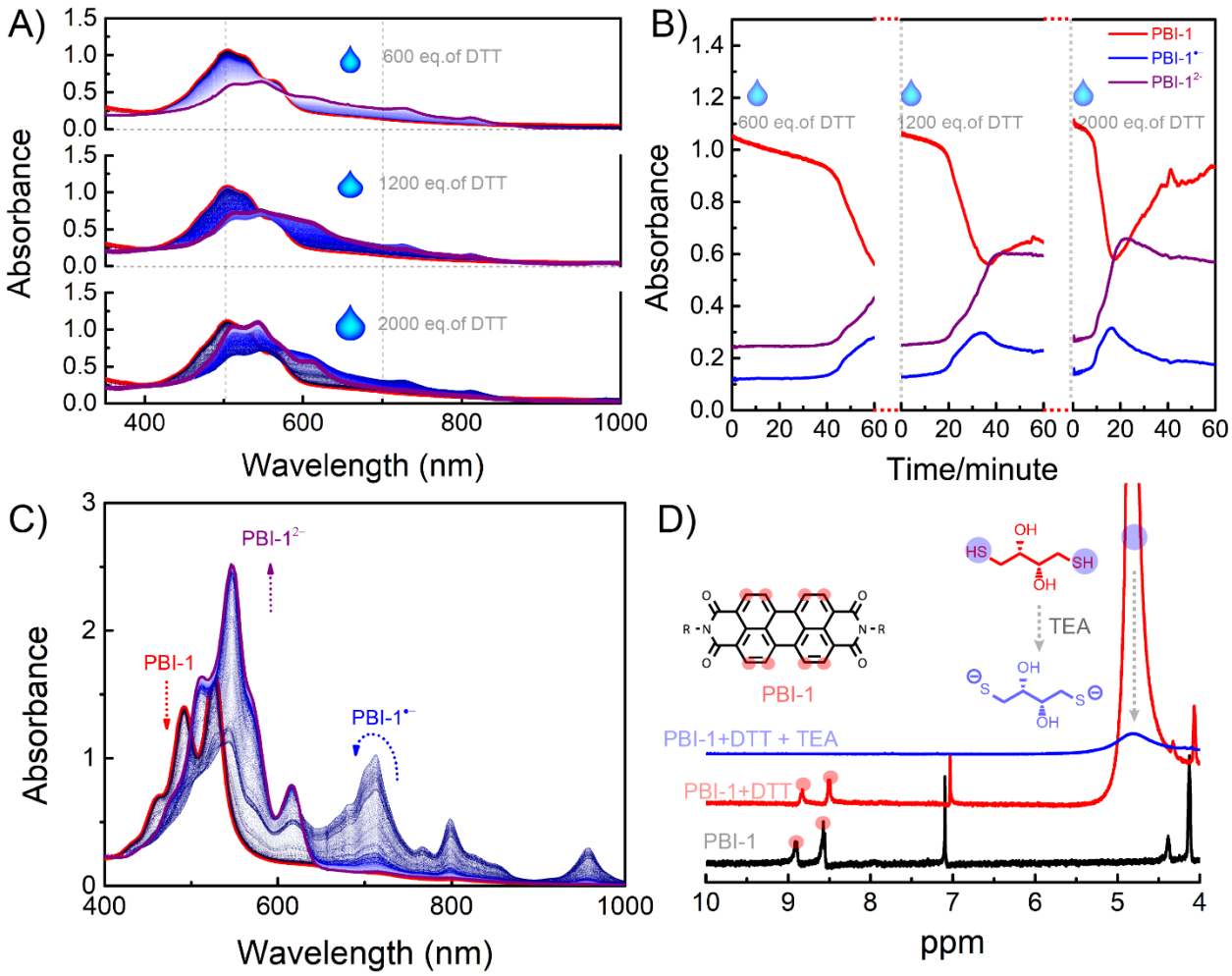

Figure 5.3. **Chemical reduction of aggregated and monomeric PBI-1 by DTT.** A) UV spectra of **PBI-1** chemical reduction in 1 hour with different amounts of DTT, 600, 1200, and 2000. eq, respectively. B) The kinetics of **PBI-1** chemical reduction in an hour with 600, 1200, and 2000 eq. of DTT, **PBI-1** neutral (red line), **PBI-1**$^{\bullet-}$ (blue line), and **PBI-1**$^{2-}$ (purple line) correspond to 502, 729, and 609 nm, respectively. (C) UV spectra of **PBI-1** chemical reduction in DMSO in 1 hour. D) NMR spectra of **PBI-1** in DMSO-d_6, PBI with 600 eq. DTT, **PBI-1** with 600 eq.DTT and 3000 eq. TEA.

Upon reduction, the aggregates are reduced into the monomeric **PBI-1**$^{\bullet-}$ with three maxima at 729, 813, and 980 nm, while **PBI-1**$^{2-}$ has three maxima at 515, 546, and 612 nm. The reduction rate starts slowly but has a significant acceleration after 43, 15, or 7 minutes for 600, 1200, or 2000 equivalent of DTT, respectively (Figure 5.3 B). In 1 hour of reduction with 2000 eq. of DTT, **PBI-1**$^{2-}$ was obtained more than the less DTT involved in (with 600 or 1200 eq.). It should be noted that the latter experiments were performed in a closed cuvette but with a volume of ~ 1 mL of air at the top. Upon shaking, and thus rigorously introducing O_2, **PBI-1**$^{\bullet-}$ and **PBI-1**$^{2-}$ were spontaneously re-oxidized (see Fig. 5.4A, re-oxidized neutral spectrum).

In a control experiment, no reduction was observed for pH values below 7 as reported in literature[44], since only the thiolate form $-S^-$ is active, whereas –SH is not. To further confirm that the evolution of **PBI-1** is an electron-transfer process instead of DTT performing a nucleophilic attack on **PBI-1** imide positions, NMR spectroscopy was used. Because the aggregated **PBI-1** in D_2O has no defined peaks, we studied monomeric **PBI-1** reduction in DMSO-d_6 (the reduction is easier to be observed with NMR). Figure 5.3 C shows the evolution of UV absorption as **PBI-1** in DMSO (with 600.eq of DTT and 3000 eq. of TEA, replacing sodium hydroxide with TEA due to the inorganic salt is insoluble in DMSO) sequentially reduced into **PBI-1**$^{\bullet-}$, and **PBI-1**$^{2-}$. This suggests that monomeric **PBI-1** also can be chemically reduced by DTT (the same as the aggregated **PBI-1**). Next, we followed the reaction of the monomeric **PBI-1** with DTT in DMSO-d_6. Figure 5.3D shows that the chemical shift of the neutral **PBI-1** has two peaks around 8.9–8.7, and 8.5–8.4 ppm, corresponds to the aromatic perylene core (as labeled in Fig. 5.3D). Adding 600 eq. of DTT, no peaks shift but with one more peak around 4.80 ppm that is assigned to the thiol group of DTT. This implies that there is no chemical reduction. But when adding 3000 eq. of TEA (triethylamine, in this case, under dark conditions thus not acting as an electron donor), the chemical reduction occurs as DTT is deprotonated; meanwhile, chemical shift at aromatic area disappeared due to that new species **PBI-1**$^{\bullet-}$ is paramagnetic (Fig 5.3C). Overall, these first experiments show that DTT can be used as a chemical reductant of **PBI-1**, which had not previously been explored for PBI derivatives in general in the literature.

More interestingly, the re-oxidized **PBI-1** (note the same sample after the first reduction performed in a closed cuvette with 1cm air on the top of solution) in aqueous solution is in a

transient state that autonomously reverts to **PBI-1**$^{\bullet-}$ /**PBI-1**$^{2-}$. The second reduction takes less time (comparing to the first reduction, see Fig. 5.3B); for instance, only 1 minute needed when **PBI-1** with 1200, or 2000 eq. of DTT in water (Figure 5.4A and B), which results from the size-dependent reduction—smaller aggregates taking less time (as our group previously characterized with DLS). Herein DTT as a dual fuel that plays a dormant role which leads to a slow chemical reduction after faster oxidation of **PBI-1**$^{\bullet-}$ /**PBI-1**$^{2-}$, contributing to **PBI-1** temporally stay. Some argue that DTT is simultaneously consumed by O_2 but in this case, the **PBI**$^{\bullet-}$ /**PBI-1**$^{2-}$ priorly reacting with molecular oxygen even in the presence of extra DTT. As we observed, **PBI-1**$^{\bullet-}$ /**PBI-1**$^{2-}$ with 2000 eq. of DTT in aqueous solution is stable in a vial with a closed cap even over half-year. This autonomous reduction provides us a possibility to build **PBI-1** transient aggregates with varied lifetime by adjusting the quantity of DTT.

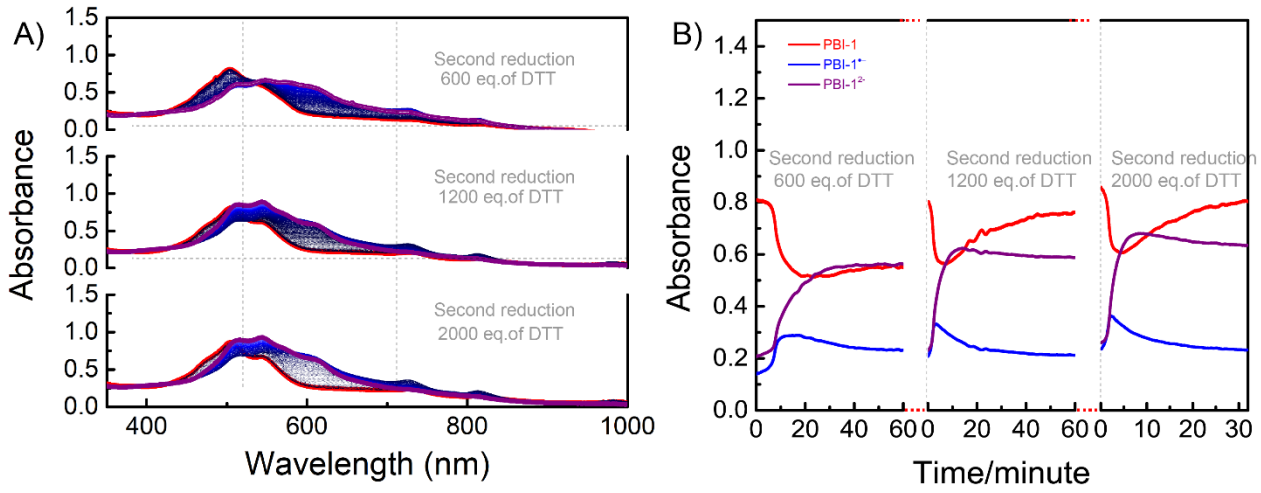

Figure 5.4. **The PBI-1 second reduction driven by dual fuel DTT.** A) UV spectra of **PBI-1** second reduction (after one redox) driven by the intrinsic dual fuel DTT with different amounts of DTT, 600, 1200, and 2000. eq. B) The kinetics of **PBI-1** chemical reduction in an hour with 600, 1200, and 2000 eq. of DTT, **PBI-1** neutral (red line), **PBI-1**$^{\bullet-}$ (blue line), and **PBI-1**$^{2-}$ (purple line) correspond to 502, 729, and 609 nm, respectively.

To construct **PBI-1** transient aggregates, we first reduced the aggregated **PBI-1** in H_2O (as above mentioned, with 600 eq. of DTT at pH=10 in a closed cuvette) into the monomeric **PBI-1**$^{\bullet-}$ and **PBI-1**$^{2-}$ (Figure 5.5 A and C) due to the electrostatic repulsion, which takes 5300 s as shown in Figure 5B (the reduction kinetics followed with UV/vis spectroscopy at 502 nm, indicating **PBI-1** evolution, as shown in step. i). When the reduction stays at a minimum plateau, 900s ensuring

that **PBI-1** is fully reduced. By a rigorous flux of O_2, **PBI-1**$^{\bullet-}$ /**PBI-1**$^{2-}$ were spontaneously re-oxidized back to the **PBI-1**.

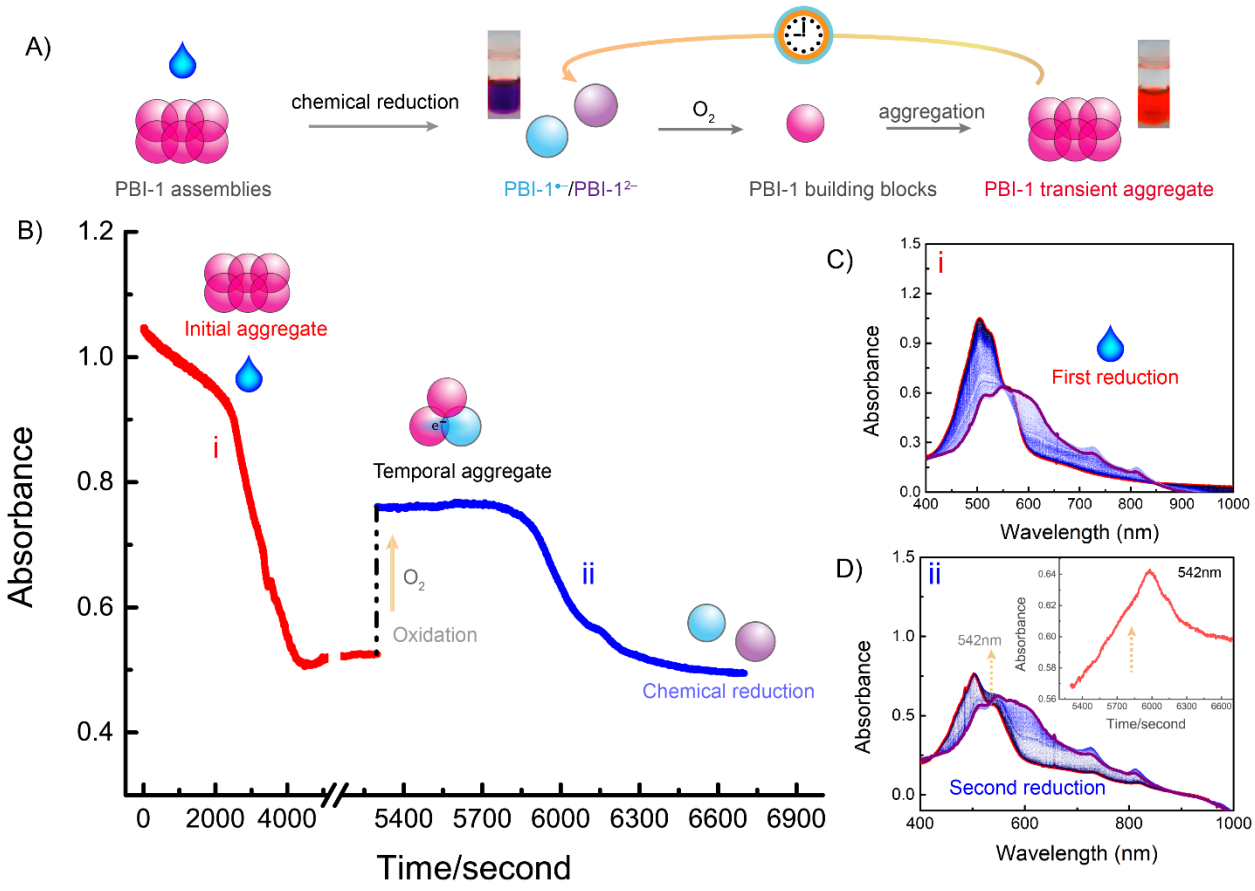

Figure 5.5 **PBI-1 transient aggregates.** A) The scheme of transient **PBI-1** aggregates. The **PBI-1** assemblies (red aggregated balls) were chemically reduced into monomeric **PBI-1**$^{\bullet-}$ /**PBI-1**$^{2-}$ (blue and purple balls). Introducing ambient O_2, the **PBI-1**$^{\bullet-}$ /**PBI-1**$^{2-}$ was re-oxidized back to the neutral **PBI-1** (single red ball) that further aggregates but in a temporally transient state. Over time, the aggregates autonomously reverted to electronically active **PBI-1**$^{\bullet-}$/**PBI-1**$^{2-}$ leading to re-disassembly. (B) The kinetics **PBI-1** chemical reduction followed by UV-diode array (502 nm as an indicator of the assembly and disassembly). The 33 µM aggregated **PBI-1** in the presence of 600 eq. of DTT at pH 10 in H_2O was chemically reduced into the monomeric **PBI-1**$^{\bullet-}$ /**PBI-1**$^{2-}$ (as step i) as UV absorbance from 1.05 to 0.52. By introducing a flux of O_2, **PBI-1**$^{\bullet-}$ /**PBI-1**$^{2-}$ is re-oxidized back to the **PBI-1** but with a small amount of **PBI-1**$^{\bullet-}$, which is a temporal aggregate. Over 500s, the **PBI-1** aggregates autonomously disassemble back to the **PBI-1**$^{\bullet-}$/**PBI-1**$^{2-}$ (as step ii). (C) UV spectra of the first chemical reduction of the aggregated **PBI-1** (step i). (D) UV spectra of the second chemical reduction after the oxidation (by O_2) **PBI-1**$^{\bullet-}$ /**PBI-1**$^{2-}$ (step ii).

UV absorbance at 502 nm (indicating neutral **PBI-1**) that only recovers to the 0.76 (a maximum plateau, step ii) from 0.52 rather than the initial absorbance at 1.05, which suggests a small amount of **PBI-1**$^{\bullet-}$ mixed with **PBI-1** (Figure 5.5D, the UV spectrum before the second reduction).

The mixture (**PBI-1**/ **PBI-1**$^{\bullet-}$) is further aggregated for 500s (as the maximum plateau shown in Figure 5.5 B). Figure 5.5 D shows that the kinetics of **PBI-1** UV absorbance at 542 nm keeps growing from 5300s to 6000s, indicative of **PBI-1** reaggregation. After that, the re-aggregates were dissembled as regeneration of **PBI-1**$^{\bullet-}$/**PBI-1**$^{2-}$ (Figure 5.5 B, step. ii.). In short, the transient **PBI-1** aggregates were built in the presence of 'dual fuel' DTT.

5.3 Photoinduced PBI-1 redox cycles

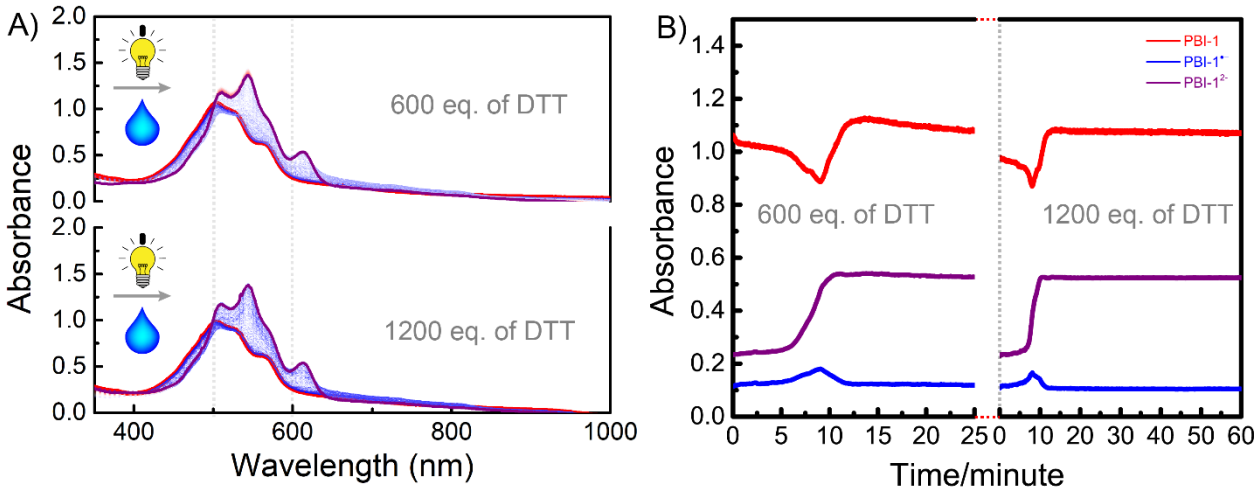

Figure 5.6. **PBI-1 photoreduction upon UVC irradiation.** A) UV-vis spectra of **PBI-1** photoreduction with DTT, 600, and 1200 eq. of DTT. B) The kinetics of **PBI-1** chemical reduction in an hour with 600 and 1200 eq. of DTT, **PBI-1** neutral (red line), **PBI-1**$^{\bullet-}$ (blue line), and **PBI-1**$^{2-}$ (purple line) correspond to 502, 729, and 609 nm, respectively.

As we reported in Chapters 2 and 3, photoinduced electron-transfer can be achieved either by TEOA or acetone radical anion being an electron-donor. In this section, we developed DTT as a novel electron donor in photoinduced electron-transfer to **PBI-1**. Upon UVC (275 nm, 5 mW) irradiation, **PBI-1** (with DTT) is quickly photoreduced. In contrast to the purely chemical reduction by DTT, which took over 1 hour to see an appreciable amount of **PBI-1**$^{2-}$, reduction upon irradiation was completed in only 5 minutes (compare Fig. 5.6B to Fig. 5.4B, both "600 eq."). Even under constant stirring in an open (to the air) cuvette, the photoreduction is fast enough to keep everything in the fully reduced **PBI-1**$^{2-}$ state. In the photoreduction, electron transfers from the DTT HOMO to excited **PBI-1** HOMO which has a much greater potential difference, as compared to the chemical reduction where the electron has to move from the DTT HOMO to the **PBI-1**

LUMO (Figure 5.2a, pathway 2, photoreduction). As a control experiment, proving that DTT is not photoexcited directly (like for acetone radical formation in Chapter 3), we used UVA (irradiating 10 mins in a closed cuvette, 316 to 400 nm, 1422 mW/m^2, DTT has no absorption at this region) excited the sample then after forming the same product **PBI-1**$^{2-}$ (see Appendix Fig. 5.10) as in the UVC. Thus, as we illustrated in Figure 5.2a (pathway 2), DTT being an electron donor in photoinduced electron-transfer.

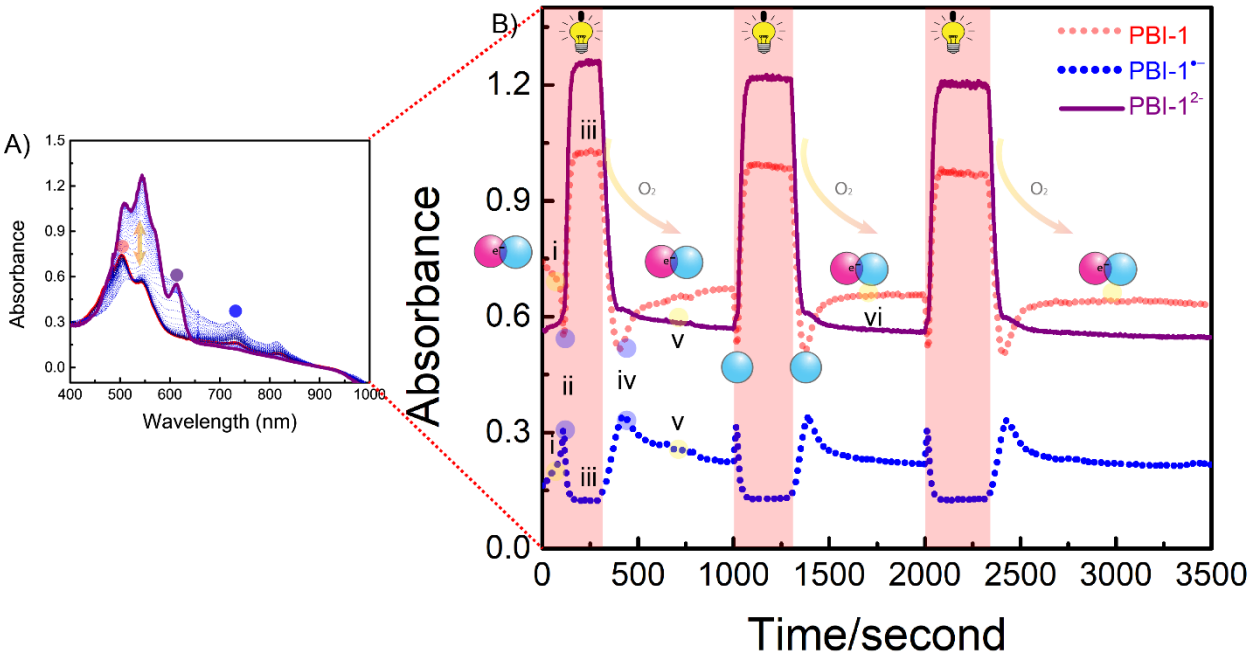

Figure 5.7. **Multiple PBI-1 photoredox cycles.** A) UV spectra of the **PBI-1** second photoreduction after the first photoredox. B) the kinetics of the **PBI-1** photoredox in the presence of 600 eq. of DTT in 1 hour by switching on and off UVC LED at 5 cm (the solution is stirred for introducing O_2 in an open cuvette). **PBI-1** neutral (red line), **PBI-1**$^{\bullet-}$ (blue line), and **PBI-1**$^{2-}$ (purple line) correspond to 502, 729, and 609 nm, respectively. The process of the photoredox: The reduction: **PBI-1** to **PBI-1**$^{\bullet-}$ (step i, light on), **PBI-1**$^{\bullet-}$ reaching to the maximum (ii), **PBI-1**$^{\bullet-}$ to **PBI-1**$^{2-}$ (from step ii to iii). The oxidation: **PBI-1**$^{2-}$ to **PBI-1**$^{\bullet-}$ (from step iii to iv), **PBI-1**$^{\bullet-}$ to **PBI-1** (v).

If one keeps introducing O_2 into **PBI-1** solution (the sample with 600 eq. of DTT after the first photoreduction in Figure 5.6A) by rigorously stirring (an open quartz cuvette), **PBI-1**$^{2-}$ would be re-oxidized back to **PBI-1** with some retaining **PBI-1**$^{\bullet-}$ (Figure 5.7A, the red line). By re-applying UVC to the solution, the faster second photoreduction (in comparison to the first photoreduction in Figure 5.6 B) only takes 3 mins reaching to **PBI-1**$^{2-}$ after passing **PBI-1**$^{\bullet-}$ (Figure 5.7 B, from step. i to iii, **PBI-1** to **PBI-1**$^{\bullet-}$, **PBI-1**$^{\bullet-}$ to **PBI-1**$^{2-}$), resulting from the monomeric **PBI-1** taking less time to be reduced comparing to the aggregated **PBI-1**. After switching off the light, **PBI-1** still has no

aggregation (Figure 5.7 B, step iv) even with a rigorous flux of O_2 due to a faster chemical reduction simultaneously occurring. This allows the mixture of **PBI-1**/ **PBI-1**$^{\bullet-}$ to stay away from equilibrium by a simultaneous chemical reduction and oxidation (Figure 5.7, step v and vi). In the third and fourth photoredox cycles, the photoreduction even only needs 90s (shorter than the second photoreduction). Thus, the **PBI-1** photoreduction can be repeated with many redox cycles without any decomposition (in general, **PBI-1** decomposes if exposed long time under UVC).

5.4 PBI-1 light-driven oscillations

Our research group has recently shown supramolecular size oscillations for the same **PBI-1** molecules.[26] In the latter work, sodium dithionite and air were continuously added to a stirred batch reactor, and large-scale color oscillations (and size oscillations confirmed by light scattering as well). In this section, the aim was to achieve light-driven oscillations in the same system. Practically, a 1 cm pathlength quartz cuvette with 33 µM **PBI-1** aqueous solution containing 1400 eq. of DTT at pH=10 was irradiated using a UVC LED (275 nm, 5 mW, 5 cm). As we reported, the oxidation and reduction rates needed to be very closely matched in order to observe oscillations.

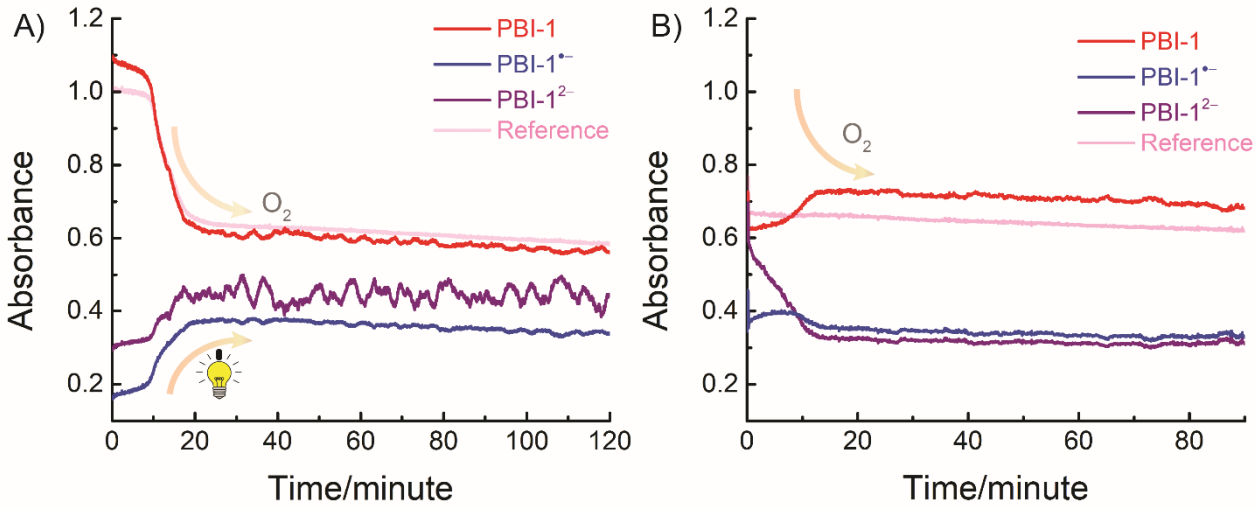

Figure 5.8 **PBI-1 oscillation in simultaneously synergistic reduction and oxidation.** (A) The oscillation between **PBI-1** aggregates and monomeric **PBI-1**$^{\bullet-}$ /**PBI-1**$^{2-}$ is tracked by UV spectroscopy. 33 µM **PBI-1** with 1400 eq. of DTT at pH 10 in a quartz cuvette was simultaneously conducted the synergistic reduction (chemical reduction and photoreduction) upon UVC LED and a constant introduction of atmospheric O_2 by stirring. The kinetics of **PBI-1** chemical reduction: **PBI-1** neutral (red line), **PBI-1**$^{\bullet-}$ (blue line), and **PBI-1**$^{2-}$ (purple line) correspond to 502, 729, and 609 nm, respectively. (B) The same experiment as the former experiment without light irradiation.

Therefore, we changed the light intensity gradually by changing the distance of the UVC LED array with respect to the quartz cuvette. After a long optimization process, we found conditions where noisy oscillations could be observed. In the previous work, it was found necessary to first fully reduce to **PBI-1**$^{2-}$ in order to see large-scale oscillations. To mimic these conditions as closely as possible, here, the sample was first fully photoreduced for 20 min (UVC light source at 2 cm). After that, the light source was turned off to allow oxidation by O_2 to occur under continuous stirring. Thirty minutes after the latter, the repositioned light sources (between 4 cm and 5 cm) were turned on and left on for the duration of the experiment (while still stirring). The results was that **PBI-1** was quickly reduced into **PBI-1**$^{\bullet-}$/**PBI-1**$^{2-}$, followed by noisy oscillations that were most visible in the **PBI-1**$^{2-}$ concentration (see Figure 5.8 A, UVC light source at 5 cm). In the oscillating regime, as our group previously reported[26], positive feedback stems from the cooperative supramolecular polymerization of **PBI-1**. That is, the assembly rate keeps increasing sharply when going from an all-monomeric state to a colloidal state. On the other hand, there is also a negative feedback mechanism. Namely, the reduction—both chemical reduction and photoreduction—is size-dependent. Larger colloids will take longer to reduce and disassemble as compared to smaller aggregates (or monomers). The nonlinearity of the kinetics of the assembly/disassembly and the reduction, are key in pushing the system far from equilibrium, and in achieving oscillations. As a control experiment—to remove the possibility that the noisy signal was caused by the stirring bar—the same sample but at pH = 7 (DTT reducing power is inactivated), no oscillation or noise signal was observed (not shown).

Notably, the oscillation here only takes place with by the dual chemical/photo-reduction in the presence of UVC light. When removing the UVC LED, no oscillations were observed (Figure 5.8 B). In fact, after 15 mins, the oxidation is dominant where **PBI-1** coexists with a small amount of **PBI-1**$^{\bullet-}$. The latter steady-state even can be maintained for 1 hour (Figure 5.8 B). Once stopping the stirring, the chemical reduction autonomously brought **PBI-1** back to **PBI-1**$^{\bullet-}$/**PBI-1**$^{2-}$ until all the fuel DTT is consumed.

Beyond oscillation, this synergistic reduction could also be promising to construct light-driven patterns. If UVC light were to be applied through a photo-mask on a **PBI-1** aqueous solution with DTT, a pattern would be created due in situ photoreduction leading to disassembly and a color

change whereas the non-irradiated region remains in the aggregated state. As we have shown (see above), the disassembly can lead to convective flows, which would result in intricate emergent patterns. We hope to explore this in the near future.

5.5 DTT as a general electron-donor in photoreduction

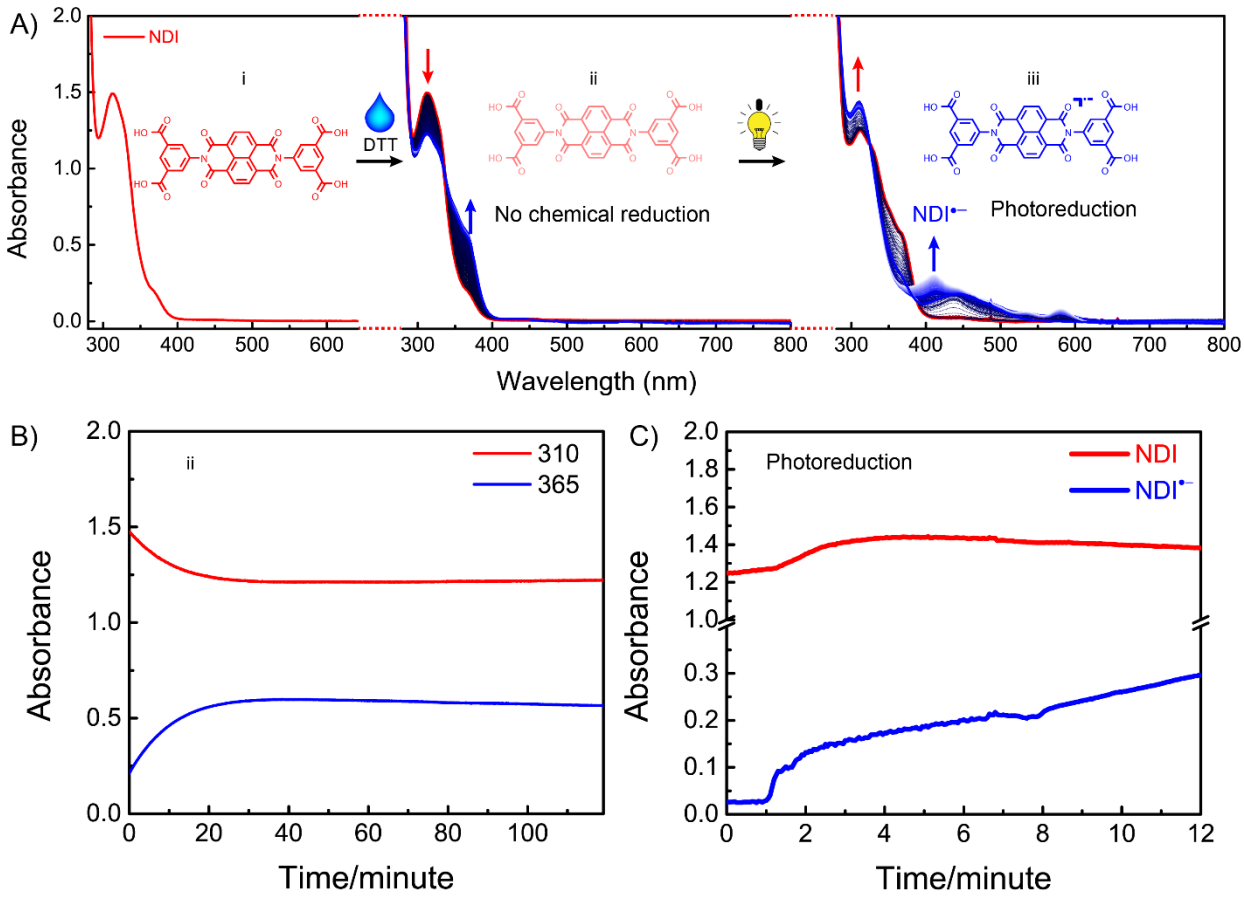

Figure 5.9. **The NDI photoredox upon UVC irradiation.** A) UV spectra of the 100 µM neutral NDI (napthalenedimide-aminoisophthalic acid) at pH 10 aqueous solution (i), the NDI with 2000 eq. of DTT (ii), the sample irradiated by UVC 12 mins (iii). B) The kinetics of the sample (ii) in 2 hours, the UV absorbance at 310 and 365 nm indicate the NDI aggregation. (C) The kinetics of NDI photoreduction (the sample iii) after the sample exposed upon UVC LED (275 nm) 12 mins, the UV absorbance at 310, and 410nm, indicative of the neutral NDI, and $NDI^{\bullet-}$, respectively.

Additionally, we developed other photoredox cycles with naphthalene bisimides (NDI). Specifically, a 100 µM napthalenedimide-aminoisophthalic acid (NDI) in water at pH=10 in the presence of 2000 eq of DTT (without stirring in a closed cuvette), had no obvious chemical

reduction for 2 hours (Figure 5.9 A, step i and ii). Figure 5.9 B shows that the kinetics of UV absorbance at 310 nm declines, whereas a new absorption rises at 365 nm, which suggests NDI aggregates without chemical reduction. But interestingly, when employing UVC light on the same sample for 12 mins, a characteristic UV absorption was observed from 360 nm to 610 nm with three maxima at 410, 535, 582 nm, corresponding to $NDI^{\bullet-}$ (NDI radical anion). Consequently, the sample are less aggregated in comparison to the former solution (Figure 5.9 A, step i and ii) with DTT. In short, DTT being an electron-donor can facilitate $NDI^{\bullet-}$ generation, even in the presence of O_2.

5.6 Conclusions

In summary, we have constructed **PBI-1** out-of-equilibrium assemblies driven by the 'dual fuel' DTT working as electron-donor both in chemical and photoreduction. In the chemical reduction (pathway 1), **PBI-1** aggregates first disassembled into the electrostatically repulsive $\mathbf{PBI^{\bullet-}}$/$\mathbf{PBI\text{-}1^{2-}}$ species. Upon shaking, oxygen was introduced, which transiently leads to neutral **PBI-1** and its aggregates. However, when shaking was stopped, reduction again became dominant. The lifetime of aggregation was predetermined by the quantity of DTT fuel. In addition, the reduction rate (chemical reduction) can be accelerated by light (pathway 2) that synergistically drives the disassembly. Upon a simultaneous reduction (chemical reduction and photoreduction) and oxidation (by O_2), we could achieve emergent oscillations between **PBI-1** aggregates and monomers. Interestingly, using DTT as an electron donor in photoreduction seems to be a general method to regulate rylene bisimide, such as NDI aggregates.

5.7 Acknowledgements

Chunfeng Chen performed the synthesis and all the experiments. Prof. Thomas Hermans supervised the research.

5.8 Experimental Section

Compound and Chemicals: The building block perylene bisimides (PBI-1) were synthesized as in chapter 2. Napthalenebisimide-aminoisophthalic acid (NDI)[45] were synthesized as literature reported by coupling napthalenebismide and aminoisophthalic acid. All the other chemicals and solvents were purchased from Sigma-Aldrich, TCI, and VWR without further purification. all.

UV-vis Measurements. UV/vis spectra were taken by Home-modified UV-diode array 8454. The holder with four windows was 3D-printed, which allows the UVC LED (275 nm, 5.0 mW) to constantly excite the sample from the sidewall of 1cm quartz cuvette.

PBI-1 Chemical Reduction. 33 μM PBI-1 with 600, 1200, and 2000 eq. DTT in water at pH 10 in a closed cuvette with 1cm air on the top of solution.

PBI-1 Photoreduction. 33 μM PBI-1 with 600, 1200, and 2000 eq. DTT in water (at pH 10, solution is stirred), was irradiated by UVC LED (275 nm, 5 mW) in a 1 cm opening cuvette. The distance between UVC LED and sample holder is 2 and 5 cm.

NDI Photoreduction. 100 μM NDI with 2000 eq. DTT in water at pH 10, was irradiated by UVC LED at 2 cm (275 nm, 5 mW) in a 1cm closed cuvette. The distance between UVC LED and sample holder is 2 cm.

5.9 References

(1) Goor, O. J. G. M.; Hendrikse, S. I. S.; Dankers, P. Y. W.; Meijer, E. W. From Supramolecular Polymers to Multi-Component Biomaterials. *Chem. Soc. Rev.* **2017**, *46* (21), 6621–6637. https://doi.org/10.1039/C7CS00564D.

(2) Xiao, T.; Zhong, W.; Yang, W.; Qi, L.; Gao, Y.; Sue, A. C.-H.; Li, Z.-Y.; Sun, X.-Q.; Lin, C.; Wang, L. Reversible Hydrogen-Bonded Polymerization Regulated by Allosteric Metal Templation. *Chem. Commun.* **2020**, *56* (92), 14385–14388. https://doi.org/10.1039/D0CC06381A.

(3) Bondarenko, A. S.; Patmanidis, I.; Alessandri, R.; Souza, P. C. T.; Jansen, T. L. C.; Vries, A. H. de; Marrink, S. J.; Knoester, J. Multiscale Modeling of Molecular Structure and Optical Properties of Complex Supramolecular Aggregates. *Chem. Sci.* **2020**, *11* (42), 11514–11524. https://doi.org/10.1039/D0SC03110K.

(4) Raymond, D. M.; Nilsson, B. L. Multicomponent Peptide Assemblies. *Chem. Soc. Rev.* **2018**, *47* (10), 3659–3720. https://doi.org/10.1039/C8CS00115D.
(5) Wang, C.; Wang, J.; Zeng, L.; Qiao, Z.; Liu, X.; Liu, H.; Zhang, J.; Ding, J. Fabrication of Electrospun Polymer Nanofibers with Diverse Morphologies. *Molecules* **2019**, *24* (5), 834. https://doi.org/10.3390/molecules24050834.
(6) Würthner, F.; Saha-Möller, C. R.; Fimmel, B.; Ogi, S.; Leowanawat, P.; Schmidt, D. Perylene Bisimide Dye Assemblies as Archetype Functional Supramolecular Materials. *Chem. Rev.* **2016**, *116* (3), 962–1052. https://doi.org/10.1021/acs.chemrev.5b00188.
(7) Cafferty, B. J.; Avirah, R. R.; Schuster, G. B.; Hud, N. V. Ultra-Sensitive PH Control of Supramolecular Polymers and Hydrogels: PKa Matching of Biomimetic Monomers. *Chem. Sci.* **2014**, *5* (12), 4681–4686. https://doi.org/10.1039/C4SC02182G.
(8) Muñoz Resta, I.; Manzano, V. E.; Cecchi, F.; Spagnuolo, C. C.; Cukiernik, F. D.; Di Chenna, P. H. Supramolecular Assembly of PH-Sensitive Triphenylene Derived π-Gelators and Their Application as Molecular Template for the Preparation of Silica Nanotubes. *Gels* **2016**, *2* (1), 7. https://doi.org/10.3390/gels2010007.
(9) Andreeva, D. V.; Kollath, A.; Brezhneva, N.; Sviridov, D. V.; Cafferty, B. J.; Möhwald, H.; Skorb, E. V. Using a Chitosan Nanolayer as an Efficient PH Buffer to Protect PH-Sensitive Supramolecular Assemblies. *Phys. Chem. Chem. Phys.* **2017**, *19* (35), 23843–23848. https://doi.org/10.1039/C7CP02618H.
(10) Matsumoto, K.; Sakikawa, N.; Miyata, T. Thermo-Responsive Gels That Absorb Moisture and Ooze Water. *Nature Communications* **2018**, *9* (1), 2315. https://doi.org/10.1038/s41467-018-04810-8.
(11) Kreuzer, L. P.; Widmann, T.; Aldosari, N.; Bießmann, L.; Mangiapia, G.; Hildebrand, V.; Laschewsky, A.; Papadakis, C. M.; Müller-Buschbaum, P. Cyclic Water Storage Behavior of Doubly Thermoresponsive Poly(Sulfobetaine)-Based Diblock Copolymer Thin Films. *Macromolecules* **2020**, *53* (20), 9108–9121. https://doi.org/10.1021/acs.macromol.0c01335.
(12) Chaudhari, A. K.; Han, I.; Tan, J.-C. Multifunctional Supramolecular Hybrid Materials Constructed from Hierarchical Self-Ordering of In Situ Generated Metal-Organic Framework (MOF) Nanoparticles. *Advanced Materials* **2015**, *27* (30), 4438–4446. https://doi.org/10.1002/adma.201501448.
(13) Huang, Y.; Kobayashi, M. Direct Observation of Relaxation of Aqueous Shake-Gel Consisting of Silica Nanoparticles and Polyethylene Oxide. *Polymers* **2020**, *12* (5), 1141. https://doi.org/10.3390/polym12051141.
(14) Salzano de Luna, M.; Marturano, V.; Manganelli, M.; Santillo, C.; Ambrogi, V.; Filippone, G.; Cerruti, P. Light-Responsive and Self-Healing Behavior of Azobenzene-Based Supramolecular Hydrogels. *Journal of Colloid and Interface Science* **2020**, *568*, 16–24. https://doi.org/10.1016/j.jcis.2020.02.038.
(15) Chen, L.; Zhao, X.; Lin, Y.; Su, Z.; Wang, Q. Dual Stimuli-Responsive Supramolecular Hydrogel of Bionanoparticles and Hyaluronan. *Polym. Chem.* **2014**, *5* (23), 6754–6760. https://doi.org/10.1039/C4PY00819G.
(16) Yan, X.; Wang, F.; Zheng, B.; Huang, F. Stimuli-Responsive Supramolecular Polymeric Materials. *Chem. Soc. Rev.* **2012**, *41* (18), 6042–6065. https://doi.org/10.1039/C2CS35091B.

(17) Nakahata, M.; Takashima, Y.; Yamaguchi, H.; Harada, A. Redox-Responsive Self-Healing Materials Formed from Host–Guest Polymers. *Nature Communications* **2011**, *2* (1), 511. https://doi.org/10.1038/ncomms1521.
(18) Yang, Y.; Urban, M. W. Self-Healing Polymeric Materials. *Chem. Soc. Rev.* **2013**, *42* (17), 7446–7467. https://doi.org/10.1039/C3CS60109A.
(19) Jones, B. A.; Facchetti, A.; Wasielewski, M. R.; Marks, T. J. Tuning Orbital Energetics in Arylene Diimide Semiconductors. Materials Design for Ambient Stability of n-Type Charge Transport. *J. Am. Chem. Soc.* **2007**, *129* (49), 15259–15278. https://doi.org/10.1021/ja075242e.
(20) Yoon, M.-H.; DiBenedetto, S. A.; Russell, M. T.; Facchetti, A.; Marks, T. J. High-Performance n-Channel Carbonyl-Functionalized Quaterthiophene Semiconductors: Thin-Film Transistor Response and Majority Carrier Type Inversion via Simple Chemical Protection/Deprotection. *Chem. Mater.* **2007**, *19* (20), 4864–4881. https://doi.org/10.1021/cm071230g.
(21) Zheng, Q.; Huang, J.; Sarjeant, A.; Katz, H. E. Pyromellitic Diimides: Minimal Cores for High Mobility n-Channel Transistor Semiconductors. *J. Am. Chem. Soc.* **2008**, *130* (44), 14410–14411. https://doi.org/10.1021/ja805746h.
(22) Katz, H. E.; Lovinger, A. J.; Johnson, J.; Kloc, C.; Siegrist, T.; Li, W.; Lin, Y.-Y.; Dodabalapur, A. A Soluble and Air-Stable Organic Semiconductor with High Electron Mobility. *Nature* **2000**, *404* (6777), 478–481. https://doi.org/10.1038/35006603.
(23) Dambenieks, A. K.; Vu, P. H. Q.; Fyles, T. M. Dissipative Assembly of a Membrane Transport System. *Chem. Sci.* **2014**, *5* (9), 3396–3403. https://doi.org/10.1039/C4SC01258E.
(24) de Jong, J. J. D.; Hania, P. R.; Pug?lys, A.; Lucas, L. N.; de Loos, M.; Kellogg, R. M.; Feringa, B. L.; Duppen, K.; van Esch, J. H. Light-Driven Dynamic Pattern Formation. *Angew. Chem. Int. Ed.* **2005**, *44* (16), 2373–2376. https://doi.org/10.1002/anie.200462500.
(25) Hwang, I.; Mukhopadhyay, R. D.; Dhasaiyan, P.; Choi, S.; Kim, S.-Y.; Ko, Y. H.; Baek, K.; Kim, K. Audible Sound-Controlled Spatiotemporal Patterns in out-of-Equilibrium Systems. *Nature Chemistry* **2020**, *12* (9), 808–813. https://doi.org/10.1038/s41557-020-0516-2.
(26) Leira-Iglesias, J.; Tassoni, A.; Adachi, T.; Stich, M.; Hermans, T. M. Oscillations, Travelling Fronts and Patterns in a Supramolecular System. *Nature Nanotech* **2018**, *13* (11), 1021–1027. https://doi.org/10.1038/s41565-018-0270-4.
(27) Maiti, S.; Fortunati, I.; Ferrante, C.; Scrimin, P.; Prins, L. J. Dissipative Self-Assembly of Vesicular Nanoreactors. *Nature Chemistry* **2016**, *8* (7), 725–731. https://doi.org/10.1038/nchem.2511.
(28) Rossum, S. A. P. van; Tena-Solsona, M.; Esch, J. H. van; Eelkema, R.; Boekhoven, J. Dissipative Out-of-Equilibrium Assembly of Man-Made Supramolecular Materials. *Chem. Soc. Rev.* **2017**, *46* (18), 5519–5535. https://doi.org/10.1039/C7CS00246G.
(29) Ragazzon, G.; Baroncini, M.; Silvi, S.; Venturi, M.; Credi, A. Light-Powered Autonomous and Directional Molecular Motion of a Dissipative Self-Assembling System. *Nature Nanotechnology* **2015**, *10* (1), 70–75. https://doi.org/10.1038/nnano.2014.260.
(30) Boekhoven, J.; Hendriksen, W. E.; Koper, G. J. M.; Eelkema, R.; van Esch, J. H. Transient Assembly of Active Materials Fueled by a Chemical Reaction. *Science* **2015**, *349* (6252), 1075–1079. https://doi.org/10.1126/science.aac6103.

(31) Rieß, B.; Grötsch, R. K.; Boekhoven, J. The Design of Dissipative Molecular Assemblies Driven by Chemical Reaction Cycles. *Chem* **2020**, *6* (3), 552–578. https://doi.org/10.1016/j.chempr.2019.11.008.
(32) Debnath, S.; Roy, S.; Ulijn, R. V. Peptide Nanofibers with Dynamic Instability through Nonequilibrium Biocatalytic Assembly. *J. Am. Chem. Soc.* **2013**, *135* (45), 16789–16792. https://doi.org/10.1021/ja4086353.
(33) Walde, P.; Umakoshi, H.; Stano, P.; Mavelli, F. Emergent Properties Arising from the Assembly of Amphiphiles. Artificial Vesicle Membranes as Reaction Promoters and Regulators. *Chem. Commun.* **2014**, *50* (71), 10177–10197. https://doi.org/10.1039/C4CC02812K.
(34) Muroyama, A.; Lechler, T. Microtubule Organization, Dynamics and Functions in Differentiated Cells. **2017**, 10.
(35) Weisenberg, R. C.; Deery, W. J.; Dickinson, P. J. Tubulin-Nucleotide Interactions during the Polymerization and Depolymerization of Microtubules. *Biochemistry* **1976**, *15* (19), 4248–4254. https://doi.org/10.1021/bi00664a018.
(36) Boekhoven, J.; Brizard, A. M.; Kowlgi, K. N. K.; Koper, G. J. M.; Eelkema, R.; van Esch, J. H. Dissipative Self-Assembly of a Molecular Gelator by Using a Chemical Fuel. *Angewandte Chemie International Edition* **2010**, *49* (28), 4825–4828. https://doi.org/10.1002/anie.201001511.
(37) Ragazzon, G.; Prins, L. J. Energy Consumption in Chemical Fuel-Driven Self-Assembly. *Nature Nanotechnology* **2018**, *13* (10), 882–889. https://doi.org/10.1038/s41565-018-0250-8.
(38) Spitzer, D.; Rodrigues, L. L.; Straßburger, D.; Mezger, M.; Besenius, P. Tuneable Transient Thermogels Mediated by a PH- and Redox-Regulated Supramolecular Polymerization. *Angewandte Chemie International Edition* **2017**, *56* (48), 15461–15465. https://doi.org/10.1002/anie.201708857.
(39) Yin Zihe; Song Guobin; Jiao Yang; Zheng Peng; Xu Jiang-Fei; Zhang Xi. Dissipative Supramolecular Polymerization Powered by Light. *CCS Chemistry 1* (4), 335–342. https://doi.org/10.31635/ccschem.019.20190013.
(40) Klajn, R.; Wesson, P. J.; Bishop, K. J. M.; Grzybowski, B. A. Writing Self-Erasing Images Using Metastable Nanoparticle "Inks." *Angewandte Chemie International Edition* **2009**, *48* (38), 7035–7039. https://doi.org/10.1002/anie.200901119.
(41) Suzuki, M.; Maruyama, Y.; Hanabusa, K. Gel-Solution Phase Transition of Organogels with Photoreversibility: L-Amino Acid Organogelators with Azobenzene. *Tetrahedron Letters* **2016**, *57* (31), 3540–3543. https://doi.org/10.1016/j.tetlet.2016.06.111.
(42) Leira-Iglesias, J.; Sorrenti, A.; Sato, A.; Dunne, P. A.; Hermans, T. M. Supramolecular Pathway Selection of Perylenediimides Mediated by Chemical Fuels. *Chem. Commun.* **2016**, *52* (58), 9009–9012. https://doi.org/10.1039/C6CC01192F.
(43) Leira-Iglesias, J.; Sorrenti, A.; Sato, A.; Dunne, P. A.; Hermans, T. M. Supramolecular Pathway Selection of Perylenediimides Mediated by Chemical Fuels. *Chem. Commun.* **2016**, *52* (58), 9009–9012. https://doi.org/10.1039/C6CC01192F.
(44) Jiang, S.; Landfester, K.; Crespy, D. Control of the Release of Functional Payloads from Redox-Responsive Nanocapsules. *RSC Adv.* **2016**, *6* (106), 104330–104337. https://doi.org/10.1039/C6RA22733C.

(45) Zhang, H.-Y.; Yao, L.-J.; Chen, X.; Huang, J.-Y. Two Coordination Polymers: Treatment Activity on the Bacterial Infection in the Hemodialysis Patients via Inhibiting *Staphylococcus Aureus* Survival. *Journal of Coordination Chemistry* **2020**, *73* (24), 3332–3343. https://doi.org/10.1080/00958972.2020.1846187.

5.10 Appendix

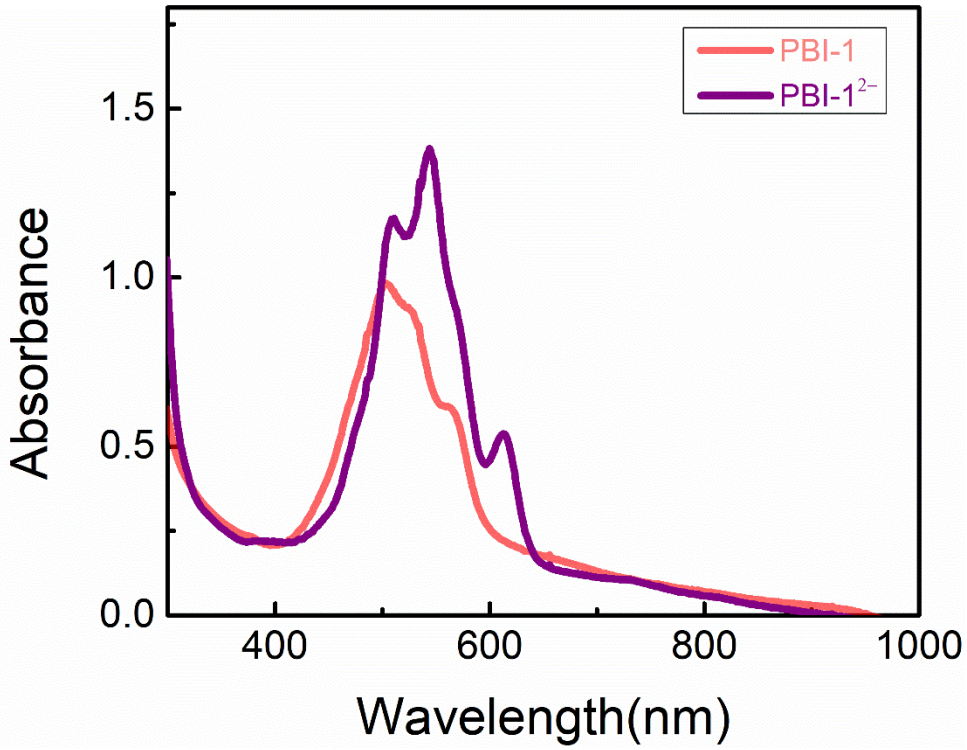

Figure 5.10. **The photoreduction of PBI-1 with DTT upon UVA irradiation.** The UV spectra of PBI-1 with 2000 eq. of DTT, at pH in aqueous solution before and after UVA irradiation (316 to 400 nm, 1422 mW/m^2) 10 mins in a closed cuvette.

Summary and outlook

Supramolecular chemistry aims to build complex dynamic materials with reversible non-covalent bonding, such as hydrogen bonding, π–π stacking, and hydrophobic interactions. In recent years, supramolecular assemblies have been extensively studied at the thermodynamical equilibrium from the nanoscale to the macroscale. For instance, well-organized π-conjugated perylene bisimides that play a leading role in constructing hierarchical structures, photocatalyst, and organic semiconductors. However, in living systems the relevant thermodynamic state is not the equilibrium, but out-of-equilibrium instead. As a result, recent reports show a shift towards developing life-like non-equilibrium systems. Living systems can only be sustained because there is a continuous supply of fuels. For example, the assembly and disassembly of microtubules are constantly driven by GTP to stay out of equilibrium that allows a cell to divide and move. To reproduce this elegant natural dynamic, scientists are striving to develop artificial dissipative systems. In general, energy must first be introduced to convert a precursor into a building block. The energy input can be chemical fuels, enzymes, or light. The resulting monomeric units can then assemble into aggregates from the relatively higher energy landscape to the lower energy landscape. Once the energy source is removed, the aggregates dissipate the energy and revert to the monomeric precursor. Meanwhile, the two reversible reactions of the activation and deactivation of the building blocks are of importance to construct the dissipative out-of-equilibrium assemblies. Recently, our group has employed sodium dithionate (for the forward reduction leading to a disassembly) and oxygen (for the backward oxidation contributing to a re-assembly) as chemical fuels to push PBI (perylene bisimides) systems far from equilibrium, which shows emergent functions, such as supramolecular oscillation, traveling fronts, and patterns.

In most cases, when trying to do multiple transient cycles, the response is damped due to the accumulation of chemical waste. Compared to chemical fuels, light is an ideal energy source to push the system out of equilibrium, which leaves no chemical waste and can be applied spatiotemporally. In this thesis, we have used light to push PBI system away from equilibrium. Unlike in current light-driven systems (e.g., azobenzenes), our approach uses light to activate a

'pre-fuel', which can be stored in large quantities in the system without being reactive itself. Thus, overall still waste is produced in our systems, but only the strictly necessary waste. The result is that reaction cycles can be efficiently operated for long times and/or many activation/deactivation cycles.

In Chapter 2, we have selectively photoinduced one or two electron-transfer of the monomeric and aggregated PBI-1 in a donor-acceptor system under vacuum conditions. We first synthesized perylene bisimide derivative (PBI-1, as our group previously reported) by coupling the perylene diamines and oligoethyleneglycol, which aggregated in sodium bicarbonate buffer, owing to the π-π stacking of conjugated perylene cores and hydrophilic intertwines, while only forms monomer in good solvents, such as DMF, DMSO. When PBI aggregates, in the presence of triethanolamine (TEOA), are irradiated with UVC, at wavelengths corresponding to the excitation of the higher energy level, light-induced two single-electron transfers to generate the PBI radical anion (PBI-$1^{\bullet-}$) followed by the PBI dianion (PBI-1^{2-}). Upon introduction of oxygen (O_2), any PBI-$1^{\bullet-}$ or PBI-1^{2-} present in solution was immediately oxidized to the neutral PBI monomer, which rapidly re-assembled and reverted to the PBI aggregates. We showed that PBI assemblies were important to obtain full reduction to the dianion state, which has so far proven difficult in the literature otherwise.

In Chapter 3, we decided to conduct PBI-1 photoreduction under ambient air conditions. Although the PBI-$1^{\bullet-}$ and PBI-1^{2-} can be easily formed with PBI aggregates under vacuum (in Chapter 2), only one photoredox cycle is achieved after oxygen is introduced into the sealed cuvette. If more photoredox cycles are required, degassing steps are necessary, which limits the application of PBI radicals. Since our ultimate goal is to build photo-driven out-of-equilibrium assemblies under ambient conditions, we realized that we needed to introduce a UV-activated chemical 'pre-fuel'—acetone, to fuel the formation of the dianion PBI-1^{2-} in the presence of oxygen, thus allowing the assembly/disassembly of the PBI aggregates under ambient conditions. Upon UVC irradiation, photoinduced electron-transfer between acetone and TEOA to generate acetone radical anion that further donates electrons to PBI-1 aggregates leading to PBI-1^{2-}even

in a rigorously stirred solutions open to the air. Interestingly, we could selectively obtain the PBI-$1^{\bullet-}$ as a final product (in contrast to the intermediate PBI-$1^{\bullet-}$ fueled by acetone) by introducing another UV-activated fuel terephthaldyhyde. The protocol is not only limited to perylene bisimide derivatives, but can be applied to naphthalene bisimide and methyl viologen.

In Chapter 4, We selectively regulated perylene bisimide gels with one or two photoinduced electron-transfer. We first synthesized the gelator perylene bisimide-aminoisophthalic acid (PDBA) that co-assembled with cetrimonium bromide (CTAB) in the presence of triethylamine (TEA) or hexylamine (HLA) into the corresponding neutral PBI gel in DMSO by heating cooling. The long and entangled nanofibers formed in PDBA/CTAB/HLA gel are reduced to $PDBA^{\bullet-}$ upon UVA irradiation. However, in the PDBA/CTAB/TEA gel, we observed the formation of the dianion $PDBA^{2-}$ which was confirmed with its characteristic UV absorption. Although PDBA/CTAB/TEA and PDBA/CTAB/HLA gel can be photoreduced, their mechanical stiffnesses are opposite. Namely, for PDBA/CTAB/HLA the storage modulus G' increases upon irradiation, whereas for PDBA/CTAB/TEA it decreased. In the former case, only partial reduction was achieved leading to delocalized electrons and stronger fibers, whereas in the latter full reduction leads to stronger electrostatic repulsion. In addition, we could control the mechanical stiffness of PDBA/CTAB/TEA gels by irradiating with varying light intensity.

In Chapter 5, we developed a novel chemical fuel DTT (1,4-Dithiothreitol) with a dual function that leads to pathway selection of PBI dianion formation. DTT herein fulfills two roles: i) it can chemically reduce PBI-1, and ii) it can act as an electron donor in photoreduction. In its chemical reduction, DTT transfers electrons to the aggregated PBI-1 forming the monomeric PBI-1 radical anion and dianion because its highest occupied molecular orbitals (HOMOs) are located above the lowest unoccupied molecular orbitals (LUMO) of PBI-1. As in chapter 3 reported, the reduced PBI-1 species are quickly re-oxidized back to the neutral PBI-1, followed by their self-assembly. Interestingly, the re-assembled PBI aggregates stay in a transient state, then automatically reverted to the monomeric $PBI^{\bullet-}$ and PBI^{2-} without any extra chemical additives or light. The

lifetime of PBI-1 transient aggregates is predetermined by the 'dual fuel' DTT added in the first reduction. Surprisingly, when the same sample was irradiated with UV light, the reduction rate of PBI was significantly accelerated as a photoreduction occurs. In photoreduction, the PBI-1 first was excited then abstract electrons from donor DTT to form PBI-1 radical anion and dianion. When a simultaneous synergistic reduction (chemical reduction and photoreduction) and oxidation occurs by constantly employing UVC irradiation and introducing molecular oxygen (by stirring), emergent properties, such as oscillation and steady-steady state, were discovered between the aggregates and the monomers. Additionally, we developed other photoredox cycles with DTT being an electron-donor, such as naphthalene bisimide (NDI).

In summary, we have developed out of equilibrium assemblies based on the photoredox chemistry of perylene bisimides with several light-activated chemical fuels under vacuum or ambient conditions. Exploring the photoreduction and oxidation under ambient oxygen opens tremendous opportunities to discover new properties of supramolecular materials, such as oscillations, light-driven programmable patterns, and steady-state gels. We believe the research in this thesis can make perylene bisimide assemblies suitable for building life-like materials with more complex and dynamic properties. We have only just started to explore out-of-equilibrium systems, but I am convinced in the supramolecular world, life-like materials with elegant functions such as those found in natural systems are not too far away.

Matériaux Mimant le Vivant Construits sur la Photoréduction et Oxidation de Bisimides de Pérylène

Résumé

1) Introduction

Traditionnellement, la chimie supramoléculaire se fait dans des conditions d'équilibre. Le domaine de la chimie supramoléculaire a évolué vers des systèmes hors équilibre qui imitent les systèmes vivants, tels que les microtubules. Les systèmes vivants ne peuvent se maintenir que grâce à un approvisionnement continu en combustibles. Par exemple, l'assemblage et le désassemblage des microtubules sont pilotés par des enzymes contrôlant temporellement les fonctions dans la cellule[1]. En général, en chimie supramoléculaire, les structures hiérarchiques sont construites par des interactions non covalentes, telles que la liaison hydrogène, l'empilement π—π et les interactions hydrophobes. L'avantage des liaisons non covalentes est la réversibilité des structures, et éventuellement l'assemblage et le désassemblage dynamiques des agrégats peut être réalisé par dissipation d'énergie. Pour construire des systèmes dissipatifs hors équilibre, l'introduction de sources d'énergie pour transformer les précurseurs en blocs de construction est la clé. Ensuite, les unités monomères obtenues s'assemblent en agrégats d'un état énergétique relativement élevé à un état énergétique inférieur[2]. Une fois les sources d'énergie retirées, les agrégats libèrent de l'énergie et redeviennent des précurseurs monomères. L'apport énergétique servant à activer les précurseurs dans les éléments de construction monomères dans un système complexe[3-5] peut être constitué de combustibles chimiques, d'enzymes ou d'un apport de lumière. Les deux réactions réversibles, d'activation et de désactivation des éléments de base sont importantes pour construire les ensembles dissipatifs hors équilibre.

Très récemment, Hermans et ses collaborateurs ont démontré l'oscillation supramoléculaire, les fronts de déplacement et les motifs en utilisant l'oxydoréduction chimique des bisimides de pérylène (PBI)[6]. Le système oscillait entre les agrégats et les unités monomériques grâce à l'introduction en continue de réducteur et d'oxydant. Dans le cycle d'oxydoréduction, les

agrégats de PBI sont réduits et désassemblés en anions radicaux $PBI^{\bullet-}$ et en dianions PBI^{2-} monomères par des combustibles chimiques. Après l'introduction de l'oxygène, $PBI^{\bullet-}$ et PBI^{2-} sont spontanément oxydés en monomère PBI neutre, puis nucléés, allongés et fragmentés. Lorsque la réduction et l'oxydation se produisent simultanément dans le réacteur semi-continu conçu, l'oscillation a été observée entre les agrégats PBI et les radicaux $PBI^{\bullet-}$ du monomère. Dans le système d'oscillation, la rétroaction positive est la nucléation-allongement-fragmentation, tandis que la rétroaction négative est la dépolymérisation des agrégats en fonction de leur taille. La non-linéarité de la cinétique de l'assemblage et du désassemblage, en d'autres termes, la réduction et l'oxydation, sont la clé pour pousser le système loin de l'équilibre. De plus, les comportements spatiotemporels, les fronts de déplacement et les motifs ont été observés en raison des différences de densité induites.

Par rapport aux combustibles chimiques, la lumière peut être un apport idéal en combustible pour entraîner localement l'assemblage et le désassemblage supramoléculaires, en raison du système photo- moteur qui peut généralement être répété de manière réversible sans aucun déchet chimique. Ainsi, mes projets ont pour but de développer des matériaux supramoléculaires proches du vivant, en utilisant l'alimentation en énergie lumineuse, qui peuvent alors réagir, se déplacer et s'adapter de la même manière que les matériaux vivants.

2） Résultats et Discussions

2.1） Assemblages de pérylène bisimides photo-entraînés hors d'équilibre dans le vide et dans les conditions ambiantes.

Les PBI représentent une classe de composés très polyvalents avec des caractéristiques pertinentes pour les applications telles que la photostabilité, la stabilité thermique et la robustesse chimique. Plus précisément, leur caractère pauvre en électrons en fait d'excellents accepteurs qui peuvent produire des anions radicaux stables. En raison de leur grande affinité pour les électrons, de leurs propriétés optiques exceptionnelles et de leur grande mobilité, les dérivés de PBI sont utilisés comme éléments de base pour construire des matériaux supramoléculaires chimiques ou photoréactifs[7,8].

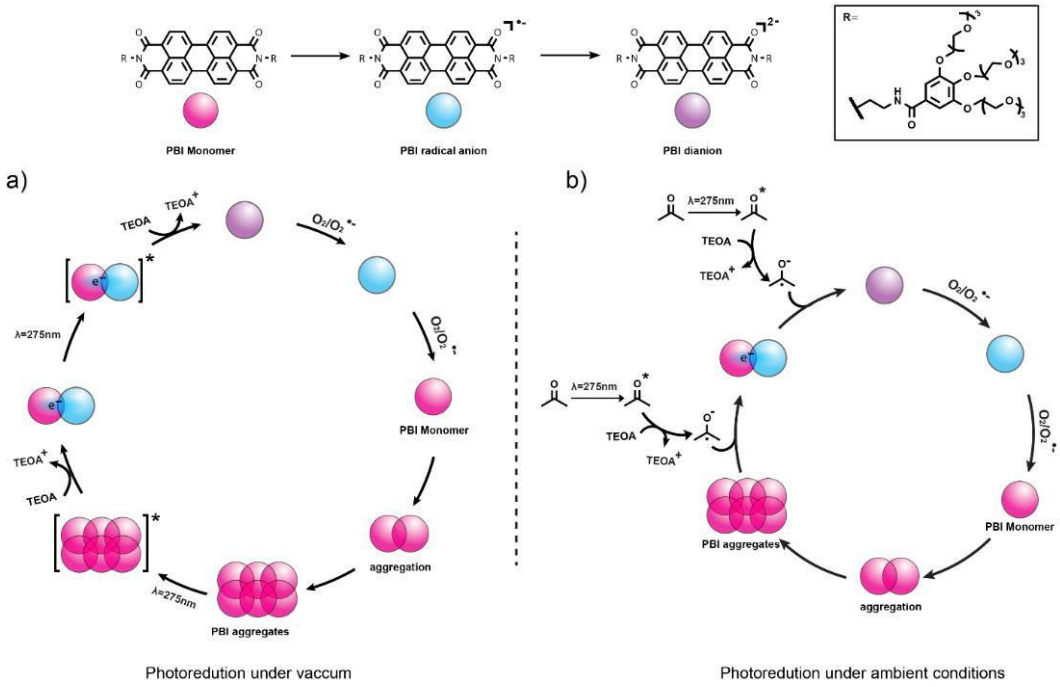

Figure 1. Les blocs de construction sont schématisés ici par les sphères roses, bleues et violettes représentant respectivement les unités monomères PBI neutres, le monomère anion radical $PBI^{\bullet-}$, et le monomère dianion PBI^{2-}. a) les agrégats de PBI à 33 µM dans 3 mL d'un tampon de bicarbonate de sodium en présence de 3000 équivalents de triéthanolamine (TEOA) ont été dégazés par des cycles de congélation-décongélation ; les agrégats PBI ont été exposés à des UVC (275nm, 5mW) pour atteindre leur état excité, puis ont reçu un électron pour former l'anion radical $PBI^{\bullet-}$ (sphères rouge et bleue fusionnées). L'électron se délocalise entre le PBI neutre et le $PBI^{\bullet-}$; le $PBI^{\bullet-}$ est alors excité et reçoit un électron supplémentaire pour former le PBI^{2-}. Lorsqu'ils sont exposés à l'O_2, le $PBI^{\bullet-}$ et le PBI^{2-} sont rapidement oxydé en PBI neutre qui s'agrège au fil du temps. b) 3 mL de PBI à 33 µM avec 3000 équivalents de TEOA dans un tampon de bicarbonate, 9% d'acétone sont utilisés comme combustible chimique dans les conditions ambiantes. L'acétone a été excitée par les UVC et a formé un anion radical d'acétone massif, puis est entrée en collision avec des agrégats de PBI, l'électron étant transféré du radical d'acétone au PBI, ce qui an entraîné la formation de $PBI^{\bullet-}$ et de PBI^{2-}. En éteignant la lumière, les espèces réduites en PBI ont été séquentiellement oxydées pour redevenir des $PBI^{\bullet-}$ et des PBI neutres. Le monomère PBI s'agrège au fil du temps.

Nous faisons ici la démonstration d'un nouveau protocole permettant de réaliser sélectivement un ou deux transferts d'électrons dans un système donneur-accepteur sous vide. Dans ce système, nous avons synthétisé un dérivé de pérylène bisimide (PBI) en couplant les pérylène diamines et l'oligoéthylèneglycol, qui s'agrègent dans un tampon de bicarbonate de sodium, grâce à l'empilement π - π de noyaux de pérylène conjugués et d'entrelacs hydrophiles, alors que le monomère ne se forme que dans de bons solvants, comme le DMF. Lorsque le PBI dégazé dans le tampon sert d'accepteur et la triéthanolamine de donneur, deux électrons peuvent être

transférés lors d'une irradiation UVC ou UVA, ce qui correspond à l'excitation du S_0-S_2[9], et à un niveau d'énergie encore plus élevé. Les agrégats neutres de PBI sont réduits en anion radical PBI ($PBI^{\bullet-}$) et en dianion PBI (PBI^{2-}). Ensuite, les agrégats de PBI se désassemblent en monomères en raison de la répulsion électronique (figure 1a). Cependant, un seul électron est transféré lorsque le PBI neutre à l'état monomère, c'est-à-dire uniquement le $PBI^{\bullet-}$ est obtenu par photoréduction. En introduisant de l'oxygène O_2, le $PBI^{\bullet-}$ et PBI^{2-} sont immédiatement oxydés en PBI neutre, puis réassemblés en agrégats de PBI. Notre hypothèse est que les agrégats contribuent à la formation de PBI^{2-}. Par conséquent, nous avons effectué une photoréduction de PBI dans le monomère et les agrégats sous vide, respectivement. Le monomère PBI préparé dans le DMSO ou le DMF ne forme que du $PBI^{\bullet-}$ (Figure 2a), alors que le PBI^{2-} se forme lorsque le PBI est agrégé dans le tampon, l'éthanol, l'acétonitrile, le toluène ou l'isopropanol (Figure 2b).

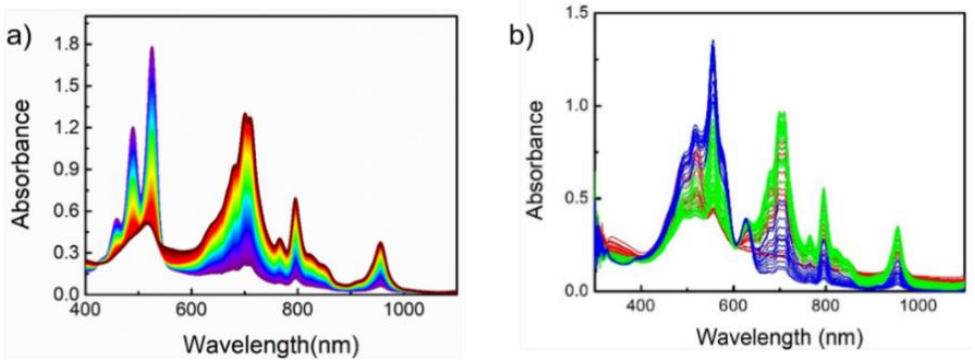

Figure 2. Spectres d'absorption UV-vis a) des monomères de PBI dans le DMF en présence de TEOA (25 °C, 33 µM, échantillon dégazé) irradié par UVC ; du PBI neutre à l'anion radical. L'absorption du PBI neutre autour de 458, 490 et 525 nm diminue avec l'irradiation UVC, tandis que l'absorption caractéristique du PBI dans l'UV-visible augmente à 703, 795 et 957 nm en haut des spectres du PBI neutre. b) Le PBI dans l'acétone (25 °C, 33 µM, échantillon dégazé) a été photoréduit du PBI neutre en anion radical et en dianion. L'absorption du PBI neutre autour de 486 et 520 nm diminue sous l'effet de l'irradiation UVC, tandis que l'absorption caractéristique du PBI dans l'UV-visible augmente à 703, 795 et 957 nm sur le sommet des spectres du PBI neutre, et que le PBI2- se forme ensuite avec la nouvelle absorption à 556 et 626 nm.

2.2) Assemblages dissipatifs hors équilibre de bisimide de pérylène entraînés par un combustible chimique activé par les UV

Bien que le $PBI^{\bullet-}$ et PBI^{2-} se forment facilement dans les agrégats de PBI sous vide, un seul cycle de photo- oxydoréduction est obtenu après l'introduction d'oxygène dans la cuvette scellée. Si d'autres cycles doivent être obtenus, des étapes de dégazage sont nécessaires, ce qui limite

l'application des radicaux $PBI^{\bullet-}$. En général, le radical est trop sensible à l'oxygène moléculaire, ce qui représente un grand défi en photochimie. Pour construire des assemblages photodéséquilibrés dans les conditions ambiantes, nous avons introduit des combustibles chimiques dans le système donneur-accepteur (figure 1b). Il n'y a pas de photoréduction si le PBI/TEOA est présent dans le monomère ou les agrégats dans les conditions ambiantes car le taux d'extinction des $PBI^{\bullet-}$ est beaucoup plus rapide que le taux de génération. En introduisant le combustible chimique, l'acétone[10], l'électron a pu être transférémême en présence d'oxygène, ainsi l'assemblage et le désassemblage des agrégats de PBI peuvent être réalisés dans les conditions ambiantes. Dans ce cycle de réaction, le combustible chimique, l'acétone, a tout d'abord été excité par les UVC et a généré une acétone radicalaire en obtenant un électron du donneur TEOA. Ensuite, l'acétone radicalaire transmet l'électron au PBI en entrant en collision avec le monomère ou les agrégats. Seulement 9 % en volume d'acétone dans le tampon ont accéléré de manière significative le taux de transfert d'électrons entre le donneur TEOA et l'accepteur PBI lors de l'irradiation UVC. Ainsi, la photoréduction et l'oxydation se produisent simultanément par l'apport constant de lumière et du flux d'oxygène, ce qui a poussé le système loin de l'équilibre et a atteint les différents états assemblés, en accordant l'intensité lumineuse au taux fixe de flux d'oxygène. Nous pouvons aussi obtenir de manière sélective le $PBI^{\bullet-}$ et le PBI^{2-} en introduisant les différents combustibles chimiques.

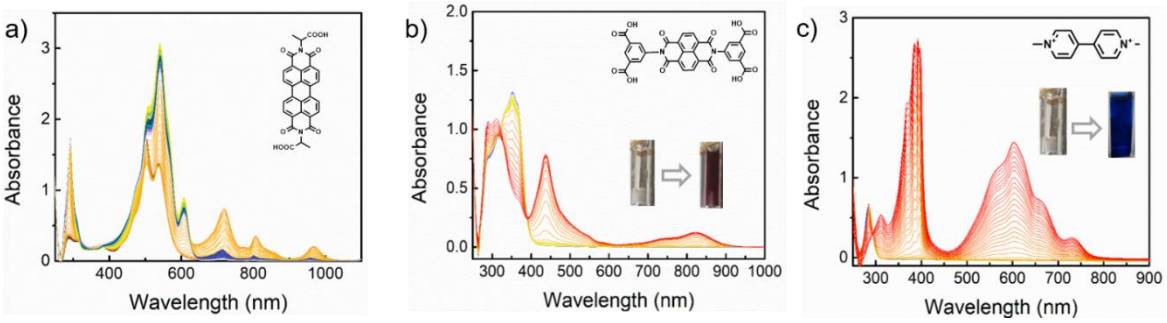

Figure 3. Spectres UV avant et après photoréduction de la PBI-alanine (PBIA), de l'acide naphtalène dimide-aminoisophtalique (NDI) et du méthyl viologène (MV) dans H_2O avec de l'acétone à 9% en présence de 3000 équivalents TEOA dans les conditions ambiantes. a) la PBI-alanine (PBIA) absorbe à 503, 537 nm ; la $PBIA^{\bullet-}$ absorbe à 717, 806, et 969 nm ; la $PBIA^{2-}$ absorbe à 510, 540, et 507 nm. b) le NDI neutre absorbe à 353 nm ; le $NDI^{\bullet-}$ absorbe à 309, 438, et 821 nm. c) le MV neutre absorbe à 285 nm ; le $MV^{\bullet-}$ absorbe à 312, 390, et 600 nm.

En outre, nous avons également développé d'autres cycles de réactions photodynamiques, comme l'alanine PBI, l'acide naphtalène-dimide-aminoisophtalique et même le méthyl viologen. La pérylène-alanine PBIA/acétone/TEOA dans l'eau peut être photoréduite séquentiellement en $PBIA^{\bullet-}$ puis $PBIA^{2-}$ (figure 3). Par rapport au PBI^{2-}, le $PBIA^{2-}$ est beaucoup plus fluorescent, résultant du fait que le pérylène alanine à pH=10 est moins assemblé. Le protocole n'est pas seulement limité aux dérivés de pérylène, qui peuvent également être appliqués dans le bisimide de naphtalène a été réduit en $NDI^{\bullet-}$, et même à la photoréduction du méthyle viologen. Par conséquent, nous avons obtenu des assemblages hors équilibre basés sur la photoréduction des bisimides de pérylène en utilisant ces combustibles chimiques photo-réduits.

2.3) Gel photosensible basé sur la photo-oxydoréduction de pérylène bidimide.

Dans cette section, nous avons réduit sélectivement le gel de pérylène bisimide en gel d'anions radicaux luminescent ou de dianions. Nous avons synthétisé le gélifiant pérylène bisimide-acide aminoisophtalique (PDBA) qui s'est co-assemblé avec le CTAB en présence de triméthylamine (TEA) ou d'helxyamine (HLA) en gel PBI neutre correspondant, dans le DMSO, par chauffage et refroidissement. Les nanofibres longues et enchevêtrées formées dans le gel PDBA/CTAB/HLA (figure 4a) peuvent être réduites en $PDBA^{\bullet-}$ lors d'une irradiation UVA (figure 4c). L'absorbance UV du PDBA neutre diminue tandis que de nouveaux pics de $PDBA^{\bullet-}$ à environ 699, 794 et 954nm apparaissent dans le haut du spectre neutre, mais il n'y a pas de formation de $PDBA^{2-}$, même si le gel a été irradié plus longtemps. Cependant, dans le gel PDBA/CTAB/TEA, nous avons observé la formation de $PDBA^{2-}$ après avoir atteint le maximum de la $PDBA^{\bullet-}$. La nouvelle absorption liée aux pics à 522nm et 570nm peut être attribuée à l'absorption UV du $PDBA^{2-}$, en particulier, les trois nouveaux pics autour de 260 nm sont la signature du $PDBA^{2-}$. Il est intéressant de noter que le gel PDBA/CTAB/TEA a rapidement été réduit et est devenu plus fluorescent après l'irradiation UVA, par rapport au gel PDBA/CTAB/HLA.

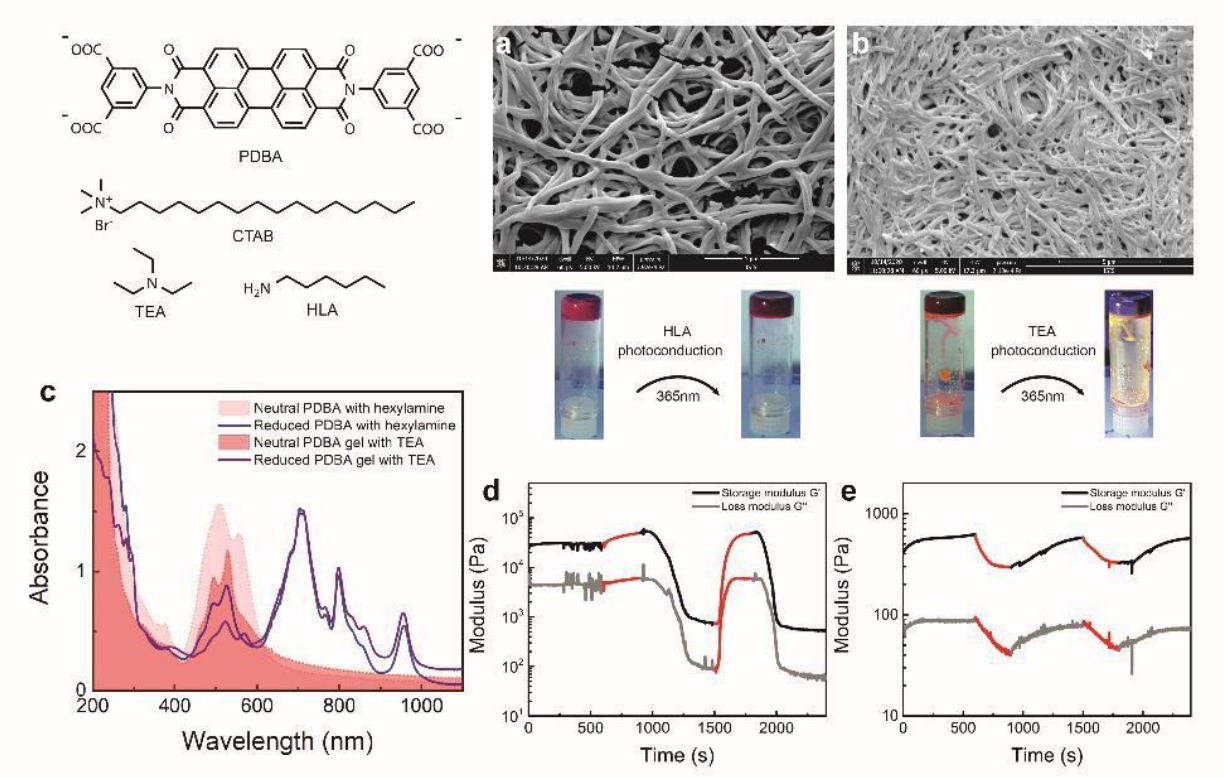

Figure 4. Structure moléculaire du gélifiant (PDBA) co-assemblé avec du bromure de cétrimonium (CTAB) en présence de triéthylamine (TEA) ou d'helxyamine (HLA) dans le gel, dans du DMSO, par chauffage-refroidissement, a, b) images MEB du xérogel de PDBA/CTAB/HLA et de PDBA/CTAB/TEA, c) spectres UV avant et après photoréduction des gels PDBA/CTAB/HLA et PDBA/CTAB/TEA, d,e) mesures rhéologiques des deux gels en mode oscillatoire au photo-rhéomètre (la contrainte de cisaillement constante est de 0.1% et le taux de cisaillement constant de 10 rad/s), les lignes rouges représentent cinq minutes d'irradiation par la lumière UVA, les autres étant sans irradiation lumineuse.

Bien que les gels PDBA/CTAB/TEA et PDBA/CTAB/HLA puissent être photoréduits, la rigidité mécanique des gels est à différente. Nous avons suivi la photoréduction des PDBA/CTAB/HLA sous photo-rhéomètre en mode oscillatoire à une contrainte et une vitesse de cisaillement constantes ; après irradiation UVA, le module de conservation G' augmente, en raison de l'anion radical généré, co-assemblé avec le PDBA neutre et ainsi renforce la rigidité mécanique du gel, ce qui est conforme au rapport de J. Adam[8]. En revanche, le module de conservation G' du gel PDBA/CTAB/TEA diminue lors de l'irradiation UVA en raison de la répulsion électronique plus forte entre les PDBA2-. En conclusion, nous avons contrôlé sélectivement le transfert d'un ou de deux électrons dans différents gels en utilisant la photoréduction des bisimides de pérylène.

2.4) Les agrégats transitoires accordables PBI construits par des combustibles photochimiques en duel.

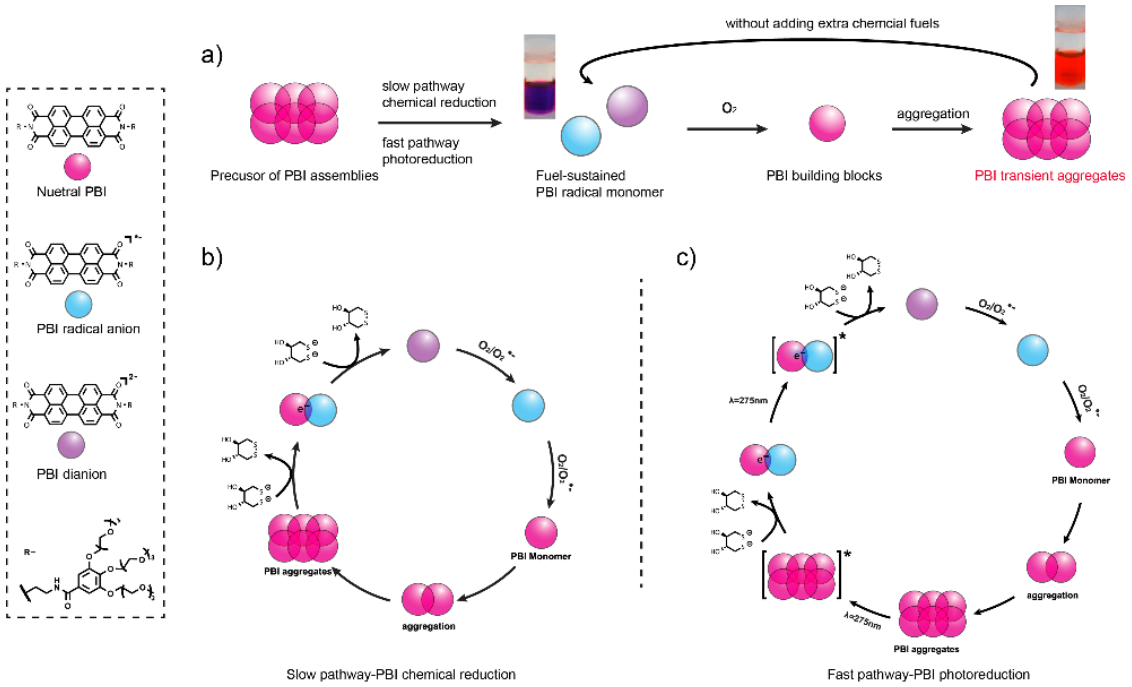

Figure 5. La structure moléculaire des blocs de construction et la représentation de la formation des matériaux transitoires. a) les agrégats PBI transitoires obtenus par les radicaux $PBI^{\bullet-}$ monomères alimentés par le carburant. Les agrégats PBI neutres (boules roses agrégées sur le côté gauche) en présence d'une quantité supplémentaire de dithiothréitol (DTT) dans l'eau peuvent être chimiquement réduits ou photoréduits en $PBI^{\bullet-}$ monomères et PBI^{2-} (boules bleues et violettes) plus ou moins rapidement. Le précurseur des radicaux $PBI^{\bullet-}$ soutenu par le carburant peut être oxydé en retour en blocs de construction monomères (une seule bille rose) en introduisant l'oxygène moléculaire, et assemblé à nouveau en agrégats PBI (billes roses agrégées sur le côté droit), mais les agrégats PBI sont instables, et retournent automatiquement au précurseur PBI soutenu par le carburant des radicaux $PBI^{\bullet-}$. b) Mécanisme de réduction chimique des PBI avec le DTT. Les agrégats PBI sont réduits en capturant les électrons libres donnés pendant la cyclisation du DTT, puis désassemblés en $PBI^{\bullet-}$ et PBI^{2-}. Après avoir introduit l'oxygène dans le système réduit, l'espèce réduite de PBI a été oxydée en PBI neutre. c) Mécanisme de photoréduction de PBI avec le DTT. Au départ, les agrégats de PBI ont été excités par les UVA à l'état excité, puis ont reçu l'électron du DTT déprotoné en $PBI^{\bullet-}$, puis un autre électron pour former le PBI^{2-}. Lorsque le PBI a été complètement réduit, les espèces réduites sont revenues au PBI neutre par l'introduction d'oxygène après avoir éteint la lumière UV.

Dans cette section, nous avons construit des agrégats PBI transitoires accordables à partir d'oxydoréduction induites de façon chimique ou lumineuse de pérylène bisimides. La réduction chimique et la photoréduction sont les forces motrices qui poussent les agrégats loin de l'équilibre. Les agrégats de PBI dans un tampon sont désassemblés en $PBI^{\bullet-}$ monomère et PBI^{2-} en introduisant du dithiothréitol (DTT), un combustible chimique. Étonnamment, lorsque le même

échantillon a été irradié par une lumière UV, le taux de réduction du PBI est considérablement accéléré. Cela implique que le PBI neutre a été excité par la lumière UV, et a de plus obtenu des électrons du DTT donneur, servant à la fois de combustible chimique et de donneur d'électrons[11]. Le $PBI^{\bullet-}$ et le PBI^{2-} ont été spontanément oxydés par l'oxygène pour redevenir des éléments de base du PBI neutre, puis allongés et fragmentés. Il est intéressant de noter que les agrégats de PBI réassemblés sont automatiquement redevenus des $PBI^{\bullet-}$ et PBI^{2-}monomères sans aucun additif chimique supplémentaire ni apport de lumière (figure 5). Lorsque le PBI neutre redevient du $PBI^{\bullet-}$ et du PBI^{2-}, la formation d'agrégats PBI transitoires peut être redéclenchée simplement en introduisant de l'oxygène. Ainsi, ce matériau transitoire semi-automatique est construit par l'ajout unique de pré-carburant DTT.

Ces agrégats PBI transitoires sont accordables avec différentes quantités de combustibles chimiques ou d'apport de lumière. Si les 60 équivalents DTT/PBI sont ajoutés dans le précurseur des assemblages PBI, aucune réduction chimique, en raison de la vitesse d'extinction des radicaux générés beaucoup plus rapide que la vitesse de réduction des PBI dans les conditions ambiantes. Le PBI est entièrement réduit en PBI^{2-} lorsque 600 équivalents de DTT sont ajoutés. Dans ce scénario, le précurseur du PBI^{2-} soutenu par le DTT a été rapidement oxydé en éléments constitutifs du PBI et agrégé. La durée pendant laquelle les agrégats peuvent s'allonger ou rester dans la phase d'agrégats dépend de la quantité de DTT de combustible chimique, les agrégats peuvent rester 10 minutes avec 600 équivalents de DTT, mais seulement 40 secondes avec 2000 équivalents de pré-carburant DTT. La raison principale qui conduit à ce matériau transitoire est les deux cycles de réaction compétitifs dans ce système, l'oxydation du $PBI^{\bullet-}$/PBI^{2-} par l'oxygène, et la réduction du PBI neutre par le DTT. Mais le taux d'oxydation est plus rapide que le taux de réduction, et la réaction de réduction est piégée par la cinétique. L'allongement des agrégats transitoires de PBI peut également être réglé par la lumière UV, les agrégats sont rapidement désassemblés et retournés à un précurseur de radicaux monomériques par irradiation UVC ou UVA. Nous devons souligner que la photostabilité de ce système est extrêmement importante. Les agrégats PBI transitoires peuvent être recyclés plus de 50 fois avec 2000 équivalents de DTT commme combustibles chimiques. Dans le même temps, nous avons

également mis au point d'autres cycles photochimiques-redox avec le bisimide de naphtalène et le méthyl viologen. Dans cette section, nous avons ainsi obtenu des agrégats PBI hors équilibre contrôlables, basés sur l'oxydoréduction photochimique des bisimides de pérylène.

3) Conclusion Générale

En conclusion, nous avons développé plusieurs matériaux émergents basés sur la photo-oxydoréduction des bisimides de pérylène. La réduction chimique ou la photoréduction dul PBI sont la clé pour pousser le système loin de l'équilibre. Nous avons contrôlé avec précision le transfert d'un ou deux électrons dans le système donneur-accepteur sous vide ou dans des conditions ambiantes. Grâce à l'acétone chimique, l'assemblage et le désassemblage dynamiques des PBI agrégés sont modulables en ajustant le taux de réduction et d'oxydation. Parallèlement, nous avons développé une double oxydoréduction : lumineuse et chimique dans un seul système pour accorder avec précision les agrégats transitoires de PBI. Enfin, nous imposons aux gels un comportement proche de celui du vivant par des cycles de réaction dissipatifs, tels que le transfert d'informations, l'adaptation et l'expression.

References

(1) Valiron, O.; Caudron, N.; Job, D. Review Microtubule Dynamics. **2001**, *58*, 16.

(2) van Rossum, S. A. P.; Tena-Solsona, M.; van Esch, J. H.; Eelkema, R.; Boekhoven, J. Dissipative Out-of-Equilibrium Assembly of Man-Made Supramolecular Materials. *Chem. Soc. Rev.* **2017**, *46* (18), 5519–5535. https://doi.org/10.1039/C7CS00246G.

(3) Dambenieks, A. K.; Vu, P. H. Q.; Fyles, T. M. Dissipative Assembly of a Membrane Transport System. *Chem. Sci.* **2014**, *5* (9), 3396–3403. https://doi.org/10.1039/C4SC01258E.

(4) Debnath, S.; Roy, S.; Ulijn, R. V. Peptide Nanofibers with Dynamic Instability through Nonequilibrium Biocatalytic Assembly. *J. Am. Chem. Soc.* **2013**, *135* (45), 16789–16792. https://doi.org/10.1021/ja4086353.

(5) de Jong, J. J. D.; Hania, P. R.; Pug?lys, A.; Lucas, L. N.; de Loos, M.; Kellogg, R. M.; Feringa, B. L.; Duppen, K.; van Esch, J. H. Light-Driven Dynamic Pattern Formation. *Angew. Chem. Int. Ed.* **2005**, *44* (16), 2373–2376. https://doi.org/10.1002/anie.200462500.

(6) Leira-Iglesias, J.; Tassoni, A.; Adachi, T.; Stich, M.; Hermans, T. M. Oscillations, Travelling Fronts and Patterns in a Supramolecular System. *Nature Nanotech* **2018**, *13* (11), 1021–1027. https://doi.org/10.1038/s41565-018-0270-4.

(7) Krieg, E.; Shirman, E.; Weissman, H.; Shimoni, E.; Wolf, S. G.; Pinkas, I.; Rybtchinski, B. Supramolecular Gel Based on a Perylene Diimide Dye: Multiple Stimuli Responsiveness, Robustness, and Photofunction. *J. Am. Chem. Soc.* **2009**, *131* (40), 14365–14373. https://doi.org/10.1021/ja903938g.

(8) Draper, E. R.; Schweins, R.; Akhtar, R.; Groves, P.; Chechik, V.; Zwijnenburg, M. A.; Adams, D. J. Reversible Photoreduction as a Trigger for Photoresponsive Gels. *Chem. Mater.* **2016**, *28* (17), 6336–6341. https://doi.org/10.1021/acs.chemmater.6b02677.

(9) Draper, E. R.; Archibald, L. J.; Nolan, M. C.; Schweins, R.; Zwijnenburg, M. A.; Sproules, S.; Adams, D. J. Controlling Photoconductivity in PBI Films by Supramolecular Assembly. *Chemistry* **2018**, *24* (16), 4006–4010. https://doi.org/10.1002/chem.201800201.

(10) Yonezawa, Y.; Sato, T.; Kuroda, S.; Kuge, K. Photochemical Formation of Colloidal Silver: Peptizing Action of Acetone Ketyl Radical. *Faraday Trans.* **1991**, *87* (12), 1905. https://doi.org/10.1039/ft9918701905.

(11) Pellegrin, Y.; Odobel, F. Sacrificial Electron Donor Reagents for Solar Fuel Production. *Comptes Rendus Chimie* **2017**, *20* (3), 283–295. https://doi.org/10.1016/j.crci.2015.11.026.

Acknowledgements

First, I would like to thank Prof. Thomas Hermans for giving me the opportunity to pursue my Ph.D. in his group. It was a great experience being able to study in such an innovative and friendly environment. In these 3.5 years, I have not only improved my fundamental knowledge of supramolecular chemistry but also had the opportunity to work at the frontier of this fascinating field. I am deeply grateful to Thomas for his continuing support and supervision. He took the time to help me with my oral presentation skills, my writing skills, as well as my laboratory work. Without him, I would not have been able to assemble the set-ups that were required for this project. Most importantly, he showed me how to be an independent researcher. A skill that will be invaluable in my career. His expertise and innovative ideas have been an inspiration to me, and, I hope, that as I continue my career, I will be able to achieve the same level of excellence.

I would also like to express my deepest appreciation to my committee—Prof. Florian Beuerle, Dr. Yannick De Decker, and Dr. Emilie Moulin. Their evaluation and comments will be essential for me as I begin to prepare for my independent career in academia.

Special thanks to Dr. Takuji Adachi, who guided me in the first year of my Ph.D. He introduced me to the field of photochemistry, and I would not have been able to accomplish all that I have done without his help. Not only did he provide me with the fundamentals to succeed in this field, but also inspired my continued fascintion. I also would thank his wife Dr. Johanna Brazard for our collaboration on the photodynamic study.

Many thanks to Dr. Antoine Bonnefont for collaborating with me on redox potential measurements. Our work together provided me with a fundamental understanding in electrochemistry that I would otherwise not have learned.

I very much appreciate Dr. Jennifer Ciesieski for her help with my CV, writing, and scientific suggestions. And I also want to thank Dr. Nishant Singh for our daily scientific discussion and his suggestions about my research.

I would like to extend my gratitude to Dr. Georges Formon for his help with my programming language study and friendly daily discussion. I also appreciate the help from Lucas Giacchetti and Dr. Caroline on my French resume. Meanwhile, I also had the pleasure of working with Dr. Alessandra Tassoni, Serena De Piccoli, and Michaela Schicho. They helped me both in administrative affairs and experiments to which I am indebted. I gratefully acknowledge the other members of the lab, both past and present, Dr. Jorge S. Valera, Dr. Dani Iglesias, Dr. Jorge Leira-Iglesia, Dr Anamali, Anastasiia Sharko, Tianheng Xu, Alvaro Acosta-Lopez, and Flor Sacarelli.

I would also like to thank all the support staff, administrators, friends in ISIS, the Doctoral school, and the department of chemistry at the University of Strasbourg. A special thank you to Annia

Bertrand, Soumia Hnin, and Nathalie Kostmann. Thanks to their support and help, I was able to finish my degree.

To my family, I am extremely grateful for their support the past 25 school-years. Without my mother Fan Xiumei and my father Chen Kai's nurture and education, I would not be here today. I am very lucky and proud to have open-minded parents who encouraged me to pursue my dreams. The love from my family has allowed me to succeed in every area of my life. I would also like to mention my younger brother. He has been the glue that has held our family together, and, without him, I would not be here today.

Finally, I would also like to thank the French doctors who helped me in one of my darkest moments. I suffered from COVID-19 in the first confinement, and, without them, I would not have survived. And, of course, to France. Even if I don't know your name, thank you for helping me integrate into this wonderful country. It's always difficult as a foreigner, and the kindness and genersoity of the French people is something I will never forget! Merci beaucoup!!

UNIVERSITÉ DE STRASBOURG

Chunfeng CHEN

EDSC École Doctorale des Sciences Chimiques

Matériaux Mimant le Vivant Construits sur la Photoréduction et Oxidation de Bisimides de Pérylène

Résumé

Notre objectif dans cette thèse est de construire des matériaux dissipatifs semblables à la vie en utilisant la photoréduction du bisimide de pérylène (PBI) dans des conditions ambiantes. Le principal défi de la photoréduction du PBI est que seul le transfert d'un électron permet d'être photo-induit dans des conditions de vide. Pour éloigner le PBI agrégé de l'équilibre en présence d'O_2 atmosphérique, notre recherche est divisée en quatre parties. Premièrement, nous avons construit le système donneur-accepteur d'électrons dans lequel les transferts photoinduits de deux électrons dans le PBI agrégé, alors que les transferts d'un électron dans le monomère dans des conditions de vide. Deuxièmement, nous avons accéléré de manière significative la photoréduction du PBI en introduisant un combustible chimique activé par les UV dans des conditions ambiantes, ce qui ouvre des possibilités d'atteindre différents états d'équilibre hors équilibre. Troisièmement, nous avons développé un combustible à double fonction, le DTT, qui est un électron à la fois dans la chimie et la photoréduction de l'PBI, ce qui nous permet de construire des agrégats transitoires d'PBI et d'observer des propriétés émergentes, comme l'oscillation. Enfin, nous avons développé la photoréduction du PBI de sa solution à des gels qui peuvent être photoinduits sélectivement par transfert d'un ou deux électrons. Ces carburants chimiques confèrent au PBI un rôle de premier plan dans le développement de matériaux hors équilibre pilotés par la lumière.

Mots clés : pérylène bisimide, photoréduction, carburants chimiques, assemblages hors équilibre, lumière, oscillation.

oscillation.

Résumé en anglais

Our aim in this thesis is to build dissipative life-like materials using photoredox of perylene bisimide (PBI) under ambient conditions. The main challenge in PBI photoreduction is that only one-electron transfer allows to be photoinduced under vacuum conditions. To drive the aggregated PBI away from equilibrium, our research is divided into four parts. First, we built the electron donor-acceptor system in which the photoinduced two-electron transfers in aggregated PBI, whereas one-electron transfers in monomer under vacuum conditions. Secondly, we significantly accelerated PBI photoreduction by introducing a UV-activated chemical fuel under ambient conditions, which opens possibilities to achieve different non-equilibrium steady states. Thirdly, we developed a dual-functional fuel DTT being an electron both in PBI chemical and photoreduction, which allows us to construct PBI transient aggregates, and observe emergent properties, such as oscillation. Lastly, we developed the PBI photoreduction from its solution to gels that can be selectively photoinduced one or two-electron transfer. These chemical fuels provide PBI a leading role in developing light-driven out-of-equilibrium materials.

Keywords: perylene bisimide, photoredox, chemical fuels, out-of-equilibrium assemblies, light, oscillation.